Programa de Doctorado "Matemáticas"

PhD Dissertation

Development of reduced numeric models to aero-thermal flows in buildings

Author
Enrique Delgado Ávila

Supervisors
Prof. Dr. *Tomás Chacón Rebollo*
Prof. Dr. *Macarena Gómez Mármol*

April 4, 2018

En memoria de mi madre, siempre fuerte y luchadora.
En memoria de mis abuelos. A mi padre y mi hermana.

Acknowledgments

En primer lugar agradecer a mis directores de Tesis, Tomás y Macarena, todo el esfuerzo que han hecho durante estos años para ayudarme en todo lo posible. Siempre estaban disponibles para ayudarme, y sacaban tiempo de donde no lo tenían. Gracias a ellos he podido madurar, con todos los conocimientos que tan bien han sabido transmitirme. Por supuesto, agradecerles también su complicidad en lo personal; tanto en los buenos momentos como en los malos he podido contar con ellos para cualquier cosa.

También agradecer a toda los compañeros con los que he tenido la suerte de compartir despacho, risas y momentos de desconectar con el trabajo. Gracias Samuele, Diego, Marta, Antonio Jesús, Javi, Antonio, Cristina y Javier, por los buenos ratos fuera y dentro del despacho. También una mención especial a los compañeros becarios del IMUS, por todas las cenas y comidas que se organizaban con cualquier excusa para tomar algo.

Por supuesto, a Jose, el compañero inseparable de los congresos nacionales. Porque aunque ha podido congelarme por las noches con el aire acondicionado, siempre estaba ahí para apoyarnos mutuamente. Por su disponibilidad casi total cuando una cerveza era necesaria para desconectar del trabajo.

A todos los compañeros del departamento EDAN, que tan bien me han acogido desde el primer día, haciéndome sentir uno más. Por supuesto, a Cristian y Soledad, que siempre han estado animando a todos los becarios, haciéndonos ver que al final el esfuerzo tiene su recompensa.

También agradecer a los compañeros del grupo de investigación M2S2M, porque han sido como una familia para mí. Por esas comidas de Navidad en Enero con ellos, y los buenos ratos después de las charlas de los congresos.

I acknowledge Prof. Yvon Maday, Prof. Gianluigi Rozza and Francesco Ballarin for all their support and guidelines in the development of this work, that has allowed improve the results in this Thesis. Also acknowledge all people in LJLL and SISSA for their support during my stays in Paris and Trieste.

Agradecer todo el apoyo de mi familia, que con las dificultades que hay para explicar la profundidad del trabajo, siempre han estado apoyando todas mis de-

cisiones y animándome en los momentos más duros. Sé que siempre los tendré a mi lado.

Por último agradecer a todos mis amigos por estar siempre cuando les he necesitado. Tanto a los que conocía antes de empezar esta aventura, como aquellos que he ido conociendo durante todos estos años, en gran medida gracias a las estancias de investigación en París y Trieste, en las que a parte de resultados, también hicieron que consiguiera grandes amigos. Del Colegio de España en París me llevé muy buenos momentos, muchísimas risas, y un gran grupo de amigos. Lo bueno de que estén repartidos por el mundo, es que cualquier excusa es buena para hacer un viaje para visitarlos.

Resumen

Esta tesis se enmarca dentro de la resolución numérica de modelos que simulan el comportamiento de flujos turbulentos mediante técnicas de orden reducido y bajo coste computacional. En particular, desarrollamos técnicas de bases reducidas que permiten reducir drásticamente el cálculo de una solución a estos modelos. El objetivo es desarrollar modelos matemáticos orientados al diseño de edificios eco-eficientes, lo que conlleva a la resolución de modelos complejos donde las incógnitas del problema aparecen acopladas. La modelización de orden reducido proporciona reducciones de varios órdenes de magnitud en el coste computacional de la simulación numérica de estos procesos y problemas de diseño, haciendo cada vez más abordable su resolución efectiva en tiempo real. Normalmente los modelos de orden reducido requieren de cientos de grados de libertad en lugar de millones como frecuentemente necesita el modelo de orden completo.

En este trabajo consideramos diferentes modelos de complejidad creciente, desarrollando las técnicas de orden reducido aplicadas a dichos modelos. Realizamos un estudio de estabilidad para dichos métodos numéricos y se completa con simulaciones numéricas que permiten validar los resultados teóricos obtenidos.

En primer lugar consideramos el modelo de turbulencia para flujos de aire conocido como modelo de Smagorinsky. Se trata de un modelo básico de turbulencia, que corresponde a las ecuaciones de Navier-Stokes donde la viscosidad es una viscosidad turbulenta, que matemática es una función no lineal de la incógnita. Para la aproximación de este término utilizamos técnicas de Interpolación Empírica, desarrollando un estimador de error *a posteriori* de acuerdo con la Teoría de Brezzi-Rappaz-Raviart. Para este modelo en su versión bidimensional, realizamos distintos test numéricos obteniendo que el tiempo de cálculo para la velocidad del flujo se divide por mil cuando utilizamos técnicas de orden reducido.

A continuacion nos ocupamos de una modificación del modelo de Smagorinsky donde consideramos que la viscosidad turbulenta actúa sólo sobre las pequeñas escalas resueltas, y además consideramos una estabilización local de proyección para el cálculo de la presión. El considerar esta estabilización de la presion nos permite evitar el enriquecimiento del espacio de velocidades para obtener

un método estable. Para este modelo hemos comprobado numéricamente que el tiempo de cálculo se reduce más que en el modelo original de Smagorinsky.

Por último consideramos un modelo acoplado de tipo Boussinesq obtenido mediante técnicas de multiescala variacional. El modelo está formado por las ecuaciones del modelo de Smagorinsky junto a la ecuación de la temperatura. Estas ecuaciones están acopladas mediante los términos de flotabilidad. El estudio realizado para este modelo se centra en aplicar técnicas de orden reducido para dos tipos de parámetros: físico y geométrico. El tratamiento para cada uno de estos parámetros es distinto desde el punto de vista matemático. Para este problema desarrollamos de nuevo un estimador de error *a posteriori* y lo validamos mediante simulaciones numéricas sencillas que representan el estudio del flujo de aire y la temperatura en habitaciones de geometría sencilla.

Abstract

This PhD dissertation addresses the numerical simulation of turbulent flows with reducer order techniques and low computational cost. Particularly, we develop reduced basis techniques that allow us to reduce drastically the computational time of the numerical solution of these models. The objective is the development mathematical models oriented to the eco-efficient buildings design, that lead us to the solution computation of complex models where the unknowns of the problem are coupled. The reduced order modelization provides reductions of several orders of magnitude in the computational cost of the numerical simulation of this processes and design problems, making possible real-time computations. Usually, reduced order models require hundreds of degree of freedom, while full-order models frequently requires millions of degree of freedom.

In this work, we consider several models with increasing complexity, for which we develop the reduced order techniques applied to these models. We perform a stability study for these models and numerical simulations that validate the theoretical results obtained.

We first construct a RB Smagorinsky model, that is the basic LES model, in which a non-linear eddy viscosity is considered for the Navier-Stokes equations. We approximate this non-linear term with the Empirical Interpolation Method, and we perform an *a posteriori* error estimation according with the Brezzi-Raviart-Rappaz theory. For this model, we perform two numerical tests, that provides us speedups rates in the computation by factor larger than 1000 in benchmark 2D flows.

Then, we construct a RB model for a Variational Multi-scale Smagorinsky model, in which the eddy viscosity only acts on the small resolved scales, with Local Projection Stabilization on the pressure. The consideration of the Local Projection Stabilization on the pressure also in the RB model let us avoid the enrichment of the reduced velocity space with the inner pressure *supremizer*. Since the dimensionality of the reduced spaces is lower, we obtain larger speedups in the computation, compared with the results obtained for the RB Smagorinsky model.

Finally, we construct a RB model for a Boussinesq VMS-Smagorinsky model,

in which we incorporate the buoyancy forces in our model. This model consists on the Smagorinsky equations coupled with the energy equation. For this model, we consider reduced order technique for both physical and geometrical parametrization. The treatment of each parameter is different from the mathematical point of view. Again, we provide an *a posteriori* error bound, and we validate our model by numerical simulations for different parameter ranges, that represent the study of the aero-thermic flow in simple geometry rooms.

Contents

List of Figures

List of Tables

Introduction

Nowadays, several industrial processes need of numerical simulations, which usually are performed with the common high-fidelity approximation techniques such as finite element (FE), finite volumes or spectral methods, and they usually take large times of computation. In many situations, the model that represents the behavior of a industrial process is given by a Partial Differential Equation (PDE) depending on parameters. Reduced-order modeling (ROM) is used in parametrized Partial Differential Equation (PDE) in order to try to reduce this high computational time, when large number of simulations with different parameter values are needed. There are different classes of ROM, such as the proper orthogonal decomposition (POD) or the reduced basis (RB) methods.

In fluid mechanics, a popular strategy is to use POD to extract the dominant structures for high-Reynolds flow, which are then used in a Galerkin approximation of the underlying equations [51, 102]. There have been a number of recent works combining POD/RB with Variational Multi-Scale models [110], in which the eddy viscosity in the Navier-Stokes equations is considered with only adding the small resolved scales with smallest energy POD modes; ensemble models [46], in which a POD is incorporate into the ensemble-basis method to significantly reduce the cost of determining multiple solutions of the Navier-Stokes equations; flow regularization models, in which a POD model is considered for a stabilized FE [4] or a regularization for the POD model is considered through a inner *supremizer* operator [7]; as well as bifurcation problems [49, 85, 86, 113], for which RB methods are used to reducing the complexity and the computational time required for the construction of bifurcation and stability diagrams.

Focusing on RB methods, them were first introduced in the ends of the 70s in [2] and [75] for structural analysis of beam and arches, where the non-linear portions of the analysis are carried out in a reduced equation system, in which the degree of freedom are the coefficients in a summation of global shape function. In the first of 80s, the use for the first time of Taylor basis functions in the context of the RB method was presented in [79], in which the modal displacement vector is expressed as a linear combination of a small number of basis vectors. Later on, on the first 80s, several works on RB methods for structural problems were presented in [1, 80, 81], by extending the theory developed in the previous works.

In the 80s, the first analysis for the RB methods were introduced in [40, 41] by Fink and Rheinboldt, where the effectiveness of the RB technique is provided by a theoretical error estimation for a general non-linear problem.

In the context of the RB method for fluid dynamic problems, the first work was presented by Peterson [83] in the ends of the 80s, in which the RB method is used in conjunction with a standard continuation technique to approximate the solution curve for the non-linear equations resulting from discretizing the Navier-Stokes equations by FE methods. Other work on this topic was presented by Gunzburger [47], also in the ends of the 80s, in the same context. Early works of reduced-order methods for control in fluid problems were proposed by Ito *et al.* in [60, 61] in the ends of the 90s, where the reduced-basis spaces are constructed by Taylor expansions.

But it was in the early 2000s, when a general mathematical background analysis was developed for the RB method. The development of an *a posteriori* error bound estimator and the design of an algorithm for the basis functions, was a milestone on the expansion of the RB method. This *a posteriori* error bound estimator is used in the snapshot selection for the reduced basis space, which is performed by a Greedy algorithm. The greedy algorithm selects in each iteration the snapshot associated with the parameter value with the highest error between the FE and RB solutions. Since compute this error is expensive from the computational point of view, the algorithm usually used in RB methods is the weak Greedy algorithm, which substitutes the exact error by an error estimator. The weak Greedy algorithm was first introduced in [88, 89, 107] in the context or RB methods. These works also exploit the parameter dependence of the problem, defining an offline phase where the parameter-independent matrices were stored, and the online phase, when the RB solution depending on the parameter value is computed. Also, general *a priori* convergence properties are first studied by Maday et *al.* in [69, 70]. From those works, several works on RB method in the context for general parametrized PDE were developed, e.g., in [50, 78, 87, 91, 94, 95, 104].

Patera et *al.* [105, 106] started on the study of free-divergence velocity spaces problem, for which *a posteriori* error bound estimator is developed. These works focused on the study of reduced-basis problem in which only the physical parameter is involved. This problem was studied by Rozza and Veroy in [97] who introduced a stabilized procedure for the pressure discretization. This procedure consist in the introduction of the inner pressure *supremizer* for the velocity-pressure stability of the reduced-basis spaces. After that, several works of RB method for Stokes equations (*cf.* [76, 96]), and Navier-Stokes equations (*cf.* [36, 38, 72]) were developed, with a deeply study on the *a posteriori* error bound estimator and the pressure stabilization via the inner pressure *supremizer* operator.

In the present work, we focus on the development of reduced basis methods for turbulence models. Turbulence models came out for the high computational cost on solving directly the Navier-Stokes equations, the so-called Direct Numerical Simulation (DNS); that need to be solved in extremely fine grids in order to solve properly all the range of energy scales involved in the flow. There exists two standard classes of turbulence models: the Reynolds Averaged Navier-Stokes (RANS) models and the Large Eddy Simulation (LES) models. RANS models rely on the so-called *Reynolds decomposition*, which consists in decomposing all the variables involved in the flow motion into a mean time value. In a counterpart, LES models relies on the solving of the large energy scales of the flow and modeling the efects of the small energy scales on the large scales. From the computational point of view, RANS models are less expensive than the LES models, but is counter-balanced with less accuracy on the numerical approximation. LES models, however, only model the interaction between the small and the large resolved scales. In the context of RANS models, the principal ones are the $K-\varepsilon$ model proposed by Jones and Launder [62], and its variant, the $K-\omega$ model proposed by Wilcox [112]. On the LES family models, we cite, e.g., the Smagorinsky model [103] and the dynamic subgrid-scale eddy viscosity model proposed by Germano et *al.* in [43].

Later on, the Variational Multi-Scale (VMS) methods appears to improve the accuracy of the numerical approximations computed by LES simulations. An important aspect of VMS models is the fact that the boundary conditions are no longer affected, since they are not preserved in the average process required for the LES models construction. The VMS method was first introduced by Hughes et *al.* in [52] for computational mechanics problems, and it generated a new approach of LES in turbulence modeling in computational fluid dynamics (*cf.* [54, 55, 56]). In classical LES models such as the Smagorinsky model, the eddy viscosity acts on both large and small scales, yielding to an over-diffusive models. With this VMS procedure for the Smagorinsky model, the eddy viscosity acts only on small resolved scales.

Even with the reduction of the computational cost provided by turbulent models with respect to the DNS, it is still expensive to compute accurately the real flows that commonly appear in industry problems. When a high number of computations for a fluid flow depending on parameters is required, Reduce Order Modeling (ROM) becomes useful. Current engineering applications for design, e.g., in which the shape of interest is modeled by free-form deformation and the RB methods are applied for the resulting parametric PDE [65]; optimization and control, where the RB approach provides reduction on the computational time for control problem for parametrized elliptic optimal control [77], or parametrized optimal flow control for the Stokes equations [76]; and uncertainly quantification problems [30], where the RB method is applied to an elliptic PDE with random input, with *a priori* and *a posteriori* error estimates. Application of the POD-

Galerkin strategy to turbulent fluid flows remains a challenging area of research. By construction, ROMs generated using only the first most energetic POD basis functions are not endowed with the dissipative mechanisms associated to the creation of lower size, and less energetic, turbulent scales. Increasing the number of modes creates very large POD-Galerkin ROMs that are still very computationally expensive to solve (*cf.* [5, 6, 101, 110]).

A developing way of research to overcome this difficulty is to adapt the standard turbulent closure techniques based upon eddy dissipation to model the effect of the un-resolved ROM modes on the resolved ones. This is based upon the analysis of [34], that shows that the transfer of energy among the POD modes is similar to the transfer of energy among Fourier modes, in fact, there is a net energy transfer from low index POD modes to higher index POD modes (*cf.* [109]).

In this work we address an alternative strategy, that consists of constructing ROMs of turbulence models, rather than using ROM to construct turbulence models. We assume that the flow under consideration (or, rather, its large scales) is well modeled by the starting turbulence model, at least up to the accuracy required by the targeted application. Our purpose is to construct fast solvers for the turbulence model which is a highly non-linear mathematical system of equations (often with larger and more complex non-linearities than the Navier-Stokes equations) and needs large computational times to be solved.

This work is part of the development of the Spanish Government Project MTM2015-64577-C2-1-R, which final objective is the development of RB models that would be applied to aero-thermal flows in buildings. For this purpose, in this work we develop RB models with increasing difficulty: from the basic RB Smagorinsky model to the RB Boussinesq VMS-Smagorinsky model with geometrical parametrization. The flow inside of a building flow may depends on several parameters, that can be both physical (Reynolds number, Rayleigh number, etc.) or geometrical (the aspect ratio of a room or a courtyard, the location of different windows and doors, etc.). In this work we get a RB model for a Boussinesq model with VMS-Smagorinsky approach for a domain in which a geometrical parametrization is considered. Previous to analyze this model in which is considered the energy equation, we deal with the development of several RB models based on turbulence models of increasing difficulty, that allows us to understand the RB framework for turbulence models.

Thus, we first develop a RB model for the Smagorinsky model, which is the basic LES turbulence model, in which the effect of the subgrid scales on the resolved scales is modeled by eddy diffusion terms (*cf.* [28, 99]). It is an intrinsically discrete model, since the eddy viscosity term depends on the mesh size. The main difficulty in the development of a RB model for the Smagorinsky turbulence model is treatment the non-linearity involved in the eddy viscosity term. To treat

the eddy viscosity term in the RB model developed in this work, we propose to use the Empirical Interpolation Method (EIM) [9, 45], to approximate properly this term and decouple the spatial dependence and the parameter dependence of the non-linear eddy viscosity term.

Once we develop the RB model for the Smagorinsky LES model, we go further considering the development of a RB model for a VMS-Smagorinsky model with a Local Projection Stabilization (LPS) of the pressure. This model relies on the consideration of a VMS procedure on the Smagorinsky eddy viscosity term, and a projection-stabilization term for the pressure. With this method we improve the numerical approximation in two ways. First, with the consideration of a VMS on the eddy viscosity, which for this model only acts on the small resolved scales. The other improvement comes from the consideration of the stabilization term for the pressure, that allows us to consider $\mathbb{P}2-\mathbb{P}2$ finite element pair, instead of the classical stable Taylor-Hood finite element $\mathbb{P}2-\mathbb{P}1$, that increments the accuracy both in velocity and pressure, and we do not enrich the velocity space with the inner pressure *supremizer*, that increases the computational time in the online phase and, therefore, the speedup.

Finally, we incorporate the buoyancy forces in our model, by means of a Boussinesq approximation. Thus leads to the so-called Boussinesq equations (see e.g. [64]), for which we also consider a VMS-Smagorinsky modeling for the eddy viscosity and eddy conductivity. This model offers a more realistic modeling of an aero-thermal flow in a building, since the buoyancy forces becomes relevant on natural convection problems, such as in a heated room. Thus, with the development of a RB model from this Boussinesq model with VMS-Smagorinsky eddy viscosity and eddy diffusivity, we can perform a realistic study of the flow inside a room with simple geometry. The consideration, in addition, of a geometrical parameter completes the study of the RB for aero-thermal flows. We consider a geometrical parameter concerning the aspect ratio (the quotient between the height and the width) of a room vertical profile, represented by a rectangle. The variability of the aspect ratio of the room reverts to flows with very different behaviors, with the same environment conditions. This highlights the importance of considering a geometrical parameter to take into account variability on the domain and not only on the physical variables of the problem.

The snapshot selection in the construction of the reduced-basis spaces of the different RB models presented in this work is done trough a (weak) greedy algorithm. Thus, the development of an *a posteriori* error bound estimator becomes essential for the different RB models presented in this work. This *a posteriori* error bound is based upon the Brezzi-Rappaz-Raviart (BRR) theory (see [18]). We derive *a posteriori* error bound estimators for all models considered in this work: RB Smagorinsky model, RB VMS-Smagorinsky model with LPS pressure stabilization and RB Boussinesq VMS-Smagorinsky model. This derivation extends

the theory existent for the development of an *a posteriori* error bound estimator for the Navier-Stokes equations [36, 38, 72, 106].

The main difference in the RB models presented in this work and the RB models for Navier-Stokes equations available in the literature is the reduction of the turbulent viscosity, highly non-linear. Also, the reduced order approximation of the stabilization coefficients that appear in the LPS stabilization of the pressure. These non-linear terms have to be approximated in a good way in order to obtain parameter-independent tensors that could be used in the online phase efficiently. The way that we propose to linearise the non-linear terms of the different models by means of the Empirical Interpolation Method (EIM) [9, 45]. Thanks to the EIM, we obtain high speedup rates in the computation of the solution on the online phase.

This work is divided in five chapters. The content and the contributions of each chapter are detailed as follows:

- In **Chapter 1** we present the basic techniques involved in the development of Reduced Basis models, that will be used in the following Chapters. In this Chapter, we first start in Section 1.2 defining the RB method for a general parametrized PDE, in which both physical and geometrical parameters can be involved. In the case of geometrical parametrization of the domain, we present the change of variable formulas involved in the transformation of the problem into an equivalent one in a reference domain, which is independent of the geometrical parameter.

  After that, we present the two procedures for the snapshot selection that will be used in the following chapters: the Greedy algorithm and the POD. (Section 1.3 and Section 1.4, respectively.)

  Then, in Section 1.5, we present how to approximate numerically the Brezzi-Rappaz-Raviart stability factor, which is the inf-sup constant of the Gateaux derivative of the problem operator. This constant is a parameter-dependent and is involved in the *a posteriori* error bound estimator. We deal with the Radial Basis Functions (RBF) algorithm in order to obtain an accurate fast approximation of the stability factor.

  Finally, in Section 1.6, we present the Empirical Interpolation Method (EIM), used in the approximation of the different non-linear terms that will appear in the following chapters. We explain how the EIM builds a reduced-basis space from snapshots of a general non-linear function.

- In **Chapter 2**, we present the first RB model developed in this work, for the Smagorinsky LES model [103]. This model is considered as a first step of our goal, since we extend the existent theory in [36, 72] of RB methods for the Navier-Stokes equations to a simple LES model, actually the Smagorinsky

model. This sets the basis for the understanding of the application of RB models to LES models. The outstanding difference between the RB method for Navier-Stokes equations and Smagorinsky model is the eddy viscosity non-linear term, that is approximated with the EIM.

In Section 2.2 we present the RB Smagorinsky model, defining first the discretization of the Smagorinsky model, and then the reduced spaces for the RB problem. In order to guarantee the inf-sup condition on the reduced-basis space, the velocity space is enriched with the inner pressure *supremizer*. In Section 2.3, we present the well possedness of the Smagorinsky FE solution by the Brezzi-Rappaz-Raviart (BRR) theory [18]. For this purpose, we define the Gateaux derivative of the problem operator, and we prove that it is continuous and inf-sup stable, respectively in Proposition 2.1 and Proposition 2.2.

In Section 2.4, we develop the *a posteriori* error bound estimator for the RB Smagorinsky model, needed for the snapshot selection with the Greedy algorithm. Theorem 2.2 gives us the condition for what the *a posteriori* error bound exists, giving us a certified error bound between the FE solution and the RB solution. The obtaining of the *a posteriori* error estimator essentially arises because the Gateaux derivative of the Smagorinsky operator is locally lipschitz in H^1 norm. Moreover, we introduce a weighted norm linked with the eddy viscosity that improves the error estimations.

In Section 2.5 we explain how we use the EIM for the approximation of the non-linear Smagorinsky eddy viscosity. We also present the parameter-independent matrices and tensors that should be stored during the offline phase.

Finally, in Section 2.6, we apply the RB Smagorinsky model in two numerical tests, the Backward-facing step problem and the Lid-driven cavity problem. In both tests, we obtain quite accurate solutions with respect to the "high fidelity" (Finite Element) solution. We also obtain a high speedup computation in the online phase, compared with the computational time for the FE solution computation. This speedup ranges from several hundreds in the Backward-facing step problem, to several thousands in the Lid-driven cavity problem.

- In **Chapter 3** we present a RB model for a VMS-Smagorinsky model with Local Projection Stabilization on the pressure, and eddy viscosity acting only on the small resolved scales. This model is an improvement of the Smagorinsky one presented in Chapter 2, since the eddy viscosity acts only on the resolved small scales instead of acting on all scales as in the Smagorinsky model, thus providing a more accurate LES turbulence model. We also consider a stabilizing term for the pressure that allows us to consider the FE

pair $\mathbb{P}2-\mathbb{P}2$, instead of the classical Taylor-Hood FE pair $\mathbb{P}2-\mathbb{P}1$. Thanks to that, we increase the accuracy on the FE solution for both velocity and pressure, while reducing the dimension of the RB space, as no *supremizer* velocity basis functions are needed to stabilize the pressure discretization.

In Section 3.2 we present the RB VMS-Smagorinsky model, with the Local Projection Stabilization for the pressure, defining first the discretization of the model, and then defining the RB spaces for this problem. The main difference with respect the RB Smagorinsky model, is that due to the stabilization considered in this VMS-Smagorinsky model, the enrichment of the velocity space with inner pressure *supremizer* is no longer necessary. Moreover, as shown in the numerical results in Section 3.6, the consideration of the *supremizer* enrichment on the velocity space leads to a reelection of a parameter value already selected in the Greedy algorithm.

In Section 3.3, we extend the well-possedness analysis done in Section 2.3 for the RB Smagorinsky, to the RB VMS-Smagorinsky model with the Local Projection Stabilization on the pressure. This is possible thanks to the linearity of the projection operator considered for both the VMS and the stabilization procedure. The non-negativity of the stabilization terms considered is essential to preserve the coercivity of the derivative of the operator.

In Section 3.4, we develop the *a posteriori* error bound estimator for the model considered in this Chapter, extending again the analysis done for the RB Smagorinsky model of Chapter 2. Again this is essentially due to the locally lipschitz nature of the Gateaux derivative of the operator involved.

In Section 3.5 we present the approximation of the non-linear terms via the Empirical Interpolation Method. In this case, we need to linearise the VMS-Smagorinsky eddy viscosity and the stabilization coefficients. We also present in this Section the parameter-independent matrices and tensors that are stored during the offline phase.

Finally, in Section 3.6, we present the same tests as for Chapter 2 in order to compare the performances of the RB Smagorinsky model and RB Smagorinsky VMS-Smagorinsky model with LPS stabilization for the pressure. For both tests, we show the speedup rate of the computational time for the RB solution in the online phase with respect to the computational time for the FE solution. For this case, the speedup rates obtained go from several thousands for the Backward-facing step problem to more than ten thousands for the Lid-driven cavity problem. This improves the speedup of the RB Smagorinsky model, possibly due to the smaller dimension of the RB spaces for the RB VMS-Smagorinsky model with LPS stabilization for the pressure.

- In **Chapter 4** when we develop a RB model for the Boussinesq equations, with VMS-Smagorinsky approximation for the eddy diffusion and eddy diffusivity terms. This model is one of the main objectives of this work, since it let us to study the aero-thermal flow inside of a room or a courtyard. Moreover, the consideration of a VMS procedure for both the eddy viscosity and eddy diffusivity leads us to a more accurate numerical approximation of the flow.

  In Section 4.2 we present the Boussinesq model with the VMS-Smagorinsky terms for the eddy viscosity and the eddy diffusivity, first defining the FE problem and then the RB one. In this Chapter, we need again the inner pressure *supremizer* enrichment for the velocity in order to guarantee the inf-sup space stability, as we do not consider LPS stabilization of the pressure, to consider a difficulty at each model studied. The non-linear terms that comes from the eddy viscosity and eddy diffusivity are again linearised with the EIM, letting us to obtain parameter-independent matrices and tensor that we store during the offline phase. Since the eddy diffusivity is proportional to the eddy viscosity, we take the same EIM approximation done in Chapter 3 for the VMS-Smagorinsky eddy viscosity.

  In Section 4.3, we study the well-possedness of the FE problem through the BRR theory, by proving the continuity and inf-sup stability of the Gateaux derivative of the problem operator. Then, in Section 4.4 we develop the *a posteriori* error bound estimator, extending the analysis done for the RB Smagorinsky model and the RB VMS-Smagorinsky model done in Chapter 2 and Chapter 3, respectively. Here, we need to consider a regularized eddy diffusivity for temperature, as the original one considered in the Boussinesq VMS-Smagorinsky model does not provide a locally lipschitz Gateaux derivative of the operator involved.

  Finally, in Section 4.5, we present the numerical results concerning the RB model studied in this Chapter. We present numerical results for a RB Boussinesq VMS-Smagorinsky model in a buoyancy-driven cavity where the flow is driven by a temperature gradient between the two vertical walls. We consider two different situations depending on the Rayleigh number value taken. First we consider the Rayleigh number ranging on $[10^3, 10^5]$, for what the heat transfer is principally in form of diffusion, since the diffusion term is dominant face to the convective term. This situation leads to an almost vertical linear contouring for the temperature, with a recirculating motion on the core of the cavity. Then we increase the Rayleigh number value range, considering that the Rayleigh number ranges on $[10^5, 10^6]$. In this situation, the velocity in the center of the domain is practically zero and present large and normal gradients near the walls. The temperature isolines are horizontal in a large domain inside the cavity, except near the

vertical walls. For both tests, we show the speedup in the computational time of the RB solution in the online phase, with respect to the FE solution computational time. In the first case, for Rayleigh numbers in $[10^3, 10^5]$, this speedup is larger than one thousand; where in the second case, for Rayleigh numbers in $[10^5, 10^6]$, the speedup is close to three hundred.

- In **Chapter 5** we present the RB Boussinesq VMS-Smagorinsky model studied in Chapter 4, applied to a buoyancy-driven cavity with a variable aspect ratio. The variability of the aspect ratio in the domain is addressed by the consideration of a geometrical parameter in the domain. When a geometrical parameter is considered, we need to transform the problem in the original parameter-dependent domain, into a reference parameter-independent domain. Once we have redefined the RB Boussinesq VMS-Smagorinsky model in the reference domain, the geometrical parameter is treated in the same way as the physical parameters, as it appears in the structure of the transformed equations, set in the reference domain.

  In Section 5.2 we present the discretization of the Boussinesq VMS-Smagorinsky model, highlighting the problem transformation from the original parameter-dependent domain to the reference parameter-independent domain. We define the new operators that are obtained due to the changes of variables applied.

  In Section 5.3 we present the RB Boussinesq VMS-Smagorinsky model, with the reduced spaces definition. The velocity space is enriched with the inner pressure *supremizer* in order to guarantee the inf-sup space stability. Again, the approximation of the non-linear terms is done with the EIM, that allows us to define the paramenter-independent matrices and tensors that we store in the offline phase, in order to solve efficiently the RB problem in the online phase. Then, in Section 5.4 we develop the *a posteriori* error bound estimator, by extending the analysis done in Chapter 4. Again, we consider a regularized eddy diffusivity to obtain a lipschitz-continuous derivative of the operator involved.

  Finally, in Section 5.5, we present two numerical tests. For the first one, we fix the Rayleigh number, taking $Ra = 10^5$, and we consider the geometrical parameter for the cavity height ranging on $[0.5, 2]$. The second test that we present includes both parameters involved in the problem. Thus, we consider the Rayleigh number ranging on $[10^3, 10^4]$, and the geometrical parameter ranging on $[0.5, 2]$. For both tests, we obtain an accurate RB solution with a speedup rate that goes from approximately three hundreds in the case of geometrical parametrization only, and fifty for the test in which we consider both parameters.

As the complexity of the problem considered increases, we need to include more basis functions in the reduced spaces, increasing the dimension of the reduced spaces, even more with more than one parameter is considered. This causes that the speedup in the RB online computation decreases. But even in the worst case, with two parameters for the Rayleigh number and the aspect ratio, this speedup is higher than 50, that is a big reduction on the computational time.

Chapter 1

Basics of Reduced order models

1.1 Introduction

In this chapter we show a review of the basics tools for Reduced Basis Method (RBM) that will be used in the following. We first start introducing the RB method for general parametrized Partial Diferencial Equations (PDEs).

The spaces for the RB problem can be constructed by two different ways: the Greedy algorithm and the Proper Orthogonal Decomposition (POD). For the Greedy algorithm the key is the construction of an *a posteriori* error bound estimator, that determines the snapshot to compute in each Greedy iteration; while, for the POD algorithm, we select from a precomputed snapshots set, the most energetic ones. In the *a posteriori* error bound, that will be developed in the following chapters, is necessary to compute a numerical approximation of the Brezzi-Rappaz-Raviart stability factor. In this Chapter, we provide techniques that allows the computation of a lower bound of the stability factor by the Radial Basis Functions (RBF).

Finally, for non-affine and non-linear problems, we also present the Empirical Interpolation Method (EIM). The EIM is used in the RB framework when we lead with non-linear or non-affine terms with respect to the parameter. The EIM computes a Lagrangian interpolant of the non-linear or non-affine terms over a set of points properly selected. With the EIM we are able to store a parameter independent matrices in the offline phase for non-linear and non-affine problems.

The chapter is structured as follows: in section 1.2, we present a parametric PDE, with the formulation in a reference domain in the case of considering geometrical parametrization. In subsection 1.2.1, we present the offline/online decomposition for a general RBM. Then, in section 1.3 we present the Greedy algorithm and in Section 1.4 we present the POD algorithm, both involved in the construction of the reduced space for the RB problem. We explain in Section

1.5 the eigenvalue problem associated to the computation of the stability factor, with the RBF algorithm used for the online computation of its approximation in subsection 1.5.1. Finally in Section 1.6, we introduce the EIM algorithm, used for non-affine and non-linear problems.

1.2 Partial Differential Equations depending on parameters

In this section we work with parametized PDEs, that are partial differentials equation which depend on parameters of different nature. Depending on the nature of the parameter, we distinguish physical and geometrical parameters. Physical parameters are those that arise from the physic of the problem, like the Reynolds number in incompressible fluid flows problems or the conductivity in thermal problems. On the other hand, the geometrical parameters are involved in the shape of the problem domain. From now, we will denote by $\boldsymbol{\mu} = (\mu_1, \dots, \mu_P) \in \mathcal{D} \subset \mathbb{R}^P$ the parameter vector, which can contain both physical and geometrical parameters, being $\mathcal{D}$ the parametric set that will contain the ranges of the different parameters.

If we consider geometrical parameters on our problem formulation, we need to solve the Reduced Basis Model in a reference domain $\Omega_r \subset \mathbb{R}^d$, that must correspond to a selected reference value of the geometrical parameters. Then, the solution corresponding to the problem in the original domain $\Omega_o(\boldsymbol{\mu}) \subset \mathbb{R}^d$ will be obtained by a transformation, that corresponds to a change of variables.

Let us define a general parametrized PDE in variational form. We look for solutions in a suitable Hilbert space defined on the reference domain $X = X(\Omega_r)$:

$$\begin{cases} \text{Given } \boldsymbol{\mu} \in \mathcal{D}, \text{ find } u(\boldsymbol{\mu}) \in X \text{ such that} \\ A(u(\boldsymbol{\mu}), v; \boldsymbol{\mu}) = F(v; \boldsymbol{\mu}) \quad \forall v \in X, \end{cases} \tag{1.1}$$

where $A : X \times X \to \mathbb{R}$ is a continuous and coercive bilinear operator, and $F : X \to \mathbb{R}$ a is continuous linear operator for a selected value of $\boldsymbol{\mu} \in \mathcal{D}$.

Let us introduce the discretization of problem (1.1), by defining a discrete subspace $X_h = X_h(\Omega_r) \subset X$, of dimension $\mathcal{N}_h$, where here the subscript $h > 0$ is related with the mesh size. Through this work, X_h will be a finite element space. Thus, the discrete problem can be stated as

$$\begin{cases} \text{Given } \boldsymbol{\mu} \in \mathcal{D}, \text{ find } u_h(\boldsymbol{\mu}) \in X_h \text{ such that} \\ A(u_h(\boldsymbol{\mu}), v_h; \boldsymbol{\mu}) = F(v_h; \boldsymbol{\mu}) \quad \forall v_h \in X_h. \end{cases} \tag{1.2}$$

Let us suppose that the solution of problem (1.2), computed by a Galerkin projection, is close enough to the solution of problem (1.1). We will refer the solution of problem (1.2) as the "truth" solution.

In (1.2) we are considering that both the bilinear form and the linear form depend on the parameter $\boldsymbol{\mu} \in \mathcal{D}$. There are several mapping techniques for geometrical parametrization in reduced order models. For simple parametrizations, it is possible to consider an affine (or non-affine) transformation maps, that can be defined easily. Other possible techniques are the *free shape representations*. These techniques are commonly used for shape optimization problems and are based on a set of control points [90]. The Free-Form Deformation (FFD) [8, 100] or the Radial Basis Functions (RBF) [21, 111] are two techniques included in this group.

For the sake of simplicity, let us consider an inversible affine transformation map $T : \Omega_r \times \mathcal{D} \to \mathbb{R}^d$, such that $\Omega_o = T(\Omega_r; \boldsymbol{\mu}), \forall \boldsymbol{\mu} \in \mathcal{D}$. The map T can be written as

$$T(x; \boldsymbol{\mu}) = \mathbf{A}(\boldsymbol{\mu})x + \mathbf{b}(\boldsymbol{\mu}),$$

where $A \in \mathbb{R}^{d \times d}$, and $\mathbf{b} \in \mathbb{R}^d$. For this case, is straightforward that the Jacobian matrix is defined by $\mathbf{J}(x; \boldsymbol{\mu}) = \mathbf{A}(\boldsymbol{\mu})$, and both the Jacobian and its determinant will depend on $\boldsymbol{\mu} \in \mathcal{D}$. Consequently, let denote by $\mathbf{J}^{-1}(x; \boldsymbol{\mu})$ the inverse of Jacobian matrix $\mathbf{J}(x; \boldsymbol{\mu})$.

Remark 1.1. *In the case that we do not consider geometrical parameters, and the problem will only depend on physical parameter, the map T considered is the identity.*

Remark 1.2. *Due to the definition of $T(\cdot; \boldsymbol{\mu})$, it holds that $\Omega_r = T^{-1}(\Omega_o, \boldsymbol{\mu})$, where $T(\cdot; \boldsymbol{\mu})$ is the inverse map of $T(\cdot; \boldsymbol{\mu})$.*

Given an integrable function $u_o : \Omega_o(\boldsymbol{\mu}) \to \mathbb{R}^d$, it holds from the change of variable formula that

$$\int_{\Omega_o(\boldsymbol{\mu})} u_o(x_o)\, d\Omega_o = \int_{\Omega_r} u(x) |\mathbf{J}(x; \boldsymbol{\mu})|\, d\Omega_r, \tag{1.3}$$

where here, $u = u_o \circ T$. Furthermore, following to the chain rule, we can obtain that

$$\nabla_o u_o(x_o) = \nabla u(x) (\mathbf{J}(x; \boldsymbol{\mu}))^{-1}, \tag{1.4}$$

where we are denoting by ∇_o and ∇ the gradient with respect the original and reference coordinates respectively.

Let $u_o, v_o \in H^1(\Omega_o)$ and $\mathbf{b}_o : \Omega_o \to \mathbb{R}^d$ a vector field. Taking into account

(1.3) and (1.4), we can obtain

$$\int_{\Omega_o(\boldsymbol{\mu})} \nabla_o u_o \cdot \nabla_o v_o \, d\Omega_o = \int_{\Omega_r} (\nabla u \, \mathbf{J}(x;\boldsymbol{\mu})^{-1}) \cdot (\nabla v \, \mathbf{J}(x;\boldsymbol{\mu})^{-1}) |\mathbf{J}(x;\boldsymbol{\mu})| \, d\Omega_r, \quad (1.5)$$

$$\int_{\Omega_o(\boldsymbol{\mu})} (\mathbf{b}_o \cdot \nabla_o u_o) v_o \, d\Omega_o = \int_{\Omega_r} \mathbf{b} \cdot (\nabla u \, \mathbf{J}(x;\boldsymbol{\mu})^{-1}) v \, |\mathbf{J}(x;\boldsymbol{\mu})| \, d\Omega_r, \quad (1.6)$$

where $u = u_o \circ T$, $v = v_o \circ T$, and $\mathbf{b} = \mathbf{b}_o \circ T$. In a equivalent way, we can obtain analogous formulas for the vectorial case.

Thus, let $\mathbf{u}_o, \mathbf{v}_o, \mathbf{w}_o \in (H^1(\Omega_o))^d$, it holds

$$\int_{\Omega_o(\boldsymbol{\mu})} \nabla_o \mathbf{u}_o \cdot \nabla_o \mathbf{v}_o \, d\Omega_o = \int_{\Omega_r} (\nabla \mathbf{u} \, \mathbf{J}(x;\boldsymbol{\mu})^{-1}) \cdot (\nabla \mathbf{v} \, \mathbf{J}(x;\boldsymbol{\mu})^{-1}) |\mathbf{J}(x;\boldsymbol{\mu})| \, d\Omega_r, \quad (1.7)$$

$$\int_{\Omega_o(\boldsymbol{\mu})} (\mathbf{u}_o \cdot \nabla_o \mathbf{v}_o) \, \mathbf{w}_o \, d\Omega_o = \int_{\Omega_r} \big(\mathbf{u} \cdot (\nabla \mathbf{v} \, \mathbf{J}(x;\boldsymbol{\mu})^{-1})\big) \mathbf{w} |\mathbf{J}(x;\boldsymbol{\mu})| \, d\Omega_r, \quad (1.8)$$

$$\int_{\Omega_o(\boldsymbol{\mu})} u_o (\nabla_o \cdot \mathbf{v}_o) \, d\Omega_o = \int_{\Omega_r} u \left((\nabla \cdot \mathbf{v}) \, \mathbf{J}(x;\boldsymbol{\mu})^{-1}\right) |\mathbf{J}(x;\boldsymbol{\mu})| \, d\Omega_r, \quad (1.9)$$

where $\mathbf{u} = \mathbf{u}_o \circ T$, $\mathbf{v} = \mathbf{v}_o \circ T$, and $\mathbf{w} = \mathbf{w}_o \circ T$.

In some cases, transformation T does not preserve the physical properties of the functions involved in the problem and is no longer valid. For example, in some deformations, the free-divergence property for a solution needed in incompressible fluids problems is not guaranteed with this kind of transformation. To solve this issue for vectorial fields, it can be used the *Piola* transformation. Further information for *Piola* transformation can be founded in [37, 59, 90].

1.2.1 Offline/online decomposition

Reduced Order Methods in general, and the Reduced Basis Method in particular, lie on the computation of solutions for parametric PDE in low-dimensional spaces. These low-dimensional spaces can be constructed using different strategies, like the Greedy algorithm (*cf.* [88, 89]) or the POD algorithm (*cf.* [63, 84]). The construction of the low-dimensional space is done once, in the called offline phase. Then in the online phase, we solve the reduced problem.

Let consider the reduced space $X_N = X_N(\Omega_r) \subset X_h$, of dimension N, with $N << \mathcal{N}_h$. The reduced problem related to the discrete problem (1.2) reads

$$\begin{cases} \text{Given } \boldsymbol{\mu} \in \mathcal{D}, \text{ find } u_N(\boldsymbol{\mu}) \in X_N \text{ such that} \\ A(u_N(\boldsymbol{\mu}), v_N; \boldsymbol{\mu}) = F(v_N; \boldsymbol{\mu}) \quad \forall v_N \in X_N. \end{cases} \quad (1.10)$$

This problem is solved by a Galerkin projection, but in this case, the space selected has a much lower dimension that the space considered in (1.2). Thus, if we consider that $X_N = \text{span}\{\varphi_i,\ i = 1 \ldots, N\}$, the reduced solution $u_N(\boldsymbol{\mu})$ is defined by

$$u_N(\boldsymbol{\mu}) = \sum_{j=1}^{N} \underline{u}_{N_j}(\boldsymbol{\mu})\, \varphi_j, \tag{1.11}$$

where $\underline{u}_N$ is the solution of the linear system $\mathbf{A}_N \underline{u}_N = \mathbf{f}_N$, being $\mathbf{A}_N$ and $\mathbf{f}_N$ the matrix and the right-hand side respectively, associated to problem (1.10).

The computational efficiency is essential in the online phase. This efficiency is exploited building parameter-independent matrices in the offline phase. Usually, the problem and the geometrical parametrization allows us to write problem (1.2) *affinely* with respect to the parameters. This means that we can express both the bilinear operator and the linear one of the right-hand side as

$$A(\mathbf{u}, \mathbf{v}; \boldsymbol{\mu}) = \sum_{q=1}^{Q_a} \Theta_q^a(\boldsymbol{\mu}) A_q(\mathbf{u}, \mathbf{v}), \tag{1.12}$$

$$F(\mathbf{v}; \boldsymbol{\mu}) = \sum_{q=1}^{Q_f} \Theta_q^f(\boldsymbol{\mu}) F_q(\mathbf{v}), \tag{1.13}$$

where in (1.12) and (1.13), $A_q(\cdot, \cdot)$ and $F_q(\cdot)$ respectively, are parameter independent operators. With this formulation, we can rewrite the matrix $\mathbf{A}_N$ and the vector $\mathbf{f}_N$ as

$$\mathbf{A}_N = \sum_{q=1}^{Q_a} \Theta_q^a(\boldsymbol{\mu}) \mathbf{A}_N^q, \quad \mathbf{f}_N = \sum_{q=1}^{Q_f} \Theta_q^f(\boldsymbol{\mu}) \mathbf{f}_N^q. \tag{1.14}$$

Since $\mathbf{A}_N^q, \mathbf{f}_N^q$ do not longer depend on the parameter, we can store them in the offline phase, avoiding the computation of the matrices in the online phase of the reduced basis problem.

In some cases, this linear dependence with respect to the parameter is no longer verified, such as in some non-linear problems or for some geometrical parametrization. Due to that, this offline/online decomposition does not give parameter-independent matrices to compute in the offline phase. For this non-affine or non linear problems, the EIM is used in order to approximate the terms that are non-affine with respect to the parameter, letting us to compute the parameter independent matrices in the offline phase. In section 1.6 we explain this algorithm used for non-linear and non-affine problems.

1.3 Greedy algorithm

In this section we will introduce the greedy algorithm, used in the construction of the reduced space of problem (1.10). This algorithm selects in each iteration the snapshot (FE solution of the PDE for a selected vale of the parameter) that is further from the reduced basis space, i.e., the snapshot associated to the parameter value with the highest error between the FE and RB solutions.

The greedy algorithm was first introduced for optimization problems [39], being used after in the reduced basis field for the construction of the reduced space (*cf.* [12, 20]).

For the startup of the Greedy algorithm, we select randomly an initial parameter value $\boldsymbol{\mu}^1 \in \mathcal{D}_{train}$, where $\mathcal{D}_{train} \subset \mathcal{D}$ is a discrete set with the parameters values taked into account in the Greedy algorithm. Initially, we define the set of parameter values $S_1 = \{\boldsymbol{\mu}^1\}$, and the first reduced space $X_1 = \text{span}\{u_h(\boldsymbol{\mu}^1)\}$.

Then, to add a new snapshot to the reduced space, we take the parameter value that gives the worst reduced basis approximation, with respect to the finite element one, i.e, we choose $\boldsymbol{\mu}_N \in \mathcal{D}_{train}$ such that

$$\boldsymbol{\mu}_N = \arg \max_{\boldsymbol{\mu} \in \mathcal{D}_{train}} \|u_h(\boldsymbol{\mu}) - u_N(\boldsymbol{\mu})\|. \tag{1.15}$$

In practise, the computation of the error $\|u_h(\boldsymbol{\mu}) - u_N(\boldsymbol{\mu})\|$ may be hard to compute numerically, due to the fact that we have to compute the solution of the finite element problem, $u_h(\boldsymbol{\mu})$, for all $\boldsymbol{\mu} \in \mathcal{D}_{train}$. Thus, rather than compute the exact error, we consider an *a posteriori* error bound, $\Delta_N(\boldsymbol{\mu})$, that is cheaper to compute with respect to the computation of the exact error.

The algorithm resulting of the substitution of the real error by the *a posteriori* error bound is usually called Weak Greedy algorithm (*cf.* [12, 90]), and is the one that is commonly used for the Reduced Basis Method.

In each iteration of the (Weak) Greedy algorithm, we actualize the set of parameter values $S_N = \{\boldsymbol{\mu}^1, \dots, \boldsymbol{\mu}^N\}$, and the reduced space $X_N = \text{span}\{u_h(\boldsymbol{\mu}^1), \dots, u_h(\boldsymbol{\mu}^N)\}$, for $N = 1, \dots, N_{\max}$, being $N_{\max}$ the maximum number of basis that we consider in our problem. With this procedure, we construct hierarchical spaces, i.e., $X_1 \subset X_2 \subset \cdots \subset X_N$.

In each step of the the Greedy algorithmm we orthonormalize, with respect to the norm in X_h, the resulting reduced space by the Gram-Schmidt orthonormalization process. This orthonormalization process becomes essential, since it avoids large condition numbers for the reduced problem matrix.

We summarize the Greedy algorithm for a general reduced basis problem:

1. Set $\boldsymbol{\mu}^1$, compute $\mathbf{u}_h(\boldsymbol{\mu}^1)$ solving problem (1.2), and define the reduced space $X_1 = \text{span}\{\mathbf{u}_h(\boldsymbol{\mu}^1)\}$. Orthonormalize the space X_1.
2. For $k \geq 2$, compute $\Delta_{k-1}(\boldsymbol{\mu}), \forall \boldsymbol{\mu} \in \mathcal{D}_{train}$ and set $\boldsymbol{\mu}^k = \arg \max_{\boldsymbol{\mu} \in \mathcal{D}_{train}} \Delta_{k-1}(\boldsymbol{\mu})$.
3. Compute $\mathbf{u}_h(\boldsymbol{\mu}^k)$, define the reduced space X_k by adding the new computed snapshot, and orhtonormalize it.
4. Stop if $\max_{\boldsymbol{\mu} \in \mathcal{D}_{train}} \Delta_k(\boldsymbol{\mu}) < \varepsilon_{RB}$. If not, back to 2.

Remark 1.3. *When a high number of basis functions are selected in the Greedy algorithm, the Gram-Schmidt orthonormalization process may loose the orhtonormality of the reduced space, due to numerical instabilities [44]. As proposed in [74] a two orthogonalization steps for each Greedy iteration can be performed in order to avoid this issue, i.e., we apply twice the Gram-Schmidt orthonormatization procedure on the reduced space.*

Remark 1.4. *Note that the norm in X_h chosen for the Gram-Schmidt orthonormalization process must be independent of $\boldsymbol{\mu}$ for realizable computations. In some applications, the energy norm (see e.g. [91]) or the natural norm (cf. [36]), which depends on the parameter, is used for the a posteriori error bound estimator by prescribing one or several parameter values a priori.*

The development of the *a posteriori* error bound for the different problems heated in this work will be detailed in the following chapters.

1.4 Proper Orthogonal Decomposition

In this section, we introduce the Proper Orthogonal Decomposition (POD). The POD is a reduced-order modelling technique that allows to obtain, as with the Greedy algorithm, a ROM from a parametric PDE.

The main difference between POD and Greedy algorithm for the construction of reduced spaces is that, for the POD, we need to have precomputed a set of N_P snapshots, while in the Greedy algorithm, we compute N_G snapshots, given by the *a posteriori* error estimator in each Greedy step. Usually $N_P >> N_G$, thus the computational effort in the construction of the reduced space is, in most cases, lower in the Greedy algorithm. The POD algorithm is usually used for problems for which the construction of the *a posteriori* error estimator is not feasible.

With the POD algorithm, we obtain a reduced space such that the error in terms of least squares is minimum, i.e., it minimizes the quantity

$$\sqrt{\frac{1}{N_P}\sum_{\boldsymbol{\mu}\in\mathcal{D}}\inf_{u_N\in X_N}\|u_h(\boldsymbol{\mu})-u_N(\boldsymbol{\mu})\|_X^2}, \tag{1.16}$$

over all N-dimensional subspaces X_N of the span $X_{N_P} = \text{span}\{u_h(\boldsymbol{\mu}) \,|\, \boldsymbol{\mu} \in \mathcal{D}_{train}\}$ of elements of the manifold $\mathcal{M} = \{u_h(\boldsymbol{\mu}) \,|\, \boldsymbol{\mu} \in \mathcal{D}_{train}\}$.

For the construction of the POD reduced space, let us consider a parameter-value set $\mathcal{D}_{POD} = \{\boldsymbol{\mu}^1, \ldots, \boldsymbol{\mu}^{N_P}\}$, with the corresponding set of snapshots associated to it, $\mathcal{U} = \{u_h(\boldsymbol{\mu}^1), \ldots, u_h(\boldsymbol{\mu}^{N_P})\}$.

We construct the correlation matrix, defined as

$$\mathbf{C}_{ij} = \frac{1}{N_P}(u_h(\boldsymbol{\mu}^i), u_h(\boldsymbol{\mu}^j))_X, \quad 1 \le i,j \le N_P, \tag{1.17}$$

and solve the eigenvalue problem associated to the correlation matrix:

$$\begin{cases} \text{Find the eigenvalue-eigenvector pair } (\lambda_n, \mathbf{v}_n) \in \mathbb{R}\times\mathbb{R}^{N_P} \text{ such that} \\ \mathbf{C}\,\mathbf{v}_n = \lambda_h \mathbf{v}_n, \quad 1 \le n \le N_P. \end{cases} \tag{1.18}$$

The resolution of this problem provides N_P eigenvalues sorted in descending order, $\lambda_1 \ge \lambda_2 \ge \cdots \ge \lambda_{N_P}$. With the N larger eigenvalues, we define the POD modes that gives us the POD reduced space $X_N = \text{span}\{\xi_1, \ldots, \xi_N\}, N \le N_P$. This POD modes are defined as

$$\xi_n = \sum_{k=1}^{N_P} (\mathbf{v}_n)_k \, u_h(\boldsymbol{\mu}^k), \quad 1 \le n \le N, \tag{1.19}$$

where we are denoting by $(\mathbf{v}_n)_k$ the k-th coefficient of the eigenvector $\mathbf{v}_n \in \mathbb{R}^{N_P}$.

The N largest eigenvalues are the ones that retains the most of the internal energy. We introduce a criteria, $I(N)$ that gives us the percentage of the energy of the N first modes. This quantity is defined as

$$I(N) = \frac{\sum_{k=1}^{N}\lambda_k}{\sum_{k=1}^{N_P}\lambda_k} \ge 1 - \varepsilon_{POD}. \tag{1.20}$$

In (1.20), the tolerance ε_{POD} points out that the energy retained by the last $N_P - N$ modes is equal or smaller than ε_{POD} [84].

Once we have constructed the POD reduced space, we solve the reduced problem (1.10) by a Galerkin projection onto the POD reduced space X_N.

1.5 Stability factor approximation

The *a posteriori* error estimator that will be developed in the following chapters, for different reduced basis models, which will be presented in this work, needs the computation of a coercive or a inf-sup constant, the so-called stability factor, which depends on the parameter value. Since the computation of this stability factor is quite expensive, due to the fact that it is necessary to solve a generalized eigenvalue problem for each parameter value, we are interested in the computation of a lower bound, that gives us a fast approximation of this quantity.

The Successive Constraint Method (SCM) [57, 73], is the classical algorithm to obtain the lower bound of the stability factor. This algorithm was introduced in [58], being a good way to compute the stability factor for the Stokes problem [91, 96] and also the Navier-Stokes problem with the *natural norm* approach [36, 72]. This algorithm usually needs of an offline phase, that in many times could be so much expensive, especially in non-linear problem, for which the SCM needs a high number of iterations to converge, or when the number of parameters is high. This issue led us to consider other strategies in order to obtain a fast and accurate lower bound.

For the stability factor definition, we first need to introduce the directional derivative of operator $A(\cdot,\cdot;\boldsymbol{\mu})$ defined in problem (1.1).

Definition 1.1. *Let the operator $A(\cdot,\cdot;\boldsymbol{\mu}) : X \times X \to \mathbb{R}$. We define the directional derivative of $A(\cdot,\cdot;\boldsymbol{\mu})$ with respect to the first variable, in the direction $\boldsymbol{z} \in X$, for all $\boldsymbol{u}, \boldsymbol{v} \in X$, as*

$$\partial_1 A(u, v; \boldsymbol{\mu})(\boldsymbol{z}) = \lim_{\lambda \to 0} \frac{A(u + \lambda z, v; \boldsymbol{\mu}) - A(u, v; \boldsymbol{\mu})}{\lambda}, \tag{1.21}$$

if this limit exists.

The stability factor of problem (1.2) is defined in the framework of the Brezzi-Rappaz-Raviart theory (*cf.* [18]), for the stability of non-linear problems. Thus, the stability factor, $\beta_h(\boldsymbol{\mu})$, of problem (1.2) is defined as follows:

$$0 < \beta_h(\boldsymbol{\mu}) := \inf_{z_h \in X_h} \sup_{v_h \in X_h} \frac{\partial_1 A(u_h(\boldsymbol{\mu}), v_h; \boldsymbol{\mu})(z_h)}{\|v_h\|_X \|z_h\|_X}, \tag{1.22}$$

where in (1.22), $u_h(\boldsymbol{\mu})$ is a Finite Element solution of problem (1.2).

For the numerical approximation of the stability factor, let us introduce the *supremizer* operator $T^{\boldsymbol{\mu}} : X_h \to X_h$ defined as

$$(T^{\boldsymbol{\mu}} z_h, \mathbf{v}_h)_X = \partial_1 A(u_h(\boldsymbol{\mu}), v_h; \boldsymbol{\mu})(z_h) \quad \forall z_h, v_h \in X_h. \tag{1.23}$$

This operator $T^{\boldsymbol{\mu}}$ is called *supremizer* since by the Riesz theorem it is held

$$T^{\boldsymbol{\mu}} z_h = \arg \sup_{v_h \in X_h} \frac{\partial_1 A(u_h(\boldsymbol{\mu}), v_h; \boldsymbol{\mu})(z_h)}{\|v_h\|_X}. \tag{1.24}$$

Taking into account the definition of this *supremizer* operator and (1.22), we have that

$$\beta_h(\boldsymbol{\mu}) = \inf_{z_h \in X_h} \frac{\|T^{\boldsymbol{\mu}} z_h\|_X}{\|z_h\|_X}. \tag{1.25}$$

We can rewrite (1.25) in an algebraic way. Denoting by $\{\phi_i\}_{i=1}^{\mathcal{N}_h}$ the basis functions of the FE space X_h, we can define the matrices

$$\begin{aligned} &(\mathbf{X})_{ij} = (\phi_j, \phi_i)_X, && i,j = 1, \dots, \mathcal{N}_h, \\ &(\mathbf{F}(\boldsymbol{\mu}))_{ij} = \partial_1 A(u_h(\boldsymbol{\mu}), \phi_j; \mu)(\phi_i), && i,j = 1, \dots, \mathcal{N}_h. \end{aligned} \tag{1.26}$$

The matrix $\mathbf{X}$ in (1.26) represents the matrix norm of X_h, while the matrix $\mathbf{F}(\boldsymbol{\mu})$ is the matrix corresponding to the FE discretization of the directional derivative. Considering the vector of components $\mathbf{t}_i^{\boldsymbol{\mu}} = T^{\boldsymbol{\mu}} z_h(x_i)$, we obtain from (1.23) that $\underline{v_h}\mathbf{X}\mathbf{t}^{\boldsymbol{\mu}} = \underline{v_h}\mathbf{F}(\boldsymbol{\mu})\underline{z_h}$, where we are denoting by $\underline{v_h} \in \mathbb{R}^{\mathcal{N}_h}$ the vector representation of a element v_h of X_h.

Thus, with this notation, we can rewrite (1.25) in a algebraic way as

$$\beta_h(\boldsymbol{\mu}) = \inf_{\underline{z_h} \in \mathbb{R}^{\mathcal{N}_h}} \frac{\underline{z_h}^T \mathbf{F}(\boldsymbol{\mu})^T \mathbf{X}^{-1} \mathbf{F}(\boldsymbol{\mu}) \underline{z_h}}{\underline{z_h}^T \mathbf{X} \underline{z_h}}. \tag{1.27}$$

Then, given a $\boldsymbol{\mu} \in \mathcal{D}$, we consider the following generalized eigenvalue problem in order to compute the stability factor:

$$\begin{cases} \text{Find } (\lambda, v_h) \in \mathbb{R} \times X_h, v_h \neq 0, \text{ such that} \\ \mathbf{F}(\mu)^T \mathbf{X}^{-1} \mathbf{F}(\mu) v_h = \lambda\, \mathbf{X} v_h, \quad \forall \mathbf{v}_h \in X_h. \end{cases} \tag{1.28}$$

From (1.25), we reach that $\beta_h(\boldsymbol{\mu}) = (\lambda_{min})^{1/2}$, with λ_{min} the minimum eigenvalue of (1.28). The numerical computation of this eigenvalue can be affordable with the Power iteration method (see [92], Chapter 5).

Remark 1.5. *The Power iteration method only computes the largest eigenvalue. In practice to obtain the lower eigenvalue, λ_{min}, of a matrix $\boldsymbol{A}$, is enough to compute the largest eigenvalue, λ_{max}, of the inverse matrix $\boldsymbol{A}^{-1}$, and then set $\lambda_{min} = 1/\lambda_{max}$. In our case, to compute the minimum eigenvalue of problem (1.28), we compute the largest eigenvalue of the matrix $\boldsymbol{F}^{-1}(\boldsymbol{\mu})\boldsymbol{X}\boldsymbol{F}^{-T}(\mu)\boldsymbol{X}$.*

Since the computation of the stability factor requires to solve a FE problem

plus an eigenvalue problem, the online computation of the stability factor becomes unaffordable. For this reason in [66], besides the Successive Constraint Method, is proposed to compute an interpolant which is computed offline, and then, given a $\boldsymbol{\mu} \in \mathcal{D}$, compute online the corresponding stability factor online. In the following, we explain how to compute this interpolant with the RBF algorithm.

1.5.1 The Radial Basis Function algorithm

The strategy considered in this work is the approximation of the stability factor by the Radial Basis Function (RBF) algorithm (see e.g. [21, 111] for a general introduction). The RBF technique was first used in Reduced Basis problems for shape parametrization. With the RBF technique it is possible to obtain parametrizations of volumes and surfaces when using polynomial or spline interpolation is not possible to be applied [71].

The RBF algorithm for the approximation of the stability factor can be found in [90] and [73]. Let us consider a discrete set of parameter values $\mathcal{D}_{disc} \subset \mathcal{D} \subset \mathbb{R}^P$. For the startup of the interpolant computation, we consider a set with an initial number, n_I, of parameter values $\mathcal{D}_I = \{\boldsymbol{\mu}^i\}_{i=1}^{n_I} \subset \mathcal{D}_{disc}$.

For each parameter value in $\boldsymbol{\mu} \in \mathcal{D}_I$, we compute the corresponding stability factor $\beta_h(\boldsymbol{\mu}^i)$, for $i = 1, \dots, n_I$, by solving problem (1.28). The radial basis interpolator $\beta_I(\boldsymbol{\mu})$, for all $\boldsymbol{\mu} \in \mathcal{D}$ is defined as

$$\beta_I(\boldsymbol{\mu}) = \omega_0 + \boldsymbol{\omega}^T \boldsymbol{\mu} + \sum_{k=1}^{n_I} \gamma_k \, \phi(\|\boldsymbol{\mu} - \boldsymbol{\mu}^k\|), \tag{1.29}$$

with $\phi : \mathbb{R} \to \mathbb{R}$ the radial function properly selected. Here, the coefficients ω_0, $\boldsymbol{\omega} = (\omega_1, \dots, \omega_p)$ and $\{\gamma_k\}_{k=1}^{n_I}$ are computed imposing the following conditions

$$\begin{gathered} \beta_I(\boldsymbol{\mu}^k) = \beta_h(\boldsymbol{\mu}^k), \quad k = 1, \dots, n_I, \\ \sum_{k=1}^{n_I} \gamma_k = 0, \qquad \sum_{k=1}^{n_I} \gamma_k \mu_p^k = 0, \quad p = 1, \dots, P. \end{gathered} \tag{1.30}$$

These conditions leads to the following symmetric linear system

$$\begin{pmatrix} \mathbf{M} & \mathbf{P}^T & \mathbf{1}^T \\ \mathbf{P} & 0 & 0 \\ \mathbf{1} & 0 & 0 \end{pmatrix} \begin{pmatrix} \boldsymbol{\gamma} \\ \boldsymbol{\omega} \\ \omega_0 \end{pmatrix} = \begin{pmatrix} \boldsymbol{\beta} \\ 0 \\ 0 \end{pmatrix}, \tag{1.31}$$

where $\mathbf{1} = (1, \dots, 1) \in \mathbb{R}^{n_I}, \boldsymbol{\beta} = (\beta_h(\boldsymbol{\mu}^1), \dots, \beta_h(\boldsymbol{\mu}^{n_I})) \in \mathbb{R}^{n_I}$ and

$$(\mathbf{M})_{ij} = \phi(\|\boldsymbol{\mu}^i - \boldsymbol{\mu}^j\|), \quad (\mathbf{P})_{pj} = \mu_p^j, \quad i, j = 1, \dots, n_I, \ p = 1, \dots, P.$$

Remark 1.6. *Several radial basis function $\phi(r)$ in (1.29) can be chosen. In [71] (Chapter 2) there are a list with the common choices for the radial function, such as the Gaussian $\phi(r) = e^{-r^2}$ and the thin plane splines $\phi(r) = r^2 \log(r+1)$.*

Note that the positivity of the interpolated stability factor $\beta_I(\boldsymbol{\mu})$ is not guaranteed for all $\boldsymbol{\mu} \in \mathcal{D}_{disc}$ at this point. For this reason, in [73] is proposed different enrichments of the interpolation set $\mathcal{D}_I$, that will take into account new parameter values for the radial basis interpolation, in order to guarantee the positivity of $\beta_I(\boldsymbol{\mu})$ for all $\boldsymbol{\mu} \in \mathcal{D}_{disc}$.

In [73] there are two proposals of enrichment. One proposal is simple, add the parameters values for which the stability factor is negative, until having assured that the stability factor is positive. The other proposal is the called *Adaptive RBF interpolation*, and for the enrichment of the set $\mathcal{D}_I$ takes into account not only the positivity but also the high local variations on the stability factor, that could have been neglected for a initial coarse selection of the set $\mathcal{D}_I$.

This *Adaptive RBF interpolation* selects new parameter values for $\mathcal{D}_I$, applying a Greedy technique for which is defined a criterion $C(\boldsymbol{\mu})$, derived from [66], which will selects the parameter value that maximizes it. This means that in the k-th step of the *Adaptive RBF interpolation*, we take

$$\boldsymbol{\mu}^k = \arg \max_{\boldsymbol{\mu} \in \mathcal{D}_{disc}} C(\boldsymbol{\mu}). \tag{1.32}$$

The criterion $C(\boldsymbol{\mu})$ is defined as

$$C(\boldsymbol{\mu}) = (\|\nabla \beta_I(\boldsymbol{\mu})\| + \epsilon)(|\Delta \beta_I(\boldsymbol{\mu})| + \epsilon) \left(\frac{h(\mu)}{\max h(\mu)} \right)^2 g_{neg}(\beta_I(\boldsymbol{\mu})), \tag{1.33}$$

where

$$h(\boldsymbol{\mu}) = \min_{\boldsymbol{\mu}^j \in \mathcal{D}_I} \|\boldsymbol{\mu} - \boldsymbol{\mu}^j\|_2, \quad g_{neg}(x) = \begin{cases} 1 & x > 0 \\ \alpha e^{-x} & x \leq 0 \end{cases},$$

with $\alpha > 0$ a prescribed parameter.

The two first factors in criterion $C(\boldsymbol{\mu})$ defined in (1.33) measure the local variations through the gradient and the laplacian operator of the interpolated stability factor. The parameter $\epsilon > 0$ ensures that $C(\boldsymbol{\mu}) > 0$ in the case of $\|\nabla \beta_I(\boldsymbol{\mu})\| = 0$ or $|\Delta \beta_I(\boldsymbol{\mu})| = 0$. Note that both the gradient and the laplacian can be computed analytically, and it is not necessary to compute a numerical approximation of them for the computation of the criterion $C(\boldsymbol{\mu})$.

The third factor depending on function $h(\boldsymbol{\mu})$, penalizes the parameters values which are close to the ones already selected, giving more weight to the parameter values further from the already selected. The last factor pretend to prioritize the selection of the parameter values for which the stability factor interpolant is

negative. With the constant $\alpha > 0$, we can increase the weight of this factor, making it crucial for the selection of the parameter value.

We stop the *Adaptive RBF* algorithm when the addition of a new parameter value does not essentially change the radial basis interpolant of the stability factor. That is when for a prescribed tolerance, the norm of the difference of two consecutive iterates is under this tolerance.

Related to the computational complexity of this algorithm, note that the evaluation of $C(\boldsymbol{\mu})$ is independent of $\mathcal{N}_h$, and it only depend on the number of elements of $\mathcal{D}_I$ and $\mathcal{D}_{disc}$. On the other hand, the online computation of $\beta_I(\boldsymbol{\mu})$ only needs to solve a linear system with a symmetric matrix of dimension $n_I + P + 1$. This allows us to compute a fast approximation of the stability factor.

1.6 Empirical Interpolation Method

In this section we introduce the Empirical Interpolation Method (EIM), which was first presented in [9], and then extended in [45]. This algorithm allows the treatment of non-linear and non-affine terms (with respect to the parameter) in the reduced basis method. This method relies in the computation of a Lagrangian interpolant function over a set of points, called *magic points* (*cf.* [68]), properly selected.

When we arise with non-affine and non-linear problems, being able to approximate those terms is crucial. With the EIM we are able to tensorize non-affine and non-linear terms, decoupling the parameter dependency with respect to the spatial variables.

For the suitability of the EIM, we define a family of parameter-dependent functions $\mathcal{W} = \{g(\cdot;\boldsymbol{\mu}), \boldsymbol{\mu} \in \mathcal{D}\} \subset L^\infty(\Omega)$. With the EIM, we construct the reduced-space $W_M = \text{span}\{q_1(x), \dots, q_M(x)\} \subset \mathcal{W}$, by selecting properly snapshots of functions of the space $\mathcal{W}$. The selection of those snapshots is given by a greedy procedure, in the same way as the algorithm explained in section 1.3. The EIM also provides a set of interpolation points $T_M = \{x_1, \dots, x_M\}$ and a set of parameter values $S_M = \{\boldsymbol{\mu}^1_{EIM}, \dots, \boldsymbol{\mu}^M_{EIM}\}$, defined during the EIM procedure.

Thank to the EIM, we can approximate any function $g \in \mathcal{W}$ as a linear combination of elements of the EIM-reduced space W_M, i.e.,

$$g(x;\boldsymbol{\mu}) \approx \mathcal{I}_M[g] = \sum_{k=1}^{M} \sigma_k(\boldsymbol{\mu}) q_k(x), \tag{1.34}$$

where we are denoting by $\mathcal{I}_M[g]$ the empirical interpolant of the function $g \in \mathcal{W}$, with respect to the space W_M.

Let M_{max} the maximum number of basis we consider for the EIM. We describe the EIM algorithm below:

1. First, we randomly select a parameter value $\boldsymbol{\mu}_1 \in \mathcal{D}_{EIM}$, where here $\mathcal{D}_{EIM}$ is the discrete set where we select the possible values of $\boldsymbol{\mu}$ in the EIM. We set

$$x_1 = \arg\sup_{x\in\Omega} |g_1(x)|, \quad q_1(x) = \frac{g_1(x)}{g_1(x_1)}, \quad \mathbf{B}^1_{11} = 1, \tag{1.35}$$

   and define $S_1 = \{\boldsymbol{\mu}_1\}, T_1 = \{x_1\}$ and $W_1 = \text{span}\{q_1\}$.

2. Then, for $2 \leq M \leq M_{max}$, solve for each $\boldsymbol{\mu} \in \mathcal{D}_{EIM}$ the linear system

$$\sum_{j=1}^{M-1} \mathbf{B}^{M-1}_{ij} \sigma_j(\boldsymbol{\mu}) = g(x_i; \mathbf{w}_h(\boldsymbol{\mu})), \quad 1 \leq i \leq M-1. \tag{1.36}$$

   We define the empirical interpolation of $g(\boldsymbol{\mu})$ on W_{M-1} as

$$\mathcal{I}_{M-1}[g(\boldsymbol{\mu})] = \sum_{j=1}^{M-1} \sigma_j(\boldsymbol{\mu}) q_j(x).$$

3. Select the next parameter value as

$$\boldsymbol{\mu}_M = \arg\max_{\boldsymbol{\mu}\in\mathcal{D}_{EIM}} \|g(\boldsymbol{\mu}) - \mathcal{I}_{M-1}[g(\boldsymbol{\mu})]\|_\infty, \tag{1.37}$$

4. Finally, we define $r_M(x) = g(x; \boldsymbol{\mu}_M) - \sum_{j=1}^{M-1} \sigma_j^{M-1}(\boldsymbol{\mu}_M) q_j(x)$. Finally, we set

$$x_M = \arg\sup_{x\in\Omega} |r_M(x)|, \quad q_M(x) = \frac{r_M(x)}{r_M(x_M)}, \quad \mathbf{B}^M_{ij} = q_j(x_i),\ 1 \leq i,j \leq M,$$

   and set $S_M = \{\boldsymbol{\mu}_1, \ldots, \boldsymbol{\mu}_M\}, T_M = \{x_1, \ldots, x_M\}$ and $W_M = \text{span}\{q_1, \ldots, q_M\}$.

5. Stop if $\max_{\boldsymbol{\mu}\in\mathcal{D}_{EIM}} \|g(\boldsymbol{\mu}) - \mathcal{I}_M[g(\boldsymbol{\mu})]\|_\infty \leq \varepsilon_{EIM}$.

The EIM algorithm is supported for the following result (see e.g. [9] or [90] for the proof).

Lemma 1.1. *The construction of the interpolation points is well-defined, and the functions $\{q_1, \ldots, q_M\}$ form a basis of W_M, which has dimension M. Moreover, the matrix $\boldsymbol{B}_M$ is lower triangular with $(\boldsymbol{B}_M)_{ii} = 1$, for $i = 1, \ldots, M$.*

In [9] there is also the numerical analysis of the error for the EIM, with an *a posteriori* error estimator for regular non-linear functions. The *a posteriori* error bound estimator for the EIM defined in [9] is given by

$$\Delta_M^{EIM} = |g(x_{M+1}; \boldsymbol{\mu}) - \mathcal{I}_M[g(x_{M+1}; \boldsymbol{\mu})]|, \tag{1.38}$$

with x_{M+1} the magical point in the $(M+1)$-th iteration of the Greedy algorithm in the EIM. The deduction of this *a posteriori* error bound estimator can be found in [9] (Section 3.2). In practice, this *a posteriori* error bound is useful only when the non-linear function only depends on the parameter and the domain. For high non-linear problems, where we have to approximate via EIM a function that depends on the solution, this *a posteriori* error bound is no longer valid.

Alternatively to the EIM, the Discrete Empirical Interpolation Method (DEIM) (*cf.* [29]) is also used for the approximation of non-linear and non-affine terms. The philosophy of DEIM is the same that the EIM, but in the DEIM the construction of the space $W_M \in \mathcal{W}$ is done with a POD sample instead a Greedy algorithm like in the EIM.

Chapter 2

A Smagorinsky Reduced Basis turbulence model

2.1 Introduction

In this chapter we present a reduced basis Smagorinsky turbulence model for steady flows, that is a Large Eddy Simulation (LES) model. We first start defining the FE problem, and then, by selecting snapshots properly with the greedy algorithm, we obtain the low-dimensional spaces for which we define the Smagorinsky RB model. The eddy viscosity is modeled by a non-linear term, that depends on the mesh size and the modulus of the velocity gradient. We approximate this non-linear term using the Empirical Interpolation Method (section 1.6), in order to obtain a linearised decomposition of the reduced basis Smagorinsky model.

We address the construction of a Reduced Basis (RB) Smagorinsky turbulence model (*cf.* [103]), which is the basic Large Eddy Simulation (LES) turbulence model, in which the effect of the subgrid scales on the resolved scales is modeled by eddy diffusion terms (*cf.* [28, 99]). It is an intrinsically discrete model, since the eddy viscosity term depends on the mesh size. Although it is well known that the Smagorinsky model is over-diffusive, the construction of this RB Smagorinsky turbulence model represents a first step complex enough, essential for the RB models presented in the following Chapters.

The RB Smagorinsky model is based upon an *a posteriori* error estimation, essential in the snapshots selection in the greedy algorithm. The theoretical development of the *a posteriori* error estimation is based on [36] and [72], according to the Brezzi-Rappaz-Raviart stability theory, and adapted for the non-linear eddy diffusion term, extending the work done for the Navier-Stokes equations to the Smagorinsky turbulence model.

Thanks to the EIM, the RB Smagorinsky turbulence model can be decoupled

in a online/offline procedure. First, in the offline stage, we construct hierarchical bases in each iteration of the Greedy algorithm, by selecting the snapshots which have the maximum *a posteriori* error estimation value. To assure the Brezzi inf-sup condition on our Reduced Basis space, we have to define a *supremizer* operator on the pressure solution, and enrich the reduced velocity space. Then, in the Online stage, we are able to compute a speedup solution of our problem, with a good accuracy.

We have performed several tests of the reduced model to solve 2D step and cavity flows, with Reynolds number ranging in intervals in which a steady solution is known to exist. We obtain speed-up rates of several thousands, with normalized errors with respect to the finite element solution below 10^{-4}.

This chapter is structured as follows: in section 2.2 we present the Finite Element Smagorinsky turbulence model (subsection 2.2.1) and the Reduced Basis Smagorinsky turbulence model (subsection 2.2.2). After that, in section 2.3, we present the numerical analysis that we need in order to assure the well-possedness, based on the BRR theory, of the discrete problem presented in subsection 2.2.1. The construction and analysis of the *a posteriori* error bound estimator is presented in section 2.4. Then, in section 2.5, we explain more in detail how we treat the non-linear eddy viscosity corresponding with the Smagorinsky term. Finally, we present some numerical results in section 2.6, where we show the reduction of the computational time in two different tests.

2.2 Smagorinsky turbulence model

In this section we present the Smagorinsky turbulence model, that is the basic LES turbulence model, in which the effect of the subgrid scales on the resolved scales is modeled by eddy diffusion terms (see [28, 99, 103]). We first present the Finite Element problem, and then we derive to the Reduced Basis one, by constructing low-dimensional spaces from snapshots given by the FE problem throughout the Greedy algorithm (see sec. 1.3).

2.2.1 Finite Element problem

To formulate the Smagorinsky turbulence model, let be Ω a bounded polyhedral domain in $\mathbb{R}^d, (d = 2, 3)$. We assume that its boundary is split into $\Gamma = \Gamma_D \cup \Gamma_N$, where $\Gamma_D = \Gamma_{D_g} \cup \Gamma_{D_0}$ is the boundary relative to the homogeneous and non-homogeneous Dirichlet boundary conditions, and Γ_N to the Neumann conditions.

Let $\{\mathcal{T}_h\}_{h>0}$ a family of affine-equivalent and conforming triangulations of $\overline{\Omega}$, formed by triangles or quadrilaterals ($d = 2$), tetrahedra or hexaedra ($d = 3$). As

usual the parameter h is the maximum diameter h_K among the elements $K \in \mathcal{T}_h$. Given an integer $l \geq 0$, and an element $K \in \mathcal{T}_h$, we denote by $\mathbb{R}_l(K)$ either $\mathbb{P}_l(K)$, the space of Lagrange polynomials of degree $\leq l$, defined on K, if the grids are formed by triangles ($d = 2$) or tetrahedra ($d = 3$); or $\mathbb{Q}_l$, the space of Lagrange polynomials of degree $\leq l$ on each variable, defined on K, if the family of triangulations is formed by quadrilaterals ($d = 2$) or hexaedra ($d = 3$).

Although the Smagorinsky model is intrinsically discrete, it can be interpreted as a discretization of a continuous model. We next present this model to clarify its relationship with the Navier-Stokes one. In this way, the "continuous" Smagorinsky turbulence model is formulated as

$$\begin{cases} \mathbf{w} \cdot \nabla \mathbf{w} + \nabla p - \nabla \cdot \left(\left(\dfrac{1}{\mathrm{Re}} + \nu_T(\mathbf{w}) \right) \nabla \mathbf{w} \right) = \mathbf{f} & \text{in } \Omega \\ \nabla \cdot \mathbf{w} = 0 & \text{in } \Omega \\ \mathbf{w} = \mathbf{g}_D & \text{on } \Gamma_{D_g} \\ \mathbf{w} = 0 & \text{on } \Gamma_{D_0} \\ -p\mathbf{n} + \left(\dfrac{1}{\mathrm{Re}} + \nu_T(\mathbf{w}) \right) \dfrac{\partial \mathbf{w}}{\partial \mathbf{n}} = 0 & \text{on } \Gamma_N \end{cases} \tag{2.1}$$

where here Re is the Reynolds number, $\mathbf{w}$ is the velocity field and p is the pressure; both depending on the Reynolds number.

Also, the eddy diffusion term is given by

$$\nu_T(\mathbf{w}) = C_S^2 \sum_{K \in \mathcal{T}_h} h_K^2 \left| \nabla \mathbf{w}_{|_K} \right| \chi_K, \tag{2.2}$$

where $\left|\cdot\right|$ denotes the Frobenius norm in $\mathbb{R}^{d \times d}$, and C_S is the Smagorinsky constant [98].

Remark 2.1. *For this problem, the Reynolds number is the only parameter considered thus, since $\mathcal{D} \subset \mathbb{R}$, let us denote the parameter as $\mu \in \mathcal{D}$ instead of $\boldsymbol{\mu}$.*

Let us consider the spaces $Y = \{\mathbf{v} \in H^1(\Omega) : \mathbf{v}|_{\Gamma_D} = 0\}$ for velocity and $M = L^2(\Omega)$ for pressure. We assume that there exists a lift function $\mathbf{u}_D \in (H^1(\Omega))^d$, such that $\mathbf{u}_D|_{\Gamma_{D_g}} = \mathbf{g}_D$, $\mathbf{u}_D|_{\Gamma_{D_0}} = 0$, and $\nabla \cdot \mathbf{u}_D = 0$ in Ω. With those conditions, we assure that the reduced velocity $\mathbf{u} = \mathbf{w} - \mathbf{u}_D$ is still incompressible and satisfies the homogeneous Dirichlet boundary conditions on Γ_D. We will assume that $\mathbf{f} \in (L^2(\Omega))^d$, and $\mathbf{g} \in (H^{1/2}(\Omega))^d$.

Let $Y_h \subset Y$ and $M_h \subset M$ two finite subspaces of Y and M. We consider the following variational discretization of problem (2.1), actually, the "true" Smagorinsky model:

$$\begin{cases} \text{Find } (\mathbf{u}_h, p_h) = (\mathbf{u}_h(\mu), p_h(\mu)) \in Y_h \times M_h \text{ such that} \\ a(\mathbf{u}_h, \mathbf{v}_h; \mu) + b(\mathbf{v}_h, p_h; \mu) + a_S(\mathbf{w}_h; \mathbf{w}_h, \mathbf{v}_h; \mu) \\ +c(\mathbf{u}_h, \mathbf{u}_h, \mathbf{v}_h; \mu) + c(\mathbf{u}_D, \mathbf{u}_h, \mathbf{v}_h; \mu) \\ +c(\mathbf{u}_h, \mathbf{u}_D, \mathbf{v}_h; \mu) = F(\mathbf{v}_h; \mu) \qquad \forall \mathbf{v}_h \in Y_h \\ b(\mathbf{u}_h, q_h; \mu) = 0 \qquad \forall q_h \in M_h \end{cases} \tag{2.3}$$

where $\mathbf{w}_h = \mathbf{u}_h + \mathbf{u}_D$; the bilinear forms $a(\cdot, \cdot; \mu)$ and $b(\cdot, \cdot; \mu)$ are defined by

$$a(\mathbf{u}, \mathbf{v}; \mu) = \frac{1}{\mu} \int_\Omega \nabla \mathbf{u} : \nabla \mathbf{v} \, d\Omega, \qquad b(\mathbf{v}, q; \mu) = -\int_\Omega (\nabla \cdot \mathbf{v}) q \, d\Omega; \tag{2.4}$$

the trilinear form, $c(\cdot, \cdot, \cdot; \mu)$, and the non-linear Smagorinsky term, $a_S(\cdot; \cdot, \cdot; \mu)$, are given by

$$c(\mathbf{z}, \mathbf{u}, \mathbf{v}; \mu) = \int_\Omega (\mathbf{z} \cdot \nabla \mathbf{u}) \mathbf{v} \, d\Omega, \qquad a_S(\mathbf{z}; \mathbf{u}, \mathbf{v}; \mu) = \int_\Omega \nu_T(\mathbf{z}) \nabla \mathbf{u} : \nabla \mathbf{v} \, d\Omega. \tag{2.5}$$

Finally, the linear form $F(\cdot; \mu)$ is defined by

$$F(\mathbf{v}; \mu) = \langle \mathbf{f}, \mathbf{v} \rangle - a(\mathbf{u}_D, \mathbf{v}; \mu) - c(\mathbf{u}_D, \mathbf{u}_D, \mathbf{v}; \mu),$$

where $\langle \cdot, \cdot \rangle$ stands for the duality pairing between Y' and Y, Y' being the dual space of Y.

The solution of problem (2.3) is intended to approximate the large-scales component of the solution of the Navier-Stokes problem (i.e., problem (2.1) with $\nu_T = 0$).

Let us define the norms relative to the spaces Y and M. For the velocity space Y, we consider a weighted inner product, $(\cdot, \cdot)_T$, defined as

$$(\mathbf{u}, \mathbf{v})_T = \int_\Omega \left[\frac{1}{\overline{\mu}} + \nu_T^* \right] \nabla \mathbf{u} : \nabla \mathbf{v} \, d\Omega \qquad \forall \mathbf{u}, \mathbf{v} \in Y, \tag{2.6}$$

where $\nu_T^* = \nu_T(\mathbf{w}(\overline{\mu}))$ and $\overline{\mu} = \arg\min_{\mu \in \mathcal{D}} \sum_{K \in \mathcal{T}_h} (C_S h_K)^2 \min_{x \in K} |\nabla \mathbf{w}(\mu)|(x) \chi_K(x)$, and $\mathbf{w}(\mu)$ is the velocity solution of (2.1). This inner product induces a norm linked to the eddy diffusion term, $\| \cdot \|_T = (\cdot, \cdot)_T^{1/2}$. As the functions of Y vanish on Γ_D, then, this norm is equivalent to the usual H^1 norm. This norm will turn out to be crucial to apply our error estimator in the RB construction by the Greedy algorithm. For the pressure space M, we will use the usual L^2-norm.

For the sake of simplicity of notation, let us denote by X the product space

$X = Y \times M$ and, by extension, $X_h = Y_h \times M_h \subset X$. We also define the X-norm as

$$\|U\|_X = \sqrt{\|\mathbf{u}\|_T^2 + \|p_u\|_{0,2,\Omega}^2} \qquad \forall U = (\mathbf{u}, p_u) \in X. \tag{2.7}$$

With this notation, we can rewrite the variational problem (2.3) as:

$$\begin{cases} \text{Find } U_h(\mu) \in X_h \text{ such that} \\ A(U_h(\mu), V_h; \mu) = F(V_h; \mu) \qquad \forall V_h \in X_h. \end{cases} \tag{2.8}$$

In this formulation, the operator A is given by,

$$A(U_h, V_h; \mu) = \frac{1}{\mu} A_0(U_h, V_h) + A_1(U_h, V_h) + A_2(U_h; V_h) + A_3(U_h; V_h), \tag{2.9}$$

where we denote $V_h = (\mathbf{v}_h, p_h^v)$, and

$$\begin{aligned} A_0(U, V) &= \int_\Omega \nabla \mathbf{u} : \nabla \mathbf{v} \, d\Omega, \\ A_1(U, V) &= \int_\Omega (\nabla \cdot \mathbf{u}) p^v \, d\Omega - \int_\Omega (\nabla \cdot \mathbf{v}) p^u \, d\Omega \\ &\quad + \int_\Omega (\mathbf{u}_D \cdot \nabla \mathbf{u}) \mathbf{v} \, d\Omega + \int_\Omega (\mathbf{u} \cdot \nabla \mathbf{u}_D) \mathbf{v} \, d\Omega, \\ A_2(U; V) &= \int_\Omega (\mathbf{u} \cdot \nabla \mathbf{u}) \mathbf{v} \, d\Omega, \\ A_3(U; V) &= \int_\Omega \nu_T(\mathbf{u} + \mathbf{u}_D) \, \nabla(\mathbf{u} + \mathbf{u}_D) : \nabla \mathbf{v} \, d\Omega. \end{aligned}$$

2.2.2 Reduced Basis Problem

In this section, we present the reduced basis method for the Smagorinsky turbulence model. This is a direct adaptation of the RB method for Navies-Stokes equations (*cf.* [36, 72]). We assume that the Reynolds number ranges on a compact interval $\mathcal{D} \subset \mathbb{R}$.

The idea to solve the Smagorinsky model by the reduced basis method is the same to solve it by the finite element method. We solve the Smagorinsky model by a Galerkin projection, but the main difference between finite element and reduced basis methods falls on the dimension of the spaces where we do the Galerkin projection. The reduced basis space is low-dimensional meanwhile the finite element one may be a high-dimensional space.

The construction of these low-dimensional spaces can be affordable with different techniques as the Greedy algorithm (see sec. 1.3) or the POD algorithm (see sec. 1.4). In this work, we focus on the construction of the reduced spaces

by the Greedy algorithm. The RB variational problem is defined as

$$\begin{cases} \text{Given } \mu \in \mathcal{D}, \text{ find } U_N(\mu) \in X_N \text{ such that} \\ A(U_N(\mu), V_N; \mu) = F(V_N; \mu) \qquad \forall V_N \in X_N, \end{cases} \tag{2.10}$$

where here, $X_N = Y_N \times M_N \subset X_h$ is the reduced basis space, being Y_N the reduced velocity space and M_N the reduced pressure space. Considering the Greedy algorithm, this space is the span of certain snapshots properly selected.

In order to guarantee the inf-sup stability of the RB approximation, let us consider the so-called inner pressure *supremizer* operator $T_p^\mu : M_h \to Y_h$, as

$$\left(T_p^\mu q_h, \mathbf{v}_h\right)_T = b(q_h, \mathbf{v}_h; \mu) \quad \forall \mathbf{v}_h \in Y_h. \tag{2.11}$$

Thus, the reduced space, $X_N = Y_N \times M_N$, is defined as

$$M_N = \text{span}\{\xi_k^p := p_h(\mu^k), \quad k = 1, \dots, N\}, \tag{2.12}$$

$$Y_N = \text{span}\{\zeta_{2k-1}^{\mathbf{v}} := \mathbf{u}_h(\mu^k),\ \zeta_{2k}^{\mathbf{v}} := T_p^\mu \xi_k^p, \quad k = 1, \dots, N\}. \tag{2.13}$$

2.3 Well-posedness analysis

The well-posedness of the Smagorinsky problem is provided in [28] by the classical Brezzi theory (*cf.* [16]). The boundedness of the FE solution is provided by this analysis. However, in this section, we analyse the well-posedness of the Smagorinsky FE solution using the more general Brezzi-Rappaz-Raviart (BRR) theory (see e.g. [18]). The finality of using the BRR theory instead the Brezzi theory is the construction of the error estimator provided by the BRR for the reduced basis problem.

Taking the directional derivative (definition 1.1), we derive each operator term in (2.9), obtaining

$$\begin{aligned}
\partial_1 A_0(U, V)(Z) &= A_0(Z, V), \\
\partial_1 A_1(U, V)(Z) &= A_1(Z, V), \\
\partial_1 A_2(U; V)(Z) &= \int_\Omega (\mathbf{u} \cdot \nabla \mathbf{z})\mathbf{v}\, d\Omega + \int_\Omega (\mathbf{z} \cdot \nabla \mathbf{u})\mathbf{v}\, d\Omega, \\
\partial_1 A_3(U; V)(Z) &= \int_\Omega \nu_T(\mathbf{u} + \mathbf{u}_D)\, \nabla \mathbf{z} : \nabla \mathbf{v}\, d\Omega \\
&\quad + \sum_{K \in \mathcal{T}} \int_K (C_S h_K)^2 \frac{\nabla(\mathbf{u} + \mathbf{u}_D) : \nabla \mathbf{z}}{|\nabla(\mathbf{u} + \mathbf{u}_D)|} \big(\nabla(\mathbf{u} + \mathbf{u}_D) : \nabla \mathbf{v}\big)\, d\Omega,
\end{aligned}$$

The following local inverse inequalities for polynomial functions will be used in the sequel. Its proof consist in the application of norm equivalence on finite dimensional spaces (*cf.*[11]).

Lemma 2.1. *Let q_1, q_2 be two real numbers such that $1 \leq q_1, q_2 \leq +\infty$. Let k_1, k_2 be two non-negative integer numbers. Assume that $k_2 \leq k_1$ and $k_2 - d/q_2 \leq k_1 - d/q_1$. In addition, suppose that the family of triangulations $\{\mathcal{T}_h\}_{h>0}$ is regular. Then, for each non-negative integer l there exists a constant $C > 0$ such that:*

$$\forall K \in \mathcal{T}_h, \quad \forall p \in \mathbb{R}_l(K), \quad |p|_{k_1,q_1,K} \leq C h_K^{k_2-k_1-\frac{d}{q_2}+\frac{d}{q_1}} |p|_{k_2,q_2,K}, \tag{2.14}$$

for all $\mathcal{T}_h$, where the constant C only depends on q_1, q_2, k_1, k_2, d, l, and the aspect ratio of the triangulations.

For the well posedness of the problem, we have to guarantee the uniform coerciveness and the boundedness of $\partial_1 A$ in the sense that for any solution $U_h(\mu)$ of (2.8), there exist $\beta_0 > 0$ and $\gamma_0 \in \mathbb{R}$ such that $\forall \mu \in \mathcal{D}$,

$$\begin{aligned} 0 < \beta_0 < \beta_h(\mu) &\equiv \inf_{Z_h \in X_h} \sup_{V_h \in X_h} \frac{\partial_1 A(U_h(\mu), V_h; \mu)(Z_h)}{\|Z_h\|_X \|V_h\|_X}, \\ \infty > \gamma_0 > \gamma_h(\mu) &\equiv \sup_{Z_h \in X_h} \sup_{V_h \in X_h} \frac{\partial_1 A(U_h(\mu), V_h; \mu)(Z_h)}{\|Z_h\|_X \|V_h\|_X}. \end{aligned} \tag{2.15}$$

Then, according to the BRR theory (*cf.* [18, 22]), it will follow that in a neighbourhood of $U_h(\mu)$ the solution of (2.8) is unique and bounded in $\|\cdot\|_X$ in terms of the data. We will prove this in Section 2.4, and as consequence we shall construct the *a posteriori* error bound estimator.

Since $H^1(\Omega)$ is embedded in $L^4(\Omega)$, let us denote by C_T the Sobolev embedding constant such that $\|\mathbf{v}\|_{0,4,\Omega} \leq C_T \|\mathbf{v}\|_T$, for all $\mathbf{v} \in Y$. Also, let us denote by $C_{\overline{\mu}}$ the constant such that $\|\mathbf{v}\|_T \leq C_{\overline{\mu}} \|\nabla \mathbf{v}\|_{0,2,\Omega}$, for all $\mathbf{v} \in Y$. These constant will be used in the following propositions. It holds:

Proposition 2.1. *There exists $\gamma_0 \in \mathbb{R}$ such that $\forall \mu \in \mathcal{D}$*

$$|\partial_1 A(U_h(\mu), V_h; \mu)(Z_h)| \leq \gamma_0 \|Z_h\|_X \|V_h\|_X \quad \forall Z_h, V_h \in X_h.$$

Proof. It holds,

$$\begin{aligned} |\partial_1 A(U_h(\mu), V_h; \mu)(Z_h)| \leq & \frac{1}{\mu} |\partial_1 A_0(U_h(\mu), V_h)(Z_h)| + |\partial_1 A_1(U_h(\mu), V_h)(Z_h)| \\ & + |\partial_1 A_2(U_h(\mu), V_h)(Z_h)| + |\partial_1 A_3(U_h(\mu); V_h)(Z_h)|. \end{aligned}$$

We bound each term separately. Denoting by $V_h = (\mathbf{v}_h, p_h^v) = (v_1, v_2, p_h^v)$ and

$Z_h = (\mathbf{z}_h, p_h^z) = (z_1, z_2, p_h^z)$, we have

$$\begin{aligned}|\partial_1 A_0(U_h(\mu), V_h)(Z_h)| &\leq \int_\Omega |\nabla \mathbf{z}_h||\nabla \mathbf{v}_h| \, d\Omega \leq \|\nabla \mathbf{z}_h\|_{0,2,\Omega}\|\nabla \mathbf{v}_h\|_{0,2,\Omega} \\ &\leq C^2\|\mathbf{z}_h\|_T\|\mathbf{v}_h\|_T \leq C_0\|Z_h\|_X\|V_h\|_X.\end{aligned}$$

In the following two terms, we will use the Sobolev embedding constant C_T. Thus,

$$\begin{aligned}|\partial_1 A_1(U_h(\mu), V_h)(Z_h)| &\leq \int_\Omega |\nabla \cdot \mathbf{v}_h||p_h^z| \, d\Omega + \int_\Omega |\nabla \cdot \mathbf{z}_h||p_h^v| \, d\Omega \\ &+ \int_\Omega |\mathbf{u}_D||\nabla \mathbf{z}_h||\mathbf{v}_h| \, d\Omega + \int_\Omega |\mathbf{z}_h||\nabla \mathbf{u}_D||\mathbf{v}_h| \, d\Omega \\ &\leq \int_\Omega \Big(|\partial_x v_1||p_h^z| + |\partial_y v_2||p_h^z| + |\partial_x z_1||p_z^v| + |\partial_y z_2||p_h^v|\Big) \, d\Omega \\ &+ \int_\Omega |\mathbf{u}_D||\nabla \mathbf{z}_h||\mathbf{v}_h| \, d\Omega + \int_\Omega |\mathbf{z}_h||\nabla \mathbf{u}_D||\mathbf{v}_h| \, d\Omega \\ &\leq 2\|\nabla \mathbf{v}_h\|_{0,2,\Omega}\|p_h^z\|_{0,2,\Omega} + 2\|\nabla \mathbf{z}_h\|_{0,2,\Omega}\|p_z^v\|_{0,2,\Omega} \\ &+ \|\mathbf{u}_D\|_{0,4,\Omega}\|\nabla \mathbf{z}_h\|_{0,2,\Omega}\|\mathbf{v}_h\|_{0,4,\Omega} \\ &+ \|\mathbf{z}_h\|_{0,4,\Omega}\|\nabla \mathbf{u}_D\|_{0,2,\Omega}\|\mathbf{v}_h\|_{0,4,\Omega} \leq C_1\|Z_h\|_X\|V_h\|_X.\end{aligned}$$

Similarly, $|\partial_1 A_2(U_h(\mu), V_h)(Z_h)| \leq C_2\|Z_h\|_X\|V_h\|_X$. For the last term, we will use the local inverse inequalities introduced in Lemma 2.1, and the fact that $(C_S h_K)^2 \leq (C_S h)^2, \forall K \in T_h$

$$\begin{aligned}|\partial_1 A_3(U_h(\mu); V_h)(Z_h)| &\leq \int_\Omega (C_S h)^2 |\nabla \mathbf{w}_h(\mu)||\nabla \mathbf{z}_h||\nabla \mathbf{v}_h| \, d\Omega \\ &+ \int_\Omega (C_S h)^2 \frac{|\nabla \mathbf{w}_h(\mu)||\nabla \mathbf{z}_h|}{|\nabla \mathbf{w}_h(\mu)|}|\nabla \mathbf{w}_h(\mu)||\nabla \mathbf{v}_h| \, d\Omega \\ &\leq 2(C_S h)^2\|\nabla \mathbf{w}_h(\mu)\|_{0,3,\Omega}\|\nabla \mathbf{z}_h\|_{0,3,\Omega}\|\nabla \mathbf{v}_h\|_{0,3,\Omega} \\ &\leq 2C_S^2 h^{2-d/3}\|\nabla \mathbf{w}_h(\mu)\|_{0,3,\Omega}\|\nabla \mathbf{z}_h\|_{0,2,\Omega}\|\nabla \mathbf{v}_h\|_{0,2,\Omega} \\ &\leq 2C^2 C_S^2 h^{2-d/3}\|\nabla \mathbf{w}_h(\mu)\|_{0,3,\Omega}\|\mathbf{z}_h\|_T\|\mathbf{v}_h\|_T \\ &\leq C_3\|Z_h\|_X\|V_h\|_X.\end{aligned}$$

So, we have indeed proved that there exists γ_0 such that

$$\infty > \gamma_0 > \gamma_h(\mu) = \sup_{Z_h \in X_h} \sup_{V_h \in X_h} \frac{\partial_1 A(U_h(\mu), V_h; \mu)(Z_h)}{\|Z_h\|_X \|V_h\|_X}.$$

□

Proving that the $\beta_h(\mu)$ inf-sup condition in (2.15) is satisfied, we assure that we are in a smooth branch of solutions for the Smagorinsky problem. It holds:

Proposition 2.2. *Let* $C^\star = C_T^2(C_{\overline{\mu}} + 1)$. *Suppose that* $\|\nabla \boldsymbol{u}_D\|_{0,2,\Omega} < \dfrac{1}{C^\star}$, *and* $\|\nabla \boldsymbol{u}_h\|_{0,2,\Omega} \leq \dfrac{1}{C^\star} - \|\nabla \boldsymbol{u}_D\|_{0,2,\Omega}$. *Then, there exists* $\tilde{\beta}_h > 0$ *such that,*

$$\partial_1 A(U_h, V_h; \mu)(V_h) \geq \tilde{\beta}_h \|\boldsymbol{v}_h\|_T^2 \qquad \forall V_h \in X_h. \tag{2.16}$$

Proof. We consider $Z_h = V_h$ in $\partial_1 A(U_h, V_h; \mu)(Z_h)$, having

$$\begin{aligned} \partial_1 A(U_h, V_h; \mu)(V_h) \;&= \frac{1}{\mu} \partial_1 A_0(U_h, V_h)(V_h) + \partial_1 A_1(U_h, V_h)(V_h) \\ &\quad + \partial_1 A_2(U_h, V_h)(V_h) + \partial_1 A_3(U_h; V_h)(V_h). \end{aligned} \tag{2.17}$$

As,

$$\begin{aligned} \frac{1}{\mu} \partial_1 A_0(U_h, V_h)(V_h) + \partial_1 A_3(U_h; V_h)(V_h) \;&= \int_\Omega \left(\frac{1}{\mu} + \nu_T(\mathbf{w}_h) \right) |\nabla \mathbf{v}_h|^2 \, d\Omega \\ &\quad + \sum_{K \in \mathcal{T}} \int_K (C_S h_K)^2 \frac{|\nabla \mathbf{w}_h : \nabla \mathbf{v}_h|^2}{|\nabla \mathbf{w}_h|} \, d\Omega. \end{aligned} \tag{2.18}$$

and,

$$\begin{aligned} \partial_1 A_1(U_h, V_h)(V_h) + \partial_1 A_2(U_h; V_h)(V_h) &= \int_\Omega (\mathbf{w}_h \cdot \nabla \mathbf{v}_h) \mathbf{v}_h \, d\Omega + \int_\Omega (\mathbf{v}_h \cdot \nabla \mathbf{w}_h) \mathbf{v}_h \, d\Omega \\ &\leq C_T^2 \big(\|\mathbf{w}_h\|_T + \|\nabla \mathbf{w}_h\|_{0,2,\Omega} \big) \|\mathbf{v}_h\|_T^2 \leq C_T^2 (C_{\overline{\mu}} + 1) \|\nabla \mathbf{w}_h\|_{0,2,\Omega} \|\mathbf{v}_h\|_T^2. \end{aligned} \tag{2.19}$$

Since $\displaystyle\sum_{K \in \mathcal{T}} \int_K (C_S h_K)^2 \frac{|\nabla \mathbf{w}_h : \nabla \mathbf{v}_h|^2}{|\nabla \mathbf{w}_h|} \, d\Omega \geq 0$, we have, thanks to (2.18) and

(2.19),

$$\begin{aligned}\partial_1 A(U_h, V_h; \mu)(V_h) &\geq \int_\Omega \left(\frac{1}{\mu} + \nu_T(\mathbf{w}_h)\right) |\nabla \mathbf{v}_h|^2 \, d\Omega \\ &\quad -C_T^2(C_{\overline{\mu}}+1)\|\nabla \mathbf{w}_h\|_{0,2,\Omega}\|\mathbf{v}_h\|_T^2 \\ &\geq \|\mathbf{v}_h\|_T^2 - \|\mathbf{v}_h\|_{0,4,\Omega}^2\|\nabla \mathbf{w}_h\|_{0,2,\Omega} \geq \|\mathbf{v}_h\|_T^2 \\ &\quad -C_T^2(C_{\overline{\mu}}+1)\|\mathbf{v}_h\|_T^2\|\nabla \mathbf{w}_h\|_{0,2,\Omega} \\ &\geq (1 - C_T^2(C_{\overline{\mu}}+1)\|\nabla \mathbf{w}_h\|_{0,2,\Omega})\|\mathbf{v}_h\|_T^2 \\ &\geq \big(1 - C_T^2(C_{\overline{\mu}}+1)\|\nabla \mathbf{u}_D\|_{0,2,\Omega} \\ &\quad -C_T^2(C_{\overline{\mu}}+1)\|\nabla \mathbf{u}_h\|_{0,2,\Omega}\big)\|\mathbf{v}_h\|_T^2.\end{aligned} \tag{2.20}$$

Thus, if $\|\nabla \mathbf{u}_h\|_{0,2,\Omega} \leq \dfrac{1}{C^\star} - \|\mathbf{u}_D\|_{0,2,\Omega}$ and $\|\mathbf{u}_D\|_{0,2,\Omega} \leq \dfrac{1}{C^\star}$, then there exists $\tilde{\beta}_h > 0$ such that,

$$\partial_1 A(U_h, V_h; \mu)(V_h) \geq \tilde{\beta}_h \|\mathbf{v}_h\|_T^2, \qquad \forall V_h \in X_h.$$

□

Remark 2.2. *Since the operator $b(\boldsymbol{v}_h, q_h; \mu)$ satisfies the discrete inf-sup condition $\alpha\|q_h\|_{0,2,\Omega} \leq \sup_{\boldsymbol{v}_h \in Y_h} \dfrac{b(\boldsymbol{v}_h, p_h; \mu)}{\|\boldsymbol{v}\|_{1,2,\Omega}}$, and thanks to Proposition 2.2, we can prove that the operator $\partial_1 A$ satisfies the inf-sup condition in (2.15). See [24] for more details.*

Observe that as $\|\mathbf{g}_D\|_{1/2,\Gamma_D} \leq \|\mathbf{w}_h\|_{1,\Omega} \leq C_\Omega \|\nabla \mathbf{w}_h\|_{0,2,\Omega}$, the condition needed in proposition 2.2, $\|\nabla \mathbf{w}_h\|_{0,2,\Omega} \leq \dfrac{1}{C_T^2(C_{\overline{\mu}}+1)}$, will only be possible if $\|\mathbf{g}_D\|_{1/2,\Gamma_D} \leq \dfrac{C_\Omega}{C_T^2(C_{\overline{\mu}}+1)}$; thus the Dirichlet boundary data should be sufficiently small.

2.4 *A posteriori* error estimator

In this section we construct the *a posteriori* error bound estimator for the Greedy algorithm, which selects the snapshots for the reduced space X_N. In order to obtain this *a posteriori* error bound estimator, we will take into account the well-posedness analysis of the reduced problem (2.8) done in the previous section.

We start by proving that the directional derivative of the operator $A(\cdot, \cdot; \mu)$ is locally lipschitz.

Lemma 2.2. *There exists a positive constant ρ_T such that*

$$\left|\partial_1 A(U_h^1, V_h; \mu)(Z_h) - \partial_1 A(U_h^2, V_h; \mu)(Z_h)\right| \leq \rho_T \|U_h^1 - U_h^2\|_X \|Z_h\|_X \|V_h\|_X, \tag{2.21}$$

for all $U_h^1, U_h^2, Z_h, V_h \in X_h$.

Proof. We have that

$$\begin{aligned}
\partial_1 A(U_h^1, V_h; \mu)(Z_h) - \partial_1 A(U_h^2, V_h; \mu)(Z_h) &= \int_\Omega ((\mathbf{u}_h^1 - \mathbf{u}_h^2) \cdot \nabla \mathbf{z}_h)\mathbf{v}_h \, d\Omega \\
&+ \int_\Omega (\mathbf{z}_h \cdot \nabla(\mathbf{u}_h^1 - \mathbf{u}_h^2))\mathbf{v}_h \, d\Omega + \int_\Omega \left(\nu_T(\mathbf{u}_h^1) - \nu_T(\mathbf{u}_h^2)\right) \nabla \mathbf{z}_h : \nabla \mathbf{v}_h \, d\Omega \\
&+ \sum_{K \in \mathcal{T}_h} \int_K (C_S h_K)^2 \frac{\nabla \mathbf{u}_h^1 : \nabla \mathbf{z}_h}{|\nabla \mathbf{u}_h^1|} (\nabla \mathbf{u}_h^1 : \nabla \mathbf{v}_h) \, d\Omega \\
&- \sum_{K \in \mathcal{T}_h} \int_K (C_S h_K)^2 \frac{\nabla \mathbf{u}_h^2 : \nabla \mathbf{z}_h}{|\nabla \mathbf{u}_h^2|} (\nabla \mathbf{u}_h^2 : \nabla \mathbf{v}_h) \, d\Omega.
\end{aligned}$$

So, thanks to the triangular inequality, it follows

$$\begin{aligned}
|\partial_1 A(U_h^1, V_h; \mu)(Z_h) - \partial_1 A(U_h^2, V_h; \mu)(Z_h)| \leq &\left| \int_\Omega ((\mathbf{u}_h^1 - \mathbf{u}_h^2) \cdot \nabla \mathbf{z}_h)\mathbf{v}_h \, d\Omega \right| \\
&+ \left| \int_\Omega (\mathbf{z} \cdot \nabla(\mathbf{u}_h^1 - \mathbf{u}_h^2)) \, d\Omega \right| \\
&+ \left| \sum_{K \in \mathcal{T}_h} \int_K (C_S h_K)^2 \left(|\nabla \mathbf{u}_h^1| - |\nabla \mathbf{u}_h^2|\right) \nabla \mathbf{z}_h : \nabla \mathbf{v}_h \, d\Omega \right| \\
&+ \left| \sum_{K \in \mathcal{T}_h} \int_K (C_S h_K)^2 \frac{\nabla \mathbf{u}_h^1 : \nabla \mathbf{z}_h}{|\nabla \mathbf{u}_h^1|} (\nabla \mathbf{u}_h^1 : \nabla \mathbf{v}_h) \, d\Omega \right. \\
&\left. - \sum_{K \in \mathcal{T}_h} \int_K (C_S h_K)^2 \frac{\nabla \mathbf{u}_h^2 : \nabla \mathbf{z}_h}{|\nabla \mathbf{u}_h^2|} (\nabla \mathbf{u}_h^2 : \nabla \mathbf{v}_h) \, d\Omega \right|.
\end{aligned} \tag{2.22}$$

We bound each term separately in (2.22). For the first two terms, we use the relation between $\|\cdot\|_{0,4,\Omega}$ and $\|\cdot\|_T$ used in Proposition 2.1, and the fact that the T-norm is equivalent to the H^1-seminorm.

$$\begin{aligned}
\left| \int_\Omega ((\mathbf{u}_h^1 - \mathbf{u}_h^2) \cdot \nabla \mathbf{z}_h)\mathbf{v}_h \, d\Omega \right| &\leq \int_\Omega |\mathbf{u}_h^1 - \mathbf{u}_h^2||\nabla \mathbf{z}_h||\mathbf{v}_h|| \, d\Omega \\
\leq \|\mathbf{u}_h^1 - \mathbf{u}_h^2\|_{0,4,\Omega} \|\nabla \mathbf{z}_h\|_{0,2,\Omega} \|\mathbf{v}_h\|_{0,4,\Omega} &\leq C_T \|\mathbf{u}_h^1 - \mathbf{u}_h^2\|_T \|\mathbf{z}_h\|_T \|\mathbf{v}_h\|_T \\
&\leq C_T \|U_h^1 - U_h^2\|_X \|Z_h\|_X \|V_h\|_X,
\end{aligned}$$

$$\left|\int_\Omega (\mathbf{z}_h \cdot \nabla(\mathbf{u}_h^1 - \mathbf{u}_h^2))\mathbf{v}_h \, d\Omega\right| \leq \int_\Omega |\mathbf{z}_h||\nabla(\mathbf{u}_h^1 - \mathbf{u}_h^2)||\mathbf{v}_h| \, d\Omega$$
$$\leq \|\mathbf{z}_h\|_{0,4,\Omega}\|\nabla(\mathbf{u}_h^1 - \mathbf{u}_h^2)\|_{0,2,\Omega}\|\mathbf{v}_h\|_{0,4,\Omega} \leq C_T\|\mathbf{z}_h\|_T\|\mathbf{u}^1 - \mathbf{u}_h^2\|_T\|\mathbf{v}_h\|_T$$
$$\leq C_T\|Z_h\|_X\|U_h^1 - U_h^2\|_X\|V_h\|_X.$$

To bound the third term in (2.22), we use the local inverse inequalities of Lemma 2.1,

$$\left|\sum_{K\in\mathcal{T}_h}\int_K (C_S h_K)^2 \left(|\nabla\mathbf{u}_h^1| - |\nabla\mathbf{u}_h^2|\right)\nabla\mathbf{z}_h : \nabla\mathbf{v}_h \, d\Omega\right|$$

$$\leq \sum_{K\in\mathcal{T}_h}\int_K (C_S h_K)^2 \left||\nabla\mathbf{u}_h^1| - |\nabla\mathbf{u}_h^2|\right| |\nabla\mathbf{z}_h||\nabla\mathbf{v}_h| \, d\Omega$$

$$\leq (C_S h)^2 \int_\Omega |\nabla(\mathbf{u}_h^1 - \mathbf{u}_h^2)||\nabla\mathbf{z}_h||\nabla\mathbf{v}_h| \, d\Omega$$
$$\leq (C_S h)^2\|\nabla(\mathbf{u}_h^1 - \mathbf{u}_h^2)\|_{0,3,\Omega}\|\nabla\mathbf{z}_h\|_{0,3,\Omega}\|\nabla\mathbf{v}_h\|_{0,3,\Omega}$$
$$\leq C_S^2 h^{2-d/2} C\|\nabla(\mathbf{u}_h^1 - \mathbf{u}_h^2)\|_{0,2,\Omega}\|\nabla\mathbf{z}_h\|_{0,2,\Omega}\|\nabla\mathbf{v}_h\|_{0,2,\Omega}$$
$$\leq C_S^2 h^{2-d/2} C\|U_h^1 - U_h^2\|_X\|Z_h\|_X\|V_h\|_X.$$

The last term in (2.22) is bounded as follows:

$$\left|\sum_{K\in\mathcal{T}_h}\int_K (C_S h_K)^2 \frac{\nabla\mathbf{u}_h^1 : \nabla\mathbf{z}_h}{|\nabla\mathbf{u}_h^1|}(\nabla\mathbf{u}_h^1 : \nabla\mathbf{v}_h) \, d\Omega\right.$$

$$\left. - \sum_{K\in\mathcal{T}_h}\int_K (C_S h_K)^2 \frac{\nabla\mathbf{u}_h^2 : \nabla\mathbf{z}_h}{|\nabla\mathbf{u}_h^2|}(\nabla\mathbf{u}_h^2 : \nabla\mathbf{v}_h) \, d\Omega\right|$$
$$= \left|\sum_{K\in\mathcal{T}_h}\int_K (C_S h_K)^2 \left[\frac{\nabla\mathbf{u}_h^1 : \nabla\mathbf{z}_h}{|\nabla\mathbf{u}_h^1|}\left(\nabla(\mathbf{u}_h^1 - \mathbf{u}_h^2) : \nabla\mathbf{v}_h\right)\right.\right.$$
$$\left.\left. + \frac{\nabla(\mathbf{u}_h^1 - \mathbf{u}_h^2) : \nabla\mathbf{z}_h}{|\nabla\mathbf{u}_h^2|}(\nabla\mathbf{u}_h^2 : \nabla\mathbf{v}_h)\right] \, d\Omega\right.$$
$$\left. + \sum_{K\in\mathcal{T}_h}\int_K (C_S h_K)^2 \frac{(|\nabla\mathbf{u}_h^2| - |\nabla\mathbf{u}_h^1|)\nabla\mathbf{u}_h^1 : \nabla\mathbf{z}_h}{|\nabla\mathbf{u}_h^1||\nabla\mathbf{u}_h^2|}(\nabla\mathbf{u}_h^2 : \nabla\mathbf{v}_h) \, d\Omega\right|$$

$$
\begin{aligned}
&\leq \sum_{K\in\mathcal{T}_h}\int_K (C_S h_K)^2 |\nabla \mathbf{z}_h||\nabla(\mathbf{u}_h^1-\mathbf{u}_h^2)||\nabla \mathbf{v}_h|\, d\Omega \\
&+ \sum_{K\in\mathcal{T}_h}\int_K (C_S h_K)^2 |\nabla(\mathbf{u}_h^1-\mathbf{u}_h^2)||\nabla \mathbf{z}_h||\nabla \mathbf{v}_h|\, d\Omega \\
&+ \sum_{K\in\mathcal{T}_h}\int_K (C_S h_K)^2 \left||\nabla \mathbf{u}_h^1|-|\nabla \mathbf{u}_h^2|\right| |\nabla \mathbf{z}_h||\nabla \mathbf{v}_h|\, d\Omega \\
&\leq 3(C_S h)^2 \|\nabla(\mathbf{u}_h^1-\mathbf{u}_h^2)\|_{0,3,\Omega}\|\nabla \mathbf{z}_h\|_{0,3,\Omega}\|\nabla \mathbf{v}_h\|_{0,3,\Omega} \\
&\leq 3C_S^2 h^{2-d/2} C \|\nabla(\mathbf{u}_h^1-\mathbf{u}_h^2)\|_{0,2,\Omega}\|\nabla \mathbf{z}_h\|_{0,2,\Omega}\|\nabla \mathbf{v}_h\|_{0,2,\Omega} \\
&\leq 3C_S^2 h^{2-d/2} C \|U_h^1-U_h^2\|_X \|Z_h\|_X \|V_h\|_X.
\end{aligned}
$$

Thus, we have just proved that

$$
|\partial_1 A(U_h^1, V_h;\mu)(Z_h) - \partial_1 A(U_h^2, V_h;\mu)(Z_h)| \leq \rho_T \|U_h^1-U_h^2\|_X \|Z_h\|_X \|V_h\|_X,
$$

where,

$$
\rho_T = 2C_T + 4C_S h^{2-d/2} C. \tag{2.23}
$$

□

We introduce the following *supremizer* operator $T_N : X_h \to X_h$, defined as

$$
(T_N Z_h, V_h)_X = \partial_1 A(U_N(\mu), V_h;\mu)(Z_h) \quad \forall V_h, Z_h \in X_h, \tag{2.24}
$$

such that

$$
T_N Z_h = \arg\sup_{V_h\in X_h} \frac{\partial_1 A(U_N(\mu), V_h;\mu)(Z_h)}{\|V_h\|_X}. \tag{2.25}
$$

Taking account this definition, in order to guarantee the well-posedness of the reduced basis problem (2.10), in the same way as in the finite element problem (2.8), we define the inf-sup and continuity constants:

$$
0 < \beta_N(\mu) \equiv \inf_{Z_h\in X_h}\sup_{V_h\in X_h} \frac{\partial_1 A(U_N(\mu), V_h;\mu)(Z_h)}{\|Z_h\|_X\|V_h\|_X} = \inf_{Z_h\in X_h} \frac{\|T_N Z_h\|_X}{\|Z_h\|_X}, \tag{2.26}
$$

$$
\infty > \gamma_N(\mu) \equiv \sup_{Z_h\in X_h}\sup_{V_h\in X_h} \frac{\partial_1 A(U_N(\mu), V_h;\mu)(Z_h)}{\|Z_h\|_X\|V_h\|_X} = \sup_{Z_h\in X_h} \frac{\|T_N Z_h\|_X}{\|Z_h\|_X}. \tag{2.27}
$$

Theorem 2.1. *Let $\mu \in \mathcal{D}$, and assume that $\beta_N(\mu) > 0$. If problem (2.8) admits*

a solution $U_h(\mu)$ such that

$$\|U_h(\mu) - U_N(\mu)\|_X \leq \frac{\beta_N(\mu)}{\rho_T},$$

then this solution is unique in the ball $B_X\left(U_N(\mu), \dfrac{\beta_N(\mu)}{\rho_T}\right)$.

Proof: The proof of this theorem is an extension of the proof of Lemma 3.1 in [36]. We define the following operators:

- $\mathcal{R}(\cdot;\mu) : X_h \to X_h'$, defined as

$$\langle \mathcal{R}(Z_h;\mu), V_h\rangle = A(Z_h, V_h;\mu) - F(V_h;\mu), \quad \forall Z_h, V_h \in X_h \tag{2.28}$$

- $\mathcal{DA}(U_h(\mu);\mu) : X_h \to X_h'$, defined, for $U_h(\mu) \in X_h$, as

$$\langle \mathcal{DA}(U_h(\mu);\mu)Z_h, V_h\rangle = \partial_1 A(U_h(\mu), V_h;\mu)(Z_h), \quad \forall Z_h, V_h \in X_h \tag{2.29}$$

- $H : X_h \to X_h$, defined as

$$H(Z_h;\mu) = Z_h - \mathcal{DA}(U_N(\mu);\mu)^{-1}\mathcal{R}(Z_h;\mu), \quad \forall Z_h \in X_h \tag{2.30}$$

Note that $\mathcal{DA}(U_N(\mu);\mu)$ is invertible thanks to the assumption $\beta_N(\mu) > 0$. Also note that it is straightforward from (2.29) and (2.24), that $\mathcal{DA}(U_N(\mu);\mu) = T_N$ in X_h'. We express

$$H(Z_h^1;\mu) - H(Z_h^2;\mu) = (Z_h^1 - Z_h^2) - \mathcal{DA}(U_N(\mu);\mu)^{-1}(\mathcal{R}(Z_h^1;\mu) - \mathcal{R}(Z_h^2;\mu)). \tag{2.31}$$

It holds

$$\mathcal{R}(Z_h^1;\mu) - \mathcal{R}(Z_h^2;\mu) = \mathcal{DA}(\xi;\mu)(Z_h^1 - Z_h^2), \tag{2.32}$$

where $\xi = \lambda Z_h^1 - (1-\lambda)Z_h^2$, for some $\lambda \in (0,1)$. To prove this, we define the operator $T : [0,1] \to \mathbb{R}$, by $T(t) = \langle \mathcal{R}(tZ_h^1 + (1-t)Z_h^2;\mu), V_h\rangle$, for all $V_h \in X_h$. Then, $T(0) = \langle \mathcal{R}(Z_h^2;\mu), V_h\rangle$ and $T(1) = \langle \mathcal{R}(Z_h^1;\mu), V_h\rangle$. The operator T is differentiable in $(0,1)$ and continuous in $[0,1]$, and

$$T'(t) = \left\langle \mathcal{DA}(tZ_h^1 + (1-t)Z_h^2;\mu)(Z_h^1 - Z_h^2), V_h \right\rangle.$$

Thus, (2.32) follows from the Mean Value Theorem in $\mathbb{R}$. Now, multiplying (2.31) by $\mathcal{DA}(U_N(\mu);\mu)$ and applying this last property, we can write

$$\mathcal{DA}(U_N(\mu);\mu)(H(Z_h^1;\mu) - H(Z_h^2;\mu)) = \left[\mathcal{DA}(U_N(\mu);\mu) - \mathcal{DA}(\xi;\mu)\right](Z_h^1 - Z_h^2).$$

Then, thanks to (2.21) and this last equality, it follows

$$\left\langle \mathcal{DA}(U_N(\mu);\mu)(H(Z_h^1;\mu)-H(Z_h^2;\mu)), V_h \right\rangle \leq \rho_T \|U_N(\mu)-\xi\|_X \|Z_h^1 - Z_h^2\|_X \|V_h\|_X.$$

Now, applying the definitions of $\beta_N(\mu)$, T_N, $\mathcal{DA}(U_N(\mu);\mu)$, and this last property, we can obtain

$$\begin{aligned}
&\beta_N(\mu)\|H(Z_h^1;\mu)-H(Z_h^2;\mu)\|_X \|T_N(H(Z_h^1;\mu)-H(Z_h^2;\mu))\|_X \\
&\qquad \leq \|T_N(H(Z_h^1;\mu)-H(Z_h^2;\mu))\|_X^2 \\
&\quad = \left(T_N(H(Z_h^1;\mu)-H(Z_h^2;\mu);\mu), T_N(H(Z_h^1;\mu)-H(Z_h^2;\mu);\mu)\right)_X \\
&= \left\langle \mathcal{DA}(U_N(\mu);\mu)(H(Z_h^1;\mu)-H(Z_h^2;\mu)), T_N(H(Z_h^1;\mu)-H(Z_h^2;\mu);\mu)\right\rangle \\
&\quad \leq \rho_T \|U_N(\mu)-\xi\|_X \|Z_h^1 - Z_h^2\|_X \|T_N(H(Z_h^1;\mu)-H(Z_h^2;\mu);\mu)\|_X
\end{aligned}$$

So, we have proved that

$$\|H(Z_h^1;\mu)-H(Z_h^2;\mu)\|_X \leq \frac{\rho_T}{\beta_N(\mu)} \|U_N(\mu)-\xi\|_X \|Z_h^1 - Z_h^2\|_X.$$

If Z_h^1 and Z_h^2 are in $B_X(U_N(\mu),\alpha)$ then, $\|U_N(\mu)-\xi\|_X \leq \alpha$, and,

$$\|H(Z_h^1;\mu)-H(Z_h^2;\mu)\|_X \leq \frac{\rho_T}{\beta_N(\mu)} \alpha \|Z_h^1 - Z_h^2\|_X.$$

Then, $H(\cdot;\mu)$ is a contraction if $\alpha < \dfrac{\beta_N(\mu)}{\rho_T}$. So it follows that there can exist at most one fixed point of $H(\cdot;\mu)$ inside $B_X\left(U_N(\mu), \dfrac{\beta_N(\mu)}{\rho_T}\right)$, and hence, at most one solution $U_h(\mu)$ to (2.8) in this ball.

□

At this point, we are in a position to define the *a posteriori* error bound estimator by

$$\Delta_N(\mu) = \frac{\beta_N(\mu)}{2\rho_T}\left[1-\sqrt{1-\tau_N(\mu)}\right], \tag{2.33}$$

where $\tau_N(\mu)$ is given by:

$$\epsilon_N(\mu) = \|\mathcal{R}(U_N(\mu);\mu)\|_{X'}, \tag{2.34}$$

$$\tau_N(\mu) = \frac{4\epsilon_N(\mu)\rho_T}{\beta_N^2(\mu)}. \tag{2.35}$$

The suitability of this *a posteriori* error bound estimator is stated by the following theorem:

Theorem 2.2. *Assume that $\beta_N(\mu) > 0$ and $\tau_N(\mu) \leq 1$ for all $\mu \in \mathcal{D}$. Then there exists a unique solution $U_h(\mu)$ of (2.8) such that the error with respect $U_N(\mu)$, solution of (2.10), is bounded by the a posteriori error bound estimator, i.e.,*

$$\|U_h(\mu) - U_N(\mu)\|_X \leq \Delta_N(\mu), \tag{2.36}$$

with effectivity

$$\Delta_N(\mu) \leq \left[\frac{2\gamma_N(\mu)}{\beta_N(\mu)} + \tau_N(\mu)\right] \|U_h(\mu) - U_N(\mu)\|_X. \tag{2.37}$$

Proof: To prove (2.36), let $\alpha > 0$ and $Z_h \in X_h$ such that $\|U_N(\mu) - Z_h\|_X \leq \alpha$. We use the notations introduced in the proof of Theorem 2.1. We consider

$$\begin{aligned} H(Z_h;\mu) - U_N(\mu) &= Z_h - U_N(\mu) - \mathcal{DA}(U_N(\mu);\mu)^{-1}\mathcal{R}(Z_h;\mu) \\ &= Z_h - U_N(\mu) - \mathcal{DA}(U_N(\mu);\mu)^{-1}\left[\mathcal{R}(Z_h;\mu) - \mathcal{R}(U_N(\mu);\mu)\right] \\ &\quad -\mathcal{DA}(U_N(\mu);\mu)^{-1}\mathcal{R}(U_N(\mu);\mu) \end{aligned}$$

Multiplying by $\mathcal{DA}(U_N(\mu);\mu)$, we obtain

$$\begin{aligned} \langle \mathcal{DA}(U_N(\mu);\mu)(H(Z_h;\mu) - U_N(\mu)), V_h\rangle &= \langle \mathcal{DA}(U_N(\mu);\mu)(Z_h - U_N(\mu)), V_h\rangle \\ - \langle \mathcal{R}(Z_h;\mu) - \mathcal{R}(U_N(\mu);\mu), V_h\rangle &- \langle \mathcal{R}(U_N(\mu);\mu), V_h\rangle, \quad \forall V_h \in X_h. \end{aligned}$$

As in the proof of Theorem 2.1, it holds

$$\mathcal{R}(Z_h;\mu) - \mathcal{R}(U_N(\mu);\mu) = \mathcal{DA}(\xi(\mu);\mu)(Z_h - U_N(\mu)),$$

where $\xi(\mu) = t^* Z_h + (1-t^*)U_N(\mu)$, $t^* \in (0,1)$.

By this way, and thanks to Lemma 2.2, we obtain:

$$\begin{aligned} \langle \mathcal{DA}(U_N(\mu);\mu)(H(Z_h;\mu) - U_N(\mu)), V_h\rangle &= \langle \mathcal{DA}(U_N(\mu);\mu)(Z_h - U_N(\mu)), V_h\rangle \\ - \langle \mathcal{DA}(\xi(\mu);\mu)(Z_h - U_N(\mu)), V_h\rangle &- \langle \mathcal{R}(U_N(\mu);\mu), V_h\rangle \\ = \left\langle \left(\mathcal{DA}(U_N(\mu);\mu) - \mathcal{DA}(\xi(\mu);\mu)\right)(Z_h - U_N(\mu)), V_h\right\rangle &- \langle \mathcal{R}(U_N(\mu);\mu), V_h\rangle \\ \leq \rho_T \|U_N(\mu) - \xi(\mu)\|_X \|Z_h - U_N(\mu)\|_X \|V_h\|_X &+ \epsilon_N(\mu)\|V_h\|_X \\ \leq \left(\rho_T \|Z_h - U_N(\mu)\|_X^2 + \epsilon_N(\mu)\right)\|V_h\|_X & \end{aligned}$$

Then, using the same arguments as in Theorem 2.1,

$$\begin{aligned}
\beta_N(\mu)\|H(Z_h;\mu)-U_N(\mu)\|_X\|T_N^\mu(H(Z_h;\mu)-U_N(\mu))\|_X \\
\leq \|T_N^\mu(H(Z_h;\mu)-U_N(\mu))\|_X^2 \\
= \Big(T_N^\mu\big(H(Z_h;\mu)-U_N(\mu)\big),\, T_N^\mu\big(H(Z_h;\mu)-U_N(\mu)\big)\Big)_X \\
= \langle \mathcal{DA}(U_N(\mu);\mu)(H(Z_h;\mu)-U_N(\mu)), T_N^\mu(H(Z_h;\mu)-U_N(\mu))\rangle \\
\leq \big(\rho_T\|Z_h-U_N(\mu)\|_X^2+\epsilon_N(\mu)\big)\|T_N^\mu(H(Z_h;\mu)-U_N(\mu))\|_X.
\end{aligned}$$

Then, as $Z_h \in B_X\left(U_N(\mu),\alpha\right)$, we have

$$\|H(Z_h;\mu)-U_N(\mu)\|_X < \frac{\rho_T}{\beta_N(\mu)}\alpha^2+\frac{\epsilon_N(\mu)}{\beta_N(\mu)}. \tag{2.38}$$

In order to ensure that H maps $B_X(U_N(\mu),\alpha)$ into a part of itself, we are seeking the values of α such that

$$\frac{\rho_T}{\beta_N(\mu)}\alpha^2+\frac{\epsilon_N(\mu)}{\beta_N(\mu)} \leq \alpha. \tag{2.39}$$

This holds if α is between the two roots of the second order equation

$$\rho_T\alpha^2-\beta_N(\mu)\alpha+\epsilon_N(\mu)=0,$$

which are,

$$\alpha_\pm = \frac{\beta_N(\mu)\pm\sqrt{\beta_N(\mu)^2-4\rho_T\epsilon_N(\mu)}}{2\rho_T} = \frac{\beta_N(\mu)}{2\rho_T}\left[1\pm\sqrt{1-\frac{4\rho_T\epsilon_N(\mu)}{\beta_N(\mu)^2}}\right]. \tag{2.40}$$

Observe that as $\tau_N(\mu)\leq 1$, then $\alpha_-\leq\alpha_+\leq\dfrac{\beta_N(\mu)}{\rho_T}$. Consequently, if $\alpha_-\leq\alpha\leq\alpha_+$, there exists a unique solution $U_h(\mu)$ to (2.8) in the ball $B_X(U_N(\mu),\alpha)$.

To obtain (2.36) observe that from (2.40), the lowest value (i.e. the best error bound) corresponds to $\alpha=\alpha_-=\Delta_N(\mu)$.

To prove (2.37), let us define the error $E_h(\mu)=U_h(\mu)-U_N(\mu)$, and the residual $R(\mu)$, such that

$$\begin{aligned}
(R(\mu),V_h)_X &= -\langle\mathcal{R}(U_N(\mu);\mu),V_h\rangle = F(V_h;\mu)-A(U_N(\mu),V_h;\mu) \\
&= A(U_h(\mu),V_;\mu)-A(U_N(\mu),V_h;\mu).
\end{aligned}$$

Note that, from (2.34), $\|R(\mu)\|_X=\epsilon_N(\mu)$. We observe that the following relation

holds, for some $t^* \in (0,1)$:

$$A(U_h(\mu), V_h; \mu) - A(U_N(\mu), V_h; \mu) = \partial_1 A\big(t^* U_h(\mu) + (1-t^*)U_N(\mu), V_h; \mu\big)(E_h(\mu)).$$

Thus, we have that

$$\|R(\mu)\|_X^2 = \Big[\partial_1 A\big(t^* U_h(\mu) + (1-t^*)U_N(\mu), R(\mu); \mu\big) - \partial_1 A(U_N(\mu), R(\mu); \mu)\Big](E_h(\mu))$$
$$+\partial_1 A(U_N(\mu), R(\mu); \mu)(E_h(\mu)).$$

Thus, thanks to Lemma 2.2, and taking into account the definition of $\gamma_N(\mu)$ by (2.27), we obtain

$$\|R(\mu)\|_X^2 \leq \rho_T \|t^*(U_h(\mu) - U_N(\mu))\|_X \|E_h(\mu)\|_X \|R(\mu)\|_X$$
$$+\gamma_N(\mu)\|E_h(\mu)\|_X \|R(\mu)\|_X.$$

Then $\epsilon_N(\mu) = \rho_T \|E_h(\mu)\|_X^2 + \|R(\mu)\|_X \leq \gamma_N(\mu)\|E_h(\mu)\|_X$. Since $0 \leq \tau_N(\mu) \leq 1$ and $1 - \sqrt{1-\tau_N(\mu)} \leq \tau_N(\mu)$, we have that

$$\frac{2\rho_T}{\beta_N(\mu)} \Delta_N(\mu) \leq \tau_N(\mu),$$

and then

$$\Delta_N(\mu) \leq \frac{2\epsilon_N(\mu)}{\beta_N(\mu)}.$$

It follows that

$$\Delta_N(\mu) \leq \frac{2\rho_T}{\beta_N(\mu)} \|E_h(\mu)\|_X^2 + \frac{2\gamma_N(\mu)}{\beta_N(\mu)} \|E_h(\mu)\|_X.$$

Thanks to (2.36), we know that $\|E_h(\mu)\|_X \leq \Delta_N(\mu)$, then $\frac{2\rho_T}{\beta_N(\mu)} \|E_h(\mu)\|_X \leq \tau_N(\mu)$. It follows (2.37), i.e.,

$$\Delta_N(\mu) \leq \left[\frac{2\gamma_N(\mu)}{\beta_N(\mu)} + \tau_N(\mu)\right] \|U(\mu) - U_N(\mu)\|_X.$$

□

2.5 Approximation of the eddy viscosity term

In this section we approximate the non-linear turbulent eddy viscosity term by the Empirical Interpolation Method (*cf.* [45, 9]), explained in section 1.6.

Let us denote $g(\mu) := g(x; \mathbf{w}_h(\mu)) = |\nabla \mathbf{w}_h(\mu)|(x)$. The finality of using the EIM in the Smagorinsky reduced basis model is decoupling the parameter dependence from the spatial dependence of the function $g(\mu)$, i.e.,

$$g(\mu) \approx \mathcal{I}_M[g(\mu)], \tag{2.41}$$

With the EIM, we construct a reduced-basis space $W_M = \text{span}\{q_1(\mu), \ldots, q_M(\mu)\}$, selecting these bases functions by a greedy procedure, with snapshots of $g(\mu)$. Thanks to that, we are able to approximate the non-linear Smagorinsky term by a trilinear form, in the following way

$$a_S(\mathbf{w}_N; \mathbf{w}_N, \mathbf{v}_N; \mu) \approx \hat{a}_S(\mathbf{w}_N, \mathbf{v}_N; \mu), \tag{2.42}$$

where,

$$\hat{a}_S(\mathbf{w}_N; \mathbf{v}_N; \mu) = \sum_{k=1}^{M} \sigma_k(\mu) s(q_k, \mathbf{w}_h, \mathbf{v}_h), \tag{2.43}$$

with

$$s(q_k, \mathbf{w}_h, \mathbf{v}_h) = \sum_{K \in \mathcal{T}_h} \int_K (C_S h_K)^2 q_k \nabla \mathbf{w} : \nabla \mathbf{v} \, d\Omega. \tag{2.44}$$

Here $\sigma_k(\mu)$, for $k = 1, \ldots, M$, is the solution of a lower-triangular linear system, where the second member is the value of $g(x; \mathbf{w}_h(\mu))$ in some certain points x_i. For more details, see section 1.6. Futhermore,

$$\hat{a}_S(q_k, \mathbf{w}_N, \mathbf{v}_N) = \sum_{K \in \mathcal{T}_h} \int_K (C_S h_K)^2 q_k \nabla \mathbf{w} : \nabla \mathbf{v} \, d\Omega. \tag{2.45}$$

This technique allows us to linearise the eddy viscosity term. Let us recall the RB problem, with this last approximation of the Smagorinsky term:

$$\begin{cases} \text{Find } (\mathbf{u}_N, p_N) \in Y_N \times M_N \text{ such that} & \\ a(\mathbf{u}_N, \mathbf{v}_N; \mu) + b(\mathbf{v}_N, p_N; \mu) + \hat{a}_S(\mathbf{w}_N; \mathbf{v}_N; \mu) & \\ +c(\mathbf{u}_D, \mathbf{u}_N, \mathbf{v}_N; \mu) + c(\mathbf{u}_N, \mathbf{u}_D, \mathbf{v}_N; \mu) & \\ +c(\mathbf{u}_N, \mathbf{u}_N, \mathbf{v}_N; \mu) = F(\mathbf{v}_N; \mu) & \forall \mathbf{v}_N \in Y_N \\ b(\mathbf{u}_N, q_N; \mu) = 0 & \forall q_N \in M_N \end{cases} \tag{2.46}$$

The solution $(\mathbf{u}_N(\mu), p_N(\mu)) \in X_N$ of (2.46) can be expressed as a linear combination of the basis functions:

$$\mathbf{u}_N(\mu) = \sum_{j=1}^{2N} u_j^N(\mu)\zeta_j^{\mathbf{v}}, \quad p_N(\mu) = \sum_{j=1}^{N} p_j^N(\mu)\xi_j^p.$$

Taking into account this representation, for the bilinear terms in (2.46), we store the parameter-independent matrices during the offline phase, as in [72], defined as:

$$\begin{array}{ll} (\mathbb{A}_N)_{ij} = a(\zeta_j^{\mathbf{v}}, \zeta_i^{\mathbf{v}}) & i,j = 1,\dots,2N, \\ (\mathbb{D}_N)_{ij} = c(\mathbf{u}_D, \zeta_j^{\mathbf{v}}, \zeta_i^{\mathbf{v}}) + c(\zeta_j^{\mathbf{v}}, \mathbf{u}_D, \zeta_i^{\mathbf{v}}), & i,j = 1,\dots,2N, \\ (\mathbb{B}_N)_{li} = b(\zeta_i^{\mathbf{v}}, \xi_l^p), & i = 1,\dots,2N,\ l = 1,\dots,N. \end{array} \tag{2.47}$$

For the convective and the Smagorinsky terms, we need to store a parameter-independent tensors of order three during the offline phase, defined as:

$$\begin{array}{ll} (\mathbb{C}_N(\zeta_s^{\mathbf{v}}))_{ij} = c(\zeta_s^{\mathbf{v}}, \zeta_j^{\mathbf{v}}, \zeta_i^{\mathbf{v}}), & i,j,s = 1,\dots,2N, \\ (\mathbb{S}_N(q_s))_{ij} = s(q_s, \zeta_j^{\mathbf{v}}, \zeta_i^{\mathbf{v}}), & i,j = 1,\dots,2N, s = 1,\dots,M. \end{array} \tag{2.48}$$

With this tensor representation, it holds that

$$c(\mathbf{u}_N, \zeta_j^{\mathbf{v}}, \zeta_i^{\mathbf{v}}; \mu) = \sum_{s=1}^{2N} u_s^N(\mu)\mathbb{C}_N(\zeta_s^{\mathbf{v}}) \quad \text{and} \quad \hat{a}_S(\zeta_j^{\mathbf{v}}; \zeta_i^{\mathbf{v}}; \mu) = \sum_{s=1}^{M} \sigma_s(\mu)\mathbb{S}_N(q_s),$$

and thanks to that, we are able to solve problem (2.46), linearised by a semi-implicit evolution approach. Remark that the treatment of the approximation of the eddy viscosity term in the offline/online phase is similar to the treatment of the convective term, thanks to the tensorization done in this section.

2.6 Numerical results

In this section, we present some numerical tests for the reduced order Smagorinsky model, programmed in FreeFem++ (*cf.* [48]). We will consider two test cases: the Backward-facing step problem and the Lid-driven cavity problem. For both cases, the Reynolds numbers for which it is known that a steady regime takes place. We obtain rates of speed-up of the computational time from several hundreds to several thousands.

2.6.1 Backward-facing step flow (2D)

In this test, we show the numerical results of a Smagorinsky reduced order model for the backward-facing step (*cf.* [3]). In Figure 2.1, we represent the geometry of our problem, with the boundaries properly identified.

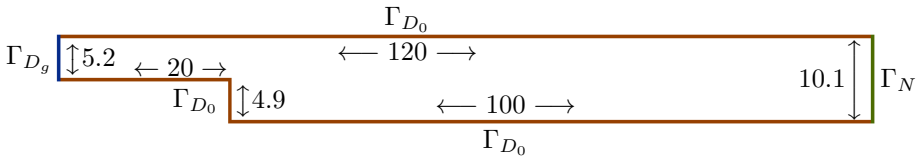

Figure 2.1: Domain Ω with the different boundaries identified.

The backward-facing step flow is laminar and reaches an steady state solution roughly up to $Re \simeq 1000$, then it becomes transitional up to $Re \simeq 5000$. For larger values, the regime become turbulent. (*cf.* [28]). The parameter that we are considering for this numerical is the Reynolds number, with values $\mu = Re \in [50, 450]$. This means that the regime we consider in this test is fully laminar.

For the offline phase, we compute the FE approximation with the Taylor-Hood finite element, i.e, we consider $\mathbb{P}2 - \mathbb{P}1$ for velocity-pressure. The mesh selected for this problem is composed by 10842 triangles and 5703 nodes. The FE steady state solution is computed trough a semi-implicit evolution approach, and we conclude that the steady solution is reached when the relative error between two iterators is below $\varepsilon_{FE} = 10^{-10}$. The numerical scheme to solve the Smagorinsky model in each time step reads

$$\begin{cases} \text{Find } (\mathbf{u}_h^{n+1}, p_h^{n+1}) \in Y_h \times M_h \text{ such that } \forall \mathbf{v}_h \in Y_h, \forall q_h \in M_h \\ \left(\dfrac{\mathbf{u}_h^{n+1} - \mathbf{u}_h^n}{\Delta t}\right)_\Omega + a(\mathbf{u}_h^{n+1}, \mathbf{v}_h; \mu) + b(\mathbf{v}_h, p_h^{n+1}; \mu) \\ + a_S(\mathbf{w}_h^n; \mathbf{w}_h^{n+1}, \mathbf{v}_h; \mu) + c(\mathbf{u}_h^n, \mathbf{u}_h^{n+1}, \mathbf{v}; \mu) \\ + c(\mathbf{u}_D, \mathbf{u}_h^{n+1}, \mathbf{v}; \mu) + c(\mathbf{u}_h^{n+1}, \mathbf{u}_D, \mathbf{v}; \mu) = F(\mathbf{v}_h; \mu) \\ b(\mathbf{u}_h^{n+1}, q_h; \mu) = 0 \end{cases} \tag{2.49}$$

To implement the Greedy algorithm, we previously compute the inf-sup constant $\beta_N(\mu)$, (2.26), and the Sobolev embedding constant C_T, as both appear in the *a posteriori* error bound estimator. Due to the fact that $U_N(\mu)$ is intended to be a good approximation of $U_h(\mu)$, in practise we substitute the value of $\beta_N(\mu)$

with the value of $\beta_h(\mu)$. To compute the inf-sup stability factor, we consider the adaptive Radial Basis Function algorithm described in section 1.5), for some selected values of $\mu \in \mathcal{D}$. On the other hand, to compute the Sobolev embedding constant, we use the fixed point algorithm described in appendix A.

In Figure 2.2 we compare $\rho_{\overline{\mu}}/\beta_{\overline{\mu}}(\mu)$, described in [36], and $\rho_T/\beta_h(\mu)$. These quantities are crucial for the number of bases necessaries to assure that $\tau_N(\mu) < 1$. Since for our problem, $\rho_T/\beta_h(\mu) < \rho_{\overline{\mu}}/\beta_{\overline{\mu}}(\mu)$, the number of bases needed to guarantee $\tau_N(\mu) < 1$ is lower when we use the norm $\|\cdot\|_T$ instead the natural norm.

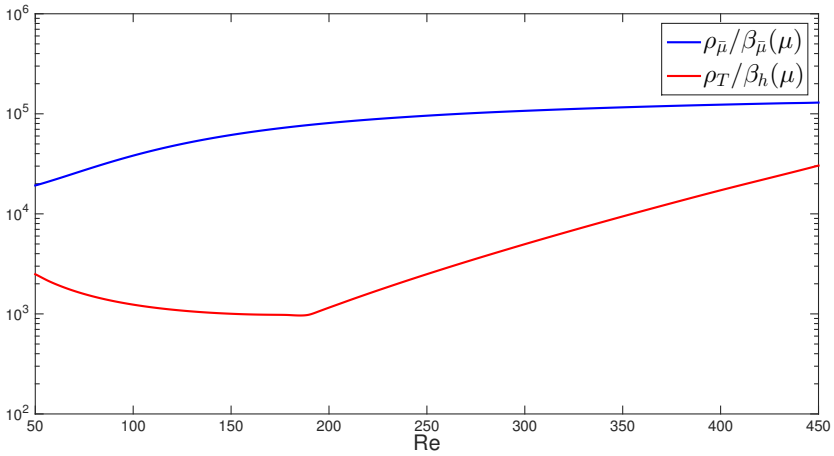

Figure 2.2: Plot of the radial basis interpolant of $\beta_h(\mu)$

To compute our reduced-basis space, we start by computing the basis functions to construct the EIM to approximate the eddy diffusion term. To evaluate the error between $g(\mu)$ and the empirical interpolation, we precompute a certain number of snapshots $\mathbf{u}_h(\mu)$, $\mu \in \mathcal{D}_{EIM}$. We stop the construction of the EIM bases when we reach a relative error below $\varepsilon_{EIM} = 5 \cdot 10^{-3}$. This error is reached for 75 basis functions for the EIM. In Figure 2.3, we show the evolution of the relative error, in the infinite norm, between $g(\mu)$ and its empirical interpolate.

Also, to obtain an initial guess such that $\tau_N \lesssim 1$, as needed by our error estimator, we first approximate the reduced manifold with some POD modes (see e.g. [7]), and then we start our Greedy algorithm. We select 10 POD modes using the snapshots computed for the EIM to start the Greedy algorithm.

In Figure 2.4, we can observe the evolution of the *a posteriori* error bound within the Greedy algorithm. We observe that it is indeed a good error estimator, with an efficiency factor close to 10 for all $\mu \in \mathcal{D}$. Due to Theorem 2.2, $\Delta_N(\mu)$ exists when $\tau_N(\mu) \leq 1$. While $\tau_N(\mu) > 1$, we use as *a posteriori* error bound estimator the proper $\tau_N(\mu)$. We stop the Greedy algorithm when we reach a

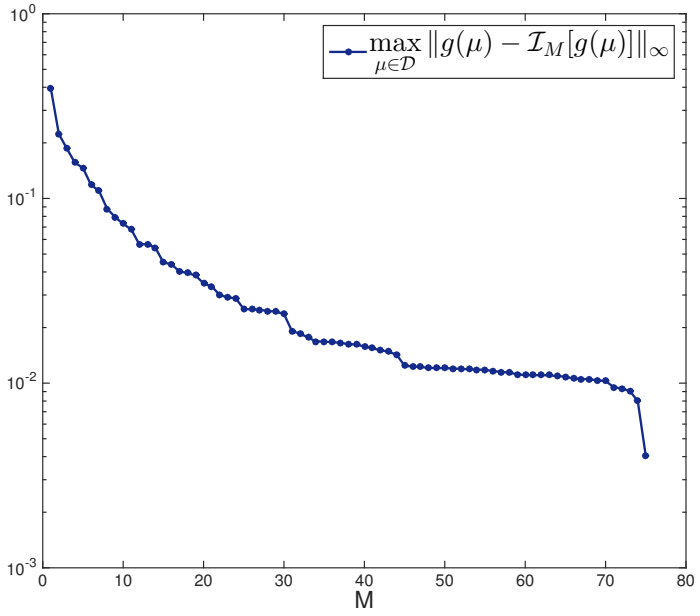

Figure 2.3: Convergence of the EIM algorithm

tolerance of $\varepsilon_{RB} = 7 \cdot 10^{-5}$, obtained when $N = N_{max} = 17$. In Figure 2.5 we show the value of the *a posteriori* error bound estimator and the relative error for all $\mu \in \mathcal{D}$, at $N = N_{\max}$.

To compute the error in the EIM approximation of the Smagorinsky eddy-viscosity term, we define the following errors:

$$e_S(\mu) = \sup_{\mathbf{v}\in V} \frac{|a_S(\mathbf{w}_h; \mathbf{w}_h, \mathbf{v}; \mu) - a_S(\mathbf{w}_N; \mathbf{w}_N, \mathbf{v}; \mu)|}{\|\mathbf{v}\|_{1,2,\Omega}} \tag{2.50}$$

$$n_S(\mu) = \sup_{\mathbf{v}\in V} \frac{a_S(\mathbf{w}_h; \mathbf{w}_h, \mathbf{v}; \mu)}{\|\mathbf{v}\|_{1,2,\Omega}} \tag{2.51}$$

In Figure 2.6 we show the value of e_S/n_S, the normalized error of the Smagorinsky term EIM approximation, for all μ in $\mathcal{D}$.

We can observe that the good approximation of the RB solution provides a good approximation for the Smagorinsky term, since the error between FE and RB solution in Figure 2.5 and the error in Figure 2.6 are similar.

In Figure 2.7 we show a comparison between the FE velocity solution (top) and the RB velocity solution (bottom) for a chosen parameter value $\mu = 320$. Note that both images are practically equal, as the error between both solutions

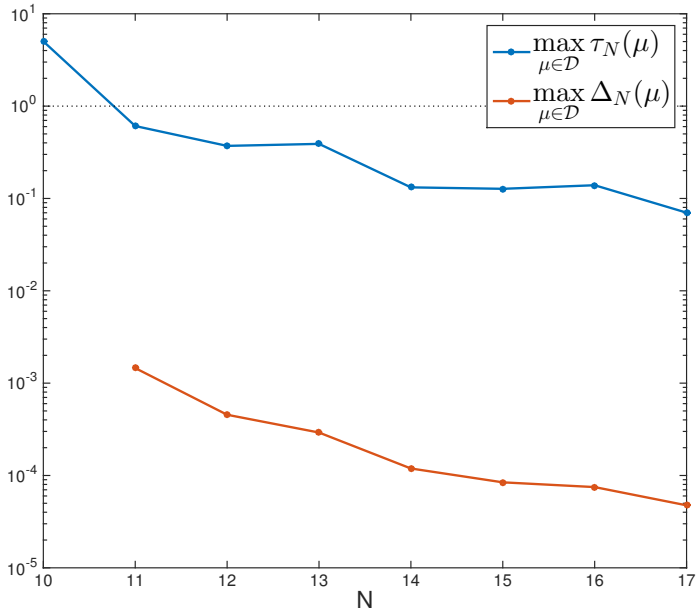

Figure 2.4: Convergence of the Greedy algorithm.

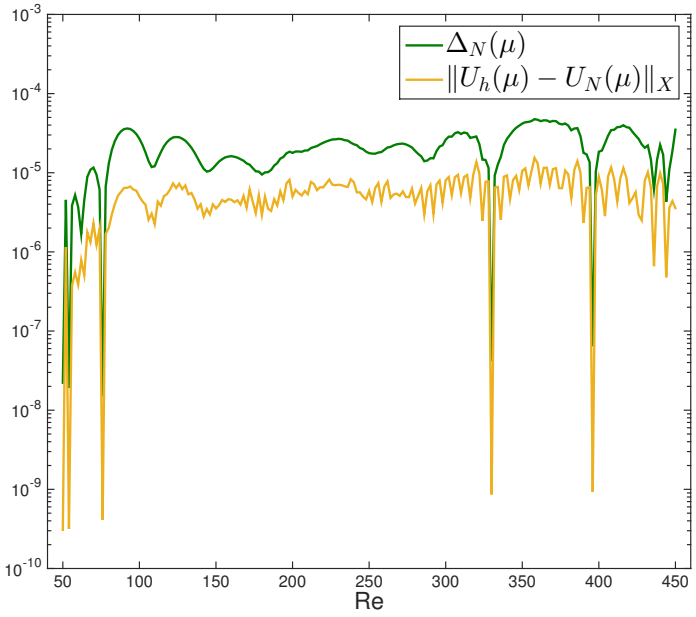

Figure 2.5: Value of $\Delta_{N_{\max}(\mu)}$ and the error between the FE solution and the RB solution.

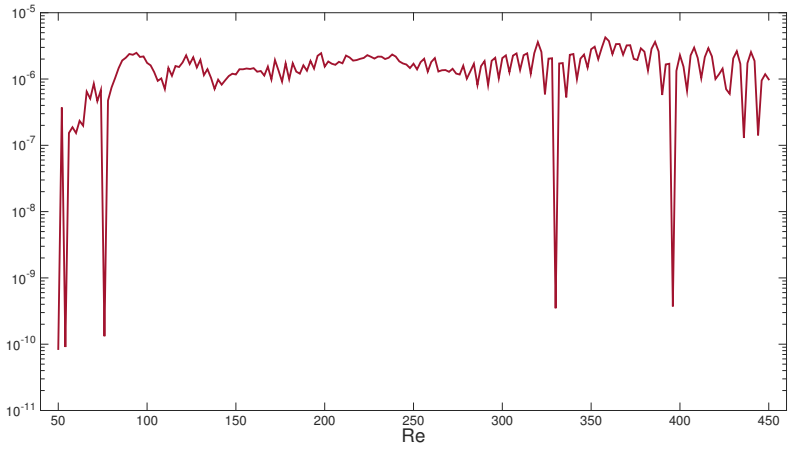

Figure 2.6: Normalized error of the EIM Smagorinsky term approximation.

is of order 10^{-6}.

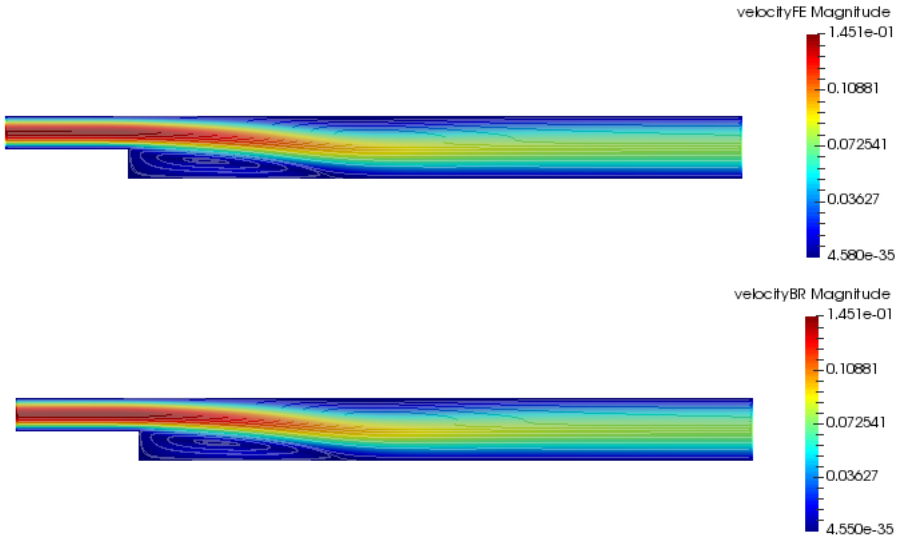

Figure 2.7: FE solution (top) and RB solution (bottom) for $\mu = 320$.

In Table 2.1, we show the results obtained for several values of μ in $\mathcal{D}$, in particular, we compare the computational time for the computation of the FE solution and the RB solution in the online phase. We also show the speedup rate in the computation of the RB solution, and the relative errors in H^1-norm for velocity and in L^2 for pressure. We observe a dramatic reduction of the computational time, with speed-up rates over 1000 for large Reynolds, with relative errors below the Greedy tolerance. The offline phase took 3 days and 10 hours to be completed. In this offline time, we are considering the time spent to constructing

the RBF functions for the stability factor β_h, the computation of the snapshots necessaries for the EIM, and the Greedy algorithm.

Data	$\mu = 56$	$\mu = 132$	$\mu = 236$	$\mu = 320$	$\mu = 450$
T_{FE}	237.88s	503.57s	1055.91s	1737.74s	2948.11s
T_{online}	1.40s	1.51s	1.69s	1.72s	2.02s
speedup	169	333	622	1008	1458
$\|\mathbf{u}_h - \mathbf{u}_N\|_T$	$3.77 \cdot 10^{-7}$	$5.33 \cdot 10^{-6}$	$6.58 \cdot 10^{-6}$	$1.36 \cdot 10^{-5}$	$3.57 \cdot 10^{-6}$
$\|p_h - p_N\|_0$	$1.94 \cdot 10^{-8}$	$6.97 \cdot 10^{-8}$	$2.1 \cdot 10^{-7}$	$4.82 \cdot 10^{-7}$	$9.02 \cdot 10^{-8}$

Table 2.1: Computational time for FE solution and RB online phase, with the speedup and the relative error.

2.6.2 Lid-driven Cavity flow (2D)

In this test, we apply the reduced-order Smagorinsky turbulence model to the Lid-driven cavity problem. In Figure 2.8, we represent the geometry with the boundaries described. We consider the non homogeneous Dirichlet boundary condition is given by $g(x) = 1$ on the lid boundary Γ_{D_g}.

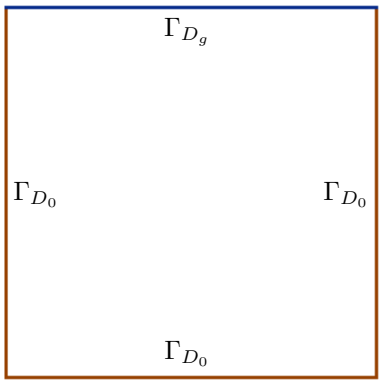

Figure 2.8: Domain Ω with the different boundaries identified.

For this test, we also consider the Reynolds number as parameter, ranging in $[1000, 5100]$. The 2D lid-driven cavity flow has a steady solution up to Reynolds 7500 (*cf.* [28]); thus in this range, a steady solution is well known to exist. We consider the same finite elements as the previous problem (Taylor-Hood), and we use a regular mesh with 5000 triangles and 2601 nodes.

In Figure 2.9, we show the comparison between $\rho_{\overline{\mu}}/\beta_{\overline{\mu}}(\mu)$ and $\rho_T/\beta_h(\mu)$ as in Section 2.6.1. In this case, the value of $\rho_{\overline{\mu}}/\beta_{\overline{\mu}}(\mu)$ (see [36] for more details) is

greater than $\rho_T/\beta_h(\mu)$. Again, thanks to that election in the norm, the number of bases needed to guarantee that $\tau_N(\mu) < 1$ in this problem is lower if we chose the norm $\|\cdot\|_T$ instead choosing the natural norm.

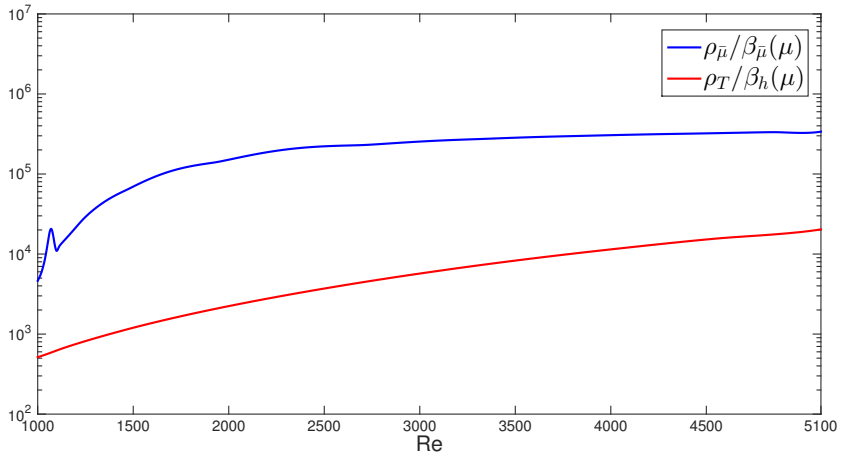

Figure 2.9: Plot of the radial basis interpolant of $\beta_h(\mu)$.

In this numerical test, we need $M_{\max} = 22$ bases in the EIM algorithm until reaching the tolerance for the relative error of $\varepsilon_{EIM} = 5 \cdot 10^{-4}$. In Figure 2.10, we show the convergence of the EIM algorithm.

For the Greedy algorithm, we prescribe a tolerance of $\varepsilon_{RB} = 5 \cdot 10^{-5}$. This tolerance is reached for $N_{\max} = 12$ basis functions. Note that, in this case, $N = 8$ bases are needed in order to assure that $\tau_N(\mu) < 1$ for all μ in $\mathcal{D}$. In Figure 2.11 we show the convergence of the Greedy algorithm, and in Figure 2.12 we show the value of the error and the a posteriori error bound for all μ in $\mathcal{D}$.

As in Section 2.6.1, we compute the error $e_S(\mu)/n_S(\mu)$, in order to compute the error in the EIM approximation of the Smagorinsky term. In Figure 2.13, we show this error for this numerical test. Again, a good approximation between FE and RB solution, provides a good EIM approximation of the Smagorinsky term.

In Figure 2.14 we show a comparison between the FE velocity solution (top) and the RB velocity solution (bottom) for a chosen parameter value $\mu = 4521$. Again, both images are practically equal, as the error between both solutions is of order 10^{-7}.

Finally, we show in Table 2.2 a summary of the results obtained for several values of μ in $\mathcal{D}$. For this test, we also observe a dramatic speedup in the computation of the numerical solution, even larger than in the Backward-facing step test. These large speed-up factors are possibly due to the high turbulent levels of viscosity introduced by the Smagorinsky turbulence model. The offline phase of this test took 2 days to be completed.

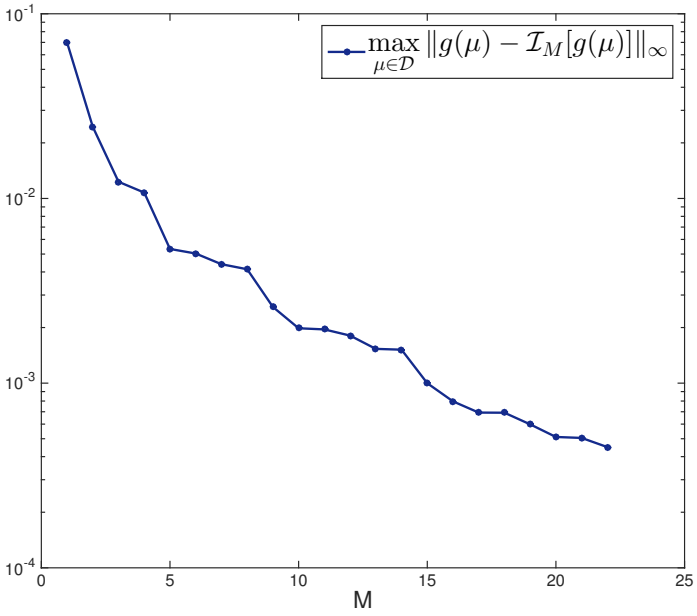

Figure 2.10: Convergence of the EIM algorithm.

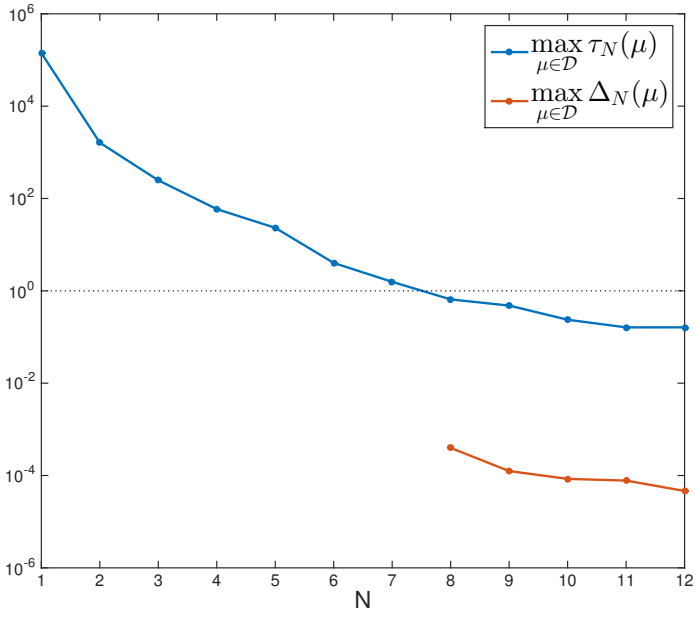

Figure 2.11: Convergence of the Greedy algorithm.

2.7 Conclusions

In this chapter we have developed a reduced basis Smagorinsky model, using the EIM to linearise the non-linear eddy viscosity of the Smagorinsky model.

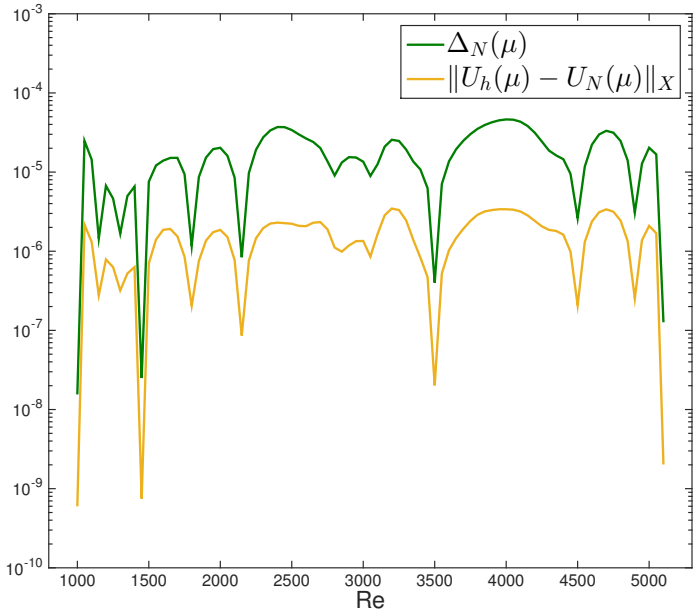

Figure 2.12: Value of $\Delta_{N_{\max}}(\mu)$ and the error between the FE solution and the RB solution.

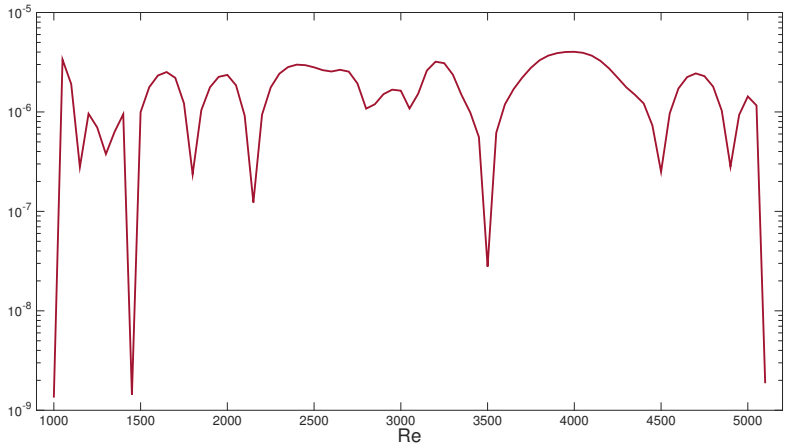

Figure 2.13: Normalized error of the EIM Smagorinsky term approximation.

We have developed an *a posteriori* error bound estimator for the Smagorinsky model, extending the theory in the literature for the incompressible Navier-Stokes equations (*e.g* [72],[36]). With the *a posteriori* error bound estimator we can compute the offline phase in a efficient way, including the computation of the inf-sup stability interpolator, that provides a fast reliable approximation of the

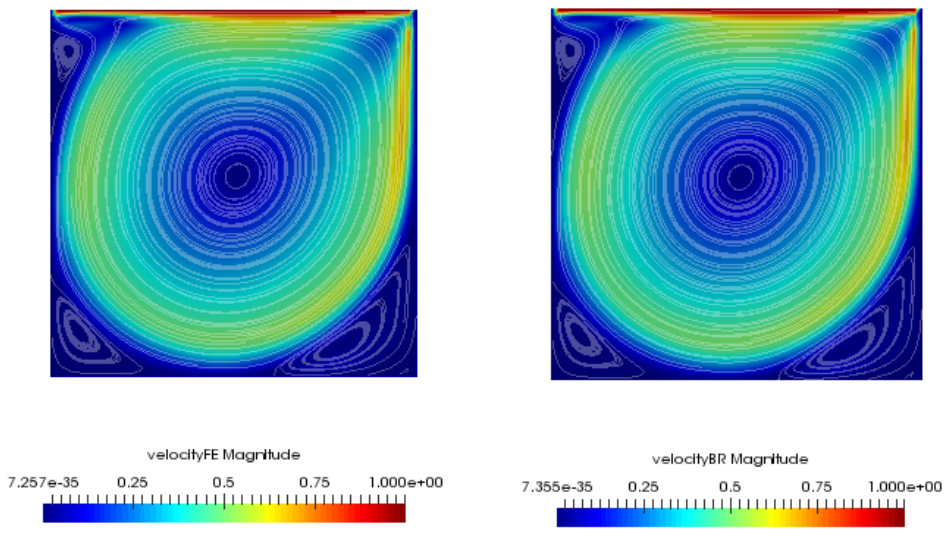

Figure 2.14: FE solution (left) and RB solution (right) for $\mu = 4521$.

Data	$\mu = 1610$	$\mu = 2751$	$\mu = 3886$	$\mu = 4521$	$\mu = 5100$
T_{FE}	638.02s	1027.62s	1369.49s	1583.08s	1699.52s
T_{online}	0.47s	0.47s	0.47s	0.49s	0.52s
speedup	1349	2182	2899	3243	3227
$\|\mathbf{u}_h - \mathbf{u}_N\|_T$	$1.91 \cdot 10^{-6}$	$1.87 \cdot 10^{-6}$	$3.28 \cdot 10^{-6}$	$6.26 \cdot 10^{-7}$	$3.17 \cdot 10^{-9}$
$\|p_h - p_N\|_0$	$1.18 \cdot 10^{-7}$	$3.65 \cdot 10^{-7}$	$3.78 \cdot 10^{-7}$	$8.34 \cdot 10^{-8}$	$1.88 \cdot 10^{-9}$

Table 2.2: Computational time for FE solution and RB online phase, with the speedup and the relative error.

inf-sup stability factor value for each parameter value.

We have presented numerical results for two benchmark cases, where we have shown the accuracy of our reduced model and the dramatic reduction of the computational time for both cases, which is typically divided by nearly 1000. This high speed-up rate is possibly due to the high dissipative effect of the Smagorinsky turbulence model. Extensions to less dissipative turbulence models of VMS kind are presented in the following chapters.

Chapter 3

A Reduced basis VMS-Smagorinsky with local projection pressure stabilization model

3.1 Introduction

In this Chapter we present a reduced basis VMS-Smagorinsky model with local projection stabilization on the pressure. This model differs from the reduced basis Smagorinsky model presented in Chapter 2 fundamentally in two aspects. In the VMS-Smagorinsky model presented in this Chapter, the eddy viscosity term acts only on the resolved small scales while in the Smagorinsky model presented in the previous Chapter, the eddy viscosity acts on both the large and resolved small scales.

We consider a local projection stabilization term for the pressure, derived from the high order term-by-term stabilization method (*cf.* [23, 25]). This methodology allows to obtain more accuracy with respect to the classic penalty stabilization procedure, with a reduced computational cost [25]. The consideration of a pressure stabilization term let us to consider a non-stable pair of finite elements, such as $\mathbb{P}2 - \mathbb{P}2$, with the consequent increase of accuracy in both velocity and the pressure.

Previous works on stabilization for RB methods in advection-diffusion problems (*cf.* [67, 82]) shows the necessity of consider an offline/online stabilization, i.e., to consider the stabilization term both in the FE model and the RB model, instead of only offline stabilization, in order to preserve the consistency of the RB approximation. In our case, we consider the offline/online stabilization for

the pressure without enriching the velocity space with the *supremizer*. The use of this *supremizer* enrichment for the velocity space leads us to a non-consistent RB approximation as shown in section 3.6.

The development of the *a posteriori* error bound estimator for the RB VMS-Smagorinsky model with local projection stabilization on the pressure is done following the same procedure considered in Chapter 2, using the BRR theory. In the online phase, we will also need the EIM to approximate the non-linear and non-affine terms, with respect to the parameter, that takes part in the model considered in this Chapter. Thus, we need to approximate through the EIM the eddy-viscosity term, and the pressure stabilization coefficient. Finally, we present numerical results for the 2D backward-facing step and the 2D cavity steady problems, for which we obtain speed-up rates of several thousands, even larger than for the RB VMS-Smagorinsky model.

The structure of this Chapter is as follows. In section 3.2, we present the VMS-Smagorinsky model with local projection stabilization for the pressure. In subsection 3.2.1, we present the FE model, while the reduced basis method is considered in 3.2.2. The numerical analysis for the well-posedness is presented in section 3.3, and the sub-sequent development of the *a posteriori* error bound estimator in section 3.4. Then, in section 3.5, we present the approximation of the eddy-viscosity and the pressure stabilization constant by the EIM. Finally, we present two numerical tests in section 3.6, in which we highlight the speed-up rates for the computation of solution with the present RB model presented in this Chapter.

3.2 Pressure local projection stabilized VMS-Smagorinsky model

In this section we describe a local projection-stabilized VMS-Smagorinsky model. In this model, we consider that the eddy-viscosity only acts on the small resolved scales. This leads to a less diffusive model than the Smagorinsky one presented in Chapter 2, where the eddy viscosity acts on both large and small resolved scales. We also consider a projection stabilization coefficient for the pressure, that allows us to use non-stable pairs of finite element.

3.2.1 Finite element problem

In this section, we define the FE problem that will be used to compute the snapshots for the RB method. As in Chapter 2, let Ω be a bounded domain of $\mathbb{R}^d (d = 2, 3)$, with Lipschitz-continuous boundary Γ, which we suppose is split

into $\Gamma = \Gamma_D \cup \Gamma_N$. Here, Γ_D is decoupled into $\Gamma_D = \Gamma_{D_0} \cup \Gamma_{D_g}$, where Γ_{D_0} and Γ_{D_g} respectively are the homogeneous and non-homogeneous Dirichlet boundary, while Γ_N is the Neumann one.

To set the VMS-Smagorinsky model, we decompose the velocity and pressure spaces (defined in section 2.2.1), Y and M respectively, as

$$Y = \overline{Y_h} \oplus Y', \quad M = \overline{M_h} \oplus M',$$

where $\overline{Y_h}$ and $\overline{M_h}$ are respectively the large-scale finite dimensional spaces for velocity and pressure, while Y' and M' are the small-scale complementary spaces. We suppose that the large and small scales are separated, by assuming that the sum is direct, i.e., $\overline{Y_h} \cap Y' = \{0\}$ and $\overline{M_h} \cap M' = \{0\}$.

The VMS-Smagorinsky modeling is a discretization of a set of macro-micro scales equations derived from the previous decomposition (see [28] for more details), based upon the following procedure:

(i) Approximate the small-scale spaces Y' and M' by finite-dimensional subspaces of *small resolved scales* Y'_h and M'_h, respectively. Then, $Y' = Y'_h \oplus Y''$, $M' = M'_h \oplus M''$, where Y'' and M'' are complementary spaces of *small unresolved scales* of finite dimension. This yield the unique decompositions

$$\begin{array}{ll} \mathbf{u} = \overline{\mathbf{u}}_h + \mathbf{u}'_h + \mathbf{u}'' & \text{for all } \mathbf{w} \in Y, \\ p = \overline{p}_h + p'_h + p'' & \text{for all } p \in M, \end{array}$$

with obvious notation.

(ii) Neglect the interaction between the large and small unresolved scales. It is assumed that in the interaction of large-small unresolved scales is weak whenever the latter lay inside the inertial spectrum.

(iii) Model the action of small unresolved scales on small resolved in the Navier-Stokes equations by the eddy viscosity procedure.

We denote $Y_h = \overline{Y}_h \oplus Y'_h$ and $M_h = \overline{M}_h \oplus M'_h$. Thus, $\mathbf{u}_h = \overline{\mathbf{u}}_h + \mathbf{u}'_h \in Y_h$ and $p_h = \overline{p}_h + p'_h$.

Let us denote the discrete space $V_h^l(\Omega) = \{r \in C^0(\overline{\Omega}) : r_{|K} \in \mathbb{P}_l(K), \forall K \in \mathcal{T}_h\}$. Thus, we define the velocity and pressure finite element spaces as $Y_h = (V_h^l(\Omega) \cap H_0^1)^d$, and $M_h = V_h^m \cap L^2$. For the sub-grid eddy viscosity modeling in the VMS-Smagorinsky model, let us consider $\overline{Y}_h = \Pi_h Y_h$, with Π_h a uniformly stable interpolation operator on $\overline{Y}_h$, where

$$\overline{Y}_h = [V_h^{l-1}(\Omega)]^d. \tag{3.1}$$

We can also define $\overline{Y}_h = [V_H^l(\Omega)]^d$, where $V_H^l(\Omega)$ a subspace of $V_h^l(\Omega)$ with a larger grid size $H > h$; tipically, $H = 2h$ or $H = 3h$.

With that notation, we are identifying $\overline{Y}_h$ as the large-scales velocity space, and $Y_h' = (Id - \Pi_h)Y_h$ as the resolved small-scales velocity space.

Applying assumptions (i)-(iii) on the Navier-Stokes equations (see [28]) we leads to the VMS-Smagorinsky model. We denote by $\mu \in \mathcal{D} \subset \mathbb{R}$ the parameter considered for the RB problem, which is again the Reynolds number, leading to the following variational formulation problem:

$$\begin{cases} \text{Find } (\mathbf{u}_h, p_h) = (\mathbf{u}_h(\mu), p_h(\mu)) \in Y_h \times M_h \text{ such that} \\ \\ a(\mathbf{u}_h, \mathbf{v}_h; \mu) + b(\mathbf{v}_h, p_h; \mu) + a_S'(\mathbf{w}_h; \mathbf{w}_h, \mathbf{v}_h; \mu) \\ +c(\mathbf{u}_h, \mathbf{u}_h, \mathbf{v}_h; \mu) + c(\mathbf{u}_D, \mathbf{u}_h, \mathbf{v}_h; \mu) \\ +c(\mathbf{u}_h, \mathbf{u}_D, \mathbf{v}_h; \mu) = F(\mathbf{v}_h; \mu) & \forall \mathbf{v}_h \in Y_h \\ b(\mathbf{u}_h, q_h; \mu) = 0 & \forall q_h \in M_h \end{cases} \tag{3.2}$$

were here again, we are denoting $\mathbf{w}_h = \mathbf{u}_h + \mathbf{u}_D$, with $\mathbf{u}_D$ a lift function in the same way as in Chapter 2 (see Sect. 2.2.1). The bilinear forms in (3.2), $a(\cdot, \cdot; \mu)$ and $b(\cdot, \cdot; \mu)$, are defined in the same way that in (2.4); as the trilinear form $c(\cdot, \cdot, \cdot; \mu)$, defined in (2.5).

The non-linear form $a_S'(\cdot; \cdot, \cdot; \mu)$, is a multi-scale Smagorinksy modeling for the eddy viscosity term, and it is given by

$$a_S'(\mathbf{z}_h; \mathbf{u}_h, \mathbf{v}_h; \mu) = \int_\Omega \nu_T(\Pi_h^* \mathbf{z}_h) \nabla(\Pi_h^* \mathbf{u}_h) : \nabla(\Pi_h^* \mathbf{v}_h) \, d\Omega, \tag{3.3}$$

where $\Pi_h^* = Id - \Pi_h$. This interpolation operator Π_h satisfies the following properties of Prop. 3.1, which proof can be found in [11] (Chap. IX).

Definition 3.1. *A family of triangulation $\{\mathcal{T}_h\}_{h>0}$ is regular, in the sense of Ciarlet (cf. [31]), if there exists a constant $\sigma > 0$ independent of h such that*

$$\forall K \in \mathcal{T}_h, \quad \frac{h_K}{\rho_K} \leq \sigma, \tag{3.4}$$

where ρ_K is the diameter of the ball inscribed in K. Moreover, $\{\mathcal{T}_h\}_{h>0}$ is uniformly regular or quasi-uniform if there exists a constant $\kappa > 0$ independent of h such that

$$\forall K \in \mathcal{T}_h, \quad \kappa h \leq h_K \leq \sigma \rho_K. \tag{3.5}$$

In the following, for technical reasons, we are going to consider that $\{\mathcal{T}_h\}_{h>0}$ is uniformly regular. The analysis can be extended in a more general case considering that $\{\mathcal{T}_h\}_{h>0}$ is regular [25].

Proposition 3.1. *Let $\{\mathcal{T}_h\}_{h>0}$ a regular family of triangulations of $\overline{\Omega}$, and $l \geq 1$. Then, there exists an interpolation operator $\Pi_h : L^1(\Omega) \to V_h^l(\Omega)$ that satisfies the following properties:*

1. *For any $v \in L^p(\Omega), 1 \leq p < \infty$:*

$$\|\Pi_h(v)\|_{0,p,K} \leq C_f \|v\|_{0,p,\omega_K} \quad \forall K \in \mathcal{T}_h, \tag{3.6}$$

where we denote by ω_k the union of all elements of $\mathcal{T}_h$ that intersect a element K of $\mathcal{T}_h$. Moreover,

$$\|\Pi_h(v)\|_{0,p,\Omega} \leq C_f \|v\|_{0,p,\Omega}, \tag{3.7}$$

2. *For any $v \in W^{1,p}(\Omega)$:*

$$\|\Pi_h(v)\|_{1,p,\Omega} \leq C_f \|v\|_{1,p,\Omega}. \tag{3.8}$$

The constant $C_f > 0$ in (3.6)-(3.8) only depends on p, Ω, d and the aspect ratio of the family of triangulations.

In VMS terminology, this corresponds to the *Small-Small* setting eddy viscosity term (*cf.* [56]). Other possibilities are the *Large-Small* setting that correspond to model the turbulent viscosity by a function of the whole resolved velocity, taking

$$a'_S(\mathbf{z}_h; \mathbf{u}_h, \mathbf{u}_h) = \int_\Omega \nu_T(\mathbf{z}_h) \nabla(\Pi_h^* \mathbf{u}_h) : \nabla(\Pi_h^* \mathbf{v}_h) \, d\Omega. \tag{3.9}$$

Also, in the standard Smagorinsky LES model, which was developed in Chapter 2, the eddy viscosity term acts both in the large and small scales. Consider either the *Small-Small* or the *Large-Small* setting, rather than the standard Smagorinsky model, avoids over-diffusive effects that leads to more accurate results.

For the practical point of view, in order to obtain good accuracy in the solution, we are interested in consider $\mathbb{P}2$ polynomial approximation for both velocity and pressure. This FE setting needs of a stabilization procedure since it does not verify a discrete inf-sup condition, unless we enrich the velocity space with stabilizing degree of freedom that do not improve the accuracy.

Depending on the stabilization procedure we can distinguish two different kind of methods, the residual-based methods and the penalty methods. As the residual-based stabilization methods let us mention the Galerkin-Least Squares (GALS) (*cf.* [53]) and modifications of this method as the Streamline Upwind Galerkin (SUPG) method (*cf.* [19, 93]), or the Adjoint-Stabilized method (*cf.* [42]). On the other hand, on the penalty methods we particularly mention the

penalty term-by-term stabilized method (*cf.* [23]), that is an extension of the penalty method introduced in [17]. In the latter method, the penalty term acts on the discretization of the pressure gradient.

The stabilization procedure that we consider in this work is a local projection-stabilization, which was introduced in [32], on the pressure gradient.The stabilization procedure considered here is based upon the high-order term-by-term stabilized method (*cf.* [25]), that stabilizes each single operator such as the convection term or pressure grandient. We further consider the stabilization on the pressure gradient.

Thus, we consider the LPS-VMS-Smagorinsky model, with stabilization on the pressure gradient, as

$$\begin{cases} \text{Find } (\mathbf{u}_h, p_h) = (\mathbf{u}_h(\mu), p_h(\mu)) \in Y_h \times M_h \text{ such that} \\ a(\mathbf{u}_h, \mathbf{v}_h; \mu) + b(\mathbf{v}_h, p_h; \mu) + a'_S(\mathbf{w}_h; \mathbf{w}_h, \mathbf{v}_h; \mu) \\ +c(\mathbf{u}_h, \mathbf{u}_h, \mathbf{v}_h; \mu) + c(\mathbf{u}_D, \mathbf{u}_h, \mathbf{v}_h; \mu) \\ +c(\mathbf{u}_h, \mathbf{u}_D, \mathbf{v}_h; \mu) = F(\mathbf{v}_h; \mu) \qquad \forall \mathbf{v}_h \in Y_h, \\ b(\mathbf{u}_h, q_h; \mu) + s_{pres}(p_h, q_h; \mu) = 0 \qquad \forall q_h \in M_h, \end{cases} \tag{3.10}$$

where here $s_{pres}(\cdot, \cdot; \mu)$ is the projection-stabilization term for the pressure, defined as

$$s_{pres}(p_h, q_h; \mu) = \sum_{K \in \mathcal{T}_h} \tau_{p,K}(\mu)(\sigma_h^*(\nabla p_h), \sigma_h^*(\nabla q_h))_K. \tag{3.11}$$

Here, $\tau_{p,K}(\mu)$ is the stabilization coefficient in (3.11), that must verify the following hypotesis:

Hypothesis 3.1. *There exists two positive constants α_1, α_2, independent of h, such that*

$$\alpha_1 h_K^2 \leq \tau_{K,p}(\mu) \leq \alpha_2 h_K^2, \quad \forall \mu \in \mathcal{D}, \forall K \in \mathcal{T}_h, \forall h > 0. \tag{3.12}$$

In the following, we will use the stabilization pressure coefficient $\tau_{p,K}(\mu)$ proposed by Codina in [32], and used in [27, 98]:

$$\tau_{p,K}(\mu) = \left[c_1 \frac{1/\mu + \overline{\nu}_{T_{|K}}(\mu)}{h_K^2} + c_2 \frac{U_K(\mu)}{h_K} \right]^{-1}, \tag{3.13}$$

where $\overline{\nu}_{T_{|K}}$ is some local eddy viscosity, U_K is a local velocity and c_1, c_2 some positive experimental constants. Taking $\tau_{p,K}(\mu)$ by this way, we are ensuring (3.12).

By denoting $X_h = Y_h \times M_h$, we rewrite problem (3.2) as follows

$$\begin{cases} \text{Find } U_h(\mu) = (\mathbf{u}_h, p_h) \in X_h \text{ such that} \\ A(U_h(\mu), V_h; \mu) = F(V_h; \mu) \qquad \forall V_h \in X_h, \end{cases} \tag{3.14}$$

where,

$$\begin{aligned} A(U_h(\mu), V_h; \mu) \; &= \frac{1}{\mu} A_0(U_h, V_h) + A_1(U_h, V_h) + A_2(U_h; V_h) \\ &\quad + A_3(U_h; V_h) + A_{pres}(U_h, V_h), \end{aligned} \tag{3.15}$$

where, denoting $U = (\mathbf{u}, p^u)$, $V = (\mathbf{v}, p^v)$ and $\mathbf{w} = \mathbf{u} + \mathbf{u}_D$, the various terms are defined by

$$\begin{aligned} A_0(U, V) &= \int_\Omega \nabla \mathbf{u} : \nabla \mathbf{v} \; d\Omega, \\ A_1(U, V) &= \int_\Omega (\nabla \cdot \mathbf{u}) p^v \; d\Omega - \int_\Omega (\nabla \cdot \mathbf{v}) p^u \; d\Omega \\ &\quad + \int_\Omega (\mathbf{u}_D \cdot \nabla \mathbf{u}) \mathbf{v} \; d\Omega + \int_\Omega (\mathbf{u} \cdot \nabla \mathbf{u}_D) \mathbf{v} \; d\Omega, \\ A_2(U; V) &= \int_\Omega (\mathbf{u} \cdot \nabla \mathbf{u}) \mathbf{v} \; d\Omega \\ A_3(U; V) &= \int_\Omega \nu_T(\Pi_h^* \mathbf{w}) \, \nabla(\Pi_h^* \mathbf{w}) : \nabla(\Pi_h^* \mathbf{v}) \; d\Omega \\ A_{pres}(U, V) &= \sum_{K \in \mathcal{T}_h} \int_K \tau_{p,K}(\mu) \, \sigma_h^*(\nabla p_u) \cdot \sigma_h^*(\nabla p_v) \; d\Omega \end{aligned}$$

3.2.2 Reduced basis problem

In this section we present the Reduced Basis (RB) model derived from the FE problem (3.14). The computation of the reduced spaces is done through the Greedy algorithm (see section 1.3). The RB problem reads

$$\begin{cases} \text{Find } U_N(\mu) \in X_N \text{ such that} \\ A(U_N(\mu), V_N; \mu) = F(V_N; \mu) \qquad \forall V_N \in X_N. \end{cases} \tag{3.16}$$

Here, the reduced space is defined as $X_N = Y_N \times M_N$, where the reduced velocity space, Y_N, and the pressure reduced space M_N are given by

$$Y_N = \text{span}\{\zeta_i^{\mathbf{v}} := \mathbf{u}(\mu^i), \; i = 1, \ldots, N\}, \tag{3.17}$$

$$M_N = \text{span}\{\xi_i^p := p(\mu^i),\ i = 1, \ldots, N\}. \tag{3.18}$$

In this case, we do not longer consider the *supremizer* for the velocity space enrichment as in the Smagorinsky RB presented in Chapter 2, due to the offline/online stabilization proposed for the RB problem (3.16). With this offline/online stabilization, the inner pressure *supremizer* operator is no longer necessary to recover the pressure. Moreover, as we show in section 3.6, the consideration of the *supremizer* operator for the velocity space enrichment is counterproductive, because the RB solution is no longer consistent with respect to the FE solution, i.e., the fact that

$$U_N(\mu^k) = U_h(\mu^k), \quad \forall \mu^k \in S = \{\mu^1, \ldots, \mu^N\}, \tag{3.19}$$

where $S = \{\mu^1, \ldots, \mu^N\}$ is the set of parameter values chosen in the Greedy algorithm. The fact of losing the consistency causes that the Greedy algorithm rechooses a parameter value previously chosen, making the matrix of the RB problem singular.

Remark 3.1. *Note that the reduced space X_N in problem 3.16 has dimension $2N$, in contrast with the reduced space of problem 2.10 that has dimension $3N$, due to the supremizer velocity space enrichment. This is relevant for strongly non-linear problems, as in the case here, where N may be large.*

3.3 Well-posedness analysis

In this section we study the well-posedness of problem (3.14). The numerical analysis of the projection-based VMS-Smagorinsky model can be found in [27]. In this section, we analyse the projection-stabilized VMS-Smagorinsky model using the BRR theory as done in Chapter 2 for the Smagorinsky model.

Let us introduce the following scalar product

$$(f, g)_{\tau_p} = \sum_{K \in \mathcal{T}_h} \int_K \tau_{p,K}\ f\ g\ d\Omega, \quad \forall f, g \in L^2(\Omega), \tag{3.20}$$

and its associated norm $\|f\|_{\tau_p} = (f, f)_{\tau_p}^{1/2}$. The following bound is satisfied:

Lemma 3.1. *Assume Hypothesis 3.1 holds, and let $q_h \in V_h^l(\Omega)$. Then,*

$$\|\sigma_h^*(\nabla q_h)\|_{\tau_p} \leq C_\tau \|q_h\|_{0,2,\Omega} \tag{3.21}$$

Proof. Taking into account Hypothesis 3.1, and Proposition 3.1, it holds

$$\|\sigma_h^*(\nabla q_h)\|_{\tau_p}^2 \leq Ch^2 \|\sigma_h^*(\nabla q_h)\|_{0,2,\Omega}^2 \leq Ch^2 \|\nabla q_h\|_{0,2,\Omega}^2. \tag{3.22}$$

Considering the local inverse inequalities of Lemma 2.1 in (3.22), we have that

$$\|\sigma_h^*(\nabla q_h)\|_{\tau_p}^2 \leq Ch^2 \|\nabla q_h\|_{0,2,\Omega}^2 \leq C\|q_h\|_{0,2,\Omega}^2,$$

deducing (3.21). □

We also consider a modification in the weight of the scalar product introduced in (2.6). Taking the same notation as in (2.6), let

$$(\mathbf{u}_h, \mathbf{v}_h)_T = \int_\Omega \left[\frac{1}{\overline{\mu}} + \nu_T'^*\right] \nabla \mathbf{u}_h : \nabla \mathbf{v}_h \, d\Omega \qquad \forall \mathbf{u}_h, \mathbf{v}_h \in Y_h, \tag{3.23}$$

where $\nu_T'^* = \nu_T(\Pi_h^* \mathbf{w}_h(\overline{\mu}))$, and

$$\overline{\mu} = \arg\min_{\mu \in \mathcal{D}} \sum_{K \in \mathcal{T}_h} (C_S h_K)^2 \min_{x \in K} |\nabla(\Pi_h^* \mathbf{w}_h)(\mu)|(x) \chi_K(x),$$

with $\mathbf{w}_h(\mu)$ the velocity solution of (3.10). Here again, we define the norm of space X_h as

$$\|U_h\|_X = \sqrt{\|\mathbf{u}_h\|_T^2 + \|p_h\|_{0,2,\Omega}^2} \qquad \forall U_h = (\mathbf{u}_h, p_h) \in X_h. \tag{3.24}$$

The analysis of the convergence and stability of the projection-stabilized VMS-Smagorinsky can be found in [27]. Particularly, for a uniformly regular triangulation, it holds

Proposition 3.2. *The following discrete inf-sup condition is verified*

$$\|q_h\|_{0,2,\Omega} \leq \alpha \left(\sup_{\boldsymbol{v}_h \in Y_h} \frac{(q_h, \nabla \cdot \boldsymbol{v}_h)_\Omega}{\|\nabla \boldsymbol{v}_h\|_{0,2,\Omega}} + \|\sigma_h^*(\nabla q_h)\|_{\tau_p}^2 \right) \quad \forall q_h \in M_h, \tag{3.25}$$

with $\alpha > 0$, independent of h.

The demonstration of this inf-sup condition can be derived from [25]. This result can be extended considering that the triangulation $\{\mathcal{T}_h\}_{h>0}$ is regular rather than uniformly regular. For further details, see [25].

Let us consider the directional derivative of the operator $A(\cdot, \cdot; \mu)$. If we derive

each operator term in (3.15), we get

$$\begin{aligned}
\partial_1 A_0(U,V)(Z) &= A_0(Z,V),\\
\partial_1 A_1(U,V)(Z) &= A_1(Z,V),\\
\partial_1 A_2(U;V)(Z) &= \int_\Omega (\mathbf{u}\cdot\nabla\mathbf{z})\mathbf{v}\; d\Omega + \int_\Omega (\mathbf{z}\cdot\nabla\mathbf{u})\mathbf{v}\; d\Omega,\\
\partial_1 A_3(U;V)(Z) &= \int_\Omega \nu_T(\Pi_h^*\mathbf{w})\,\nabla(\Pi_h^*\mathbf{z}) : \nabla(\Pi_h^*\mathbf{v})\; d\Omega,\\
&\quad + \sum_{K\in\mathcal{T}_h}\int_K (C_S h_K)^2 \frac{\nabla(\Pi_h^*\mathbf{w}) : \nabla(\Pi_h^*\mathbf{z})}{|\nabla(\Pi_h^*\mathbf{w})|}\big(\nabla(\Pi_h^*\mathbf{w}) : \nabla(\Pi_h^*\mathbf{v})\big)\; d\Omega,\\
\partial_1 A_{pres}(U,V)(Z) &= A_{pres}(Z,V).
\end{aligned}$$

According to the BRR theory (*cf.* [18, 22]), the well-posedness problem (3.14) is guaranteed by the following continuity and inf-sup conditions:

$$\infty > \gamma_0 < \gamma_h(\mu) \equiv \sup_{Z_h\in X_h}\sup_{V_h\in X_h} \frac{\partial_1 A(U_N(\mu),V_h;\mu)(V_h)}{\|Z_h\|_X\|V_h\|_X}. \tag{3.26}$$

$$0 < \beta_0 < \beta_h(\mu) \equiv \inf_{Z_h\in X_h}\sup_{V_h\in X_h} \frac{\partial_1 A(U_N(\mu),V_h;\mu)(Z_h)}{\|Z_h\|_X\|V_h\|_X}. \tag{3.27}$$

The existence of $\gamma_0 \in \mathbb{R}$ and $\beta_0 > 0$ satisfying (3.26) and (3.27), respectively, are given by the following results:

Proposition 3.3. *There exists* $\gamma_0 \in \mathbb{R}$ *such that* $\forall \mu \in \mathcal{D}$

$$|\partial_1 A(U_h(\mu),V_h;\mu)(Z_h)| \le \gamma_0 \|Z_h\|_X\|V_h\|_X \quad \forall Z_h, V_h \in X_h.$$

Proof. It holds,

$$|\partial_1 A(U_h(\mu),V_h;\mu)(Z_h)| \le \frac{1}{\mu}|\partial_1 A_0(U_h(\mu),V_h)(Z_h)| + |\partial_1 A_1(U_h(\mu),V_h)(Z_h)|$$

$$+|\partial_1 A_2(U_h(\mu),V_h)(Z_h)| + |\partial_1 A_3(U_h(\mu);V_h)(Z_h)| + |\partial_1 A_{pres}(U_h(\mu),V_h)(Z_h)|.$$

From Prop. 2.1, we can deduce the boundedness of $|\partial_1 A_0(U_h(\mu),V_h;\mu)(Z_h)|$, $|\partial_1 A_1(U_h(\mu),V_h)(Z_h)|$, and $|\partial_1 A_2(U_h(\mu);V_h)(Z_h)|$. To bound $|\partial_1 A_3(U_h(\mu);V_h)(Z_h)|$,

we consider Prop. 3.1, and the inverse inequalities of Lemma 2.1. It holds,

$$\begin{aligned}
|\partial_1 A_3(U_h(\mu);V_h)(Z_h)| \leq & \int_\Omega (C_S h)^2 |\nabla(\Pi_h^* \mathbf{w})||\nabla(\Pi_h^* \mathbf{z})||\nabla(\Pi_h^* \mathbf{v})| \, d\Omega, \\
& + \int_\Omega (C_S h)^2 \frac{|\nabla(\Pi_h^* \mathbf{w})||\nabla(\Pi_h^* \mathbf{z})|}{|\nabla(\Pi_h^* \mathbf{w})|} |\nabla(\Pi_h^* \mathbf{w})||\nabla(\Pi_h^* \mathbf{v})| \, d\Omega, \\
& \leq 2(C_S h)^2 \|\nabla(\Pi_h^* \mathbf{w})\|_{0,3,\Omega} \|\nabla(\Pi_h^* \mathbf{z})\|_{0,3,\Omega} \|\nabla(\Pi_h^* \mathbf{v})\|_{0,3,\Omega} \\
& \leq 2C_S^2 h^{2-d/3} \|\nabla(\Pi_h^* \mathbf{w})\|_{0,3,\Omega} \|\nabla(\Pi_h^* \mathbf{z})\|_{0,2,\Omega} \|\nabla(\Pi_h^* \mathbf{v})\|_{0,2,\Omega} \\
& \leq 2C_f^2 C_S^2 h^{2-d/3} \|\nabla(\Pi_h^* \mathbf{w})\|_{0,3,\Omega} \|\nabla \mathbf{z}\|_{0,2,\Omega} \|\nabla \mathbf{v}\|_{0,2,\Omega} \\
& \leq 2C^2 C_f^2 C_S^2 h^{2-d/3} \|\nabla(\Pi_h^* \mathbf{w})\|_{0,3,\Omega} \|\nabla \mathbf{z}\|_T \|\nabla \mathbf{v}\|_T \\
& \leq C_3 \|Z_h\|_X \|V_h\|_X.
\end{aligned}$$

The last term can be bounded using Lemma 3.1, and Cauchy-Schwartz inequality:

$$\begin{aligned}
|\partial_1 A_{pres}(U_h(\mu);V_h)(Z_h)| \leq & \sum_{K \in \mathcal{T}_h} \int_K \tau_{p,K}(\mu) |\sigma_h^*(\nabla p_h^z)||\sigma_h^*(\nabla p_h^v)| \, d\Omega \\
& \leq \|\sigma_h^*(\nabla p_h^z)\|_{\tau_p} \|\sigma_h^*(\nabla p_h^v)\|_{\tau_p} \leq C_\tau^2 \|p_h^z\|_{0,2,\Omega} \|p_h^v\|_{0,2,\Omega} \\
& \leq C_4 \|Z_h\|_X \|V_h\|_X.
\end{aligned}$$

Thus, we have proved that there exists γ_0 such that

$$\infty > \gamma_0 > \gamma_h(\mu) = \sup_{Z_h \in X_h} \sup_{V_h \in X_h} \frac{\partial_1 A(U_h(\mu), V_h; \mu)(Z_h)}{\|Z_h\|_X \|V_h\|_X}.$$

□

Proposition 3.4. *Let* $C^\star = C_T^2(C_{\overline{\mu}} + 1)$. *Suppose that*

$$\|\nabla \boldsymbol{u}_D\|_{0,2,\Omega} < \frac{1}{\mu C_{\overline{\mu}}^2 C^\star}, \text{ and } \|\nabla \boldsymbol{u}_h\|_{0,2,\Omega} \leq \frac{1}{\mu C_{\overline{\mu}}^2 C^\star} - \|\nabla \boldsymbol{u}_D\|_{0,2,\Omega}.$$

Then, there exists $\tilde{\beta}_h(\mu) > 0$ *such that,*

$$\partial_1 A(U_h, V_h; \mu)(V_h) \geq \tilde{\beta}_h(\mu) \|\boldsymbol{v}_h\|_T^2 \qquad \forall V_h \in X_h. \tag{3.28}$$

Proof. We consider $Z_h = V_h$ in $\partial_1 A(U_h, V_h; \mu)(Z_h)$, having

$$\begin{aligned}
\partial_1 A(U_h, V_h; \mu)(V_h) = & \frac{1}{\mu} \partial_1 A_0(U_h, V_h)(V_h) + \partial_1 A_1(U_h, V_h)(V_h) \\
& + \partial_1 A_2(U_h, V_h)(V_h) + \partial_1 A_3(U_h; V_h)(V_h) + \partial_1 A_{pres}(U_h, V_h)(V_h).
\end{aligned} \tag{3.29}$$

First of all, note that $\partial_1 A_{pres}(U_h, V_h)(V_h) = \|\sigma_h^*(p_h^v)\|_{\tau_p}^2 \geq 0$. Moreover,

$$\partial_1 A_3(U_h; V_h)(V_h) = \int_\Omega \nu_T(\nabla(\Pi_h^* \mathbf{w}_h))|\nabla(\Pi_h^* \mathbf{v}_h)|^2 \, d\Omega$$

$$+ \sum_{K \in \mathcal{T}_h} \int_K (C_S h_K)^2 \frac{|\nabla(\Pi_h^* \mathbf{w}_h) : \nabla(\Pi_h^* \mathbf{v}_h)|^2}{|\nabla(\Pi_h^* \mathbf{w}_h)|} \, d\Omega \geq 0.$$

Thus,

$$\partial_1 A(U_h, V_h; \mu)(V_h) \geq \frac{1}{\mu}\|\nabla \mathbf{v}\|_{0,2,\Omega}^2 + \int_\Omega (\mathbf{w}_h \cdot \nabla \mathbf{v}_h)\mathbf{v}_h \, d\Omega + \int_\Omega (\mathbf{v}_h \cdot \nabla \mathbf{w}_h)\mathbf{v}_h \, d\Omega$$

$$\geq \frac{1}{\mu C_{\overline{\mu}}^2}\|\mathbf{v}_h\|_T^2 - \|\mathbf{w}_h\|_{0,4,\Omega}\|\nabla \mathbf{v}_h\|_{0,2,\Omega}\|\mathbf{v}_h\|_{0,4,\Omega} - \|\mathbf{v}_h\|_{0,4,\Omega}^2\|\nabla \mathbf{w}_h\|_{0,2,\Omega}$$

$$\geq \frac{1}{\mu C_{\overline{\mu}}^2}\|\mathbf{v}_h\|_T^2 - C_T^2 C_{\overline{\mu}}\|\nabla \mathbf{w}_h\|_{0,2,\Omega}\|\mathbf{v}_h\|_T - C_T^2\|\nabla \mathbf{w}_h\|_{0,2,\Omega}\|\mathbf{v}_h\|_T^2$$

$$\geq \left[\frac{1}{\mu C_{\overline{\mu}}^2} - (C_{\overline{\mu}} + 1)C_T^2\|\nabla \mathbf{w}_h\|_{0,2,\Omega}\right] \|\mathbf{v}_h\|_T^2$$

$$\geq \left[\frac{1}{\mu C_{\overline{\mu}}^2} - (C_{\overline{\mu}} + 1)C_T^2\|\nabla \mathbf{u}_h\|_{0,2,\Omega} - (C_{\overline{\mu}} + 1)C_T^2\|\nabla \mathbf{u}_D\|_{0,2,\Omega}\right] \|\mathbf{v}_h\|_T^2.$$

If $\|\nabla \mathbf{u}_D\|_{0,2,\Omega} < \dfrac{1}{\mu C_{\overline{\mu}}^2 C^\star}$, and $\|\nabla \mathbf{u}_h\|_{0,2,\Omega} \leq \dfrac{1}{\mu C_{\overline{\mu}}^2 C^\star} - \|\nabla \mathbf{u}_D\|_{0,2,\Omega}$, then there exists $\tilde{\beta}_h(\mu) > 0$ such that,

$$\partial_1 A(U_h, V_h; \mu)(V_h) \geq \tilde{\beta}_h(\mu)\|\mathbf{v}_h\|_T^2 \qquad \forall V_h \in X_h.$$

□

The inf-sup condition (3.27) is verified thanks to the fact that the operator $b(v_h, q_h; \mu)$ satisfies the discrete inf-sup condition (3.2). Moreover, the condition of proposition 3.4 is verified when the Dirichlet boundary data is sufficiently small.

3.4 *A posteriori* error bound estimator

In this section we develop the *a posteriori* error bound estimator used in the hierarchical construction of the reduced space during the Greedy algorithm. We use the Brezzi-Rapaz-Raviart (BRR) theory [18].

Lemma 3.2. *There exists a positive constant ρ_T such that, $\forall U_h^1, U_h^2, Z_h, V_h \in X_h$,*

$$\left|\partial_1 A(U_h^1, V_h; \mu)(Z_h) - \partial_1 A(U_h^2, V_h; \mu)(Z_h)\right| \leq \rho_T \|U_h^1 - U_h^2\|_X \|Z_h\|_X \|V_h\|_X. \tag{3.30}$$

Proof. We have that

$$\begin{aligned}
&\partial_1 A(U_h^1, V_h; \mu)(Z_h) - \partial_1 A(U_h^2, V_h; \mu)(Z_h) = \int_\Omega ((\mathbf{u}_h^1 - \mathbf{u}_h^2) \cdot \nabla \mathbf{z}_h)\mathbf{v}_h \, d\Omega \\
&+\int_\Omega (\mathbf{z}_h \cdot \nabla(\mathbf{u}_h^1 - \mathbf{u}_h^2))\mathbf{v}_h \, d\Omega + \int_\Omega \left[\nu_T(\Pi_h^* \mathbf{u}_h^1) - \nu_T(\Pi_h^* \mathbf{u}_h^2)\right] \nabla(\Pi_h^* \mathbf{z}_h) : \nabla(\Pi_h^* \mathbf{v}_h) \, d\Omega \\
&+ \sum_{K \in \mathcal{T}_h} \int_K (C_S h_K)^2 \frac{\nabla(\Pi_h^* \mathbf{u}_h^1) : \nabla(\Pi_h^* \mathbf{z}_h)}{|\nabla(\Pi_h^* \mathbf{u}_h^1)|} \left(\nabla(\Pi_h^* \mathbf{u}_h^1) : \nabla(\Pi_h^* \mathbf{v}_h)\right) \, d\Omega \\
&- \sum_{K \in \mathcal{T}_h} \int_K (C_S h_K)^2 \frac{\nabla(\Pi_h^* \mathbf{u}_h^2) : \nabla(\Pi_h^* \mathbf{z}_h)}{|\nabla(\Pi_h^* \mathbf{u}_h^2)|} \left(\nabla(\Pi_h^* \mathbf{u}_h^2) : \nabla(\Pi_h^* \mathbf{v}_h)\right) \, d\Omega.
\end{aligned}$$

Thanks to the triangular inequality, it holds

$$\begin{aligned}
|\partial_1 A(U_h^1, V_h; \mu)(Z_h) - \partial_1 A(U_h^2, V_h; \mu)(Z_h)| \leq &\left| \int_\Omega ((\mathbf{u}_h^1 - \mathbf{u}_h^2) \cdot \nabla \mathbf{z}_h)\mathbf{v}_h \, d\Omega \right| \\
&+ \left| \int_\Omega (\mathbf{z}_h \cdot \nabla(\mathbf{u}_h^1 - \mathbf{u}_h^2))\mathbf{v}_h \, d\Omega \right| \\
&+ \left| \int_\Omega \left[\nu_T(\Pi_h^* \mathbf{u}_h^1) - \nu_T(\Pi_h^* \mathbf{u}_h^2)\right] \nabla(\Pi_h^* \mathbf{z}_h) : \nabla(\Pi_h^* \mathbf{v}_h) \, d\Omega \right| \\
&+ \left| \sum_{K \in \mathcal{T}_h} \int_K (C_S h_K)^2 \frac{\nabla(\Pi_h^* \mathbf{u}_h^1) : \nabla(\Pi_h^* \mathbf{z}_h)}{|\nabla(\Pi_h^* \mathbf{u}_h^1)|} \left(\nabla(\Pi_h^* \mathbf{u}_h^1) : \nabla(\Pi_h^* \mathbf{v}_h)\right) \, d\Omega \right. \\
&\left. - \sum_{K \in \mathcal{T}_h} \int_K (C_S h_K)^2 \frac{\nabla(\Pi_h^* \mathbf{u}_h^2) : \nabla(\Pi_h^* \mathbf{z}_h)}{|\nabla(\Pi_h^* \mathbf{u}_h^2)|} \left(\nabla(\Pi_h^* \mathbf{u}_h^2) : \nabla(\Pi_h^* \mathbf{v}_h)\right) \, d\Omega \right|.
\end{aligned} \tag{3.31}$$

We bound each term in (3.31) separately. The two first terms are bounded as in Lemma 2.2. For the third term, we use use the local inverse inequalities of Lemma 2.1 and the properties of proposition 3.1

$$\begin{aligned}
&\left| \int_\Omega \left(\nu_T(\Pi_h^* \mathbf{u}_h^1) - \nu_T(\Pi_h^* \mathbf{u}_h^2)\right) \nabla(\Pi_h^* \mathbf{z}_h) : \nabla(\Pi_h^* \mathbf{v}_h) \, d\Omega \right| \\
&\leq \sum_{K \in \mathcal{T}_h} \int_K (C_S h_K)^2 \left| |\nabla(\Pi_h^* \mathbf{u}_h^1)| - |\nabla(\Pi_h^* \mathbf{u}_h^2)| \right| |\nabla(\Pi_h^* \mathbf{z}_h)| |\nabla(\Pi_h^* \mathbf{v}_h)| \, d\Omega \\
&\leq (C_S h)^2 \int_\Omega |\nabla\left(\Pi_h^*(\mathbf{u}_h^1 - \mathbf{u}_h^2)\right)| |\nabla(\Pi_h^* \mathbf{z}_h)| |\nabla(\Pi_h^* \mathbf{v}_h)| \, d\Omega
\end{aligned}$$

$$\leq (C_S h)^2 \|\nabla\big(\Pi_h^*(\mathbf{u}_h^1 - \mathbf{u}_h^2)\big)\|_{0,3,\Omega} \|\nabla(\Pi_h^*\mathbf{z}_h)\|_{0,3,\Omega} \|\nabla(\Pi_h^*\mathbf{v}_h)\|_{0,3,\Omega}$$
$$\leq C_S^2 h^{2-d/2} C \|\nabla\big(\Pi_h^*(\mathbf{u}_h^1 - \mathbf{u}_h^2)\big)\|_{0,2,\Omega} \|\nabla(\Pi_h^*\mathbf{z}_h)\|_{0,2,\Omega} \|\nabla(\Pi_h^*\mathbf{v}_h)\|_{0,2,\Omega}$$
$$\leq C_S^2 h^{2-d/2} C C_f^3 \|\nabla(\mathbf{u}_h^1 - \mathbf{u}_h^2)\|_{0,2,\Omega} \|\nabla\mathbf{z}_h\|_{0,2,\Omega} \|\nabla\mathbf{v}_h\|_{0,2,\Omega}$$
$$\leq C_S^2 h^{2-d/2} C C_f^3 \|U_h^1 - U_h^2\|_X \|Z_h\|_X \|V_h\|_X$$

The last term in (3.31) is bounded as follows:

$$\left| \sum_{K\in\mathcal{T}_h} \int_K (C_S h_K)^2 \frac{\nabla(\Pi_h^*\mathbf{u}_h^1) : \nabla(\Pi_h^*\mathbf{z}_h)}{|\nabla(\Pi_h^*\mathbf{u}_h^1)|} \big(\nabla(\Pi_h^*\mathbf{u}_h^1) : \nabla(\Pi_h^*\mathbf{v}_h)\big)\, d\Omega \right.$$
$$\left. - \sum_{K\in\mathcal{T}_h} \int_K (C_S h_K)^2 \frac{\nabla(\Pi_h^*\mathbf{u}_h^2) : \nabla(\Pi_h^*\mathbf{z}_h)}{|\nabla(\Pi_h^*\mathbf{u}_h^2)|} \big(\nabla(\Pi_h^*\mathbf{u}_h^2) : \nabla(\Pi_h^*\mathbf{v}_h)\big)\, d\Omega \right|$$
$$= \left| \sum_{K\in\mathcal{T}_h} \int_K (C_S h_K)^2 \left[\frac{\nabla(\Pi_h^*\mathbf{u}_h^1) : \nabla(\Pi_h^*\mathbf{z}_h)}{|\nabla(\Pi_h^*\mathbf{u}_h^1)|} \big(\nabla(\Pi_h^*\mathbf{u}_h^1 - \Pi_h^*\mathbf{u}_h^2) : \nabla(\Pi_h^*\mathbf{v}_h)\big) \right.\right.$$
$$+ \frac{\nabla(\Pi_h^*\mathbf{u}_h^1 - \Pi_h^*\mathbf{u}_h^2) : \nabla(\Pi_h^*\mathbf{z}_h)}{|\nabla(\Pi_h^*\mathbf{u}_h^2)|} \big(\nabla(\Pi_h^*\mathbf{u}_h^2) : \nabla(\Pi_h^*\mathbf{v}_h)\big)$$
$$\left.\left. + \frac{(|\nabla(\Pi_h^*\mathbf{u}_h^2)| - |\nabla(\Pi_h^*\mathbf{u}_h^1)|)\nabla(\Pi_h^*\mathbf{u}_h^1) : \nabla(\Pi_h^*\mathbf{z}_h)}{|\nabla(\Pi_h^*\mathbf{u}_h^1)||\nabla(\Pi_h^*\mathbf{u}_h^2)|} \big(\nabla(\Pi_h^*\mathbf{u}_h^2) : \nabla(\Pi_h^*\mathbf{v}_h)\big) \right] d\Omega \right|$$
$$\leq \sum_{K\in\mathcal{T}_h} \int_K (C_S h_K)^2 |\nabla(\Pi_h^*\mathbf{z}_h)||\nabla(\Pi_h^*\mathbf{u}_h^1 - \Pi_h^*\mathbf{u}_h^2)||\nabla(\Pi_h^*\mathbf{v}_h)|\, d\Omega$$
$$+ \sum_{K\in\mathcal{T}_h} \int_K (C_S h_K)^2 |\nabla(\Pi_h^*\mathbf{u}_h^1 - \Pi_h^*\mathbf{u}_h^2)||\nabla(\Pi_h^*\mathbf{z}_h)||\nabla(\Pi_h^*\mathbf{v}_h)|\, d\Omega$$
$$+ \sum_{K\in\mathcal{T}_h} \int_K (C_S h_K)^2 \big||\nabla(\Pi_h^*\mathbf{u}_h^1)| - |\nabla(\Pi_h^*\mathbf{u}_h^2)|\big| |\nabla(\Pi_h^*\mathbf{z}_h)||\nabla(\Pi_h^*\mathbf{v}_h)|\, d\Omega$$
$$\leq 3(C_S h)^2 \|\nabla(\Pi_h^*\mathbf{u}_h^1 - \Pi_h^*\mathbf{u}_h^2)\|_{0,3,\Omega} \|\nabla(\Pi_h^*\mathbf{z}_h)\|_{0,3,\Omega} \|\nabla(\Pi_h^*\mathbf{v}_h)\|_{0,3,\Omega}$$
$$\leq 3C_S^2 h^{2-d/2} C \|\nabla(\Pi_h^*\mathbf{u}_h^1 - \Pi_h^*\mathbf{u}_h^2)\|_{0,2,\Omega} \|\nabla(\Pi_h^*\mathbf{z}_h)\|_{0,2,\Omega} \|\nabla(\Pi_h^*\mathbf{v}_h)\|_{0,2,\Omega}$$
$$\leq 3C_S^2 h^{2-d/2} C C_f^3 \|\nabla(\mathbf{u}_h^1 - \mathbf{u}_h^2)\|_{0,2,\Omega} \|\nabla\mathbf{z}_h\|_{0,2,\Omega} \|\nabla\mathbf{v}_h\|_{0,2,\Omega}$$
$$\leq 3C_S^2 h^{2-d/2} C C_f^3 \|U_h^1 - U_h^2\|_X \|Z_h\|_X \|V_h\|_X.$$

Thus, we have just proved that

$$\big|\partial_1 A(U_h^1, V_h; \mu)(Z_h) - \partial_1 A(U_h^2, V_h; \mu)(Z_h)\big| \leq \rho_T \|U_h^1 - U_h^2\|_X \|Z_h\|_X \|V_h\|_X,$$

with, $\rho_T = 2C_T + 4C_S^2 h^{2-d/2} C C_f^3$. □

We define the following inf-sup and continuity constants, associated to the well-posedness of the RB problem (3.16):

$$0 < \beta_N(\mu) \equiv \inf_{Z_h \in X_h} \sup_{V_h \in X_h} \frac{\partial_1 A(U_N(\mu), V_h; \mu)(Z_h)}{\|Z_h\|_X \|V_h\|_X} = \inf_{Z_h \in X_h} \frac{\|T_N Z_h\|_X}{\|Z_h\|_X}, \tag{3.32}$$

$$\infty > \gamma_N(\mu) \equiv \sup_{Z_h \in X_h} \sup_{V_h \in X_h} \frac{\partial_1 A(U_N(\mu), V_h; \mu)(Z_h)}{\|Z_h\|_X \|V_h\|_X} = \sup_{Z_h \in X_h} \frac{\|T_N Z_h\|_X}{\|Z_h\|_X}, \tag{3.33}$$

where the *supremizer* operator T_N is defined in (2.24). Let us recall the definition of the *a posteriori* error bound estimator:

$$\Delta_N(\mu) = \frac{\beta_N(\mu)}{2\rho_T} \left[1 - \sqrt{1 - \tau_N(\mu)}\right], \tag{3.34}$$

where $\tau_N(\mu)$ is given by

$$\tau_N(\mu) = \frac{4\epsilon_N(\mu)\rho_T}{\beta_N^2(\mu)}, \tag{3.35}$$

with $\epsilon_N(\mu)$ the dual norm of the residual. The *a posteriori* error bound estimator is stated by the following result

Theorem 3.1. *Let $\mu \in \mathcal{D}$, and assume that $\beta_N(\mu) > 0$. If problem (3.14) admits a solution $U_h(\mu)$ such that*

$$\|U_h(\mu) - U_N(\mu)\|_X \leq \frac{\beta_N(\mu)}{\rho_T},$$

then this solution is unique in the ball $B_X\left(U_N(\mu), \dfrac{\beta_N(\mu)}{\rho_T}\right)$.

Moreover, assume that $\tau_N(\mu) \leq 1$ for all $\mu \in \mathcal{D}$. Then there exists a unique solution $U_h(\mu)$ of (3.14) such that the error with respect $U_N(\mu)$, solution of (3.16), is bounded by the a posteriori error bound estimator, i.e.,

$$\|U_h(\mu) - U_N(\mu)\|_X \leq \Delta_N(\mu), \tag{3.36}$$

with effectivity

$$\Delta_N(\mu) \leq \left[\frac{2\gamma_N(\mu)}{\beta_N(\mu)} + \tau_N(\mu)\right] \|U_h(\mu) - U_N(\mu)\|_X. \tag{3.37}$$

The proof of this Theorem can be derived from the proofs of Theorem 2.1 and Theorem 2.2, defining analogously the operators (2.28)-(2.30) in the same way for the operator $A(\cdot, \cdot; \mu)$ of problem 3.14 and its derivative. Thus, using in the

same way the continuity and inf-sup properties and Lemma 3.2, we can prove (3.36) and (3.37).

□

3.5 Approximation of eddy viscosity term and pressure stabilizing coefficient

In this section, we present the approximation of the non-linear terms with respect to the parameter, throughout the Empirical Interpolation Method [45, 9].

Both the Small-Small setting of the Smagorinsky eddy-diffusion term defined in (3.15), $\nu_T(\Pi_h^*(\nabla \mathbf{w})) := \nu_T(\mu)$, and the pressure stabilization coefficient, $\tau_{p,K}(\mu)$, defined in (3.11) have a non-linear representation with respect to the parameter, and consequently need to be linearised with the EIM.

As the approximation done for the Smagorinsky term in section 2.5, we consider an approximation of the eddy-viscosity term and the pressure-stabilization term. For this purpose, we need to build two reduced-basis spaces $W_{M_1}^S = \{q_1^S(\mu), \dots, q_{M_1}^S(\mu)\}$ and $W_{M_2}^P = \{q_1^P(\mu), \dots, q_{M_2}^P(\mu)\}$ by a greedy procedure selection, with $W_{M_1}^S$ and $W_{M_2}^P$ the EIM reduced spaces associated to the eddy-viscosity term and the pressure-stabilization term, respectively.

Thus, we approximate them by the following trilinear forms:

$$\begin{aligned} a'_S(\mathbf{w}_N; \mathbf{w}_N, \mathbf{v}_N; \mu) &\approx \hat{a}'_S(\mathbf{w}_N, \mathbf{v}_N; \mu), \\ s_{pres}(p_N, q_N; \mu) &\approx \hat{s}_{pres}(p_N, q_N; \mu), \end{aligned} \tag{3.38}$$

where,

$$\begin{aligned} \hat{a}'_S(\mathbf{w}_N, \mathbf{v}_N; \mu) &= \sum_{k=1}^{M_1} \sigma_k^S(\mu) s(q_k^S, \mathbf{w}_N, \mathbf{v}_N), \\ \hat{s}_{pres}(p_N, q_N; \mu) &= \sum_{k=1}^{M_2} \sigma_k^P(\mu) r(q_k^P, p_N, q_N), \end{aligned} \tag{3.39}$$

with,

$$\begin{aligned} s(q_k^S, \mathbf{w}_N, \mathbf{v}_N) &= \sum_{K \in \mathcal{T}_h} \left(q_k^S \, \nabla(\Pi_h^* \mathbf{w}_N), \nabla(\Pi_h^* \mathbf{v}_N) \right)_K, \\ r(q_k^P, p_N, q_N) &= \sum_{K \in \mathcal{T}_h} \left(q_k^P \, \sigma_h^*(\nabla p_N), \sigma_h^*(\nabla q_N) \right)_K. \end{aligned} \tag{3.40}$$

Here we are considering that the approximations given by the EIM for $\nu_T(\mu)$

and $\tau_{K,p}(\mu)$ are respectively

$$\begin{aligned} \mathcal{I}_{M_1}[\nu_T(\mu)] &= \sum_{k=1}^{M_1} \sigma_k^S(\mu) q_k^S, \\ \mathcal{I}_{M_1}[\tau_{K,p}(\mu)] &= \sum_{k=1}^{M_2} \sigma_k^P(\mu) q_k^P. \end{aligned} \tag{3.41}$$

With this representation, we lead to a linearisation of the RB problem (3.16), with an affine dependence with respect to the parameter, given by

$$\begin{cases} \text{Find } (\mathbf{u}_N, p_N) = (\mathbf{u}_N(\mu), p_N(\mu)) \in Y_N \times M_N \text{ such that} \\ a(\mathbf{u}_N, \mathbf{v}_N; \mu) + b(\mathbf{v}_N, p_N; \mu) + \hat{a}'_S(\mathbf{w}_N; \mathbf{v}_N; \mu) \\ +c(\mathbf{u}_N, \mathbf{u}_N, \mathbf{v}_N; \mu) + c(\mathbf{u}_D, \mathbf{u}_N, \mathbf{v}_N; \mu) \\ +c(\mathbf{u}_N, \mathbf{u}_D, \mathbf{v}_N; \mu) = F(\mathbf{v}_N; \mu) \qquad \forall \mathbf{v}_N \in Y_N \\ b(\mathbf{u}_N, q_N; \mu) + \hat{s}_{pres}(p_N, q_N; \mu) = 0 \qquad \forall q_N \in M_N. \end{cases} \tag{3.42}$$

We can express the solution $(\mathbf{u}_N(\mu), p_N(\mu)) \in X_N$ of (3.42) as a linear combination of the basis functions:

$$\mathbf{u}_N(\mu) = \sum_{j=1}^{N} u_j^N(\mu) \zeta_j^{\mathbf{v}}, \quad p_N(\mu) = \sum_{j=1}^{N} p_j^N(\mu) \xi_j^p.$$

The matrix representation of the bilinear terms in (3.42) and the tensor representation of the trilinear form associated to the convective term have a similar representation than in (2.47)-(2.48).

The tensor representation associated to the eddy-viscosity term and the pressure stabilization coefficient are define as follows:

$$(\mathbb{S}'_N(q_s^S))_{ij} = \sum_{K \in \mathcal{T}_h} (q_s^S \nabla(\Pi_h^* \zeta_j^{\mathbf{v}}), \nabla(\Pi_h^* \zeta_i^{\mathbf{v}}))_K, \quad i,j = 1 \ldots, N, s = 1, \ldots, M_1, \tag{3.43}$$

$$(\mathbb{P}_N(q_s^P))_{ij} = \sum_{K \in \mathcal{T}_h} (q_s^P \sigma_h^*(\nabla \xi_j^p), \sigma_h^*(\nabla \xi_i^p))_K, \quad i,j = 1, \ldots, N, s = 1, \ldots, M_2. \tag{3.44}$$

With this tensor representation for the non-linear terms in (3.16) done in the offline phase, it holds that

$$\hat{a}'_S(\zeta_j^{\mathbf{v}}; \zeta_i^{\mathbf{v}}; \mu) = \sum_{s=1}^{M_1} \sigma_s^S(\mu) \mathbb{S}'_N(q_s^S) \quad \text{and} \quad \hat{s}_{pres}(\xi_j^p, \xi_i^p; \mu) = \sum_{s=1}^{M_2} \sigma_s^P(\mu) \mathbb{P}_N(q_s^P).$$

Problem (3.42) is solved by a semi-implicit evolution approach. Remark that thanks to that representation, we are able to solve efficiently the online phase due to the linearisation of the eddy-viscosity and pressure stabilization terms.

3.6 Numerical Results

In this section, we present numerical results for the LPS-Smagorinsky reduced basis model, programmed in FreeFem++ (*cf.* [48]). We consider two different cases: the Backward-facing step and the Lid-driven cavity problems. In both cases, we obtain a speed-up of the computational time for several thousands.

3.6.1 Backward-facing step (2D)

In this numerical test, we show the numerical results for the backward-facing step (*cf.* [3]) for the LSP-VMS-Smagorinsky reduced basis model. The parameter that we consider is the Reynold number, ranging in $\mathcal{D} = [50, 450]$. As mentioned in section 2.6.1, this setting correspond to a regime fully laminar.

For the offline phase, we compute the FE solution with a non-stable finite element pair, $\mathbb{P}2 - \mathbb{P}2$ for velocity-pressure. The mesh selected for this problem is composed by 10842 triangles and 5703 nodes. The FE steady state solution is computed through a semi-implicit evolution approach, concluding that the steady solution is reached when the relative error between two successive iterations is below $\varepsilon_{FE} = 10^{-10}$. The numerical scheme to solve the LPS-VMS-Smagorinsky model in each step of the semi-implicit evolution approach reads

$$\begin{cases} \text{Find } (\mathbf{u}_h^{n+1}, p_h^{n+1}) \in Y_h \times M_h \text{ such that } \forall \mathbf{v}_h \in Y_h, \forall q_h \in M_h \\ \left(\dfrac{\mathbf{u}_h^{n+1} - \mathbf{u}_h^n}{\Delta t}\right)_\Omega + a(\mathbf{u}_h^{n+1}, \mathbf{v}_h; \mu) + b(\mathbf{v}_h, p_h^{n+1}; \mu) \\ + a_S(\mathbf{w}_h^n; \mathbf{w}_h^{n+1}, \mathbf{v}_h; \mu) + c(\mathbf{u}_h^n, \mathbf{u}_h^{n+1}, \mathbf{v}; \mu) \\ + c(\mathbf{u}_D, \mathbf{u}_h^{n+1}, \mathbf{v}; \mu) + c(\mathbf{u}_h^{n+1}, \mathbf{u}_D, \mathbf{v}; \mu) = F(\mathbf{v}_h; \mu) \\ b(\mathbf{u}_h^{n+1}, q_h; \mu) + s_{pres}(p_h^{n+1}, q_h; \mu) = 0, \end{cases} \tag{3.45}$$

where the linearised pressure stabilization term is defined as:

$$s_{pres}(p_h^{n+1}, q_h; \mu) = \sum_{K \in \mathcal{T}_h} (\tau_{K,p}^n(\mu)\, \sigma_h^*(\nabla p_h), \sigma_h^*(\nabla q_h))_K.$$

Here, the stabilization coefficient is given by the adapted Codina's form (3.13):

$$\tau^n_{p,K}(\mu) = \left[c_1 \frac{1/\mu + \overline{\nu}^n_{T_{|K}}}{h_K^2} + c_2 \frac{U^n_K}{h_K} \right]^{-1},$$

where $U^n_K = \|\mathbf{w}^n_h\|_{0,2,K}/|K|^{1/2}$, and $\overline{\nu}^n_{T_{|K}} = (C_S h_K)^2 \|\nabla(\Pi^*_h \mathbf{w}^n_h)\|_{0,2,K}/|K|^{1/2}$. For the experimental values of constants c_1 and c_2, we consider that $c_1 = 16$ and $c_2 = \sqrt{c_1}$ (*cf.* [33]).

As mentioned in sec. 3.2.2, we do not enrich the velocity space with the *supremizer* operator. In fig. 3.1 we show the comparison between the consideration or not of the inner pressure *supremizer* for the velocity enrichment. For this test, in the third iteration, the Greedy algorithm selects a parameter value already chosen, ending the algorithm. This is due to the obtaining of a singular matrix for the RB problem. Thus, from now, we will consider that the velocity space considered is the one defined in (3.17).

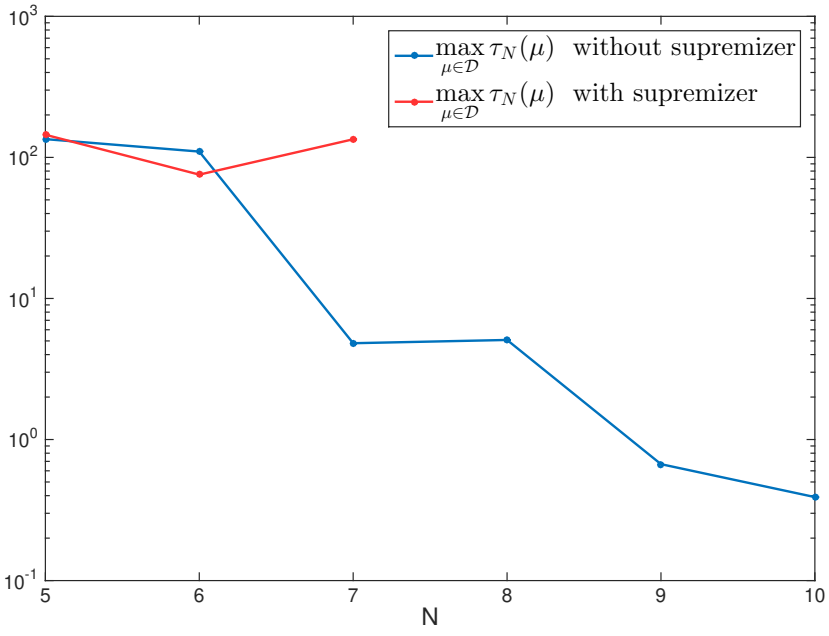

Figure 3.1: Comparison of the stabilization with/without *supremizer*

For the computation of the inf-sup constant $\beta_h(\mu)$, we deal with the RBF algorithm described in section 1.5. In Fig. 3.2, we compare the value of $\beta_h(\mu)$ for the Smagorinsky model and the LPS-VMS-Smagorinsky model. As expected, due to the fact that the Smagorinsky model is more diffusive than the VMS-Smagorinsky model, the value of the inf-sup constant for this last model is slightly

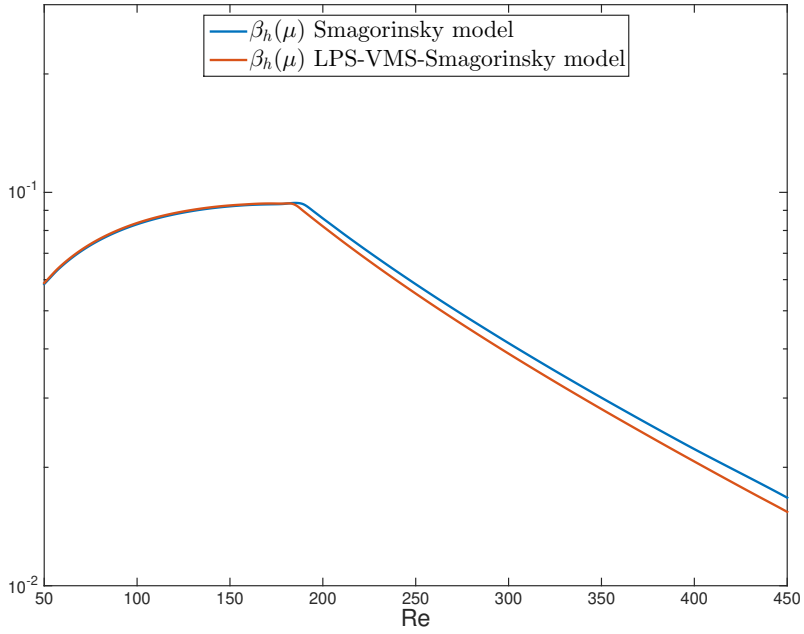

Figure 3.2: $\beta_h(\mu)$ for the Smagorinsky and the LPS-VMS-Smagorinsky model.

lower than the value of the inf-sup constant for the Smagorinsky model.

We implement two EIM algorithms, one to approximate the eddy viscosity term, $\nu_T(\mu)$; and the other one for the pressure-stabilization constant, $\tau_{p,K}(\mu)$, since this last changes at each time step of the semi-implicit numerical scheme. For the eddy viscosity term, we need $M_1 = 64$ basis of the EIM until reaching a prescribe tolerance of $\varepsilon_{EIM} = 10^{-3}$. For the approximation of the pressure stabilization constant, we need $M_2 = 79$ basis until reaching the same tolerance. In Fig. 3.3 we show the evolution on the error in both EIM.

In this numerical test, a POD is performed before starting the Greedy algorithm in order to obtain a initial guess such that $\tau_N(\mu)$ is near to 1. We select 5 POD modes (see e.g. [7]), and then we need $N = 13$ basis in order to reach the tolerance in the Greedy algorithm of $\varepsilon_{RB} = 10^{-4}$. In Fig. 3.4 we show the evolution, during the Greedy algorithm, of the maximum of the *a posteriori* error bound estimator $\Delta_N(\mu)$. Recall that when $\tau_N(\mu) > 1$, we consider as *a posteriori* error bound estimator the proper value of $\tau_N(\mu)$.

In Fig. 3.5 we show the value of the error between the FE solution and the RB one, with the value of the *a posteriori* error bound for $N = 13$. Note that the error between FE and RB solution is below of the *a posteriori*, as predicted in Theorem 3.1, about one order of magnitude.

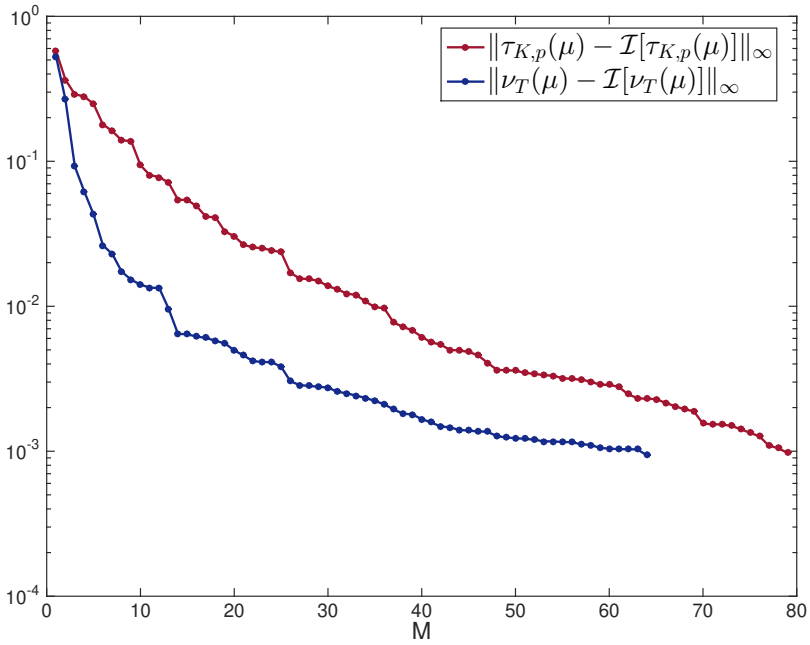

Figure 3.3: Evolution of the error in the EIM

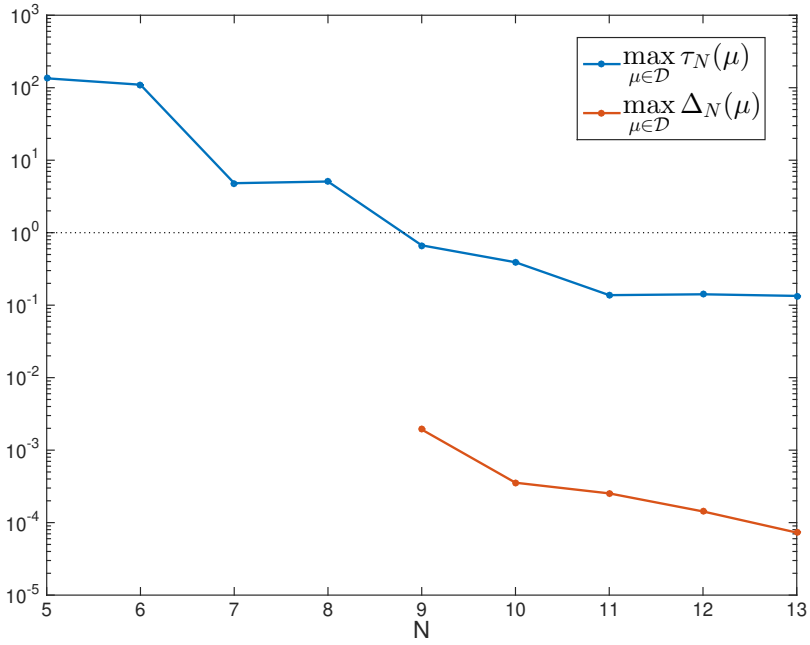

Figure 3.4: Evolution of the error in the Greedy algorithm

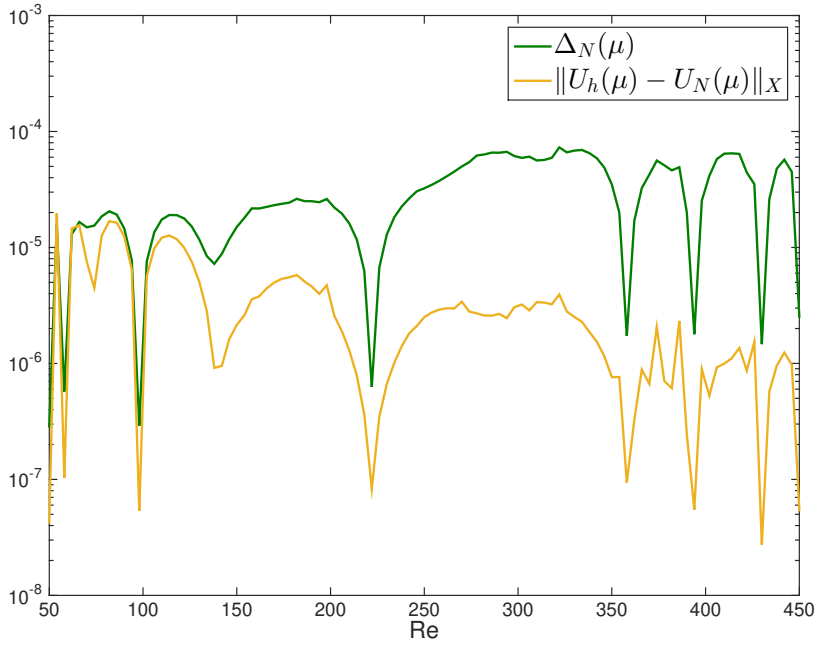

Figure 3.5: Error and *a posteriori* error bound estimator for $N = 13$.

In Fig. 3.6 we show a comparison between the FE velocity solution (top) and the RB one (bottom), for a chosen value of the Reynold number $\mu = 132$. Both solutions differ by an error of order 10^{-6}, giving images practically equal at the displayed scale.

Finally in Table 3.1 we show the results obtained for several values of $\mu \in \mathcal{D}$. In that table we show the error between the FE and RB solution, for both velocity and pressure. We also show the computational time for the computation for both solution and the speedup in the computation. As we can observe, the error is small enough and has speed-up rates of several thousands.

The increment of the speed-up rate for the LPS-VMS-Smagorinsky model with respect to the Smagorinsky model is possibly due to the increment of the degree of freedom of the FE problem by considering $\mathbb{P}2-\mathbb{P}2$ instead of $\mathbb{P}2-\mathbb{P}1$, and the decreasing of the dimension of the RB problem, thanks to the offline/online stabilization procedure that avoids us to increment the velocity space dimensionality with the inner pressure *supremizer*.

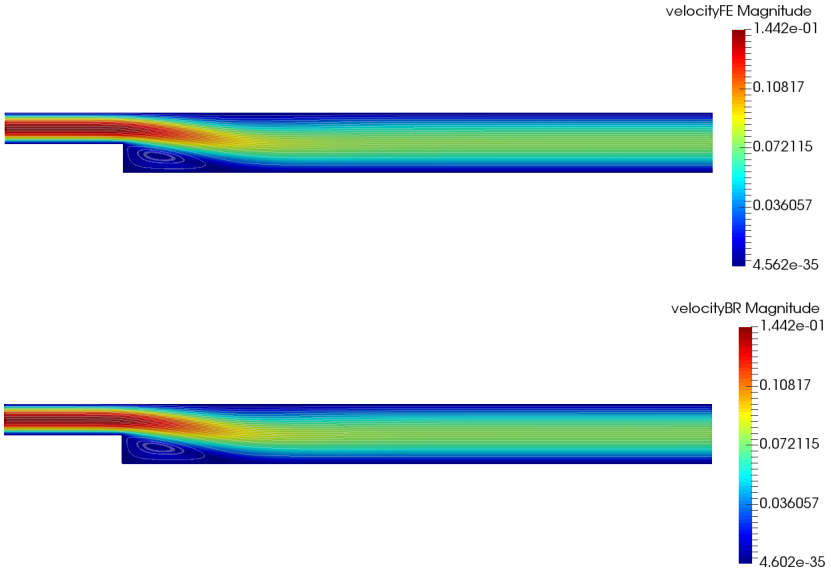

Figure 3.6: FE (top) and RB (bottom) solution for $\mu = 320$.

Data	$\mu = 56$	$\mu = 132$	$\mu = 236$	$\mu = 320$	$\mu = 450$
T_{FE}	585.68s	1281.83s	2600s	3733.37s	7007.65s
T_{online}	0.92s	1.04s	1.32s	1.39s	1.98s
speedup	631	1222	1957	2671	3525
$\|\mathbf{u}_h - \mathbf{u}_N\|_T$	$1.265 \cdot 10^{-5}$	$1.88 \cdot 10^{-6}$	$1.04 \cdot 10^{-6}$	$3.24 \cdot 10^{-6}$	$1.94 \cdot 10^{-9}$
$\|p_h - p_N\|_0$	$1.12 \cdot 10^{-5}$	$3.79 \cdot 10^{-6}$	$1.27 \cdot 10^{-6}$	$2.99 \cdot 10^{-6}$	$5.44 \cdot 10^{-8}$

Table 3.1: Computational time for FE solution and RB online phase, with the speedup and the error.

3.6.2 Lid-driven Cavity flow (2D)

In this numerical test, we show the results of the pressure LPS-Smagorinsky reduced basis model for the Lid-driven Cavity problem. We consider the Reynolds number as a parameter, ranging in $\mathcal{D} = [1000, 5100]$. We consider a regular mesh with 5000 triangles and 2601 nodes. The Finite Element pair chosen is the pair $\mathbb{P}2 - \mathbb{P}2$. We impose a non-homogeneous boundary condition $\mathbf{u}_D = 1$ on the top of the geometry, while in the rest of the boundaries, we impose homogeneous Dirichlet conditions.

For this test, again the consideration of the *supremizer* enrichment for the velocity space, leads to a reelection of a parameter value already selected in the Greedy algorithm. In Fig. 3.7 we show that in this case, in the fourth iteration,

the Greedy algorithm breaks.

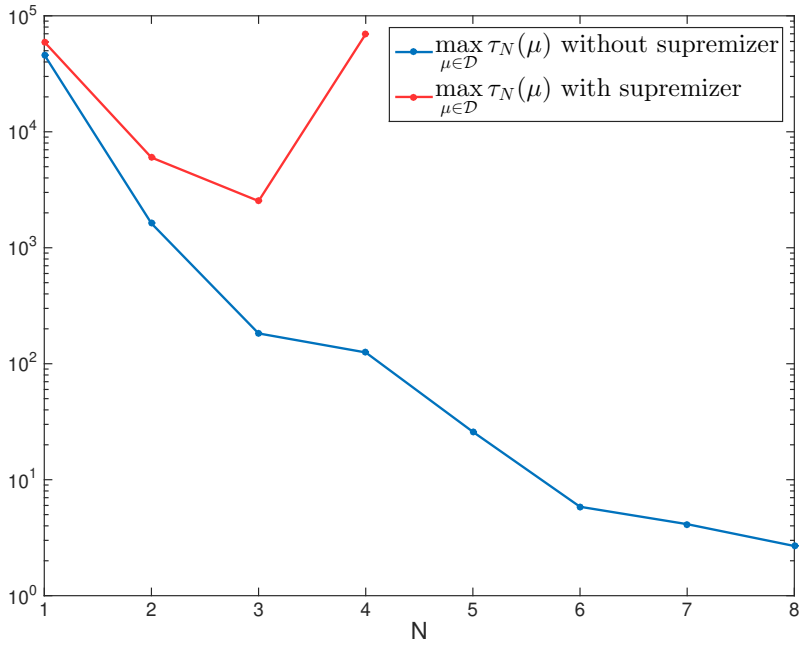

Figure 3.7: Comparison of the stabilization with/without *supremizer*

In the EIM considered in this test, we compute $M_1 = 20$ basis for the eddy viscosity approximation and $M_2 = 25$ basis for the pressure stabilization constant approximation to reach a prescribe tolerance of $\varepsilon_{EIM} = 5 \cdot 10^{-4}$. In Fig. 3.8 we show the evolution of the error for both EIM.

For the Greedy algorithm we prescribe a tolerance of $\varepsilon_{RB} = 10^{-4}$, which is reached for $N = 16$ basis. In Fig. 3.9 we show the evolution of the *a posteriori* error bound estimator during the Greedy algorithm. Then, in Fig. 3.10, we show the comparison of the error and the *a posteriori* error bound estimator. In this case, the *a posteriori* error bound estimator is about two orders of magnitude greater than the exact error.

In Fig. 3.11, we show two solutions for a prescribed value of Reynolds number $\mu = 2751$, for the FE problem (right) and the RB (problem). We can observe the similarity of both solutions, since the error between them is of order 10^{-6}.

Finally, in Table 3.2 we summarize results obtained for several values of Reynold numbers. For this test, we obtain higher speed-up rates than for the backward-facing step test, that can reach the order of tens of thousands. Again, the error between FE and RB solution is quite small.

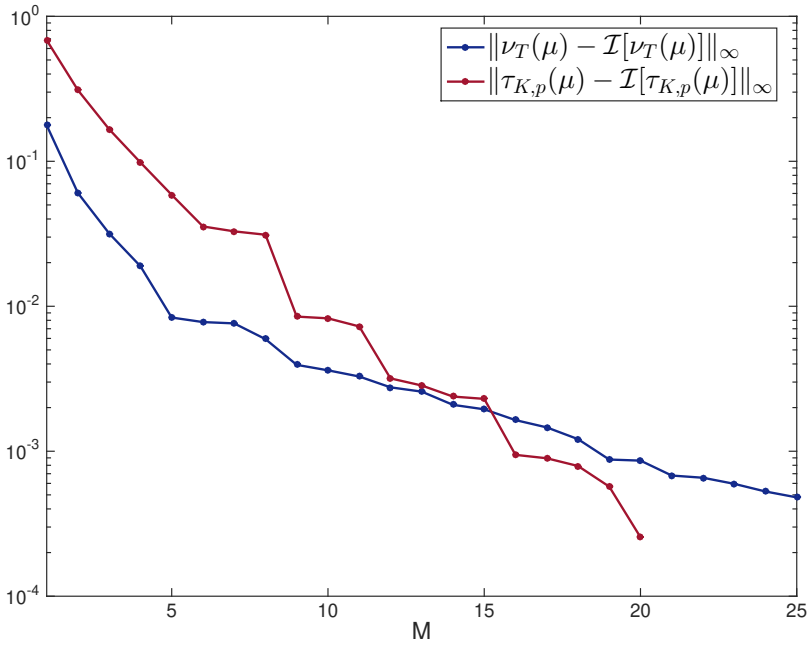

Figure 3.8: Evolution of the error in the EIM

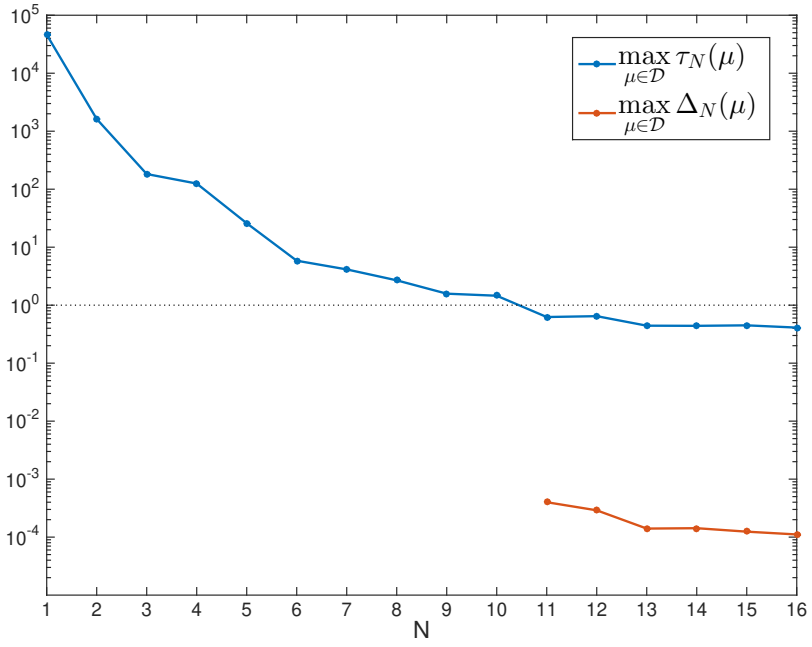

Figure 3.9: Evolution of the error in the Greedy algorithm

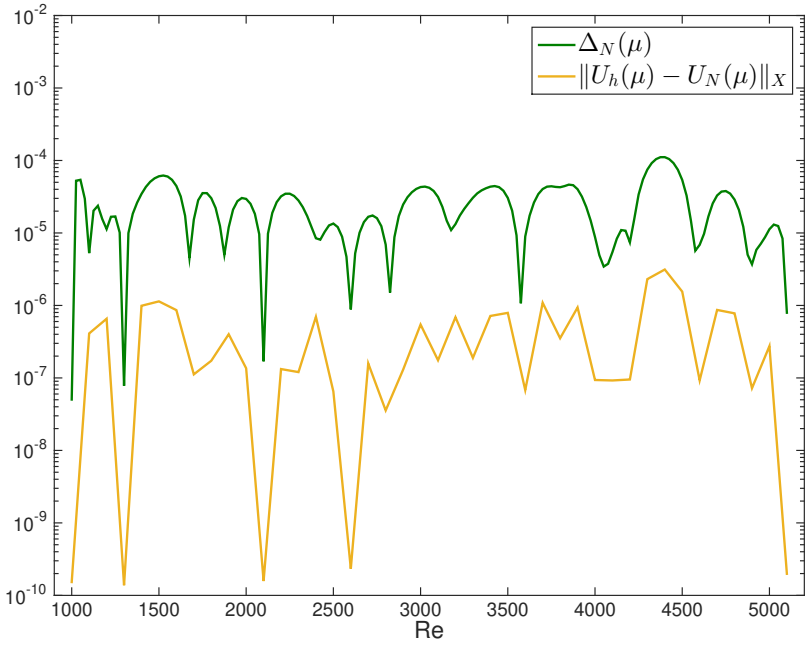

Figure 3.10: Error and *a posteriori* error bound estimator for $N = 13$.

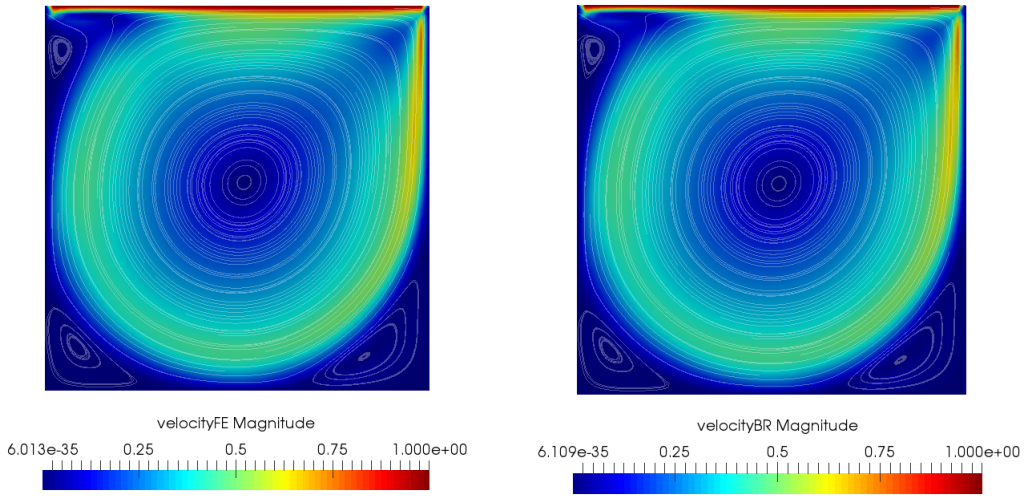

Figure 3.11: FE (top) and RB (bottom) solution for $\mu = 2751$.

Data	$\mu = 1610$	$\mu = 2751$	$\mu = 3886$	$\mu = 4521$	$\mu = 5100$
T_{FE}	4083.19s	6918.53s	9278.51s	10201.7s	11277.8s
T_{online}	0.71s	0.69s	0.69s	0.7s	0.69s
speedup	5750	10026	13280	14459	16248
$\|\mathbf{u}_h - \mathbf{u}_N\|_T$	$2.4 \cdot 10^{-5}$	$4.129 \cdot 10^{-6}$	$3.14 \cdot 10^{-5}$	$3.23 \cdot 10^{-5}$	$2.77 \cdot 10^{-8}$
$\|p_h - p_N\|_0$	$2.17 \cdot 10^{-7}$	$1.99 \cdot 10^{-8}$	$5.38 \cdot 10^{-8}$	$6.36 \cdot 10^{-8}$	$6.89 \cdot 10^{-8}$

Table 3.2: Computational time for FE solution and RB online phase, with the speedup and the error.

3.7 Conclusions

In this Chapter we have developed a LPS-VMS-Smagorinsky reduced basis model, extending the techniques used in Chapter 2 for the Smagorinsky reduced basis model. In the LPS-VMS-Smagorinsky model, the inner pressure *supremizer* is no longer necessary, since we perform an offline/online stabilization on the pressure. We use the EIM to approximate the eddy viscosity and the pressure stabilization coefficient in order to avoid the non-linearities that appear in both terms. The speedups obtained for the LPS-VMS-Smagorinsky model are larger than the speedups obtained in Chapter 2 for the Smagorinsky model, probably due to the use of stabilized methods, that avoid us to use the inner pressure *supremizer* for the velocity-pressure stabilization, reducing the dimension of the velocity reduced space.

Chapter 4

A VMS-Boussinesq-Smagorinsky Reduced Basis model

4.1 Introduction

In this Chapter, we present a Reduced Basis Boussinesq model, with VMS-Smagorinsky modelling for both the eddy viscosity and the eddy diffusivity. This model takes into account the buoyancy forces present in natural convection problems, being of big interest in the study of many physics applications and industry problems, such as the comportment of the atmosphere or the oceans, the cooling of electronic devices, room ventilation, etc.

This model differs from the ones presented in previous Chapter as it considers the energy equation, coupled with the momentum and continuous equations. In this Chapter, we assume that the temperature of the fluid becomes essential in the flow of the fluid considered. Thanks to that assumption, we deal to more realistic flows, which we are more interested in.

We perform a Reduced Basis model of Boussinesq VMS-Smagorinsky equations with the same strategy presented in the previous Chapters. We develop an *a posteriori* error bound, essential for the Greedy algorithm used in the snapshots selection. Moreover, we take into account the EIM in order to approximate the non-linear terms for the eddy viscosity and eddy diffusivity terms.

We perform two numerical tests, for different ranges of the Rayleigh number. We consider a first test with low and moderate Rayleigh numbers, in which the heat transfer is principally in form of diffusion. Then, we increase the Rayleigh numbers, getting a range of high Rayleigh numbers obtaining a flow where the heat transfer is principally by diffusion. We obtain speed-ups rate of computational time of several hundreds in both cases.

The Chapter is structured as follows: in section 4.2 we present the Boussinesq VMS-Smagorinsky model for natural convection flows, defining both the FE problem (subsection 4.2.1) and the RB problem, with the approximation via EIM of the eddy viscosity and eddy diffusivity terms (subsection 4.2.2). Then, in section 4.3 we present the numerical analysis of the model, assuring the well-possedness of the problem. After that, we develop the *a posteriori* error bound estimator in section 4.4. Finally, in section 4.5 we present the numerical results for two test, both programmed in FreeFem++ (*cf.* [48]).

4.2 Boussinesq equations for natural convection flows

In this section we present a Boussinesq model for natural convection flow problems. We deal with a square cavity problem, for what the top and the bottom are isolated walls and the vertical walls have a prescribed temperature. The difference of temperatures in the vertical wall, produces a circulation of the fluid, that is supposed to be viscous, Newtonian and incompressible, and the buoyancy forces are modelled with a Boussinesq approximation.

4.2.1 Finite element problem

For the FE problem statement, let $\Omega \in \mathbb{R}^d$ $(d = 2, 3)$ a polyhedral domain, with $\Gamma = \partial\Omega$ a Lipschitz-continuous boundary that we suppose to be splitted in two disjoints parts, $\Gamma = \Gamma_D \cup \Gamma_N$, corresponding with the Dirichlet and Neumann boundary conditions respectively.

We next present the Navier-Stokes equations with the Boussinesq approximation for the energy equation (*cf.* [10, 13, 14, 26]), for which we also include the modelling of the eddy viscosity and the eddy diffusivity by the Smagorinsky approach (see [98, 103]). We present a continuous form of the Smagorinsky eddy viscosity and eddy diffusivity:

$$\begin{cases} \mathbf{u}\cdot\nabla\mathbf{u} - Pr\Delta\mathbf{u} - \nabla\cdot(\nu_T(\mathbf{u})\nabla\mathbf{u}) + \nabla p - Pr\,Ra\,\theta\,\mathbf{e}_d = \mathbf{f} & \text{in } \Omega \\ \nabla\cdot\mathbf{u} = 0 & \text{in } \Omega \\ \mathbf{u}\cdot\nabla\theta - \Delta\theta - \nabla\cdot(K_T(\mathbf{u})\nabla\theta) = Q & \text{in } \Omega \\ \mathbf{u} = 0 & \text{on } \Gamma \\ \theta = \theta_D & \text{on } \Gamma_D \\ \partial_n\theta = 0 & \text{on } \Gamma_N \end{cases} \tag{4.1}$$

Here, $\mathbf{u}$ is the velocity field, p is the pressure and θ is the temperature. In addition, $\mathbf{e}_d$ is the last vector of the canonical basis of $\mathbb{R}^d$, while Ra and Pr are the Rayleigh and Prandtl dimensionless numbers respectively. Both the external body forces $\mathbf{f}$, and the heat source term Q, are given data for the problem. In (4.1), $\nu_T(\mathbf{u})$ is the eddy viscosity term, and $K_T(\mathbf{u})$ the eddy diffusivity that is given by

$$K_T(\mathbf{u}) = \frac{1}{Pr}\nu_T(\mathbf{u}). \tag{4.2}$$

Remark 4.1. *The Prandtl number is defined as*

$$Pr := \frac{\nu_0}{k_0},$$

with ν_0 a reference kinematic viscosity and k_0 a reference thermal diffusivity. Since the Prandtl number depends on the physics of the fluid, we consider it as a fixed value and not as a parameter. Thus, for this problem, we consider the Rayleigh number as the only parameter for the model, denoted by $\mu \in \mathcal{D} \subset \mathbb{R}$.

In (4.1), we represent by θ_D the a given temperature over the boundary Γ_D. For the simplicity of the analysis, we further consider that $\theta_D = 0$. In the case of considering non-homogeneous boundary conditions, it is enough to define a lift function θ_g such that $\theta_g|_{\Gamma_D} = \theta_D$. In Chapters 2 and 3, an analysis with the lift function is already done.

To define the variational form of problem (4.1), let us define the spaces $Y = (H_0^1(\Omega))^d$ for velocity, $\Theta = H_0^1(\Omega)$ for temperature, and $M = L_0^2(\Omega)$ for pressure. We consider the H^1-seminorm for the velocity and temperature spaces, and the L^2-norm for the pressure space. In addition, let us define the Sobolev embedding constants C_u and C_θ, associated to these norms, such that

$$\|\mathbf{v}\|_{0,4,\Omega} \leq C_u \|\nabla \mathbf{v}\|_{0,2,\Omega}, \quad \forall \mathbf{v} \in Y, \tag{4.3}$$

and

$$\|\theta\|_{0,4,\Omega} \leq C_\theta \|\nabla \theta\|_{0,2,\Omega}, \quad \forall \theta \in \Theta. \tag{4.4}$$

Moreover, we consider the tensor space $X = Y \times \Theta \times M$, with the following associated norm:

$$\|U\|_X^2 = \|\nabla \mathbf{u}\|_{0,2,\Omega}^2 + \|\nabla \theta\|_{0,2,\Omega}^2 + \|p\|_{0,2,\Omega}^2, \quad \forall U = (\mathbf{u}, \theta, p) \in X. \tag{4.5}$$

Let $\{\mathcal{T}_h\}_{h>0}$ a uniformly regular family of triangulation, and $Y_h = (H_0^1(\Omega) \cap V_h^l(\Omega))^d$, $M_h = L_0^2(\Omega) \cap V_h^m(\Omega)$, $\Theta_h = H_0^1(\Omega) \cap V_h^q(\Omega)$, with $l, m, q \in \mathbb{N}$. We consider the VMS-Smagorinsky Small-Small setting (see section 3.2) for the eddy viscosity and eddy thermal diffusivity. Denoting by $\mu \in \mathbb{R}$ the Rayleigh number,

we lead to the following variational formulation of problem 4.1:

$$\begin{cases} \text{Find } (\mathbf{u}_h, \theta_h^u, p_h^u) = (\mathbf{u}_h(\mu), \theta_h^u(\mu), p_h^u(\mu)) \in X_h \text{ such that} \\ a_u(\mathbf{u}_h, \mathbf{v}_h; \mu) + b(\mathbf{v}_h, p_h^u; \mu) + a'_{Su}(\mathbf{u}_h; \mathbf{u}_h, \mathbf{v}_h; \mu) \\ +c_u(\mathbf{u}_h, \mathbf{u}_h, \mathbf{v}_h; \mu) + f(\theta_h^u, \mathbf{v}_h; \mu) = F(\mathbf{v}_h; \mu) \qquad \forall \mathbf{v}_h \in Y_h, \\ b(\mathbf{u}_h, p_h^v; \mu) = 0 \qquad \forall p_h^v \in M_h, \\ a_\theta(\theta_h^u, \theta_h^v; \mu) + c_\theta(\mathbf{u}_h, \theta_h^u, \theta_h^v; \mu) \\ +a'_{S\theta,n}(\mathbf{u}_h; \theta_h^u, \theta_h^v; \mu) = Q(\theta_h^v; \mu) \qquad \forall \theta_h^v \in \Theta_h. \end{cases} \tag{4.6}$$

Here, the bilinear forms $a_u(\cdot,\cdot;\mu)$, $a_\theta(\cdot,\cdot;\mu)$, $b(\cdot,\cdot;\mu)$ and $f(\cdot,\cdot;\mu)$ are defined by

$$\begin{aligned} a_u(\mathbf{u}, \mathbf{v}; \mu) &= Pr \int_\Omega \nabla \mathbf{u} : \nabla \mathbf{v} \, d\Omega, \qquad a_\theta(\theta^u, \theta^v; \mu) = \int_\Omega \nabla \theta^u \cdot \nabla \theta^v \, d\Omega, \\ f(\theta^u, \mathbf{v}; \mu) &= -Pr\, \mu \int_\Omega \theta^u \, v_2 \, d\Omega, \qquad b(\mathbf{u}, p^v; \mu) = -\int_\Omega (\nabla \cdot \mathbf{u}) p^v \, d\Omega; \end{aligned} \tag{4.7}$$

the trilinear forms $c_u(\cdot,\cdot,\cdot;\mu)$, $c_\theta(\cdot,\cdot,\cdot;\mu)$ are defined by

$$c_u(\mathbf{z}, \mathbf{u}, \mathbf{v}; \mu) = \int_\Omega (\mathbf{z} \cdot \nabla \mathbf{u}) \mathbf{v} \, d\Omega, \qquad c_u(\mathbf{u}, \theta^u, \theta^v; \mu) = \int_\Omega (\mathbf{u} \cdot \nabla \theta^u) \theta^v \, d\Omega; \tag{4.8}$$

and the non-linear VMS-Smagorinsky term for eddy viscosity, $a'_{Su}(\cdot;\cdot,\cdot;\mu)$, is given by

$$a'_{Su}(\mathbf{z}; \mathbf{u}, \mathbf{v}; \mu) = \int_\Omega \nu_T(\Pi_h^* \mathbf{z}) \nabla(\Pi_h^* \mathbf{u}) : \nabla(\Pi_h^* \mathbf{v}) \, d\Omega, \tag{4.9}$$

with

$$\nu_T(\mathbf{u}) = (C_S h_K)^2 |\nabla \mathbf{u}_{|_K}|.$$

For the eddy diffusivity term, let us first introduce a mollifier $\phi \in C_c^\infty(\mathbb{R})$, with $\text{supp}(\phi) \subset B(0,1), \phi \geq 0, \|\phi\|_{0,1,\mathbb{R}} > 0$ and ϕ is even, i.e., $\phi(-x) = \phi(x)$. Let us consider the mollifier sequence $\{\phi_n(x)\}_{n\geq 1}$, with $\phi_n \in C_c^\infty(\mathbb{R})$, $\text{supp}(\phi_n) \subset B(0, 1/n), \phi_n \geq 0, \|\phi_n\|_{0,1,\mathbb{R}} = 1$, defined by

$$\phi_n(x) = \frac{n}{\|\phi\|_{0,1,\mathbb{R}}} \phi(n\, x).$$

The following result for mollifiers can be found in [15]:

Proposition 4.1. *Assume $f \in L^p(\mathbb{R}^d)$ with $1 \leq p < \infty$. Then $(\phi_n * f) \xrightarrow[n\to\infty]{} f$ in $L^p(\mathbb{R}^n)$.*

Thus, the VMS-Smagorinsky eddy diffusivity term is defined as

$$a'_{S\theta,n}(\mathbf{u}_h;\theta_h^u,\theta_h^v;\mu)=\int_\Omega \nu_{T,n}(\Pi_h^*\mathbf{u}_h)\nabla(\Pi_h^*\theta_h^u)\cdot\nabla(\Pi_h^*\theta_h^v)\,d\Omega, \tag{4.10}$$

with

$$\nu_{T,n}(\mathbf{u})=(C_S h_K)^2(\phi_n * |\nabla \mathbf{u}_{|_K}|).$$

Thanks to Prop. 4.1, it holds that $a'_{S\theta,n}$ converges uniformly to $a'_{S\theta}$, with

$$a'_{S\theta}(\mathbf{u}_h;\theta_h^u,\theta_h^v;\mu)=\int_\Omega \nu_{T}(\Pi_h^*\mathbf{u}_h)\nabla(\Pi_h^*\theta_h^u)\cdot\nabla(\Pi_h^*\theta_h^v)\,d\Omega.$$

Remark 4.2. *The eddy diffusivity $a'_{S\theta,n}$ is considered for the well-possedness analysis and the development of a posteriori error bound estimator. In practice, we consider the eddy diffusivity term in the Boussinesq VMS-Smagorinsky model as $a'_{S\theta}$.*

Recall that $\Pi_h^* = Id - \Pi_h$, were we denote both $\Pi_h \equiv \Pi_h^u$ and $\Pi_h \equiv \Pi_h^\theta$ an uniformly stable interpolation operator, on $\overline{Y}_h$ or $\overline{\Theta}_h$ respectively, where

$$\overline{Y}_h = [V_h^{l-1}(\Omega)]^d, \qquad \overline{\Theta}_h = V_h^{q-1}(\Omega), \tag{4.11}$$

with these interpolation operators satisfying the properties of Prop. 3.1 (*cf.* [11]).

Remark 4.3. *Recall that in the VMS setting, we denote by $\overline{Y}_h$ and $\overline{\Theta}_h$ the large-scale finite dimensional spaces for velocity and temperature.*

Denoting by $X_h = Y_h \times \Theta_h \times M_h$, we rewrite problem 4.6 as

$$\begin{cases} \text{Find } U_h(\mu)=(\mathbf{u}_h,\theta_h^u,p_h^u)\in X_h \text{ such that} \\ A(U_h(\mu),V_h;\mu)=F(V_h;\mu) \qquad \forall V_h\in X_h, \end{cases} \tag{4.12}$$

where,

$$A(U_h,V_h;\mu)=A_0(U_h,V_h)+\mu A_1(U_h,V_h)+A_2(U_h;V_h)+A_3(U_h;V_h). \tag{4.13}$$

Denoting $V_h=(\mathbf{v}_h,\theta_h^v,p_h^v)\in X_h$, the μ-independent operators in (4.13) are

given by

$$\begin{aligned}
A_0(U_h, V_h) &= Pr \int_\Omega \nabla \mathbf{u}_h : \nabla \mathbf{v}_h \, d\Omega + \int_\Omega \nabla \theta_h^u \cdot \nabla \theta_h^v \, d\Omega \\
&\quad - \int_\Omega (\nabla \cdot \mathbf{v}_h) p_h^u \, d\Omega + \int_\Omega (\nabla \cdot \mathbf{u}_h) p_h^v \, d\Omega, \\
A_1(U_h, V_h) &= -Pr \int_\Omega \theta_h^u \, v_2 \, d\Omega, \\
A_2(U_h; V_h) &= \int_\Omega (\mathbf{u}_h \cdot \nabla \mathbf{u}_h) \mathbf{v}_h \, d\Omega + \int_\Omega (\mathbf{u}_h \cdot \nabla \theta_h^u) \theta_h^v \, d\Omega, \\
A_3(U_h; V_h) &= \int_\Omega \nu_T(\Pi_h^* \mathbf{u}_h) \nabla(\Pi_h^* \mathbf{u}_h) : \nabla(\Pi_h^* \mathbf{v}_h) \, d\Omega \\
&\quad + \frac{1}{Pr} \int_\Omega \nu_{T,n}(\Pi_h^* \mathbf{u}_h) \nabla(\Pi_h^* \theta_h^u) \cdot \nabla(\Pi_h^* \theta_h^v) \, d\Omega.
\end{aligned}$$

Recall that the eddy viscosity term is defined as $\nu_T(\mathbf{u}) = (C_S h_K)^2 |\nabla \mathbf{u}_{|_K}|$.

4.2.2 Reduced basis problem

In this section, we present the reduced basis method for the model presented in section 4.2.1. The RB problem reads

$$\begin{cases} \text{Find } U_N(\mu) \in X_N \text{ such that} \\ A(U_N(\mu), V_N; \mu) = F(V_N; \mu) \qquad \forall V_N \in X_N, \end{cases} \tag{4.14}$$

where the reduced space is defined as $X_N = Y_N \times \Theta_N \times M_N \subset X_h$. In this case, to guarantee the inf-sup stability for the RB problem, we consider the inner-pressure *supremizer* operator T_p^μ, defined in (2.11). Thus, the reduced spaces for velocity, temperature and pressure are given by

$$M_N = \text{span}\{\xi_k^p := p_h^u(\mu^k), \quad k = 1, \ldots, N\}, \tag{4.15}$$

$$Y_N = \text{span}\{\zeta_{2k-1}^{\mathbf{v}} := \mathbf{u}_h(\mu^k), \ \zeta_{2k}^{\mathbf{v}} := T_p^\mu \xi_k^p, \quad k = 1, \ldots, N\}, \tag{4.16}$$

$$\Theta_N = \text{span}\{\varphi_k^\theta := \theta_h^u(\mu^k), \quad k = 1, \ldots, N\}. \tag{4.17}$$

With this notation, the RB solutions of problem (4.14), can be represented as

$$\mathbf{u}_N(\mu) = \sum_{j=1}^{2N} u_j^N(\mu) \zeta_j^{\mathbf{v}}, \quad \theta_N(\mu) = \sum_{j=1}^{N} \theta_j^N(\mu) \varphi_j^\theta, \quad p_N(\mu) = \sum_{j=1}^{N} p_j^N(\mu) \xi_j^p.$$

The snapshots for the construction of the RB spaces are given by the Greedy al-

gorithm (see sec. 1.3). The pressure and temperature spaces are orthonormalized with respect each respective space norm. Moreover, in the velocity space, we orthonormalize separately the velocities snapshots and the inner pressure *supremizers*. This orthonormalization for the velocity space reduces the condition number for the matrix in the reduced basis problem (4.14), with respect the orthonormalization of the velocities and the inner pressure *supremizers* snapshots together.

The efficiency in solving problem (4.14) during the online phase relies on the linearisation via Empirical Interpolation Method. More precisely, we construct a reduced-basis space for the eddy viscosity and eddy diffusivity terms. Since the eddy diffusivity is a linear function of the eddy viscosity, we only need to construct one approximation.

This approximation corresponds with the one done in Section 3.5 for $\nu_T(\Pi_h^* \mathbf{u}_h)$. By this way, we approximate the eddy viscosity term and the eddy diffusivity term as

$$\begin{aligned} a'_{Su}(\mathbf{u}_N; \mathbf{u}_N, \mathbf{v}_N; \mu) &\approx \hat{a}'_{Su}(\mathbf{u}_N, \mathbf{v}_N; \mu), \\ a'_{S\theta}(\mathbf{u}_N; \theta_N^u, \theta_N^v; \mu) &\approx \hat{a}'_{S\theta}(\theta_N^u, \theta_N^v; \mu), \end{aligned} \tag{4.18}$$

where,

$$\begin{aligned} \hat{a}'_{Su}(\mathbf{u}_N, \mathbf{v}_N; \mu) &= \sum_{k=1}^{M} \sigma_k(\mu) s_u(q_k, \mathbf{u}_N, \mathbf{v}_N), \\ \hat{a}'_{S\theta}(\theta_N^u, \theta_N^v; \mu) &= \sum_{k=1}^{M} \sigma_k(\mu) s_\theta(q_k, \theta_N^u, \theta_N^v), \end{aligned} \tag{4.19}$$

with,

$$\begin{aligned} s_u(q_k, \mathbf{u}_N, \mathbf{v}_N) &= \sum_{K \in \mathcal{T}_h} \left(q_k \, \nabla(\Pi_h^* \mathbf{u}_N), \nabla(\Pi_h^* \mathbf{v}_N) \right)_K, \\ s_\theta(q_k, \theta_N^u, \theta_N^v) &= \frac{1}{Pr} \sum_{K \in \mathcal{T}_h} \left(q_k \, \nabla(\Pi_h^* \theta_N^u), \nabla(\Pi_h^* \theta_N^v) \right)_K. \end{aligned} \tag{4.20}$$

With this representation, the problem we solve in the online phase can be read as

$$\left\{ \begin{array}{ll} \text{Find } (\mathbf{u}_N(\mu), \theta_N^u(\mu), p_N^u(\mu)) \in X_N \text{ such that} & \\ \\ a_u(\mathbf{u}_N, \mathbf{v}_N; \mu) + b(\mathbf{v}_N, p_N^u; \mu) + \hat{a}'_{Su}(\mathbf{u}_N, \mathbf{v}_N; \mu) & \\ + c_u(\mathbf{u}_N, \mathbf{u}_N, \mathbf{v}_N; \mu) + f(\theta_N^u, \mathbf{v}_N; \mu) = F(\mathbf{v}_N; \mu) & \forall \mathbf{v}_N \in Y_N, \\ b(\mathbf{u}_N, p_N^v; \mu) = 0 & \forall p_N^v \in M_N, \\ a_\theta(\theta_N^u, \theta_N^v; \mu) + c_\theta(\mathbf{u}_N, \theta_N^u, \theta_N^v; \mu) & \\ + \hat{a}'_{S\theta}(\theta_N^u, \theta_N^v; \mu) = Q(\theta_N^v; \mu) & \forall \theta_N^v \in \Theta_N. \end{array} \right. \tag{4.21}$$

The parameter-independent matrices and tensors that we store during the offline phase have a similar form that the ones presented in (2.47)-(2.48), and are

given by

$$\begin{aligned}
&(\mathbb{A}_N^u)_{ij} = a_u(\zeta_j^{\mathbf{v}}, \zeta_i^{\mathbf{v}}), (\mathbb{A}_N^\theta)_{lm} = a_\theta(\varphi_m^\theta, \varphi_l^\theta) && i,j = 1,\dots,2N,\ l,m = 1,\dots,N\\
&(\mathbb{F}_N)_{li} = f(\varphi_l^\theta, \zeta_i^{\mathbf{v}}), && i = 1,\dots,2N,\ l = 1,\dots,N,\\
&(\mathbb{B}_N)_{li} = b(\zeta_i^{\mathbf{v}}, \xi_l^p), && i = 1,\dots,2N,\ l = 1,\dots,N.\\
&(\mathbb{C}_N^u(\zeta_s^{\mathbf{v}}))_{ij} = c_u(\zeta_s^{\mathbf{v}}, \zeta_j^{\mathbf{v}}, \zeta_i^{\mathbf{v}}), && i,j,s = 1,\dots,2N,\\
&(\mathbb{C}_N^\theta(\zeta_s^{\mathbf{v}}))_{lm} = c_\theta(\zeta_s^{\mathbf{v}}, \varphi_m^\theta, \varphi_l^\theta), && l,m = 1,\dots,N,\ s = 1,\dots,2N,\\
&(\mathbb{S}_N^u(q_s))_{ij} = s_u(q_s, \zeta_j^{\mathbf{v}}, \zeta_i^{\mathbf{v}}), && i,j = 1,\dots,2N, s = 1,\dots,M,\\
&(\mathbb{S}_N^\theta(q_s))_{lm} = s_\theta(q_s, \varphi_m^\theta, \varphi_l^\theta), && l,m = 1,\dots,N, s = 1,\dots,M.
\end{aligned} \tag{4.22}$$

4.3 Well-posedness analysis

In this section, we present the well-posedness of problem (3.14) through the BRR theory [18, 22]. For this purpose, let the directional derivative of $A(\cdot,\cdot;\mu)$, deriving each term separately:

$$\begin{aligned}
\partial_1 A_0(U,V)(Z) &= A_0(Z,V),\\
\partial_1 A_1(U,V)(Z) &= A_1(Z,V),\\
\partial_1 A_2(U;V)(Z) &= \int_\Omega (\mathbf{z}\cdot\nabla\mathbf{u})\mathbf{v}\ d\Omega + \int_\Omega (\mathbf{u}\cdot\nabla\mathbf{z})\mathbf{v}\ d\Omega\\
&\quad + \int_\Omega (\mathbf{z}_h\cdot\nabla\theta^u)\theta^v\ d\Omega + \int_\Omega (\mathbf{u}\cdot\nabla\theta^z)\theta^v\ d\Omega,
\end{aligned}$$

$$\begin{aligned}
\partial_1 A_3(U;V)(Z) = &\int_\Omega \nu_T(\Pi_h^*\mathbf{u})\nabla(\Pi_h^*\mathbf{z}) : \nabla(\Pi_h^*\mathbf{v})\ d\Omega\\
&+ \sum_{K\in\mathcal{T}_h}\int_K (C_S h_K)^2 \frac{\nabla(\Pi_h^*\mathbf{u}) : \nabla(\Pi_h^*\mathbf{z})}{|\nabla(\Pi_h^*\mathbf{u})|}\nabla(\Pi_h^*\mathbf{u}) : \nabla(\Pi_h^*\mathbf{v})\ d\Omega\\
&+ \frac{1}{Pr}\int_\Omega \nu_{T,n}(\Pi_h^*\mathbf{u})\ \nabla(\Pi_h^*\theta_h^z)\cdot\nabla(\Pi_h^*\theta_h^v)\ d\Omega\\
&+ \frac{1}{Pr}\int_\Omega \partial_1\nu_{T,n}(\Pi_h^*\mathbf{u})(\Pi_h^*\mathbf{z})\ \nabla(\Pi_h^*\theta^u)\cdot\nabla(\Pi_h^*\theta^v)\ d\Omega,
\end{aligned}$$

where

$$\partial_1\nu_{T,n}(\mathbf{u})(\mathbf{z}) = (C_S h_K)^2\big[(\phi_n' * |\nabla\mathbf{u}_{|_K}|) : \nabla\mathbf{z}\big].$$

Note that we are denoting $U = (\mathbf{u},\theta^u,p^u), V = (\mathbf{v},\theta^v,p^v), Z = (\mathbf{z},\theta^z,p^z) \in X$. The directional derivative verifies the following continuity and inf-sup conditions:

$$\infty > \gamma_0 < \gamma_h(\mu) \equiv \sup_{Z_h \in X_h} \sup_{V_h \in X_h} \frac{\partial_1 A(U_N(\mu), V_h; \mu)(V_h)}{\|Z_h\|_X \|V_h\|_X}. \tag{4.23}$$

$$0 < \beta_0 < \beta_h(\mu) \equiv \inf_{Z_h \in X_h} \sup_{V_h \in X_h} \frac{\partial_1 A(U_N(\mu), V_h; \mu)(Z_h)}{\|Z_h\|_X \|V_h\|_X}. \tag{4.24}$$

The existence of $\gamma_0 \in \mathbb{R}$ and $\beta_0 > 0$ satisfying (4.23) and (4.24), respectively, are given by the following results:

Lemma 4.1. *Let $\boldsymbol{u} \in Y$, then there exists a constant $C \in \mathbb{R}$, depending on $\boldsymbol{u}$, such that*

$$\left| \int_\Omega \partial_1 \nu_{T,n}(\Pi_h^* \boldsymbol{u})(\Pi_h^* \boldsymbol{z}) \, \nabla(\Pi_h^* \theta^u) \cdot \nabla(\Pi_h^* \theta^v) \, d\Omega \right| \leq C \|\nabla \boldsymbol{z}\|_{0,2,\Omega} \|\nabla \boldsymbol{v}\|_{0,2,\Omega}. \tag{4.25}$$

Proof. It holds:

$$\left| \int_\Omega \partial_1 \nu_{T,n}(\Pi_h^* \mathbf{u})(\Pi_h^* \mathbf{z}) \, \nabla(\Pi_h^* \theta^u) \cdot \nabla(\Pi_h^* \theta^v) \, d\Omega \right|$$

$$\leq (C_S h)^2 \int_\Omega \left| (\phi_n' * |\nabla(\Pi_h^* \mathbf{u})|) \right| |\nabla(\Pi_h^* \mathbf{z})| |\nabla(\Pi_h^* \mathbf{u})| |\nabla(\Pi_h^* \mathbf{v})| \, d\Omega$$

$$\leq (C_S h)^2 \|\phi_n' * |\nabla(\Pi_h^* \mathbf{u})|\|_{0,\infty,\Omega} \|\nabla(\Pi_h^* \mathbf{u})\|_{0,3,\Omega} \|\nabla(\Pi_h^* \mathbf{z})\|_{0,3,\Omega} \|\nabla(\Pi_h^* \mathbf{v})\|_{0,3,\Omega}$$

$$\leq C \|\nabla \mathbf{z}\|_{0,2,\Omega} \|\nabla \mathbf{v}\|_{0,2,\Omega},$$

where we are using that $\|\phi_n' * |\nabla(\Pi_h^* \mathbf{u})|\|_{0,\infty,\Omega} \leq \|\phi_n'\|_{0,1,\mathbb{R}} \|\nabla(\Pi_h^* \mathbf{u})\|_{0,\infty,\Omega}$ (see e.g. [15]), the properties of the interpolation operator of Prop. 3.1, and the local inverse inequalities of Lemma 2.1.

□

Proposition 4.2. *There exists $\gamma_0 \in \mathbb{R}$ such that $\forall \mu \in \mathcal{D}$*

$$|\partial_1 A(U_h(\mu), V_h; \mu)(Z_h)| \leq \gamma_0 \|Z_h\|_X \|V_h\|_X \quad \forall Z_h, V_h \in X_h.$$

Proof. It holds

$$\begin{aligned} |\partial_1 A(U_h(\mu), V_h; \mu)(Z_h)| \; &\leq |\partial_1 A_0(U_h(\mu), V_h)(Z_h)| + \mu |\partial_1 A_1(U_h(\mu), V_h)(Z_h)| \\ &\quad + |\partial_1 A_2(U_h(\mu); V_h)(Z_h)| + |\partial_1 A_3(U_h(\mu); V_h)(Z_h)|. \end{aligned}$$

From Prop. 2.1, we can deduce the boundedness of $|\partial_1 A_0(U_h(\mu), V_h)(Z_h)|$, and from Prop. 3.3, we can deduce the boundedness of $|\partial_1 A_2(U_h(\mu); V_h)(Z_h)|$ and $|\partial_1 A_3(U_h(\mu); V_h)(Z_h)|$, using the same techniques for the eddy diffusivity term, and Lemma 4.1.

Thus, we only have to prove the boundedness of $|\partial_1 A_1(U_h(\mu), V_h)(Z_h)|$. Using the Cauchy-Schwartz's and Poincaré's inequality, we have,

$$|\partial_1 A_1(U_h(\mu), V_h)(Z_h)| \leq Pr\|\theta_h^u\|_{0,2,\Omega}\|\mathbf{v}_h\|_{0,2,\Omega}$$

$$\leq C_P Pr\|\nabla\theta_h^u\|_{0,2,\Omega}\|\nabla\mathbf{v}_h\|_{0,2,\Omega} \leq C_2\|U_h\|_X\|V_h\|_X.$$

Thus, we have proved that there exists γ_0 such that

$$\infty > \gamma_0 > \gamma_h(\mu) = \sup_{Z_h\in X_h}\sup_{V_h\in X_h}\frac{\partial_1 A(U_h(\mu), V_h;\mu)(Z_h)}{\|Z_h\|_X\|V_h\|_X}.$$

□

Proposition 4.3. *If the Dirichlet boundary data is sufficiently small, then there exists $\tilde{\beta}(\mu) > 0$ such that*

$$\partial_1 A(U_h, V_h;\mu)(V_h) \geq \tilde{\beta}(\mu)(\|\nabla \boldsymbol{v}_h\|^2_{0,2,\Omega} + \|\nabla\theta_h^v\|^2_{0,2,\Omega}) \quad \forall V_h \in \ X_h. \tag{4.26}$$

Proof. We consider $Z_h = V_h$ in $\partial_1 A(U_h, V_h;\mu)(Z_h)$, letting

$$\begin{aligned}\partial_1 A(U_h, V_h;\mu)(V_h) \ &= \partial_1 A_0(U_h, V_h)(V_h) + \mu\,\partial_1 A_1(U_h, V_h)(V_h)\\ &+ \partial_1 A_2(U_h, V_h)(V_h) + \partial_1 A_3(U_h; V_h)(V_h).\end{aligned} \tag{4.27}$$

Denoting by C_P the Poincare's constant, we have that

$$\partial_1 A_0(U_h, V_h)(V_h) \geq Pr\|\nabla\mathbf{v}_h\|^2_{0,2,\Omega} + \|\nabla\theta_h^v\|^2_{0,2,\Omega}, \tag{4.28}$$

and considering the Holder's and Young's inequalities,

$$\begin{aligned}\mu\,\partial_1 A_1(U_h, V_h)(V_h) \ &\geq -Pr\,\mu\|\theta_h^v\|_{0,2,\Omega}\|v_d\|_{0,2,\Omega}\\ &\geq -\frac{C_P Pr\,\mu}{2}(\|\nabla\theta_h^v\|^2_{0,2,\Omega} + \|\nabla\mathbf{v}_h\|^2_{0,2,\Omega}).\end{aligned} \tag{4.29}$$

Recalling the Sobolev embedding constants C_u and C_θ, defined in (4.3) and (4.4) respectively, it holds,

$$\partial_1 A_2(U_h, V_h)(V_h) \geq -2C_u^2\|\nabla\mathbf{u}_h\|_{0,2,\Omega}\|\nabla\mathbf{v}_h\|^2_{0,2,\Omega} - 2C_u C_\theta\|\nabla\theta_h^u\|_{0,2,\Omega}\|\nabla\theta_h^v\|^2_{0,2,\Omega}. \tag{4.30}$$

Finally, using the local inverse inequalities of Lemma 2.1, and taking into account that

$$\int_\Omega \nu_T(\nabla(\Pi_h^*\mathbf{u}_h))|\nabla(\Pi_h^*\mathbf{v}_h)|^2\,d\Omega + \sum_{K\in\mathcal{T}_h}\int_K (C_S h_K)^2\frac{|\nabla(\Pi_h^*\mathbf{u}_h) : \nabla(\Pi_h^*\mathbf{v}_h)|^2}{|\nabla(\Pi_h^*\mathbf{u}_h)|}\,d\Omega$$

$$+\int_\Omega \frac{\nu_T(\nabla(\Pi_h^*\mathbf{u}_h))}{Pr}|\nabla(\Pi_h^*\theta_h^v)|^2\,d\Omega \geq 0,$$

we have that

$$\partial_3 A(U_h,V_h)(V_h)=\int_\Omega \nu_T(\nabla(\Pi_h^*\mathbf{u}_h))|\nabla(\Pi_h^*\mathbf{v}_h)|^2\,d\Omega$$

$$+\sum_{K\in\mathcal{T}_h}\int_K (C_S h_K)^2\frac{|\nabla(\Pi_h^*\mathbf{u}_h):\nabla(\Pi_h^*\mathbf{v}_h)|^2}{|\nabla(\Pi_h^*\mathbf{u}_h)|}\,d\Omega+\int_\Omega\frac{\nu_{T,n}(\nabla(\Pi_h^*\mathbf{u}_h))}{Pr}|\nabla(\Pi_h^*\theta_h^v)|^2\,d\Omega$$

$$+\frac{1}{Pr}\int_\Omega \partial_1\nu_{T,n}(\Pi_h^*\mathbf{u}_h)(\Pi_h^*\mathbf{z}_h)\;\nabla(\Pi_h^*\theta_h^u)\cdot\nabla(\Pi_h^*\theta_h^v)\,d\Omega$$

$$\geq -\frac{C_S^2h^{2-d/2}C_f^4C\|\phi_n'\|_{0,1,\mathbb{R}}}{Pr}\|\nabla\mathbf{u}_h\|_{0,\infty,\Omega}\|\nabla\theta_h^u\|_{0,2,\Omega}\|\nabla\mathbf{v}_h\|_{0,2,\Omega}\|\nabla\theta_h^v\|_{0,2,\Omega}$$

$$\geq -\frac{C_S^2h^{2-d/2}C_f^4C}{2Pr}\|\nabla\mathbf{u}_h\|_{0,\infty,\Omega}\|\nabla\theta_h^u\|_{0,2,\Omega}(\|\nabla\mathbf{v}_h\|_{0,2,\Omega}^2+\|\nabla\theta_h^v\|_{0,2,\Omega}^2).$$

Thus, we have prove that for data small enough,

$$\partial_1 A(U_h,V_h;\mu)(V_h)\geq\tilde{\beta}(\mu)(\|\nabla\mathbf{v}_h\|_{0,2,\Omega}^2+\|\nabla\theta_h^v\|_{0,2,\Omega}^2)\quad\forall V_h\in\ X_h.$$

□

Since the operator $b(\mathbf{v}_h,p_h;\mu)$ satisfies the discrete inf-sup condition

$$\alpha\|p_h\|_{0,2,\Omega}\leq\sup_{\mathbf{v}_h\in Y_h}\frac{b(\mathbf{v}_h,p_h;\mu)}{\|\nabla\mathbf{v}_h\|_{0,2,\Omega}},$$

we can prove that the inf-sup (4.24) is satisfied thanks to Prop. 4.3.

4.4 A *posteriori* error bound estimator

In this section, we present the development of the a *posteriori* error bound estimator, needed in the Greedy algorithm for the construction of the reduced spaces for velocity, temperature and pressure. For this purpose, we deal with the BRR theory [18].

With the following result, we prove that the directional derivative $\partial_1 A$ is Lipschitz-continuous:

Lemma 4.2. *There exists a positive constant ρ_n such that, $\forall U_h^1,U_h^2,Z_h,V_h\in X_h$,*

$$\left|\partial_1 A(U_h^1,V_h;\mu)(Z_h)-\partial_1 A(U_h^2,V_h;\mu)(Z_h)\right|\leq\rho_n\|U_h^1-U_h^2\|_X\|Z_h\|_X\|V_h\|_X. \quad (4.31)$$

Proof. It holds that

$$\partial_1 A_n(U_h^1, V_h; \mu)(Z_h) - \partial_1 A_n(U_h^2, V_h; \mu)(Z_h) = \int_\Omega ((\mathbf{u}_h^1 - \mathbf{u}_h^2) \cdot \nabla \mathbf{z}_h)\mathbf{v}_h \, d\Omega$$

$$+ \int_\Omega (\mathbf{z}_h \cdot \nabla(\mathbf{u}_h^1 - \mathbf{u}_h^2))\mathbf{v}_h \, d\Omega + \int_\Omega ((\mathbf{u}_h^1 - \mathbf{u}_h^2) \cdot \nabla \theta_h^z)\theta_h^v \, d\Omega + \int_\Omega (\mathbf{z}_h \cdot \nabla(\theta_h^{u1} - \theta_h^{u2}))\theta_h^v \, d\Omega$$

$$+ \int_\Omega \left[\nu_T(\Pi_h^* \mathbf{u}_h^1) - \nu_T(\Pi_h^* \mathbf{u}_h^2)\right] \nabla(\Pi_h^* \mathbf{z}_h) : \nabla(\Pi_h^* \mathbf{v}_h) \, d\Omega$$

$$+ \sum_{K \in \mathcal{T}_h} \int_K (C_S h_K)^2 \frac{\nabla(\Pi_h^* \mathbf{u}_h^1) : \nabla(\Pi_h^* \mathbf{z}_h)}{|\nabla(\Pi_h^* \mathbf{u}_h^1)|} \left(\nabla(\Pi_h^* \mathbf{u}_h^1) : \nabla(\Pi_h^* \mathbf{v}_h)\right) \, d\Omega$$

$$- \sum_{K \in \mathcal{T}_h} \int_K (C_S h_K)^2 \frac{\nabla(\Pi_h^* \mathbf{u}_h^2) : \nabla(\Pi_h^* \mathbf{z}_h)}{|\nabla(\Pi_h^* \mathbf{u}_h^2)|} \left(\nabla(\Pi_h^* \mathbf{u}_h^2) : \nabla(\Pi_h^* \mathbf{v}_h)\right) \, d\Omega$$

$$+ \frac{1}{Pr} \int_\Omega \left[\nu_{T,n}(\Pi_h^* \mathbf{u}_h^1) - \nu_{T,n}(\Pi_h^* \mathbf{u}_h^2)\right] \nabla(\Pi_h^* \theta_h^z) \cdot \nabla(\Pi_h^* \theta_h^v) \, d\Omega$$

$$+ \frac{1}{Pr} \int_\Omega \partial_1 \nu_{T,n}(\Pi_h^* \mathbf{u}_h^1)(\Pi_h^* \mathbf{z}_h) \, \nabla(\Pi_h^* \theta_h^{u1}) \cdot \nabla(\Pi_h^* \theta_h^v) \, d\Omega$$

$$- \frac{1}{Pr} \int_\Omega \partial_1 \nu_{T,n}(\Pi_h^* \mathbf{u}_h^2)(\Pi_h^* \mathbf{z}_h) \, \nabla(\Pi_h^* \theta_h^{u2}) \cdot \nabla(\Pi_h^* \theta_h^v) \, d\Omega.$$

Thus, thanks to the triangular inequality, it follows

$$|\partial_1 A_n(U_h^1, V_h; \mu)(Z_h) - \partial_1 A_n(U_h^2, V_h; \mu)(Z_h)| \leq \left| \int_\Omega ((\mathbf{u}_h^1 - \mathbf{u}_h^2) \cdot \nabla \mathbf{z}_h)\mathbf{v}_h \, d\Omega \right|$$

$$+ \left| \int_\Omega (\mathbf{z}_h \cdot \nabla(\mathbf{u}_h^1 - \mathbf{u}_h^2))\mathbf{v}_h \, d\Omega \right| + \left| \int_\Omega ((\mathbf{u}_h^1 - \mathbf{u}_h^2) \cdot \nabla \theta_h^z)\theta_h^v \, d\Omega \right|$$

$$+ \left| \int_\Omega (\mathbf{z}_h \cdot \nabla(\theta_h^{u1} - \theta_h^{u2}))\theta_h^v \, d\Omega \right|$$

$$+ \left| \int_\Omega \left[\nu_T(\Pi_h^* \mathbf{u}_h^1) - \nu_T(\Pi_h^* \mathbf{u}_h^2)\right] \nabla(\Pi_h^* \mathbf{z}_h) : \nabla(\Pi_h^* \mathbf{v}_h) \, d\Omega \right|$$

$$+ \left| \sum_{K \in \mathcal{T}_h} \int_K (C_S h_K)^2 \frac{\nabla(\Pi_h^* \mathbf{u}_h^1) : \nabla(\Pi_h^* \mathbf{z}_h)}{|\nabla(\Pi_h^* \mathbf{u}_h^1)|} \left(\nabla(\Pi_h^* \mathbf{u}_h^1) : \nabla(\Pi_h^* \mathbf{v}_h)\right) \, d\Omega \right.$$

$$\left. - \sum_{K \in \mathcal{T}_h} \int_K (C_S h_K)^2 \frac{\nabla(\Pi_h^* \mathbf{u}_h^2) : \nabla(\Pi_h^* \mathbf{z}_h)}{|\nabla(\Pi_h^* \mathbf{u}_h^2)|} \left(\nabla(\Pi_h^* \mathbf{u}_h^2) : \nabla(\Pi_h^* \mathbf{v}_h)\right) \, d\Omega \right|$$

$$+ \left| \frac{1}{Pr} \int_\Omega \left[\nu_{T,n}(\Pi_h^* \mathbf{u}_h^1) - \nu_{T,n}(\Pi_h^* \mathbf{u}_h^2)\right] \nabla(\Pi_h^* \theta_h^z) \cdot \nabla(\Pi_h^* \theta_h^v) \, d\Omega \right|$$

$$+\left|\frac{1}{Pr}\int_\Omega \partial_1\nu_{T,n}(\Pi_h^*\mathbf{u}_h^1)(\Pi_h^*\mathbf{z}_h)\ \nabla(\Pi_h^*\theta_h^{u1})\cdot\nabla(\Pi_h^*\theta_h^v)\ d\Omega\right.$$
$$\left.-\frac{1}{Pr}\int_\Omega \partial_1\nu_{T,n}(\Pi_h^*\mathbf{u}_h^2)(\Pi_h^*\mathbf{z}_h)\ \nabla(\Pi_h^*\theta_h^{u2})\cdot\nabla(\Pi_h^*\theta_h^v)\ d\Omega\right|$$

In this inequality, there are eight terms, which we bound separately. Taking into account the notation of the Sobolev embedding constant introduced in (4.3), the first and second terms, associated to the convective term in the velocity equation, are bounded as in Lemma 2.2. The fifth and sixth terms, associated to the VMS-Smagorinsky term in the velocity equation, are bounded as in Lemma 3.2, with the obvious change of notation.

The third and fourth terms, associated to the convective terms of the energy equation, are bounded as follows

$$\left|\int_\Omega((\mathbf{u}_h^1-\mathbf{u}_h^2)\cdot\nabla\theta_h^z)\theta_h^v\ d\Omega\right|+\left|\int_\Omega(\mathbf{z}_h\cdot\nabla(\theta_h^{u1}-\theta_h^{u2}))\theta_h^v\ d\Omega\right|$$
$$\leq\int_\Omega|\mathbf{u}_h^1-\mathbf{u}_h^2||\nabla\theta_h^z||\theta_h^v|\ d\Omega+\int_\Omega|\mathbf{z}_h||\nabla(\theta_h^{u1}-\theta_h^{u2})||\theta_h^v|\ d\Omega$$
$$\leq\|\mathbf{u}_h^1-\mathbf{u}_h^2\|_{0,4,\Omega}\|\nabla\theta_h^z\|_{0,2,\Omega}\|\theta_h^v\|_{0,4,\Omega}+\|\mathbf{z}_h\|_{0,4,\Omega}\|\nabla(\theta_h^{u1}-\theta_h^{u2})\|_{0,2,\Omega}\|\theta_h^v\|_{0,4,\Omega}$$
$$\leq 2C_uC_\theta\|U_h^1-U_h^2\|_X\|Z_h\|_X\|V_h\|_X.$$

For the boundeness of the seventh term, associated to the VMS-Smagorinsky term in the energy equation, we use the local inverse inequalities of Lemma 2.1, the properties of Proposition 3.1, and the properties of the convolution, recalling that $\|\phi_n\|_{0,1,\mathbb{R}^d}=1$:

$$\left|\int_\Omega\left[\nu_{T,n}(\Pi_h^*\mathbf{u}_h^1)-\nu_{T,n}(\Pi_h^*\mathbf{u}_h^2)\right]\nabla(\Pi_h^*\theta_h^z)\cdot\nabla(\Pi_h^*\theta_h^v)\ d\Omega\right|$$
$$\leq\frac{(C_Sh)^2}{Pr}\int_\Omega\left|\left[\phi_n*(|\nabla(\Pi_h^*\mathbf{u}_h^1)|-|\nabla(\Pi_h^*\mathbf{u}_h^2)|)\right]\right||\nabla(\Pi_h^*\theta_h^z)||\nabla(\Pi_h^*\theta_h^v)|\ d\Omega$$
$$\leq\frac{(C_Sh)^2}{Pr}\|\phi_n\|_{0,1,\mathbb{R}}\|(\nabla(\Pi_h^*\mathbf{u}_h^1-\Pi_h^*\mathbf{u}_h^2)\|_{0,3,\Omega}\|\nabla(\Pi_h^*\theta_h^z)\|_{0,3,\Omega}\|\nabla(\Pi_h^*\theta_h^v)\|_{0,3,\Omega}$$
$$\leq\frac{C_S^2h^{2-d/2}C}{Pr}\|\nabla(\Pi_h^*\mathbf{u}_h^1-\Pi_h^*\mathbf{u}_h^2)\|_{0,2,\Omega}\|\nabla(\Pi_h^*\theta_h^z)\|_{0,2,\Omega}\|\nabla(\Pi_h^*\theta_h^v)\|_{0,2,\Omega}$$
$$\leq\frac{C_S^2h^{2-d/2}CC_f^3}{Pr}\|U_h^1-U_h^2\|_X\|Z_h\|_X\|V_h\|_X.$$

Finally, the last term is bounded as follows:

$$
\begin{aligned}
&+\left|\frac{1}{Pr}\int_\Omega \partial_1\nu_{T,n}(\Pi_h^*\mathbf{u}_h^1)(\Pi_h^*\mathbf{z}_h)\ \nabla(\Pi_h^*\theta_h^{u1})\cdot\nabla(\Pi_h^*\theta_h^v)\ d\Omega\right.\\
&\left.-\frac{1}{Pr}\int_\Omega \partial_1\nu_{T,n}(\Pi_h^*\mathbf{u}_h^2)(\Pi_h^*\mathbf{z}_h)\ \nabla(\Pi_h^*\theta_h^{u2})\cdot\nabla(\Pi_h^*\theta_h^v)\ d\Omega\right|\\
&\le\left|\frac{1}{Pr}\int_\Omega \partial_1\nu_{T,n}(\Pi_h^*\mathbf{u}_h^1)(\Pi_h^*\mathbf{z}_h)\ \nabla\left(\Pi_h^*(\theta_h^{u1}-\theta_h^{u2})\right)\cdot\nabla(\Pi_h^*\theta_h^v)\ d\Omega\right|\\
&+\left|\frac{1}{Pr}\int_\Omega \left[\partial_1\nu_{T,n}(\Pi_h^*\mathbf{u}_h^1)(\Pi_h^*\mathbf{z}_h)-\partial_1\nu_{T,n}(\Pi_h^*\mathbf{u}_h^2)(\Pi_h^*\mathbf{z}_h)\right]\nabla(\Pi_h^*\theta_h^{u2})\cdot\nabla(\Pi_h^*\theta_h^v)\ d\Omega\right|\\
&\le C_1\left(\|\nabla(\Pi_h^*\mathbf{u}_h^1)\|_{0,\infty,\Omega}\right)\|\nabla\mathbf{z}_h\|_{0,2,\Omega}\|\nabla\left(\theta_h^{u1}-\theta_h^{u2}\right)\|_{0,2,\Omega}\|\nabla\theta_h^v\|_{0,2,\Omega}\\
&+C_2\left(\|\nabla(\Pi_h^*\theta^{u2})\|_{0,\infty,\Omega}\right)\|\nabla\mathbf{z}_h\|_{0,2,\Omega}\|\nabla(\mathbf{u}_h^1-\mathbf{u}_h^2)\|_{0,2,\Omega}\|\nabla\theta_h^v\|_{0,2,\Omega}\\
&\le\left[C_1\left(\|\nabla(\Pi_h^*\mathbf{u}_h^1)\|_{0,\infty,\Omega}\right)+C_2\left(\|\nabla(\Pi_h^*\theta^{u2})\|_{0,\infty,\Omega}\right)\right]\|U_h^1-U_h^2\|_X\|Z_h\|_X\|V_h\|_X,
\end{aligned}
$$

with

$$
C_1\left(\|\nabla(\Pi_h^*\mathbf{u}_h^1)\|_{0,\infty,\Omega}\right)=\frac{C_S^2h^{2-d/2}CC_f^3\|\phi_n'\|_{0,1,\mathbb{R}}}{Pr}\|\nabla(\Pi_h^*\mathbf{u}_h^1)\|_{0,\infty,\Omega},
$$

and

$$
C_2\left(\|\nabla(\Pi_h^*\theta^{u2})\|_{0,\infty,\Omega}\right)=\frac{C_S^2h^{2-d/2}CC_f^3\|\phi_n'\|_{0,1,\mathbb{R}}}{Pr}\|\nabla(\Pi_h^*\theta^{u2})\|_{0,\infty,\Omega}.
$$

Thus, we have proved (4.31), with

$$
\begin{aligned}
\rho_n&=2C_u+2C_\theta+4C_S^2h^{2-d/2}CC_f^3\\
&+\frac{C_S^2h^{2-d/2}CC_f^3\|\phi_n'\|_{0,1,\mathbb{R}}(\|\nabla(\Pi_h^*\mathbf{u}_h^1)\|_{0,\infty,\Omega}+\|\nabla(\Pi_h^*\theta^{u2})\|_{0,\infty,\Omega})}{Pr}.
\end{aligned}
$$

□

Remark 4.4. *Note that when $h\to 0$, $\rho_n\to 2C_u+2C_\theta$, getting that $\partial_1 A$ is globally Lipschitz, since it does not depends on U_h^1 and U_h^2.*

We define the following continuity and inf-sup constants, relative to the well-posedness of the RB problem (4.14):

$$
0<\beta_N(\mu)\equiv\inf_{Z_h\in X_h}\sup_{V_h\in X_h}\frac{\partial_1 A_n(U_N(\mu),V_h;\mu)(Z_h)}{\|Z_h\|_X\|V_h\|_X}=\inf_{Z_h\in X_h}\frac{\|T_NZ_h\|_X}{\|Z_h\|_X},\qquad(4.32)
$$

$$\infty > \gamma_N(\mu) \equiv \sup_{Z_h \in X_h} \sup_{V_h \in X_h} \frac{\partial_1 A_n(U_N(\mu), V_h; \mu)(Z_h)}{\|Z_h\|_X \|V_h\|_X} = \sup_{Z_h \in X_h} \frac{\|T_N Z_h\|_X}{\|Z_h\|_X}, \quad (4.33)$$

where the *supremizer* operator T_N is defined in (2.24). The existence of these constants can be proved in the same way that the existence of the constants (4.23)-(4.24). Thus, we can define the *a posteriori* error bound estimator as

$$\Delta_N(\mu) = \frac{\beta_N(\mu)}{2\rho_n} \left[1 - \sqrt{1 - \tau_N(\mu)}\right], \quad (4.34)$$

where $\tau_N(\mu)$ is given by

$$\tau_N(\mu) = \frac{4\epsilon_N(\mu)\rho_n}{\beta_N^2(\mu)}, \quad (4.35)$$

with $\epsilon_N(\mu)$ the dual norm of the residual. The *a posteriori* error bound estimator is stated by the following result

Theorem 4.1. *Let $\mu \in \mathcal{D}$, and assume that $\beta_N(\mu) > 0$. If problem (4.12) admits a solution $U_h(\mu)$ such that*

$$\|U_h(\mu) - U_N(\mu)\|_X \leq \frac{\beta_N(\mu)}{\rho_n},$$

then this solution is unique in the ball $B_X\left(U_N(\mu), \frac{\beta_N(\mu)}{\rho_n}\right)$.

Moreover, assume that $\tau_N(\mu) \leq 1$ for all $\mu \in \mathcal{D}$. Then there exists a unique solution $U_h(\mu)$ of (4.12) such that the error with respect $U_N(\mu)$, solution of (4.14), is bounded by the a posteriori error bound estimator, i.e.,

$$\|U_h(\mu) - U_N(\mu)\|_X \leq \Delta_N(\mu), \quad (4.36)$$

with effectivity

$$\Delta_N(\mu) \leq \left[\frac{2\gamma_N(\mu)}{\beta_N(\mu)} + \tau_N(\mu)\right] \|U_h(\mu) - U_N(\mu)\|_X. \quad (4.37)$$

Proof. The proof of this problem can be derived from the proofs of Theorem 2.1 and Theorem 2.2. Since we have verified that the operator $\partial_1 A$ is Lipschitz-continuous, the technique is analogue.

□

4.5 Numerical results

In this section, we present the numerical results for the VMS-Boussinesq reduced basis model, presented in section 4.2. The numerical results have been performed with FreeFrem++ (*cf.* [48]). We consider a two-dimensional unity square cavity, in which the flow is driven by a temperature gradient between the two vertical walls. The top and the bottom of the cavity are isolated. We impose no-slip boundary conditions for the velocity in all walls, and we suppose that the gravity acts on the vertical direction. In Fig. 4.1 we show a schematic representation of the problem considered.

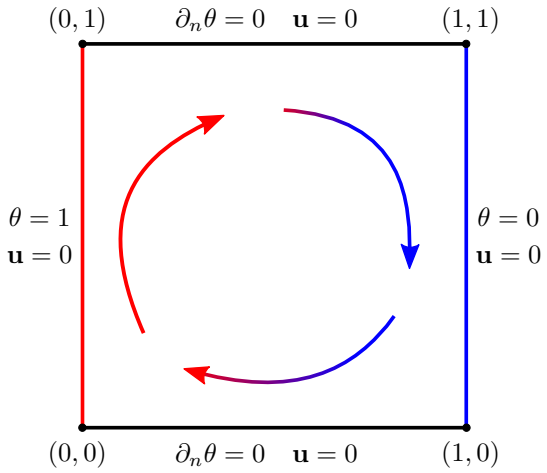

Figure 4.1: Unity cavity domain Ω, with the different boundaries identified, for problem 4.1.

We perform two tests, with different intervals for the Rayleigh number. We first start considering moderate Rayleigh numbers, taking $\mu \in [10^3, 10^5]$. Then, we consider larger Rayleigh numbers, with $\mu \in [10^5, 10^6]$, which leads to a much more complex flows. In the full range $[10^3, 10^6]$, the flow pattern experiments large changes. Considering two sub-intervals provides an accurate representation of the flow, as the flow pattern changes within each range are smaller. Since we are interested in the study of the aero-thermal flows, we consider that the Prandtl number is fixed, more precisely, we the consider $Pr = 0.71$, that is the Prandtl number for the air.

We solve steady problem (4.6) by a semi-implicit evolution approach, considering that the steady regime is reached when the error between two iterations is below $\varepsilon_{FE} = 10^{-10}$. This numerical scheme reads

$$
\begin{cases}
\text{Find } (\mathbf{u}_h^{n+1}, \theta_h^{u,n+1}, p_h^{u,n+1}) \in Y_h \times \Theta_h \times M_h \text{ such that} & \\
\left(\dfrac{\mathbf{u}_h^{n+1} - \mathbf{u}_h^n}{\Delta t}\right)_\Omega + a_u(\mathbf{u}_h^{n+1}, \mathbf{v}_h; \mu) + b(\mathbf{v}_h, p_h^{u,n+1}; \mu) & \\
+a'_{Su}(\mathbf{u}_h^n; \mathbf{u}_h^{n+1}, \mathbf{v}_h; \mu) + c_u(\mathbf{u}_h^n, \mathbf{u}_h^{n+1}, \mathbf{v}; \mu) & \\
+f(\theta_h^{u,n+1}, \mathbf{v}; \mu) = F(\mathbf{v}_h; \mu) & \forall \mathbf{v}_h \in Y_h, \\
b(\mathbf{u}_h^{n+1}, p_h^v; \mu) = 0 & \forall p_h^v \in M_h, \\
\left(\dfrac{\theta_h^{u,n+1} - \theta_h^{u,n}}{\Delta t}\right)_\Omega + a'_{S\theta}(\mathbf{u}_h^n; \theta_h^{u,n+1}, \theta_h^v; \mu) & \\
+a_\theta(\theta_h^{u,n+1}, \theta_h^v; \mu) + c_\theta(\mathbf{u}_h^n, \theta_h^{u,n+1}, \theta_h^v; \mu) = Q(\theta_h^v; \mu) & \forall \theta_h^v \in \Theta_h.
\end{cases}
\tag{4.38}
$$

4.5.1 Moderate Rayleigh numbers

In this test, we consider the Rayleigh number range $\mathcal{D} = [10^3, 10^5]$. For the lower Rayleigh values in this interval, as showed in the literature (see e.g. [26, 35, 108]) the heat transfer is principally in form of diffusion, i.e., the diffusion term in the energy equation is predominant, leading to an almost vertical linear contouring for the temperature, and a recirculating motion in the core of the region is observed. As we increase the value of the Rayleigh number in $\mathcal{D}$, the flow is stretched to the walls, specially to the vertical walls; and the heat transfer become to be due to convection. The isotherms become horizontal in a domain inside the cavity, far from the walls, that increases as the Rayleigh number increases. This behavior can be observed in Figures 4.2 and 4.3. In Fig. 4.2 we show the FE velocity magnitude and temperature for $\mu = 4363$, while in Fig. 4.3 we show the FE velocity magnitude and temperature for $\mu = 53778$.

This FE solution have been computed considering $\mathbb{P}2-\mathbb{P}2-\mathbb{P}1$ finite elements for velocity, temperature and pressure, respectively. We consider a uniform mesh, with 50 divisions in each square side, i.e., $h = 0.02\sqrt{2}$. We have considered a time step $\Delta t = 0.01$ in the evolution semi-implicit approach (4.38). For larger values of the time step, the numerical scheme does not converges to a steady solution.

In the Reduced Basis framework, we perform an EIM (see Sec. 1.6) for both the eddy viscosity and eddy diffusivity. Although for the numerical analysis performed in this Chapter we have considered a regularized eddy diffusivity, the numerical tests are done with the eddy diffusivity defined in (4.2). Since the eddy diffusivity is proportional to the eddy viscosity, we only need to perform one EIM. With the EIM we are able to decouple the parameter dependence of the non-linear eddy viscosity and eddy diffusivity terms. For this test, we need $M = 42$ basis until reaching a prescribed tolerance of $\varepsilon_{EIM} = 5 \cdot 10^{-3}$. In Fig.

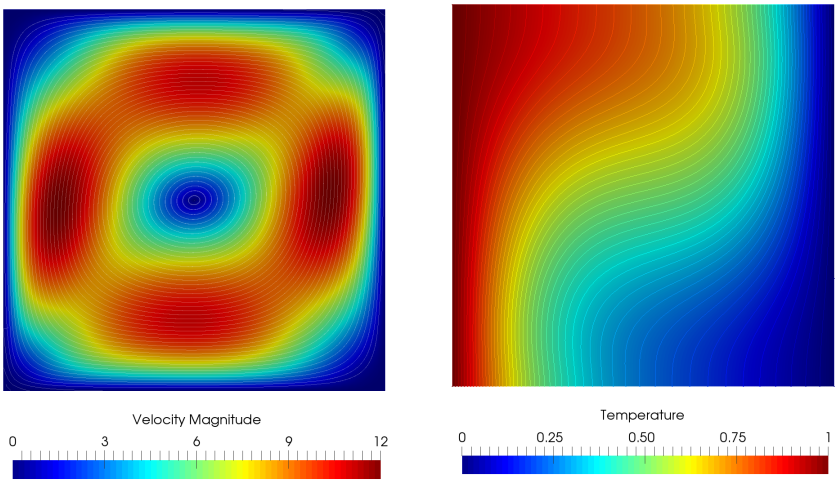

Figure 4.2: FE solution, velocity magnitude and temperature, for $Ra = 4363$

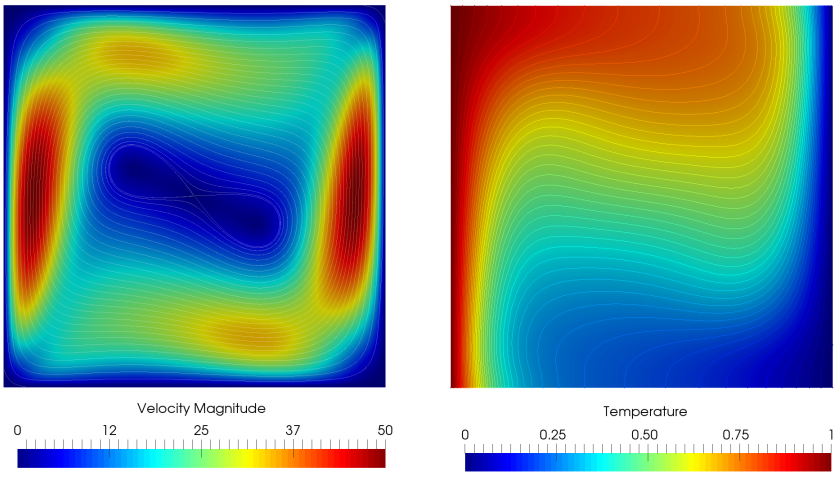

Figure 4.3: FE solution, velocity magnitude and temperature, for $Ra = 53778$

4.4 we show the evolution of this error.

For the Greedy algorithm we prescribe a tolerance of $\varepsilon_{RB} = 10^{-4}$. For this test, we need $N_{\max} = 22$ basis to reach this tolerance. When $N = 15$, holds the condition of Theorem 4.1 and $\tau_N(\mu) < 1$ for all μ in $\mathcal{D}$. From that point, the *a posteriori* error bound estimator $\Delta_N(\mu)$ exists. When $\tau_N(\mu) > 1$, we use as *a posteriori* error bound the proper $\tau_N(\mu)$. In Fig. 4.5 we show the convergence for the greedy algorithm, and in Fig. 4.6 we show the value of the *a posteriori* error bound estimator, for $N = N_{\max}$.

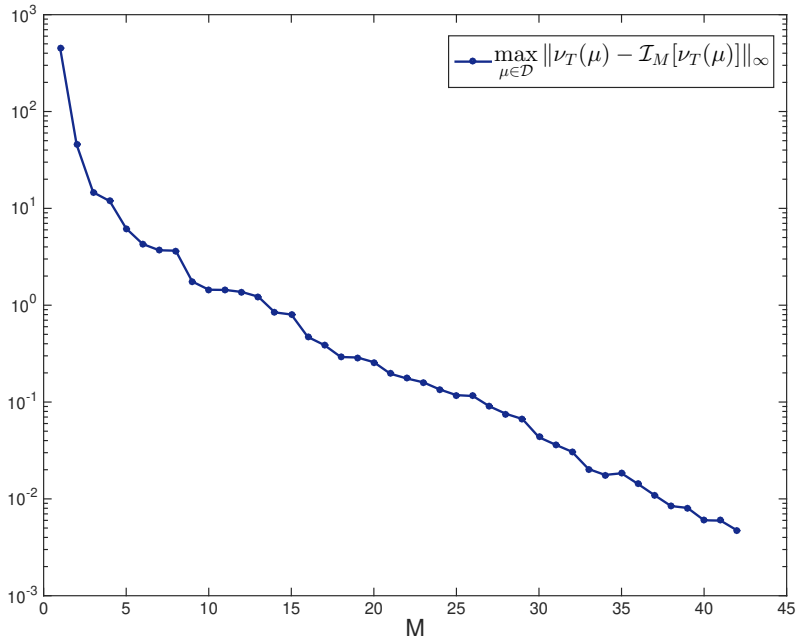

Figure 4.4: Error evolution for the EIM, for $\mu \in [10^3, 10^5]$

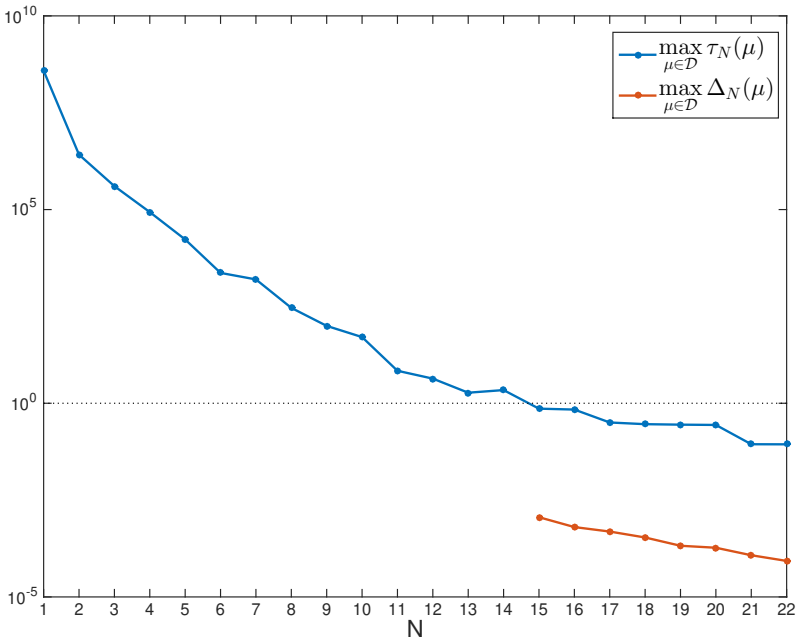

Figure 4.5: Evolution of the *a posteriori* error bound in the Greedy algorithm

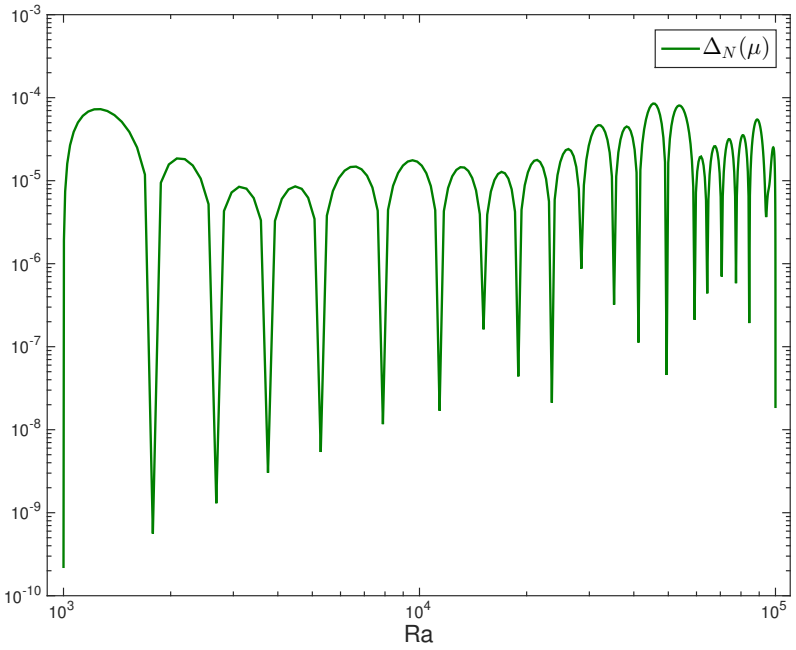

Figure 4.6: *A posteriori* error bound for $N = N_{\max} = 22$

Finally, in Table 4.1, we show a comparison between the FE and RB solutions for several Rayleigh values. We show the computational time for solving a FE solution and a RB solution in the online phase. As can be observed, the speed-up rate of the computational time is larger than one thousand. Moreover, we show the errors in H^1-norm for velocity and temperature, and in L^2-norm for pressure; for which we observe that the RB solution is close enough to the FE solution.

Data	$Ra = 4060$	$Ra = 17808$	$Ra = 53778$	$Ra = 93692$
T_{FE}	633.65s	585.83s	553.25s	677.86s
T_{online}	0.55s	0.5s	0.46s	0.49s
speedup	1133	1151	1189	1367
$\|\mathbf{u}_h - \mathbf{u}_N\|_1$	$2.26 \cdot 10^{-7}$	$5.93 \cdot 10^{-7}$	$1.04 \cdot 10^{-6}$	$1.34 \cdot 10^{-6}$
$\|\theta_h - \theta_N\|_1$	$4.57 \cdot 10^{-9}$	$5.57 \cdot 10^{-9}$	$8.9 \cdot 10^{-9}$	$8.83 \cdot 10^{-9}$
$\|p_h - p_N\|_1$	$2.49 \cdot 10^{-7}$	$3.22 \cdot 10^{-7}$	$1.11 \cdot 10^{-6}$	$2.27 \cdot 10^{-6}$

Table 4.1: Computational time for FE and RB solutions, with the speedup and the error, for problem (4.1), and $\mu \in [10^3, 10^5]$.

4.5.2 High Rayleigh numbers

In this test, we increase the Rayleigh number with respect to the previous one. We consider the Rayleigh number ranging in $\mathcal{D} = [10^5, 10^6]$. In this Rayleigh range the velocity in the center of the cavity is practically zero, and presents large and normal gradients near the vertical walls. The temperature isolines are horizontal in a large domain inside the cavity, except in the near of the vertical walls. In Fig. 4.7 we show a FE solution computed for a Rayleigh value $\mu = 667746$. This behavior agrees with the results presented in several works, e.g. [26, 35, 108].

The FE element solutions have been computed considering again $\mathbb{P}2-\mathbb{P}2-\mathbb{P}1$ finite elements for velocity, temperature and pressure, respectively. For this test, we have considered a finer mesh, in order to compute more accurately the eddies near the walls. Thus, we have considered a uniform mesh with 70 divisions in each square side, i.e., $h = 1/70 \cdot \sqrt{2}$. To obtain convergence in the semi-implicit evolution approach (4.38), we have to take a lower time step than in the previous test. More precisely, we take $\Delta t = 2 \cdot 10^{-3}$.

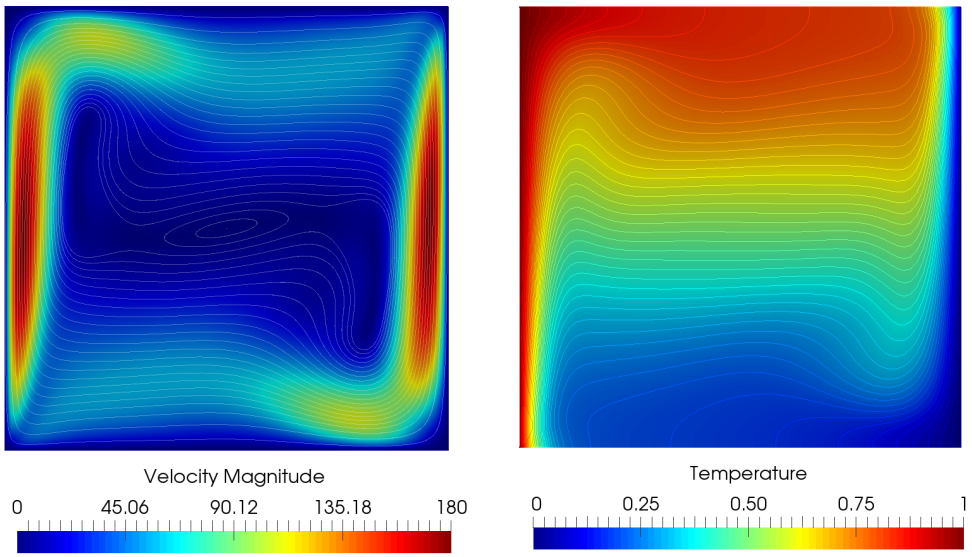

Figure 4.7: FE solution, velocity magnitude and temperature, for $Ra = 667746$

Again, we use the EIM to linearize the eddy viscosity and the eddy diffusivity. For this test, the Smagorinsky eddy viscosity and eddy diffusivity terms become more relevant. For this reason, we take a lower tolerance for this test with respect the previous one, considering $\varepsilon_{EIM} = 10^{-4}$. For this test, we need $M = 150$ basis in the EIM to reach the mentioned tolerance. In Fig. 4.8 we show the evolution of the maximum error in the Greedy algorithm performed in the EIM.

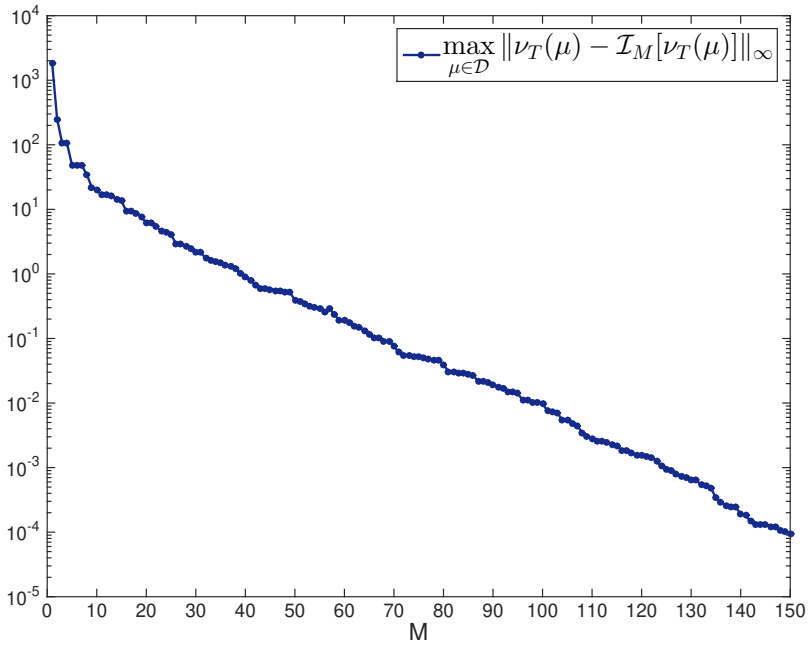

Figure 4.8: Error evolution for the EIM for $\mu \in [10^5, 10^6]$

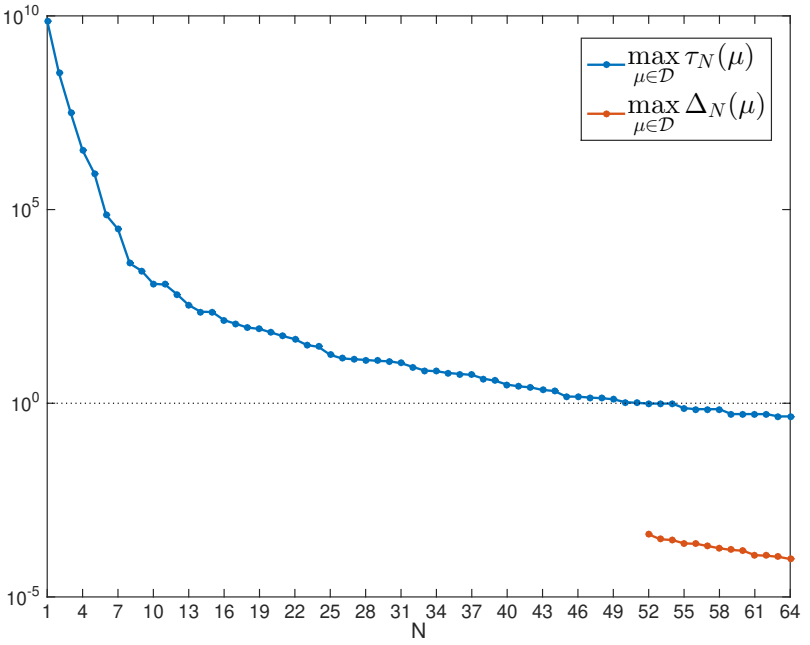

Figure 4.9: Evolution of the *a posteriori* error bound in the Greedy algorithm

In this test, for the Greedy algorithm we prescribe a tolerance of $\varepsilon_{RB} = 10^{-4}$. The complexity of this test, due to the high Rayleigh values chosen, leads to the necessity of a high number of basis functions in order to approximate accurately the RB solution. Thus, we need $N = N_{\max} = 64$ basis functions to reach the tolerance previously prescribed. Moreover, $\tau_N(\mu)$ becomes smaller than one when we get $N = 52$ basis functions. As usual, we consider as *a posteriori* error bound the proper $\tau_N(\mu)$, when it is greater than one and $\Delta_N(\mu)$ does not exist. In Fig. 4.9 we show the evolution of the *a posteriori* error bound during the Greedy algorithm. In Fig. 4.10 we show the *a posteriori* error bound when the Greedy algorithm is finished, i.e., for $N = N_{\max} = 64$.

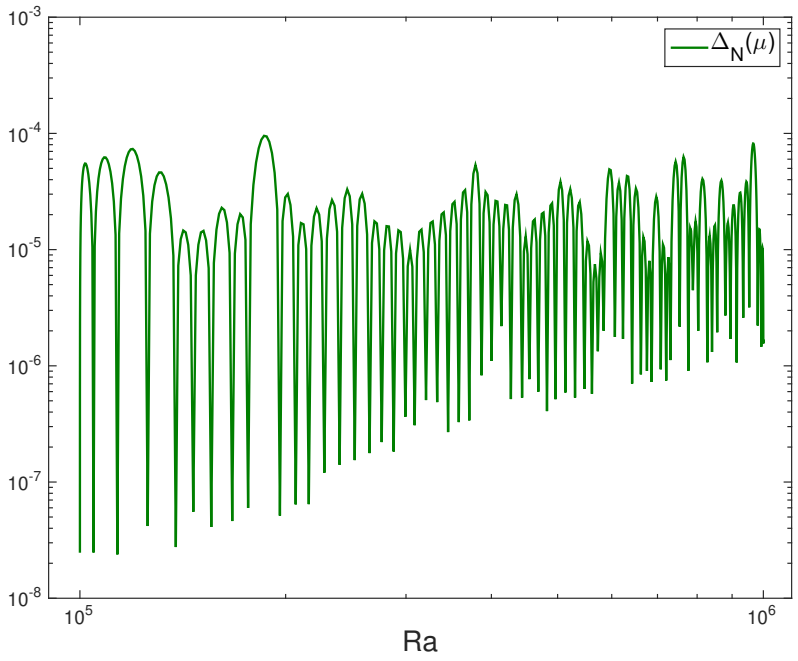

Figure 4.10: *A posteriori* error bound for $N = N_{\max} = 64$

Finally, in Table 4.2, we present a summary of the results for different parameter values. We show a comparison of the computational time for the computation of a FE solution and the computation of a RB solution in the online phase. We can observe a reduction of the computational time close to tree hundreds. The error between the FE solution and the RB solution is around 10^{-6} for velocity, 10^{-8} for temperature and 10^{-5} for pressure. Thus, we can conclude that we can compute an accurate approximation of the FE solution, with a high reduction of the computational time.

Data	$\mu = 16941$	$\mu = 355402$	$\mu = 667746$	$\mu = 921441$
T_{FE}	3563.11s	3675.01s	4354.26s	4928.37s
T_{online}	9.28s	11.34s	15.22s	16.8s
speedup	383	324	285	293
$\|\mathbf{u}_h - \mathbf{u}_N\|_1$	$1.74 \cdot 10^{-6}$	$2.77 \cdot 10^{-6}$	$2.28 \cdot 10^{-6}$	$5.35 \cdot 10^{-6}$
$\|\theta_h - \theta_N\|_1$	$1.23 \cdot 10^{-8}$	$1.33 \cdot 10^{-8}$	$1.34 \cdot 10^{-8}$	$1.33 \cdot 10^{-8}$
$\|p_h - p_N\|_1$	$6.29 \cdot 10^{-6}$	$1.43 \cdot 10^{-5}$	$2.66 \cdot 10^{-5}$	$3.54 \cdot 10^{-5}$

Table 4.2: Computational time for FE and RB solutions, with the speedup and the error, for problem (4.1), and $\mu \in [10^5, 10^6]$.

4.6 Conclusions

In this Chapter we have developed a RBM of buoyancy flows governed by a Boussinesq model with VMS-Smagorinsky modelling for the eddy viscosity and eddy diffusivity, which we need to approximate via EIM. We have developed an *a posteriori* error bound estimator, needed for the Greedy algorithm in the offline phase.

We have preformed two numerical tests, for moderate and high Rayleigh number values, in which we show high speed-up in the computation of the numerical solution of the Boussinesq model that is larger for the moderate range of Rayleigh number. Moreover, the error between the FE and RB solution is quite small.

Chapter 5

Natural convection flow in a variable height cavity

5.1 Introduction

In this Chapter we consider the application of the Reduced Basis Boussinesq VMS-Smagorinsky model studied in Chapter 4 to simulate a natural convection in a variable height cavity. Since each building is projected differently, this cavity perfectly can represent a room or a courtyard inside of a building. The study of the flow depending on the height of the room or the courtyard is of high interest in architectural applications.

The variability of the cavity height is considered through a geometrical parametrization on the domain. Since we are interested in solve efficiently the parameter-dependent problem, we need to reformulate the Boussinesq VMS-Smagorinsky model in a parameter-independent domain with a change of variables. This change of variables leads to obtain operators that depends on the geometrical parameter in the same way that they depends on the physical parameters. This setting let us to decompose affinely the operators with respect to the parameters, both physical and geometrical, letting us to store parameter-independent matrices and tensors in the offline phase.

We present two different tests for the variable height cavity. In the first one, we consider fixed the Rayleigh number, with a moderate value $Ra = 10^5$. This test intends to represent a situation in which the environmental conditions are fixed and we only are interested in simulating the flow in cavities. In the second test, both the Rayleigh and the geometric parameter are taken into account. This test is more complex since two parameters are considered, thus the number of basis functions to include in our reduced-basis spaces increases with respect to the previous one. At the same time, the speed-up ratio decreases.

The chapter is structured as follows: in section 5.2 we define the FE problem in the reference domain from the one defined in the original domain depending on the geometric parameter. Then, in section 5.3, we present the Reduced Basis problem, with the EIM approximation for the eddy viscosity and eddy diffusivity terms. In section 5.4 we construct the *a posteriori* error bound estimator. Finally in section 5.5, we present the numerical results for the tests previously described.

5.2 Problem statement

In this section consider a natural convection in a cavity, whose height is variable. Thus, we are considering a single geometrical parameter for the height, which modifies the aspect ratio of the cavity, denoted by μ_g. Let $\Omega_o(\mu_g) = [0,1] \times [0,\mu_g] \subset \mathbb{R}^2$ be the original domain and let $\Gamma = \Gamma_D \cup \Gamma_N$ the be Lipschitz-continuous boundary of $\Omega_o(\mu_g)$, where Γ_D is the part of the boundary with Dirichlet conditions and Γ_N the part of the boundary with Neumann conditions. In Fig. 5.1 we present a scheme of the problem to consider.

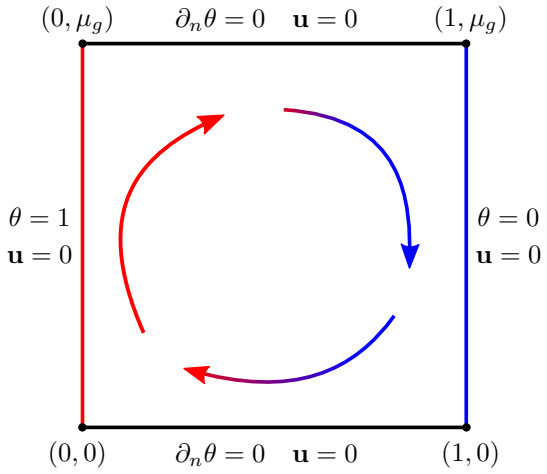

Figure 5.1: Original domain Ω_o, with the different boundaries identified, of problem (5.1).

To model this flow, we consider the Boussinesq model presented in Chapter 4, with VMS-Smagorinsky modelling for the eddy viscosity and eddy diffusivity. Besides the geometrical parameter, we also can consider the Rayleigh as a parameter, letting $\boldsymbol{\mu} = (\mu_{ph}, \mu_g) \in \mathcal{D}$, with $\mu_{ph} = Ra$, the Rayleigh number. Since we are interested in modeling the aero-thermal flow, we consider in our model $Pr = 0.71$, the Prandtl number of the air. With the same notation as in Chapter

4, the continuous form of the VMS-Boussinesq-Smagorinsky model in the original domain reads:

$$\begin{cases} \mathbf{u}_o \cdot \nabla_o \mathbf{u}_o - Pr\Delta_o \mathbf{u}_o - \nabla_o \cdot (\nu_T(\mathbf{u}_o)\nabla_o \mathbf{u}_o) & \\ +\nabla_o p_o - Pr\,\mu_{ph}\,\theta_o\,\mathbf{e}_d = \mathbf{f} & \text{in } \Omega_o(\mu_g) \\ \nabla_o \cdot \mathbf{u}_o = 0 & \text{in } \Omega_o(\mu_g) \\ \mathbf{u}_o \cdot \nabla_o \theta_o - \Delta_o \theta_o - \nabla_0 \cdot (K_T(\mathbf{u}_o)\nabla_o \theta_o) = Q & \text{in } \Omega_o(\mu_g) \\ \mathbf{u}_o = 0 & \text{on } \Gamma \\ \theta_o = \theta_D & \text{on } \Gamma_D \\ \partial_n \theta_o = 0 & \text{on } \Gamma_N \end{cases} \tag{5.1}$$

Let us consider the spaces $Y^o = (H_0^1(\Omega_o)^d$, $M^o = L_0^2(\Omega_o)$, $\Theta^o = H_0^1(\Omega_o)$. We denote $X^o = Y^o \times \Theta^o \times M^o$. The variational formulation of problem (5.1), over the parameter-dependent original domain is

$$\begin{cases} \text{Find } (\mathbf{u}_o, \theta_o^u, p_o^u) = (\mathbf{u}_o(\boldsymbol{\mu}), \theta_o^u(\boldsymbol{\mu}), p_o^u(\boldsymbol{\mu})) \in X^o \text{ such that} & \\ \tilde{a}_u(\mathbf{u}_o, \mathbf{v}_o; \boldsymbol{\mu}) + \tilde{b}(\mathbf{v}_o, p_o^u; \boldsymbol{\mu}) + \tilde{a}'_{Su}(\mathbf{u}_o; \mathbf{u}_o, \mathbf{v}_o; \boldsymbol{\mu}) & \\ +\tilde{c}_u(\mathbf{u}_o, \mathbf{u}_o, \mathbf{v}_o; \boldsymbol{\mu}) + \tilde{f}(\theta_o^u, \mathbf{v}_o; \boldsymbol{\mu}) = \tilde{F}(\mathbf{v}_o; \boldsymbol{\mu}) & \forall \mathbf{v}_o \in Y^o, \\ \tilde{b}(\mathbf{u}_o, p_o^v; \boldsymbol{\mu}) = 0 & \forall p_o^v \in M^o, \\ \tilde{a}_\theta(\theta_o^u, \theta_o^v; \boldsymbol{\mu}) + \tilde{c}_\theta(\mathbf{u}_o, \theta_o^u, \theta_o^v; \boldsymbol{\mu}) & \\ +\tilde{a}'_{S\theta}(\mathbf{u}_o; \theta_o^u, \theta_o^v; \boldsymbol{\mu}) = \tilde{Q}(\theta_o^v; \boldsymbol{\mu}) & \forall \theta_o^v \in \Theta_h^o. \end{cases} \tag{5.2}$$

Here, the forms $\tilde{a}_u(\cdot,\cdot;\boldsymbol{\mu})$, $\tilde{a}_\theta(\cdot,\cdot;\boldsymbol{\mu})$, $\tilde{b}(\cdot,\cdot;\boldsymbol{\mu})$, $\tilde{f}(\cdot,\cdot;\boldsymbol{\mu})$, $\tilde{c}_u(\cdot,\cdot,\cdot;\boldsymbol{\mu})$, $\tilde{c}_\theta(\cdot,\cdot,\cdot;\boldsymbol{\mu})$, $\tilde{a}'_{Su}(\cdot;\cdot,\cdot;\boldsymbol{\mu})$, and $\tilde{a}'_{S\theta}(\cdot;\cdot,\cdot;\boldsymbol{\mu})$ are defined in an analogous way that in (4.7)-(4.9).

To be able to store parameter independent matrices in the offline phase of the RB method, we need to compute all the integrals in a reference domain trough a transformation of the original domain. Thus, we set $\mu_g^{ref} = 1$, and we define the reference domain $\Omega_r = \Omega_o(\mu_g^{ref})$. The parameter-dependent original domain can be recovered by a transformation map, $T : \Omega_r \times \mathcal{D} \to \mathbb{R}^2$, defined as

$$T((x,y);\mu_g) = \begin{pmatrix} 1 & 0 \\ 0 & \mu_g \end{pmatrix} \begin{pmatrix} x \\ y \end{pmatrix}, \quad \forall (x,y) \in \Omega_r. \tag{5.3}$$

As this map is linear, its Jacobian matrix and its determinant are given by

$$\mathbf{J}((x,y);\mu_g) = \begin{pmatrix} 1 & 0 \\ 0 & \mu_g \end{pmatrix}, \text{ and } |\mathbf{J}((x,y);\mu_g)| = \mu_g. \tag{5.4}$$

Let $\{\mathcal{T}_h\}_{h>0}$ a uniformly regular family of triangulation on the reference domain. We denote $Y_h = (H_0^1(\Omega_r) \cap V_h^l(\Omega_r))^d$, $M_h = L_0^2(\Omega_r) \cap V_h^m(\Omega_r)$, $\Theta_h = H_0^1(\Omega_r) \cap V_h^q(\Omega_r)$, with $l, m, q \in \mathbb{N}$, respectively the discrete velocity, pressure and temperature spaces on the reference domain. Denoting $X_h = Y_h \times \Theta_h \times M_h$, we rewrite problem (5.2) with respect to the reference domain, applying the change of variables of the transformation map T, as

$$\begin{cases} \text{Find } (\mathbf{u}_h, \theta_h^u, p_h^u) = (\mathbf{u}_h(\boldsymbol{\mu}), \theta_h^u(\boldsymbol{\mu}), p_h^u(\boldsymbol{\mu})) \in X_h \text{ such that} \\ a_{u,x}(\mathbf{u}_h, \mathbf{v}_h; \boldsymbol{\mu}) + a_{u,y}(\mathbf{u}_h, \mathbf{v}_h; \boldsymbol{\mu}) + b_x(\mathbf{v}_h, p_h^u; \boldsymbol{\mu}) \\ +b_y(\mathbf{v}_h, p_h^u; \boldsymbol{\mu}) + a'_{Su,x}(\mathbf{u}_h; \mathbf{u}_h, \mathbf{v}_h; \boldsymbol{\mu}) \\ +a'_{Su,y}(\mathbf{u}_h; \mathbf{u}_h, \mathbf{v}_h; \boldsymbol{\mu}) + c_{u,x}(\mathbf{u}_h, \mathbf{u}_h, \mathbf{v}_h; \boldsymbol{\mu}) \\ +c_{u,y}(\mathbf{u}_h, \mathbf{u}_h, \mathbf{v}_h; \boldsymbol{\mu}) + f(\theta_h^u, \mathbf{v}_h; \boldsymbol{\mu}) = \tilde{F}(\mathbf{v}_h; \boldsymbol{\mu}) & \forall \mathbf{v}_h \in Y_h, \\ b_x(\mathbf{u}_h, p_h^v; \boldsymbol{\mu}) + b_y(\mathbf{u}_h, p_h^v; \boldsymbol{\mu}) = 0 & \forall p_h^v \in M_h, \\ a_{\theta,x}(\theta_h^u, \theta_h^v; \boldsymbol{\mu}) + a_{\theta,y}(\theta_h^u, \theta_h^v; \boldsymbol{\mu}) + c_{\theta,x}(\mathbf{u}_h, \theta_h^u, \theta_h^v; \boldsymbol{\mu}) \\ +c_{\theta,y}(\mathbf{u}_h, \theta_h^u, \theta_h^v; \boldsymbol{\mu}) + a'_{S\theta,x}(\mathbf{u}_h; \theta_h^u, \theta_h^v; \boldsymbol{\mu}) \\ +a'_{S\theta,y}(\mathbf{u}_h; \theta_h^u, \theta_h^v; \boldsymbol{\mu}) = \tilde{Q}(\theta_h^v; \boldsymbol{\mu}) & \forall \theta_h^v \in \Theta_h, \end{cases} \tag{5.5}$$

where the subscripts x and y denotes the addend of the corresponding operator, relatives to the partial derivative with respect to x or y, respectively. These operators have the following form:

$$a_{u,x}(\mathbf{u}_h, \mathbf{v}_h; \boldsymbol{\mu}) = Pr\, \mu_g \int_{\Omega_r} (\partial_x u_1 \partial_x v_1 + \partial_x u_2 \partial_x v_2)\, d\Omega_r,$$

$$a_{u,y}(\mathbf{u}_h, \mathbf{v}_h; \boldsymbol{\mu}) = \frac{Pr}{\mu_g} \int_{\Omega_r} (\partial_y u_1 \partial_y v_1 + \partial_y u_2 \partial_y v_2)\, d\Omega_r,$$

$$b_x(\mathbf{u}_h, p_h^u; \boldsymbol{\mu}) = -\mu_g \int_{\Omega_r} p_h^u \partial_x u_1\, d\Omega_r, \quad b_y(\mathbf{u}_h, p_h^u; \boldsymbol{\mu}) = -\int_{\Omega_r} p_h^u \partial_y u_2\, d\Omega_r,$$

$$f(\theta_h^u, \mathbf{v}_h; \boldsymbol{\mu}) = Pr\, \mu_{ph}\, \mu_g \int_{\Omega_r} \theta_h^u v_2\, d\Omega_r,$$

$$a_{\theta,x}(\theta_h^u, \theta_h^v; \boldsymbol{\mu}) = \mu_g \int_{\Omega_r} \partial_x \theta_h^u \partial_x \theta_h^v\, d\Omega_r, \quad a_{\theta,y}(\theta_h^u, \theta_h^v; \boldsymbol{\mu}) = \frac{1}{\mu_g} \int_{\Omega_r} \partial_y \theta_h^u \partial_y \theta_h^v\, d\Omega_r,$$

$$c_{u,x}(\mathbf{w}_h, \mathbf{u}_h, \mathbf{v}_h; \boldsymbol{\mu}) = \mu_g \int_{\Omega_r} \left[(w_1 \partial_x u_1) v_1 + (w_1 \partial_x u_2) v_2\right] d\Omega_r,$$

$$c_{u,y}(\mathbf{w}_h, \mathbf{u}_h, \mathbf{v}_h; \boldsymbol{\mu}) = \int_{\Omega_r} \left[(w_2 \partial_y u_1) v_1 + (w_2 \partial_y u_2) v_2\right] d\Omega_r,$$

$$c_{\theta,x}(\mathbf{u}_h, \theta_h^u, \theta_h^v; \boldsymbol{\mu}) = \mu_g \int_{\Omega_r} (u_1 \partial_x \theta_h^u) \theta_h^v\, d\Omega_r,$$

$$c_{\theta,y}(\mathbf{u}_h,\theta_h^u,\theta_h^v;\boldsymbol{\mu}) = \int_{\Omega_r} (u_2\partial_x\theta_h^u)\theta_h^v \, d\Omega_r,$$

$$a'_{Su,x}(\mathbf{w}_h;\mathbf{u}_h,\mathbf{v}_h;\boldsymbol{\mu}) = \mu_g\int_{\Omega_r}\nu_T(\Pi_h^*\mathbf{w})\left[\partial_x(\Pi_h^*u_1)\partial_x(\Pi_h^*v_1)+\partial_x(\Pi_h^*u_2)\partial_x(\Pi_h^*v_2)\right] d\Omega_r,$$

$$a'_{Su,y}(\mathbf{w}_h;\mathbf{u}_h,\mathbf{v}_h;\boldsymbol{\mu}) = \frac{1}{\mu_g}\int_{\Omega_r}\nu_T(\Pi_h^*\mathbf{w})\left[\partial_y(\Pi_h^*u_1)\partial_y(\Pi_h^*v_1)+\partial_y(\Pi_h^*u_2)\partial_y(\Pi_h^*v_2)\right] d\Omega_r,$$

$$a'_{S\theta,x}(\mathbf{u}_h;\theta_h^u,\theta_h^v;\boldsymbol{\mu}) = \frac{\mu_g}{Pr}\int_{\Omega_r}\nu_T(\Pi_h^*\mathbf{u};\mu_g)\partial_x(\Pi_h^*\theta^u)\partial_x(\Pi_h^*\theta^v) \, d\Omega_r,$$

$$a'_{S\theta,y}(\mathbf{u}_h;\theta_h^u,\theta_h^v;\boldsymbol{\mu}) = \frac{1}{Pr\,\mu_g}\int_{\Omega_r}\nu_T(\Pi_h^*\mathbf{u};\mu_g)\partial_y(\Pi_h^*\theta^u)\partial_y(\Pi_h^*\theta^v) \, d\Omega_r.$$

These integrals are derived applying the change variable formula deduced in (1.5)-(1.9). With this geometrical parametrization, the eddy viscosity $\nu_T(\cdot)$ depends also in the geometrical parameter, and is defined as

$$\nu_T(\mathbf{u};\mu_g) = C_S^2\frac{\mu_g^2+1}{N_h^2}\sqrt{(\partial_x u_1)^2+\frac{1}{\mu_g^2}(\partial_y u_1)^2+(\partial_x u_2)^2+\frac{1}{\mu_g^2}(\partial_y u_2)^2}. \tag{5.6}$$

Here we are supposing that we consider an uniform mesh in the reference domain Ω_r, with N_h partitions in each side. Since the mesh size, h_K, in the VMS-Smagorinsky eddy viscosity and eddy diffusivity term is in terms of the parameter-dependent original domain, we adapt it to the reference domain, by applying the change of variable map T defined in (5.3), obtaining that

$$h_K = \frac{\mu_g^2+1}{N_h^2}, \quad \forall K \in \mathcal{T}_h.$$

Note that problem (4.12) is a particular case of problem (5.5), taking $\mu_g = 1$.

5.3 Reduced Basis problem

In this section we present the RB problem derived from the discrete problem presented in section 5.2. We construct the low-dimensional spaces for the RB problem with the Greedy algorithm (see sect. 1.3). Both the pressure and the temperature reduced basis spaces are defined with the corresponding snapshots computed solving the FE problem (5.5).

The reduced basis velocity space is constructed with the velocity snapshot of the FE velocity solution, and the inner pressure *supremizer*, $T_p^{\boldsymbol{\mu}} : M_h \to Y_h$,

defined for this problem as

$$\int_{\Omega_r} \nabla T_p^{\boldsymbol{\mu}} q_h : \nabla \mathbf{v}_h \, d\Omega_r = -\mu_g \int_{\Omega_r} q_h \, \partial_x v_1 \, d\Omega_r - \int_{\Omega_r} q_h \, \partial_y v_2 \, d\Omega_r, \quad \forall \mathbf{v}_h \in Y_h. \tag{5.7}$$

Thus, the reduced basis spaces are given by

$$Y_N = \text{span}\{\zeta^{\mathbf{v}}_{2k-1} := \mathbf{u}_h(\boldsymbol{\mu}^k),\ \zeta^{\mathbf{v}}_{2k} := T_p^{\boldsymbol{\mu}} \xi_k^p, \quad k = 1, \ldots, N\}, \tag{5.8}$$

$$M_N = \text{span}\{\xi_k^p := p_h^u(\boldsymbol{\mu}^k), \quad k = 1, \ldots, N\}, \tag{5.9}$$

$$\Theta_N = \text{span}\{\varphi_k^\theta := \theta_h^u(\boldsymbol{\mu}^k), \quad k = 1, \ldots, N\}. \tag{5.10}$$

Denoting $X_N = Y_N \times \Theta_N \times M_N$, the RB problem is

$$\begin{cases} \text{Find } (\mathbf{u}_N, \theta_N^u, p_N^u) \in X_N \text{ such that} \\ \begin{aligned} &a_{u,x}(\mathbf{u}_N, \mathbf{v}_N; \boldsymbol{\mu}) + a_{u,y}(\mathbf{u}_N, \mathbf{v}_N; \boldsymbol{\mu}) + b_x(\mathbf{v}_N, p_N^u; \boldsymbol{\mu}) \\ &+ b_y(\mathbf{v}_N, p_N^u; \boldsymbol{\mu}) + a'_{Su,x}(\mathbf{u}_N; \mathbf{u}_N, \mathbf{v}_N; \boldsymbol{\mu}) \\ &+ a'_{Su,y}(\mathbf{u}_N; \mathbf{u}_N, \mathbf{v}_N; \boldsymbol{\mu}) + c_{u,x}(\mathbf{u}_N, \mathbf{u}_N, \mathbf{v}_N; \boldsymbol{\mu}) \\ &+ c_{u,y}(\mathbf{u}_N, \mathbf{u}_N, \mathbf{v}_N; \boldsymbol{\mu}) + f(\theta_N^u, \mathbf{v}_N; \boldsymbol{\mu}) = F(\mathbf{v}_N; \boldsymbol{\mu}) && \forall \mathbf{v}_N \in Y_N, \\ &b_x(\mathbf{u}_N, p_N^v; \boldsymbol{\mu}) + b_{(y)}(\mathbf{u}_N, p_N^v; \boldsymbol{\mu}) = 0 && \forall p_N^v \in M_N, \\ &a_{\theta,x}(\theta_N^u, \theta_N^v; \boldsymbol{\mu}) + a_{\theta,y}(\theta_N^u, \theta_N^v; \boldsymbol{\mu}) + c_{\theta,x}(\mathbf{u}_N, \theta_N^u, \theta_N^v; \boldsymbol{\mu}) \\ &+ c_{\theta,y}(\mathbf{u}_N, \theta_N^u, \theta_N^v; \boldsymbol{\mu}) + a'_{S\theta,x}(\mathbf{u}_N; \theta_N^u, \theta_N^v; \boldsymbol{\mu}) \\ &+ a'_{S\theta,y}(\mathbf{u}_N; \theta_N^u, \theta_N^v; \boldsymbol{\mu}) = Q(\theta_N^v; \boldsymbol{\mu}) && \forall \theta_N^v \in \Theta_N. \end{aligned} \end{cases} \tag{5.11}$$

The eddy viscosity $\nu_T(\mathbf{u}; \mu_g)$ must be linearized in problem (5.11), for the efficiently solving in the online phase. For this purpose, we again use the EIM (see sect. 1.6). The construction of the reduced-basis space for the EIM is done in a similar way as in section 4.2.2.

The eddy viscosity and eddy diffusivity terms are approximated as

$$a'_{Su,x}(\mathbf{w}_h; \mathbf{u}_h, \mathbf{v}_h; \boldsymbol{\mu}) \approx \hat{a}'_{Su,x}(\mathbf{u}_N, \mathbf{v}_N; \boldsymbol{\mu}),$$

$$a'_{Su,y}(\mathbf{w}_h; \mathbf{u}_h, \mathbf{v}_h; \boldsymbol{\mu}) \approx \hat{a}'_{Su,y}(\mathbf{u}_N, \mathbf{v}_N; \boldsymbol{\mu}),$$

$$a'_{S\theta,x}(\mathbf{u}_h; \theta_h^u, \theta_h^v; \boldsymbol{\mu}) \approx \hat{a}'_{S\theta,x}(\theta_N^u, \theta_N^v; \boldsymbol{\mu}),$$

$$a'_{S\theta,y}(\mathbf{u}_h; \theta_h^u, \theta_h^v; \boldsymbol{\mu}) \approx \hat{a}'_{S\theta,y}(\theta_N^u, \theta_N^v; \boldsymbol{\mu}),$$

with,

$$\hat{a}'_{Su,x}(\mathbf{u}_N, \mathbf{v}_N; \boldsymbol{\mu}) = \sum_{k=1}^{M} \sigma_k(\boldsymbol{\mu}) s_{u,x}(q_k, \mathbf{u}_N, \mathbf{v}_N),$$

$$\hat{a}'_{Su,y}(\mathbf{u}_N, \mathbf{v}_N; \boldsymbol{\mu}) = \sum_{k=1}^{M} \sigma_k(\boldsymbol{\mu}) s_{u,y}(q_k, \mathbf{u}_N, \mathbf{v}_N),$$

$$\hat{a}'_{S\theta,x}(\theta^u_N, \theta^v_N; \boldsymbol{\mu}) = \sum_{k=1}^{M} \sigma_k(\boldsymbol{\mu}) s_{\theta,x}(q_k, \theta^u_N, \theta^v_N),$$

$$\hat{a}'_{S\theta,y}(\theta^u_N, \theta^v_N; \boldsymbol{\mu}) = \sum_{k=1}^{M} \sigma_k(\boldsymbol{\mu}) s_{\theta,y}(q_k, \theta^u_N, \theta^v_N),$$

and,

$$s_{u,x}(q_k, \mathbf{u}_N, \mathbf{v}_N) = \mu_g \int_{\Omega_r} q_k \left[\partial_x(\Pi^*_h u_1)\partial_x(\Pi^*_h v_1) + \partial_x(\Pi^*_h u_2)\partial_x(\Pi^*_h v_2)\right] d\Omega_r,$$

$$s_{u,y}(q_k, \mathbf{u}_N, \mathbf{v}_N) = \frac{1}{\mu_g} \int_{\Omega_r} q_k \left[\partial_y(\Pi^*_h u_1)\partial_y(\Pi^*_h v_1) + \partial_y(\Pi^*_h u_2)\partial_y(\Pi^*_h v_2)\right] d\Omega_r,$$

$$s_{\theta,x}(q_k, \theta^u_N, \theta^v_N) = \frac{\mu_g}{Pr} \int_{\Omega_r} q_k\, \partial_x(\Pi^*_h \theta^u)\partial_x(\Pi^*_h \theta^v)\, d\Omega_r,$$

$$s_{\theta,y}(q_k, \theta^u_N, \theta^v_N) = \frac{1}{Pr\,\mu_g} \int_{\Omega_r} q_k\, \partial_y(\Pi^*_h \theta^u)\partial_y(\Pi^*_h \theta^v)\, d\Omega_r.$$

The parameter independent matrices and tensors to store during the offline phase in order to solve efficiently problem (5.11), are given in this case by

$$(\mathbb{A}^{u,x}_N)_{ij} = a_{u,x}(\zeta^{\mathbf{v}}_j, \zeta^{\mathbf{v}}_i), \quad (\mathbb{A}^{u,y}_N)_{ij} = a_{u,y}(\zeta^{\mathbf{v}}_j, \zeta^{\mathbf{v}}_i), \quad i,j = 1,\dots,2N,$$

$$(\mathbb{A}^{\theta,x}_N)_{lm} = a_{\theta,x}(\varphi^{\theta}_m, \varphi^{\theta}_l), \quad (\mathbb{A}^{\theta,y}_N)_{lm} = a_{\theta,y}(\varphi^{\theta}_m, \varphi^{\theta}_l), \quad l,m = 1,\dots,N,$$

$$(\mathbb{F}_N)_{li} = f(\varphi^{\theta}_l, \zeta^{\mathbf{v}}_i), \quad i = 1,\dots,2N,\ l = 1,\dots,N,$$

$$(\mathbb{B}^{x}_N)_{li} = b_x(\zeta^{\mathbf{v}}_i, \xi^p_l), \quad (\mathbb{B}^{(y)}_N)_{li} = b_y(\zeta^{\mathbf{v}}_i, \xi^p_l), \quad i = 1,\dots,2N,\ l = 1,\dots,N,$$

$$(\mathbb{C}^{u,x}_N(\zeta^{\mathbf{v}}_s))_{ij} = c_{u,x}(\zeta^{\mathbf{v}}_s, \zeta^{\mathbf{v}}_j, \zeta^{\mathbf{v}}_i), \quad i,j,s = 1,\dots,2N,$$

$$(\mathbb{C}^{u,y}_N(\zeta^{\mathbf{v}}_s))_{ij} = c_{u,y}(\zeta^{\mathbf{v}}_s, \zeta^{\mathbf{v}}_j, \zeta^{\mathbf{v}}_i), \quad i,j,s = 1,\dots,2N,$$

$$(\mathbb{C}^{\theta,x}_N(\zeta^{\mathbf{v}}_s))_{lm} = c_{\theta,x}(\zeta^{\mathbf{v}}_s, \varphi^{\theta}_m, \varphi^{\theta}_l), \quad l,m = 1,\dots,N,\ s = 1,\dots,2N,$$

$$(\mathbb{C}^{\theta,y}_N(\zeta^{\mathbf{v}}_s))_{lm} = c_{\theta,y}(\zeta^{\mathbf{v}}_s, \varphi^{\theta}_m, \varphi^{\theta}_l), \quad l,m = 1,\dots,N,\ s = 1,\dots,2N,$$

$$(\mathbb{S}^{u,x}_N(q_s))_{ij} = s_{u,x}(q_s, \zeta^{\mathbf{v}}_j, \zeta^{\mathbf{v}}_i), \quad i,j = 1,\dots,2N, s = 1,\dots,M,$$

$$(\mathbb{S}^{u,y}_N(q_s))_{ij} = s_{u,y}(q_s, \zeta^{\mathbf{v}}_j, \zeta^{\mathbf{v}}_i), \quad i,j = 1,\dots,2N, s = 1,\dots,M,$$

$$(\mathbb{S}^{\theta,x}_N(q_s))_{lm} = s_{\theta,x}(q_s, \varphi^{\theta}_m, \varphi^{\theta}_l), \quad l,m = 1,\dots,N, s = 1,\dots,M,$$

$$(\mathbb{S}^{\theta,y}_N(q_s))_{lm} = s_{\theta,y}(q_s, \varphi^{\theta}_m, \varphi^{\theta}_l), \quad l,m = 1,\dots,N, s = 1,\dots,M.$$

Here we are representing the reduced basis velocity, temperature and pressure solutions as a linear combination of the velocity, temperature and pressure snapshots, respectively, of the reduced spaces, i.e.,

$$\mathbf{u}_N(\boldsymbol{\mu}) = \sum_{j=1}^{2N} u_j^N(\boldsymbol{\mu})\zeta_j^{\mathbf{v}}, \quad \theta_N(\boldsymbol{\mu}) = \sum_{j=1}^{N} \theta_j^N(\boldsymbol{\mu})\varphi_j^{\theta}, \quad p_N(\boldsymbol{\mu}) = \sum_{j=1}^{N} p_j^N(\boldsymbol{\mu})\xi_j^p.$$

5.4 *A posteriori* error bound estimator

The *a posteriori* error bound estimator for the Greedy algorithm can be developed in the same way that in Chapter 4. Thus, we rewrite problem (5.5) in a more compact form as

$$\begin{cases} \text{Find } U_h(\boldsymbol{\mu}) = (\mathbf{u}_h, \theta_h^u, p_h^u) \in X_h \text{ such that} \\ A(U_h(\boldsymbol{\mu}), V_h; \boldsymbol{\mu}) = F(V_h; \boldsymbol{\mu}) \qquad \forall V_h \in X_h, \end{cases} \tag{5.12}$$

Remark 5.1. *For the numerical analysis in the development of the a posteriori error bound estimator, we consider the regularized, by a mollifier, eddy diffusivity defined in (4.10).*

In order to use the BRR theory (*cf.* [18]), we define the directional derivative of $A(\cdot, \cdot; \boldsymbol{\mu})$ in a analogous way that in Chapter 4. The directional derivative satisfies the following continuity and inf-sup conditions:

$$\infty > \gamma_0 < \gamma_h(\boldsymbol{\mu}) \equiv \sup_{Z_h \in X_h} \sup_{V_h \in X_h} \frac{\partial_1 A(U_N(\mu), V_h; \boldsymbol{\mu})(V_h)}{\|Z_h\|_X \|V_h\|_X}. \tag{5.13}$$

$$0 < \beta_0 < \beta_h(\boldsymbol{\mu}) \equiv \inf_{Z_h \in X_h} \sup_{V_h \in X_h} \frac{\partial_1 A(U_N(\mu), V_h; \boldsymbol{\mu})(Z_h)}{\|Z_h\|_X \|V_h\|_X}. \tag{5.14}$$

The existence of $\gamma_0 \in \mathbb{R}$ and $\beta_0 > 0$ satisfying (5.13) and (5.14), respectively, are given by the following results:

Proposition 5.1. *There exists* $\gamma_0 \in \mathbb{R}$ *such that* $\forall \mu \in \mathcal{D}$

$$|\partial_1 A(U_h(\boldsymbol{\mu}), V_h; \boldsymbol{\mu})(Z_h)| \leq \gamma_0 \|Z_h\|_X \|V_h\|_X \quad \forall Z_h, V_h \in X_h.$$

Proposition 5.2. *If the Dirichlet boundary data is sufficiently small, then there exists* $\tilde{\beta}(\boldsymbol{\mu}) > 0$ *such that*

$$\partial_1 A(U_h, V_h; \boldsymbol{\mu})(V_h) \geq \tilde{\beta}(\boldsymbol{\mu})(\|\nabla \boldsymbol{v}_h\|_{0,2,\Omega}^2 + \|\nabla \theta_h^v\|_{0,2,\Omega}^2) \quad \forall V_h \in \ X_h. \tag{5.15}$$

Proposition 5.1 and Proposition 5.2, can be proved analogously as in Proposition 4.2 and Proposition 4.3, respectively, taking into account that in the derivative of the operator $A(\cdot,\cdot;\boldsymbol{\mu})$ of problem (5.12) there is a re-scaling of the terms in the derivative operator $A(\cdot,\cdot;\mu)$ of problem (4.12).

With the following result, we prove that the directional derivative is Lipschitz-continuous, which proof is derived straightforwardly from Lemma 4.2:

Lemma 5.1. *There exists a positive constant $\rho_n(\mu_g)$ such that, $\forall U_h^1, U_h^2, Z_h, V_h \in X_h$,*

$$\left|\partial_1 A(U_h^1, V_h;\boldsymbol{\mu})(Z_h) - \partial_1 A(U_h^2, V_h;\boldsymbol{\mu})(Z_h)\right| \leq \rho_n(\mu_g)\|U_h^1 - U_h^2\|_X\|Z_h\|_X\|V_h\|_X, \tag{5.16}$$

with

$$\rho_n(\mu_g) = 2\max\{\mu_g,1\}C_u + 2\max\{\mu_g,1\}C_\theta + 4\max\left\{\mu_g,\frac{1}{\mu_g}\right\}C_S^2 h^{2-d/2} C C_f^3$$

$$+\max\left\{\mu_g,\frac{1}{\mu_g}\right\}\frac{C_S^2 h^{2-d/2} C C_f^3 \|\phi_n'\|_{0,1,\mathbb{R}}(\|\nabla(\Pi_h^*\boldsymbol{u}_h^1)\|_{0,\infty,\Omega} + \|\nabla(\Pi_h^*\theta^{u2})\|_{0,\infty,\Omega})}{Pr}.$$

We define the following continuity and inf-sup constants, relative to the well-posedness of the RB problem (5.11):

$$0 < \beta_N(\boldsymbol{\mu}) \equiv \inf_{Z_h\in X_h}\sup_{V_h\in X_h}\frac{\partial_1 A_n(U_N(\boldsymbol{\mu}),V_h;\boldsymbol{\mu})(Z_h)}{\|Z_h\|_X\|V_h\|_X} = \inf_{Z_h\in X_h}\frac{\|T_N Z_h\|_X}{\|Z_h\|_X}, \tag{5.17}$$

$$\infty > \gamma_N(\boldsymbol{\mu}) \equiv \sup_{Z_h\in X_h}\sup_{V_h\in X_h}\frac{\partial_1 A_n(U_N(\boldsymbol{\mu}),V_h;\boldsymbol{\mu})(Z_h)}{\|Z_h\|_X\|V_h\|_X} = \sup_{Z_h\in X_h}\frac{\|T_N Z_h\|_X}{\|Z_h\|_X}, \tag{5.18}$$

where the *supremizer* operator T_N is defined in (2.24). The existence of these constants can be proved in the same way that the existence of the constants (5.13)-(5.14). Thus, we can define the *a posteriori* error bound estimator as

$$\Delta_N(\boldsymbol{\mu}) = \frac{\beta_N(\boldsymbol{\mu})}{2\rho_n(\mu_g)}\left[1-\sqrt{1-\tau_N(\boldsymbol{\mu})}\right], \tag{5.19}$$

where $\tau_N(\boldsymbol{\mu})$ is given by

$$\tau_N(\boldsymbol{\mu}) = \frac{4\epsilon_N(\boldsymbol{\mu})\rho_n(\mu_g)}{\beta_N^2(\boldsymbol{\mu})}, \tag{5.20}$$

with $\epsilon_N(\boldsymbol{\mu})$ the dual norm of the residual. The *a posteriori* error bound estimator is stated by the following result. The proof can be derived from the proof of Theorem 4.1.

Theorem 5.1. *Let $\boldsymbol{\mu} \in \mathcal{D}$, and assume that $\beta_N(\boldsymbol{\mu}) > 0$. If problem (5.12) admits a solution $U_h(\boldsymbol{\mu})$ such that*

$$\|U_h(\boldsymbol{\mu}) - U_N(\boldsymbol{\mu})\|_X \leq \frac{\beta_N(\boldsymbol{\mu})}{\rho_n(\mu_g)},$$

then this solution is unique in the ball $B_X\left(U_N(\boldsymbol{\mu}), \dfrac{\beta_N(\boldsymbol{\mu})}{\rho_n(\mu_g)}\right)$.

Moreover, assume that $\tau_N(\boldsymbol{\mu}) \leq 1$ for all $\boldsymbol{\mu} \in \mathcal{D}$. Then there exists a unique solution $U_h(\boldsymbol{\mu})$ of (5.12) such that the error with respect $U_N(\boldsymbol{\mu})$, solution of (5.11), is bounded by the a posteriori error bound estimator, i.e.,

$$\|U_h(\boldsymbol{\mu}) - U_N(\boldsymbol{\mu})\|_X \leq \Delta_N(\boldsymbol{\mu}), \tag{5.21}$$

with effectivity

$$\Delta_N(\boldsymbol{\mu}) \leq \left[\frac{2\gamma_N(\boldsymbol{\mu})}{\beta_N(\boldsymbol{\mu})} + \tau_N(\boldsymbol{\mu})\right] \|U_h(\boldsymbol{\mu}) - U_N(\boldsymbol{\mu})\|_X. \tag{5.22}$$

5.5 Numerical results

In this section we present some numerical results for the Boussinesq VMS-Smagorinsky RB model, with geometrical parametrization. We first suppose that the Rayleigh number is fixed with $Ra = 10^5$, and we consider the geometrical parameter ranging in $\mu_g \in \mathcal{D} = [0.5, 2]$.

Next, we consider both the geometrical parameter and the Rayleigh number. For this test, we consider the Rayleigh number (physical parameter), μ_{ph}, ranging in $[10^3, 10^4]$, and the geometrical parameter, μ_g, ranging in $\mu_g \in [0.5, 2]$. Thus we are considering that the parameter domain is $\mathcal{D} = [10^3, 10^4] \times [0.5, 2]$. For both cases, the Prandtl number considered is $Pr = 0.71$, that corresponds to the air Prandtl number.

The FE solution is computed through a semi-implicit evolution approach, which is the adaptation of the numerical scheme (4.38), to problem (5.11). We also suppose that the steady state solution is reached when the error between two iterators is below $\varepsilon_{FE} = 10^{-10}$.

5.5.1 Geometrical parametrization only

In this test, we consider a moderate Rayleigh number value $Ra = 10^5$, and we consider the geometrical parameter ranging in $\mu_g \in \mathcal{D} = [0.5, 2]$. The difference in the height of the cavity affects to the buoyancy force, making it more relevant when we increase the parameter value. This behavior is observed in Fig. 5.2, in which we show four solutions for different values of the geometrical parameter.

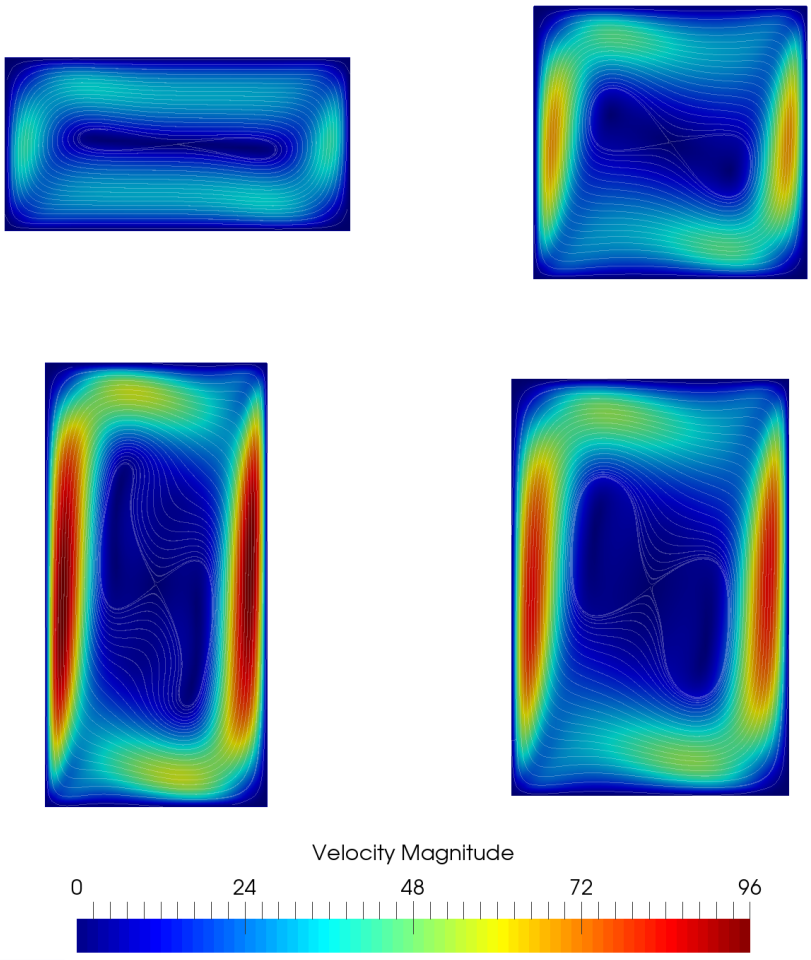

Figure 5.2: FE snapshots for $\mu_g = 0.5$ (top-left), $\mu_g = 1$ (top-right), $\mu_g = 1.5$ (bottom-right) and $\mu_g = 2$ (bottom-left).

Firstly in the offline phase, we construct the reduced-basis space corresponding to the EIM, in which we approximate properly the eddy viscosity and eddy diffusivity term. In this test, we need $M = 73$ basis functions in order to reach a prescribe tolerance of $\varepsilon_{EIM} = 10^{-4}$. In Fig. 5.3 we show the evolution of the infinity norm of the error between the eddy viscosity $\nu_T(\mu_g)$ and its EIM approximation.

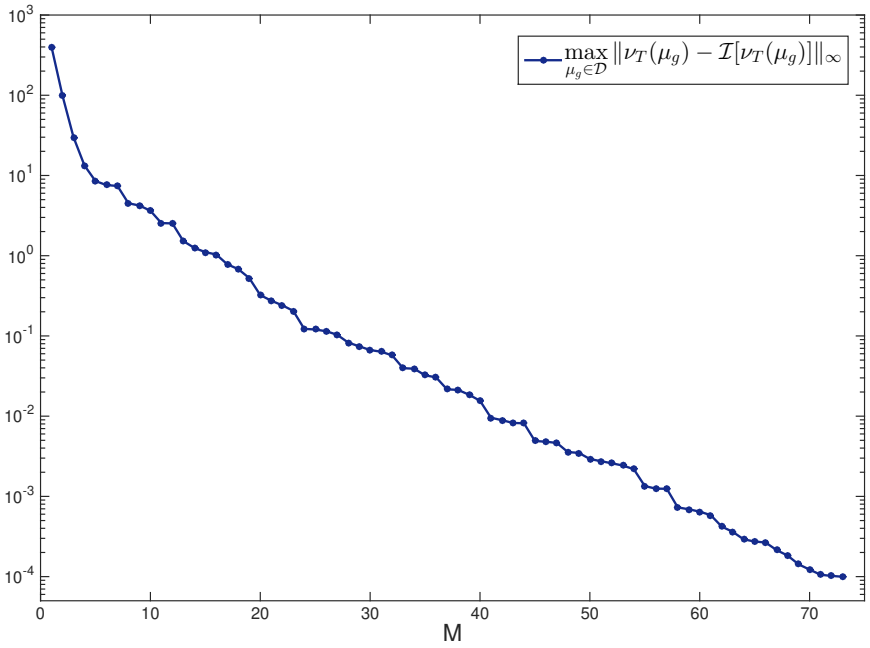

Figure 5.3: Error evolution for the EIM, for Boussinesq VMS-Smagorinsky model with $\mu_g \in [0.5, 2]$

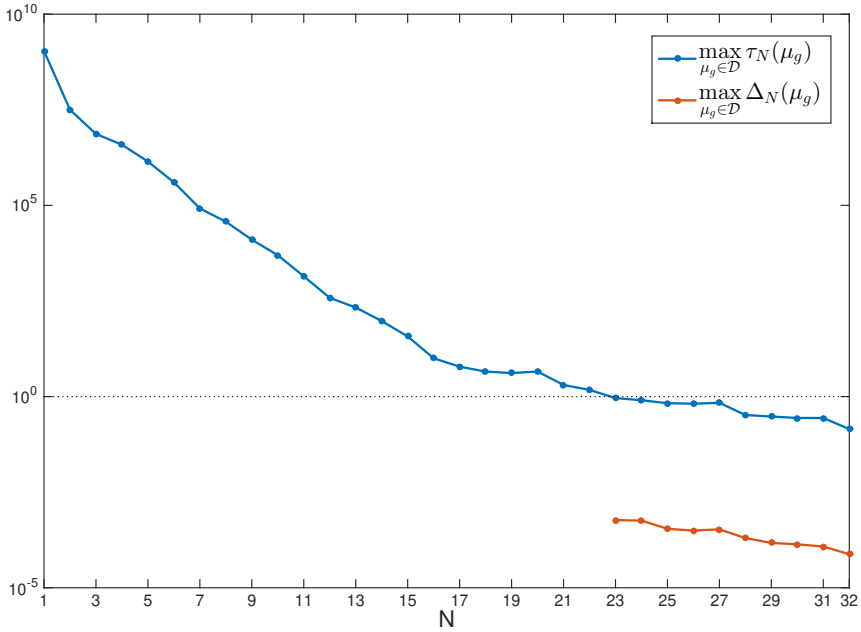

Figure 5.4: Evolution of the *a posteriori* error bound in the Greedy algorithm, for Boussinesq VMS-Smagorinsky model with $\mu_g \in [0.5, 2]$

For the Greedy algorithm, in this test, we prescribe a tolerance for the *a posteriori* error bound of $\varepsilon_{RB} = 10^{-4}$. We need $N = 23$ basis functions

until guarantee the condition of Theorem 5.1, and get $\tau_N(\mu) < 1$. Then, we reach the prescribed tolerance when $N = N_{\max} = 32$. In Fig. 5.4, we show the maximum value for all $\mu_g \in \mathcal{D}$ of the *a posteriori* error bound estimator, and $\tau_N(\mu)$, in each iteration of the Greedy algorithm. Moreover, in Fig. 5.5, we show the *a posteriori* error bound for all $\mu_g \in \mathcal{D}$, in the last iteration of the Greedy algorithm, i.e., when $N = 32$.

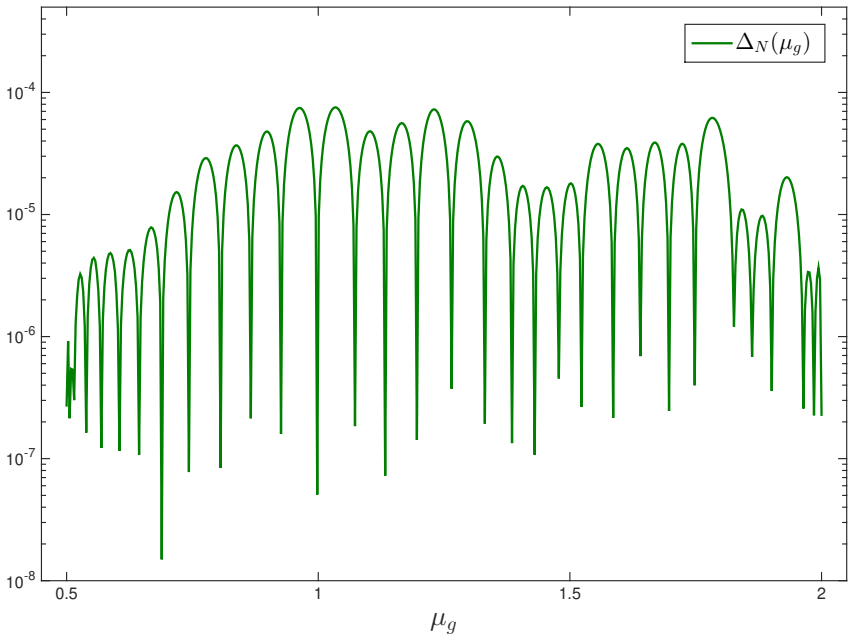

Figure 5.5: *A posteriori* error bound for $N = N_{\max} = 32$

Finally, in Table 5.1, we summarize the results for several parameter values. We show the comparison between the time for computing a FE solution, and the online phase computational time. We obtain a speed-up rate of several hundreds in the computational time. The RB solution accuracy is fairly good, since the error is approximately of order 10^{-6} for velocity, 10^{-8} for temperature, and 10^{-5} for pressure.

Data	$\mu_g = 0.64$	$\mu_g = 1.08$	$\mu_g = 1.44$	$\mu_g = 1.87$
T_{FE}	808.91s	810.16s	866.1s	851.82s
T_{online}	2.68s	2.55s	2.61s	2.52s
speedup	301	317	331	337
$\|\mathbf{u}_h - \mathbf{u}_N\|_1$	$1.13 \cdot 10^{-6}$	$1.86 \cdot 10^{-6}$	$2.82 \cdot 10^{-6}$	$3.4 \cdot 10^{-6}$
$\|\theta_h - \theta_N\|_1$	$6.28 \cdot 10^{-8}$	$8.83 \cdot 10^{-9}$	$9.37 \cdot 10^{-9}$	$9.48 \cdot 10^{-9}$
$\|p_h - p_N\|_1$	$1.69 \cdot 10^{-5}$	$3.7 \cdot 10^{-5}$	$8.35 \cdot 10^{-5}$	$8.82 \cdot 10^{-5}$

Table 5.1: Computational time for FE and RB solutions, with the speedup and the error, for Boussinesq VMS-Smagorinsky model with $\mu_g \in [0.5, 2]$.

5.5.2 Physical and geometrical parametrization

In this test, we perform a RB model in which a physical parameter (the Rayleigh), and a geometric parameter are taken into account. Due to the increasing complexity in the flux with the consideration of this two parameters, we consider low range of Rayleigh number.

Thus, we consider that $\boldsymbol{\mu} = (\mu_{ph}, \mu_g) \in \mathcal{D} = [10^3, 10^4] \times [0.5, 2]$. If we wanted to increase the Rayleigh number, we would have to consider a smaller interval for the geometric parameter. Indeed, as shown in sect. 4.5.2, the flow for high Rayleigh values is quite complex, thus the consideration of geometric parameter joint with the physical parameter is only possible if both intervals are not so much big. If a big parameter set is required, a possible strategy is split it in subsets of lower amplitude, as done in section 4.5, where the whole interval of Rayleigh number of interest $[10^3, 10^6]$ is split in two sub-intervals, $[10^3, 10^5]$ and $[10^5, 10^6]$.

Due to the physic of the problem, it is not necessary so much accuracy in the EIM for the approximation of the eddy viscosity and eddy diffusivity. Thus, for the EIM, we prescribe a tolerance of $\varepsilon_{EIM} = 10^{-3}$. The error between $\nu_T(\mathbf{u}_h; \boldsymbol{\mu})$ and its interpolant becomes below from this tolerance when $M = 138$ basis functions are included in the EIM reduced-basis space. In Fig. 5.6 we show the evolution of that error during the Greedy algorithm in the EIM.

For the Greedy algorithm in the offline phase we prescribe a tolerance of $\varepsilon_{RB} = 10^{-3}$. This tolerance is reached when $N = N_{\max} = 54$ basis functions are considered. We need $N = 46$ basis functions to get $\tau_N(\boldsymbol{\mu}) < 1$, satisfying the conditions of Theorem 5.1, and having defined the *a posteriori* error bound $\Delta_N(\boldsymbol{\mu})$. In Fig. 5.7 we show the evolution of the maximum value of $\tau_N(\boldsymbol{\mu})$ and $\Delta_N(\boldsymbol{\mu})$ in the Greedy algorithm. On the other hand, in Fig. 5.8 we show the value of the *a posteriori* error bound estimator, when $N = N_{\max} = 54$, for all $\boldsymbol{\mu} \in \mathcal{D}$.

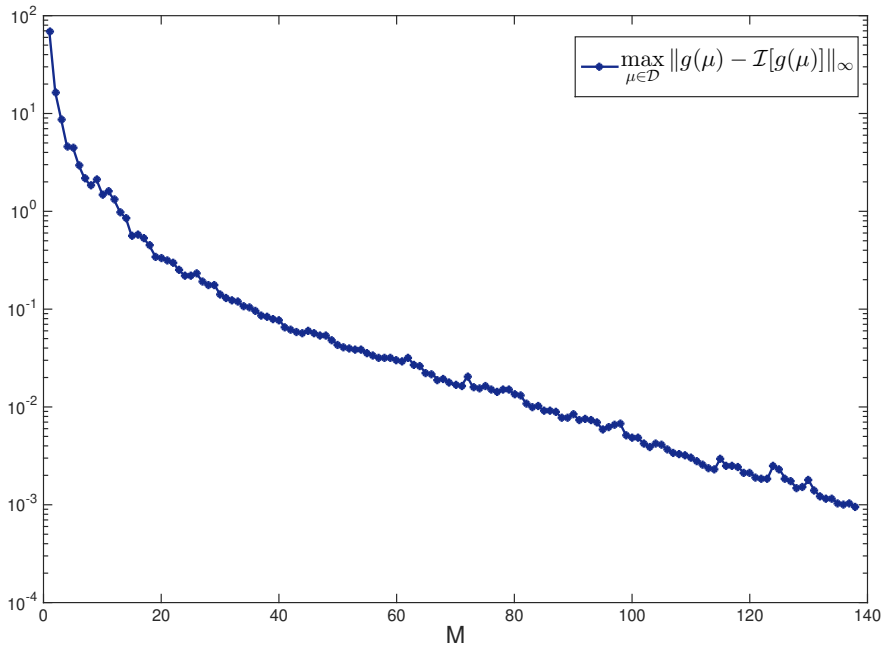

Figure 5.6: Error evolution for the EIM, for Boussinesq VMS-Smagorinsky model with $\boldsymbol{\mu} \in [10^3, 10^4] \times [0.5, 2]$.

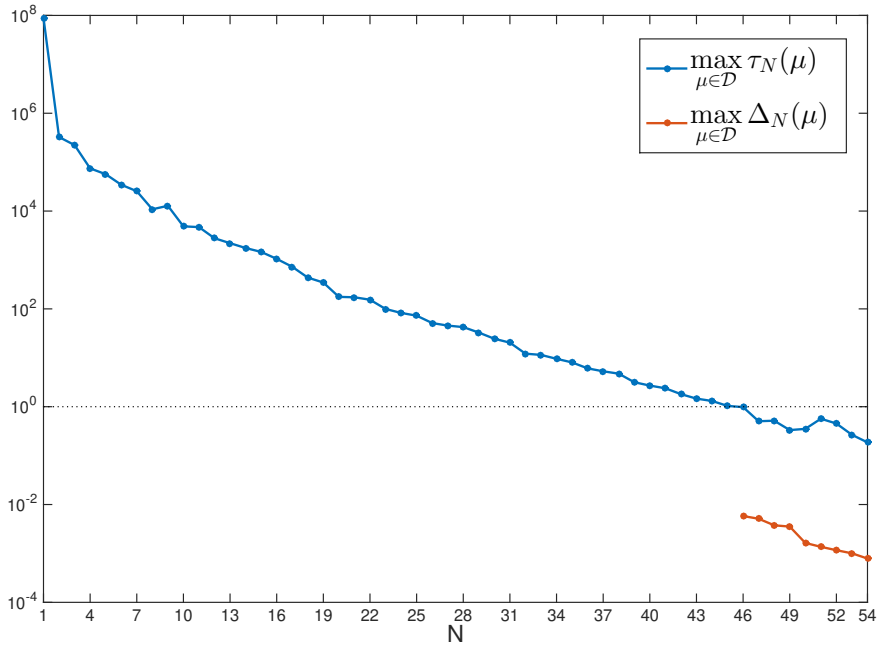

Figure 5.7: Evolution of the *a posteriori* error bound in the Greedy algorithm, for Boussinesq VMS-Smagorinsky model with $\boldsymbol{\mu} \in [10^3, 10^4] \times [0.5, 2]$

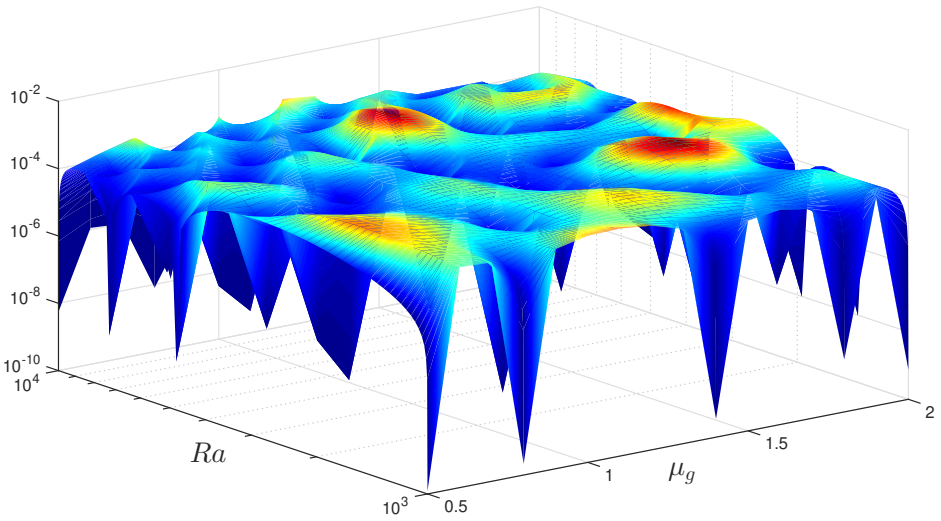

Figure 5.8: *A posteriori* error bound for $N_{\max} = 54$.

Finally, in Table 5.2 we sumarize some results obtained for some values of $\boldsymbol{\mu} \in \mathcal{D}$. There we show that the error between the FE solution and the RB solution is of order 10^{-5} for velocity, 10^{-7} for temperature, and 10^{-5} for pressure. For this test, the speedup rate obtained in the computation of the RB solution in the online phase with respect the computation of the FE solution is around fifty. Again, we have obtained a good accuracy in the RB solution with respect to the FE solution, with a worthy of consideration decrease of the computational time.

Data	$Ra = 2143$ $\mu_g = 1.95$	$Ra = 3506$ $\mu_g = 0.71$	$Ra = 5922$ $\mu_g = 1.13$	$Ra = 9618$ $\mu_g = 1.63$
T_{FE}	600.96s	914.18s	684.95s	630.94s
T_{online}	11.08s	15.73s	14.52s	11.46s
speedup	54	58	47	55
$\|\mathbf{u}_h - \mathbf{u}_N\|_1$	$1.18 \cdot 10^{-5}$	$1.27 \cdot 10^{-5}$	$5.25 \cdot 10^{-6}$	$5.65 \cdot 10^{-6}$
$\|\theta_h - \theta_N\|_1$	$1.07 \cdot 10^{-7}$	$1.67 \cdot 10^{-7}$	$3.23 \cdot 10^{-8}$	$1.51 \cdot 10^{-8}$
$\|p_h - p_N\|_1$	$6.94 \cdot 10^{-6}$	$1.15 \cdot 10^{-5}$	$4.01 \cdot 10^{-6}$	$2.49 \cdot 10^{-6}$

Table 5.2: Computational time for FE and RB solutions, with the speedup and the error, for Boussinesq VMS-Smagorinsky model with $\boldsymbol{\mu} \in [10^3, 10^4] \times [0.5, 2]$.

5.6 Conclusions

In this Chapter, we have developed the RB Boussinesq VMS-Smagorinsky model, with a parametric dependence. We have reformulated our problem in a reference domain, which does not depends on the geometric parameter.

We have present two different tests, one considering only the geometric parameter; and other with two parameters, physical (Rayleigh number) and geometrical. For both test, we obtain a accurate RB solution with a speedup rate that goes from approximately three hundreds in the case of geometrical parametrization only, and fifty for the test in which we consider both parameters.

Appendix A

Sobolev embedding constant approximation

For the computation of the *a posteriori* error bound, that have been developed in the different Chapters of this work, is necessary to compute a numerical approximation of the Sobolev embedding constant of $H^1(\Omega)$ in $L^4(\Omega)$, and the Brezzi-Rappaz-Raviart stability factor.

In this appendix, we rely on the computation of an approximation of the Sobolev embedding constant, needed in the *a posteriori* error bound for the Greedy algorithm, presented in section 1.3.

For the computation of this approximation of the Sobolev embedding constant, we address a fixed-point algorithm than can be found in [36] and [72]. The computation of this approximation of the Sobolev embedding constant is done in the offline phase since it does not longer depends on the parameter value. Even if we are considering a geometrical parametrization, all the computations in the offline phase are done in a reference domain, which does not depend on the geometrical parameter.

The Sobolev embedding constant is defined as

$$C_X^2 = \sup_{v_h \in X_h} \frac{\|v_h\|_{0,4,\Omega}^2}{\|v_h\|_X^2}. \tag{A.1}$$

To approximate it numerically, let us denote by u_* the element of X_h that satisfies

$$u_* = \arg \max_{v_h \in X_h} \frac{\|v_h\|_{0,4,\Omega}^2}{\|v_h\|_X^2}, \quad \|u_*\|_X = 1, \tag{A.2}$$

and let us consider the operator $\sigma : X_h \to L^2(\Omega_r)$, defined as $\sigma(v_h) = v_h^2/\|v\|_{0,4,\Omega}^2$. Note that $\|\sigma(v_h)\|_{0,2,\Omega} = 1$, for all $v_h \in X_h$.

Given a nonnegative function $z \in L^2(\Omega_r)$, we introduce the following eigenvalue problem:

$$\begin{cases} \text{Find } u(z) \in X_h \text{ and } \lambda(z) \in \mathbb{R}_+ \text{ such that} \\ \displaystyle\int_\Omega z\, u(z) v_h \, d\Omega = \lambda(z)(u(z), v_h)_X, \quad \text{with } \|u(z)\|_X = 1, \end{cases} \tag{A.3}$$

where we denote by $\lambda_{\max}(z)$ and $u_{\max}(z)$ the largest eigenvalue and it associated eigenfunction respectively. Taking into account that $\lambda_{\max}(\sigma(u_*)) = C_X^2$ and $u_{\max}(\sigma(u_*)) = u_*$, we consider the following fixed-point algorithm:

$$\begin{cases} \text{Let } u^0 \in X_h, \text{ for } k \geq 0, \\ u^{k+1} = u_{\max}(\sigma(u^k)), \lambda^{k+1} = \lambda_{\max}(\sigma(u^k)). \end{cases} \tag{A.4}$$

We remark that a fixed-point of this algorithm is not necessarily a supremizer of (A.1), but it is at least a local supremizer. In fact, as appears in [36] and [72],

$$\lambda^{k+1} - \lambda^k = \|u^{k-1}\|_{0,4,\Omega}^2 \int_\Omega (\sigma(u^{k-1}) - \sigma(u^{k-2}))\sigma(u^{k-1}) \, d\Omega$$

$$+ o(\|\sigma(u^{k-1}) - \sigma(u^{k-2})\|_{0,2,\Omega}),$$

and since $\|\sigma(v)\|_{0,2,\Omega} = 1$,

$$\int_\Omega (\sigma(u^{k-1}) - \sigma(u^{k-2}))\sigma(u^{k-1}) \, d\Omega \geq 0.$$

Note that if $\sigma(u^{k-1})$ and $\sigma(u^{k-2})$ are not equal, this integral is strictly positive, thus at least each fixed-point iteration heads in the right direction.

Bibliography

[1] B. O. Almroth, P. Stelhin and F. A. Brogan, *Use of global functions for improvement in efficiency of nonlinear analysis*, in 22nd Structures, Structural Dynamics and Materials Conference, American Institute of Aeronautics and Astronautics, apr 1981.

[2] B. O. Almroth, P. Stern and F. A. Brogan, *Automatic choice of global shape functions in structural analysis*, AIAA Journal, 16 (1978), pp. 525–528.

[3] B. Armali, F. Durst, J. Pereira and B. Schönung, *Experimental and theoretical investigation of backward-facing step flow*, J . Fluid Mech., 127 (1983), pp. 473–496.

[4] J. Baiges, R. Codina and S. Idelsohn, *Explicit reduced-order models for the stabilized finite element approximation of the incompressible navier-stokes equations*, Int. J. Numer. Meth. Fluids, 72 (2013), pp. 1219–1243.

[5] J. Bailon-Cuba, O. Shishkina, C. Wagner and J. Schumacher, *Low-dimensional model of turbulent mixed convection in a complex domain*, Physics of Fluids, 24 (2012), p. 107101.

[6] M. J. Balajewicz, E. H. Dowell and B. R. Noack, *A novel model order reduction approach for Navier-Stokes equations at high Reynolds number*, J. Fluid Mech., 729 (2013), pp. 285–308.

[7] F. Ballarin, A. Manzoni, A. Quarteroni and G. Rozza, *Supremizer stabilization of POD-Galerkin approximation of parametrized steady incompressible Navier-Stokes equations.*, Int J Numer Methods Eng, (2014), pp. 1136–1161.

[8] F. Ballarin, A. Manzoni, G. Rozza and S. Salsa, *Shape optimization by free-form deformation: Existence results and numerical solution for stokes flows*, Journal of Scientific Computing, 60 (2013), pp. 537–563.

[9] M. Barrault, Y. Maday, N. C. Nguyen and A. T. Patera, *An 'empirical interpolation' method: application to efficient reduced-basis discretization of partial differential equations*, C.R. Acad. Sci. Paris Sér. I Math., 339 (2004), pp. 667–672.

[10] M. Benítez and A. Bermúdez, *A second order characteristics finite element scheme for natural convection problems*, Journal of Computational and Applied Mathematics, 235 (2011), pp. 3270–3284.

[11] C. Bernardi, Y. Maday and F. Rapetti, *Discrétisations variationnelles de problèmes aux limites elliptiques*, Springer Berlin Heidelberg, 2004.

[12] P. Binev, A. Cohen, W. Dahmen, R. DeVore, G. Petrova and P. Wojtaszczyk, *Convergence rates for greedy algorithms in reduced basis methods*, SIAM J. Num. Anal., 43 (2010), p. 1457–1472.

[13] J. Boland and W. Layton, *An analysis of the finite element method for natural convection problems*, Numerical Methods for Partial Differential Equations, 6 (1990), pp. 115–126.

[14] J. Boland and W. Layton, *Error analysis for finite element methods for steady natural convection problems*, Numerical Functional Analysis and Optimization, 11 (1990), pp. 449–483.

[15] H. Brezis, *Analyse Fonctionnelle: Theorie Et Applications*, Dunod, 2002.

[16] F. Brezzi, *On the existence, uniqueness, and approximation of saddle point problems arising from Lagrangian multipliers.*, R.A.I.R.O., Anal. Numér., 2 (1974), pp. 129–151.

[17] F. Brezzi and J. Pitkäranta, *On the stabilization of finite element approximations of the stokes equations*, in Efficient Solutions of Elliptic Systems, Vieweg+Teubner Verlag, 1984, pp. 11–19.

[18] F. Brezzi, J. Rappaz and P. Raviart, *Finite dimensional approximation of nonlinear problems*, Numer. Maht., 36 (1980), pp. 1–25.

[19] A. N. Brooks and T. J. Hughes, *Streamline upwind/petrov-galerkin formulations for convection dominated flows with particular emphasis on the incompressible navier-stokes equations*, Computer Methods in Applied Mechanics and Engineering, 32 (1982), pp. 199–259.

[20] A. Buffa, Y. Maday, A. T. Patera, C. Prud'homme and G. Turinici, A priori *convergence of the Greedy algorithm for the parametrized reduced basis method*, ESAIM: M2AN, 46 (2012), pp. 595 – 603.

[21] M. Buhmann, *Radial Basis Functions: Theory and Implementations*, vol. 12, Cambridge monographs on applied and computational mathematics, UK, 2003.

[22] G. Caloz and J. Rappaz, *Numerical Analysis for nonlinear and bifurcation problems*, Handbook of numerical analysis, Vol. V, 1997.

[23] T. Chacón Rebollo, *A term by term stabilization algorithm for finite element solution of incompressible flow problems*, Numerische Mathematik, 79 (1998), pp. 283–319.

[24] T. Chacón Rebollo, *An analysis technique for stabilized finite element solution of incompressible flows*, ESAIM: Mathematical Modelling and Numerical Analysis, 35 (2001), pp. 57–89.

[25] T. Chacón Rebollo, M. Gómez Mármol, V. Girault and I. Sánchez Muñoz, *A high order term-by-term stabilization solver for incompressible flow problems*, IMA Journal of Numerical Analysis, 33 (2012), pp. 974–1007.

[26] T. Chacón Rebollo, M. Gómez Mármol, F. Hecht, S. Rubino and I. Sánchez Muñoz, *A high-order local projection stabilization method for natural convection problems*, Journal of Scientific Computing, (2017).

[27] T. Chacón Rebollo, M. Gómez Mármol and S. Rubino, *Numerical analysis of a finite element projection-based VMS turbulence model with wall laws*, Computer Methods in Applied Mechanics and Engineering, 285 (2015), pp. 379–405.

[28] T. Chacón Rebollo and R. Lewandowski, *Mathematical and Numerical Foundations of Turbulence Models and Applications*, Springer New York, 2014.

[29] S. Chaturantabut and D. C. Sorensen, *Nonlinear model reduction via discrete empirical interpolation*, SIAM Journal on Scientific Computing, 32 (2010), pp. 2737–2764.

[30] P. Chen, A. Quarteroni and G. Rozza, *Reduced basis methods for uncertainty quantification*, SIAM/ASA Journal on Uncertainty Quantification, 5 (2017), pp. 813–869.

[31] P. G. Ciarlet, *The finite element method for elliptic problems*, Amsterdam: North-Holland, 1978.

[32] R. Codina, *Stabilization of incompressibility and convection through orthogonal sub-scales in finite element methods*, Computer Methods in Applied Mechanics and Engineering, 190 (2000), pp. 1579–1599.

[33] R. Codina, *A stabilized finite element method for generalized stationary incompressible flows*, Computer Methods in Applied Mechanics and Engineering, 190 (2001), pp. 2681–2706.

[34] M. Couplet, P. Sagaut and C. Basdevant, *Intermodal energy transfers in a proper orthogonal decomposition-Galerkin representation of a turbulent separated flow*, J. Fluid Mech., 491 (2003), pp. 257–284.

[35] G. De Vahl Davis, *Natural convection of air in a square cavity: A bench mark numerical solution*, International Journal for Numerical Methods in Fluids, 3 (1983), pp. 249–264.

[36] S. Deparis, *Reduced basis error bound computation of parameter-dependent Navier-Stokes equations by the natural norm approach*, SIAM J. Sci. Comput., 46 (2008), pp. 2039–2067.

[37] S. Deparis and A. E. Løvgren, *Stabilized reduced basis approximation of incompressible three-dimensional navier-stokes equations in parametrized deformed domains*, J. Sci. Comput., 50 (2012), pp. 198–212.

[38] S. Deparis and G. Rozza, *Reduced basis method for multi-parameter-dependent steady Navier-Stokes equations: Applications to natural convection in a cavity*, Journal of Computational Physics, 228 (2009), pp. 4359–4378.

[39] J. Edmonds, *Matroids and the greedy algorithm*, Math. Program., 1 (1971), pp. 127–136.

[40] J. P. Fink and W. C. Rheinboldt, *On the discretization error of parametrized nonlinear equations*, SIAM Journal on Numerical Analysis, 20 (1983), pp. 732–746.

[41] J. P. Fink and W. C. Rheinboldt, *On the error behavior of the reduced basis technique for nonlinear finite element approximations*, ZAMM - Zeitschrift für Angewandte Mathematik und Mechanik, 63 (1983), pp. 21–28.

[42] L. P. Franca and C. Farhat, *Bubble functions prompt unusual stabilized finite element methods*, Computer Methods in Applied Mechanics and Engineering, 123 (1995), pp. 299–308.

[43] M. Germano, U. Piomelli, P. Moin and W. H. Cabot, *A dynamic subgrid-scale eddy viscosity model*, Physics of Fluids A: Fluid Dynamics, 3 (1991), pp. 1760–1765.

[44] L. Giraud, J. Langou and M. Rozloznik, *The loss of ortorthogonal in the gram-schmidt orthogonalization process.*, Computers and Mathematics with Applications, 50 (2005), pp. 1069–1075.

[45] M. A. Grepl, Y. Maday, N. C. Nguyen and A. T. Patera, *Efficient reduced-basis treatment of nonaffine and nonlinear partial differential equations*, ESAIM: Mathematical Modelling and Numerical Analysis, 41 (2007), pp. 575–605.

[46] M. Gunzburger, N. Jiang and M. Schneier, *An ensemble-Proper Orthogonal decomposition method for the nonstationary Navier-Stokes equations*, https://arxiv.org/abs/1603.04777, (2016).

[47] M. D. Gunzburger, *Finite Element Methods for Viscous Incompressible Flows: A Guide to Theory, Practice, and Algorithms (Computer Science and Scientific Computing)*, Academic Press, 1989.

[48] F. Hecht, *New development in FreeFem++*, J. Numer. Math., 20 (2012), pp. 251–265.

[49] H. Herrero, Y. Maday and F. Pla, *RB (Reduced basis) for RB (Rayleigh–Bénard)*, Comput. Methods Appl. Mech. Eng., 261-262 (2013), pp. 132–141.

[50] J. S. Hesthaven, G. Rozza and B. Stamm, *Certified Reduced Basis Methods for Parametrized Partial Differential Equations*, Springer, 2015.

[51] P. Holmes, J. L. Lumley and G. Berkooz., *Turbulence, Coherent Structures, Dynamical Systems and Symmetry*, Cambridge, 1996.

[52] T. J. Hughes, G. R. Feijóo, L. Mazzei and J.-B. Quincy, *The variational multiscale method—a paradigm for computational mechanics*, Computer Methods in Applied Mechanics and Engineering, 166 (1998), pp. 3–24.

[53] T. J. Hughes, L. P. Franca and G. M. Hulbert, *A new finite element formulation for computational fluid dynamics: VIII. the galerkin/least-squares method for advective-diffusive equations*, Computer Methods in Applied Mechanics and Engineering, 73 (1989), pp. 173–189.

[54] T. J. Hughes, L. Mazzei and K. E. Jansen, *Large eddy simulation and the variational multiscale method*, Computing and Visualization in Science, 3 (2000), pp. 47–59.

[55] T. J. R. Hughes, L. Mazzei, A. A. Oberai and A. A. Wray, *The multiscale formulation of large eddy simulation: Decay of homogeneous isotropic turbulence*, Physics of Fluids, 13 (2001), pp. 505–512.

[56] T. J. R. Hughes, A. A. Oberai and L. Mazzei, *Large eddy simulation of turbulent channel flows by the variational multiscale method*, Physics of Fluids, 13 (2001), pp. 1784–1799.

[57] D. Huynh, D. Knezevic, Y. Chen, J. Hesthaven and A. Patera, *A natural-norm successive contraint method for inf-sup lower bounds*, Comp. Meth. Appl Mech. Engrg., 199 (2010), pp. 1963–1975.

[58] D. Huynh, G. Rozza, S. Sen and A. Patera, *A successive constraint linear optimization method for lower bounds of parametric coercivity and inf–sup stability constants*, Comptes Rendus Mathematique, 345 (2007), pp. 473–478.

[59] L. Iapichino, A. Quarteroni and G. Rozza, *A reduced basis hybrid method for the cou of parametrized doma represented by fluidic networks*, Comput. Meth. Appl. Mech. Engrg., 221-222 (2012), pp. 63–82.

[60] K. Ito and S. Ravindran, *A reduced-order method for simulation and control of fluid flows*, Journal of Computational Physics, 143 (1998), pp. 403–425.

[61] K. Ito and S. Ravindran, *Reduced basis method for optimal control of unsteady viscous flows*, International Journal of Computational Fluid Dynamics, 15 (2001), pp. 97–113.

[62] W. Jones and B. Launder, *The prediction of laminarization with a two-equation model of turbulence*, International Journal of Heat and Mass Transfer, 15 (1972), pp. 301–314.

[63] K. Kunisch and S. Volkwein, *Galerkin proper orthogonal decomposition methods for a general equation in fluid dynamics*, SIAM Journal on Numerical Analysis, 40 (2002), pp. 492–515.

[64] L. Landau, *Fluid Mechanics: Vol 6 (Course of Theoretical Physics)*, Butterworth-Heinemann Ltd, 1987.

[65] T. Lassila and G. Rozza, *Parametric free-form shape design with PDE models and reduced basis method*, Computer Methods in Applied Mechanics and Engineering, 199 (2010), pp. 1583–1592.

[66] T. J. MackMan and C. B. Allen, *Investigation of an adaptive sampling method for data interpolation using radial basis functions*, Int. J. Numer. Methods Eng., 83 (2010), p. 915–938.

[67] Y. Maday, A. Manzoni and A. Quarteroni, *An online intrinsic stabilization strategy for the reduced basis approximation of parametrized*

advection-dominated problems, Comptes Rendus Mathematique, 354 (2016), pp. 1188–1194.

[68] Y. Maday, N. C. Nguyen, A. T. Patera and G. S. H. Pau, *A general, multipurpose interpolation procedure: the magic points*, Commun. Pure Appl. Anal., 8 (2009), pp. 383–404.

[69] Y. Maday, A. T. Patera and G. Turinici, *Global a priori convergence theory for reduced-basis approximations of single-parameter symmetric coercive elliptic partial differential equations*, Comptes Rendus Mathematique, 335 (2002), pp. 289–294.

[70] Y. Maday, A. T. Patera and G. Turinici, *A priori convergence theory for reduced-basis approximations of single-parameter elliptic partial differential equations*, Journal of Scientific Computing, 17 (2002), pp. 437–446.

[71] A. Manzoni, *Reduced Models for Optimal Control, Shape Optimization and Inverse Problems in Haemodynamics*, PhD thesis, École Polytechnique Fédérale de Laussane, 2012.

[72] A. Manzoni, *An efficient computational framework for reduced basis approximation and a posteriori error estimation of parametrized Navier-Stokes flows*, ESAIM: Mathematical Modelling and Numerical Analysis, 48 (2014), pp. 1199–1226.

[73] A. Manzoni and F. Negri, *Heuristic strategies for the approximation of stability factors in quadratically nonlinear parametrized PDEs.*, Adv. Comput. Math., 41 (2015), pp. 1255–1288.

[74] I. Martini, B. Haasdonk and G. Rozza, *Certified reduced basis approximation for the coupling of viscous and inviscid parametrized flow models*, Journal of Scientific Computing, (2017).

[75] D. A. Nagy, *Modal representation of geometrically nonlinear behavior by the finite element method*, Computers & Structures, 10 (1979), pp. 683–688.

[76] F. Negri, A. Manzoni and G. Rozza, *Reduced basis approximation of parametrized optimal flow control problems for the Stokes equations*, Computers and Mathematics with Applications, 69 (2015), pp. 319–336.

[77] F. Negri, G. Rozza, A. Manzoni and A. Quarteroni, *Reduced basis method for parametrized elliptic optimal control problems*, SIAM Journal on Scientific Computing, 35 (2013), pp. A2316–A2340.

[78] N. Ngoc Cuong, K. Veroy and A. T. Patera, *Certified real-time solution of parametrized partial differential equations*, in Handbook of Materials Modeling, Springer Netherlands, 2005, pp. 1529–1564.

[79] A. K. Noor, *Reduced basis technique for nonlinear analysis of structures*, AIAA Journal, 18 (1980), pp. 455–462.

[80] A. K. Noor and J. M. Peters, *Recent advances in reduction methods for instability analysis of structures*, Computers & Structures, 16 (1983), pp. 67–80.

[81] A. K. Noor, J. M. Peters and C. M. Andersen, *Reduced basis technique for collapse analysis of shells*, AIAA Journal, 19 (1981), pp. 393–397.

[82] P. Pacciarini and G. Rozza, *Stabilized reduced basis method for parametrized advection–diffusion PDEs*, Computer Methods in Applied Mechanics and Engineering, 274 (2014), pp. 1–18.

[83] J. S. Peterson, *The reduced basis method for incompressible viscous flow calculations*, SIAM Journal on Scientific and Statistical Computing, 10 (1989), pp. 777–786.

[84] R. Pinnau, *Model reduction via proper orthogonal decomposition*, in Mathematics in Industry, W. Schilders, H. van der Vorst and J. Rommes, eds., Springer Berlin Heidelberg, 2008, pp. 95–109.

[85] G. Pitton, A. Quaini and G. Rozza, *Computational reduction strategies for the detection of steady bifurcations in incompressible fluid-dynamics: Applications to Coanda effect in cardiology*, J Comput Phys, 344 (2017), pp. 534–557.

[86] G. Pitton and G. Rozza, *On the application of Reduced Basis methods to bifurcation problems in incompressible fluid dynamics*, J Sci Comput, (2017). In press.

[87] C. Prud'homme and A. Patera, *Reduced-basis output bounds for approximately parametrized elliptic coercive partial differential equations*, Computing and Visualization in Science, 6 (2004), pp. 147–162.

[88] C. Prud'homme, D. V. Rovas, K. Veroy, L. Machiels, Y. Maday and A. T. Patera, *Reliable real-time solution of parametrized partial differential equations: Reduced-basis output bound methods*, J. Fluids Eng., 124(1) (2002), pp. 70–80.

[89] C. Prud'homme, D. V. Rovas, K. Veroy and A. T. Patera, *A mathematical and computational framework for reliable real-time solution of parametrized partial differential equations*, ESAIM: Mathematical Modelling and Numerical Analysis, 36 (2002), pp. 747–771.

[90] A. Quarteroni, A. Manzoni and F. Negri, *Reduced Basis Methods for Partial Differential Equations: An Introduction*, Springer, 2015.

[91] A. Quarteroni, A. Manzoni and G. Rozza, *Certified reduced basis approximation for parametrized partial differential equations and applications*, Journal of Mathematics in Industry, 1 (2011).

[92] A. Quarteroni, R. Sacco and F. Saleri, *Numerical mathematics*, Springer-Verlag Berlin Heidelberg, 2007.

[93] A. Quarteroni and A. Valli, *Numerical Approximation of Partial Differential Equations*, vol. 23, Springer Berlin Heidelberg, 1994.

[94] D. Rovas, *Reduced-basis output bound methods for parametrized partial differential equations*, PhD thesis, MIT – Massachusetts Institute of Technology, 2003.

[95] G. Rozza, D. B. P. Huynh and A. T. Patera, *Reduced basis approximation and a posteriori error estimation for affinely parametrized elliptic coercive partial differential equations*, Archives of Computational Methods in Engineering, 15 (2008), pp. 229–275.

[96] G. Rozza, D. P. Huynh and A. Manzoni, *Reduced basis approximation and a posteriori error estimation for Stokes flows in parametrized geometries: roles of the inf-sup stability constant*, Numer. Maht., (2013), pp. 115–152.

[97] G. Rozza and K. Veroy, *On the stability of the reduced basis method for Stokes equations in parametrized domains*, Comput. Meth. Appl. Mech. Engrg., (2007), pp. 1244–1260.

[98] S. Rubino, *Numerical modeling of turbulence by Richardson number-based and VMS models*, PhD thesis, University of Seville, 2014.

[99] P. Sagaut, *Large Eddy Simulation for Incompressible Flows: an introduction.*, Springer-Verlag, 2006.

[100] T. W. Sederberg and S. R. Parry, *Free-form deformation of solid geometric models*, ACM SIGGRAPH Computer Graphics, 20 (1986), pp. 151–160.

[101] S. Sirisup and G. Karniadakis, *A spectral viscosity method for correcting the long-term behavior of POD models*, Journal of Computational Physics, 194 (2004), pp. 92–116.

[102] L. Sirovich, *Turbulence and the dynamics of coherent structures. parts i-iii.*, Quart. Appl. Math., 45(3) (1987), pp. 561–590.

[103] J. Smagorinsky, *General circulation experiments with the primitive equations. i. the basic experiment.*, Mon. Weather Rev., 91 (1963), pp. 99–164.

[104] K. Veroy, *Reduced-basis methods applied to problems in elasticity*, PhD thesis, MIT – Massachusetts Institute of Technology, 2003.

[105] K. Veroy and A. Patera, *Reduced-basis approximation of the viscosity parametrized incompressible navier–stokes equations: rigorous a posteriori error bounds*, in Proceedings Singapore–MIT Alliance Symposium, Jan. 2004.

[106] K. Veroy and A. T. Patera, *Certified real-time solution of the parametrized steady incompressible Navier-Stokes equations: rigorous reduced-basis a posteriori error bounds*, Int. J. Numer. Methods Fluids, 47 (2005), p. 773–788.

[107] K. Veroy, C. Prud'homme, D. Rovas and A. Patera, *A posteriori error bounds for reduced-basis approximation of parametrized noncoercive and nonlinear elliptic partial differential equations*, in 16th AIAA Computational Fluid Dynamics Conference, American Institute of Aeronautics and Astronautics, jun 2003.

[108] D. Wan, B. Patnaik and G. Wei, *A new benchmark quality solution for the buoyancy-driven cavity by discrete singular convolution*, Numerical Heat Transfer, Part B: Fundamentals, 40 (2001), pp. 199–228.

[109] Z. Wang, I. Akhtar, J. Broggaard and T. Iliescu, *Proper orthogonal decomposition closure models for turbulent flows: A numerical comparison*, Comp. Meth. Appl Mech. Engrg., 237-240 (2012), pp. 10–26.

[110] Z. Wang and T. Iliescu, *Variational multiscale proper orthogonal decomposition: Navier-Stokes equations*, Num. Meth. PDEs, 30 (2014), pp. 641–663.

[111] H. Wendland, *Scattered Data Approximation*, vol. 17, Cambridge monographs on applied and computational mathematics, Cambridge, 2005.

[112] D. C. Wilcox, *Turbulence Modeling for CFD*, DCW Industries, 1993.

[113] M. Yano and A. T. Patera, *A space–time variational approach to hydrodynamic stability theory*, Proc. R. Soc. A, 469 (2013).